

**GREEN COMPOSITES OF POLYLACTIC ACID FILLED WITH NATURAL
FIBER FOR BIODEGRADATION APPLICATION**

Chamaiporn Yamoum

A Dissertation Submitted in Partial Fulfillment of the Requirements
for the Degree of Doctor of Philosophy
The Petroleum and Petrochemical College, Chulalongkorn University
in Academic Partnership with
The University of Michigan, The University of Oklahoma,
and Case Western Reserve University
2018

บทคัดย่อและแฟ้มข้อมูลฉบับเต็มของวิทยานิพนธ์ตั้งแต่ปีการศึกษา 2554 ที่ให้บริการในคลังปัญญาจุฬาฯ (CUIR)
เป็นแฟ้มข้อมูลของนิสิตเจ้าของวิทยานิพนธ์ที่ส่งผ่านทางบัณฑิตวิทยาลัย

The abstract and full text of theses from the academic year 2011 in Chulalongkorn University Intellectual Repository (CUIR)
are the thesis authors' files submitted through the Graduate School.

Thesis Title: Green Composites of Polylactic Acid Filled with Natural
Fiber for Biodegradable Application
By: Chamaiporn Yamoum
Program: Polymer Science
Thesis Advisor: Prof. Rathanawan Magaraphan

Accepted by the Petroleum and Petrochemical College, Chulalongkorn University, in
partial fulfillment of the requirements for the Degree of Doctor of Philosophy

..... College Dean
(Prof. Suwabun Chirachanchai)

Thesis Committee:

.....
(Asst. Prof. Pomthong Malakul) (Prof. Rathanawan Magaraphan)

.....
(Asst. Prof. Thanyalak Chaisuwan) (Asst. Prof. Manit Nithitanakul)

.....
(Assoc.Prof. Ittipol Jangchud)

ABSTRACT

5282004063: POLYMER SCIENCE PROGRAM

Chamaiporn Yamoum: Green Composites of Polylactic Acid

Filled with Natural Fiber for Biodegradable Application

Thesis Advisors: Prof. Rathanawan Magaraphan 242 pages

Keywords: polylactic acid/ natural fiber/ plasticizer/ biocomposite/chemical crosslinking

This research focuses on how to use natural fibers available from agricultural residues to produce biodegradable materials such as mulch films. Green composites were prepared from natural fibers (peanut shell and bagasse fiber) and polylactic acid (PLA) together with plasticizers. The presence of plasticizers improved PLA molecular mobility as seen by the reduction of glass transition, cold crystallization, and melting temperatures. The addition of natural fibers into PLA brought down decomposition temperature when compared to PLA. The morphological study of the composites showed poor interfacial adhesion between natural fibers and PLA matrix. Moreover, the loading of plasticizers improved distribution of natural fibers in PLA matrix. The composites revealed that tensile strength decreased while Young's modulus increased with increasing natural fibers content. The added plasticizers into the composites showed increase elongation at break and impact strength. Thermo-mechanical properties revealed improvement of PLA performance at high temperature use by the addition of natural fibers together with plasticizers due to cold crystallization at a high temperature, which developed high storage modulus. The composites showed low water vapor permeability which reduced moisture loss by evaporation and increased the efficiency of water use. The enhancements in degradation of the composites were due to the presence of natural fibers. Furthermore, the study of chemical crosslinking PLA in the presence of crosslinking agent showed that the optimum of thermal, thermo-mechanical, and rheological properties were at 5 phr crosslinking agent content.

บทคัดย่อ

หมั่ยพร แยม่อ่ม: คอมพอสิตสีเขียวจากพอลิแลคติกแอซิดและเส้นใยธรรมชาติสำหรับการใช้งานด้านการย่อยสลายทางชีวภาพ (Green Composites of Polylactic Acid Filled with Natural Fiber for Biodegradable Application) อ. ที่ปรึกษา: ศ. ดร. รัตนาวรรณ มกรพันธุ์ 242 หน้า

งานวิจัยนี้มุ่งเน้นการใช้เส้นใยธรรมชาติที่เป็นวัสดุที่เหลือใช้ทางการเกษตรมาพัฒนาเป็นผลิตภัณฑ์ที่สามารถย่อยสลายได้เรียกว่าคอมพอสิตชีวภาพ โดยคอมพอสิตชีวภาพเตรียมจากเส้นใยธรรมชาติ และพอลิแลคติกแอซิดร่วมกับพลาสติกโพลีเอทิลีนเพื่อปรับปรุงประสิทธิภาพการทำงานของพอลิแลคติกแอซิดให้สามารถใช้เป็นฟิล์มคลุมดิน จากการศึกษาพบว่า การเติมพลาสติกโพลีเอทิลีนทำให้สายโซ่ของพอลิแลคติกแอซิดเคลื่อนไหวได้ดีขึ้นและลดอุณหภูมิการเปลี่ยนสถานะคล้ายแก้ว อุณหภูมิตกผลึกเย็นและอุณหภูมิหลอมละลาย ผลของการเติมเส้นใยธรรมชาติทำให้ลดอุณหภูมิสลายตัวของพอลิแลคติกแอซิด การศึกษาลักษณะทางสัณฐานวิทยาของคอมพอสิตแสดงให้เห็นถึงการยึดเกาะที่ไม่ดีระหว่างเส้นใยธรรมชาติและเมทริกซ์ การเติมพลาสติกโพลีเอทิลีนพบว่าสามารถปรับปรุงการกระจายตัวของเส้นใยธรรมชาติในคอมพอสิต และผลของสมบัติเชิงกลพบว่าการต้านแรงดึงและโมดูลัสลดลงในขณะที่การยึดตัวที่จุดขาดเพิ่มขึ้นเมื่อปริมาณการเติมพลาสติกโพลีเอทิลีนเพิ่มขึ้น ในกรณีเติมปริมาณเส้นใยธรรมชาติเพิ่มขึ้นพบว่าโมดูลัสเพิ่มขึ้นด้วย การศึกษาสมบัติเชิงกลพลวัตพบการปรับปรุงประสิทธิภาพการทำงานของพอลิแลคติกแอซิดที่อุณหภูมิสูงซึ่งเป็นผลมาจากการตกผลึกเย็นที่อุณหภูมิต่ำ เส้นใยธรรมชาติปรับปรุงการย่อยสลายของคอมพอสิต นอกจากนี้การศึกษาระบบการเชื่อมขวางทางเคมีของพอลิแลคติกแอซิดด้วยสารที่ทำให้เกิดการเชื่อมขวาง ผลลัพธ์ที่ได้แสดงให้เห็นว่าสมบัติทางความร้อน สมบัติเชิงกลพลวัต และสมบัติการไหล ปรับปรุงขึ้นเมื่อเติมสารเชื่อมขวางปริมาณ 5 phr

ACKNOWLEDGEMENTS

The author would like to thank her supervisor, Professor Dr Rathanawan Magaraphan, who gave her intensive recommendation, constructive criticism, suggestions, constant encouragement, inspiration, and the opportunity to study and have more experiences in The Petroleum and Petrochemical College, Chulalongkorn University, Thailand. Furthermore, she would like to express her appreciation to Center for Petroleum, Petrochemicals and Advanced Materials, Chulalongkorn University, National Research Council of Thailand (NRCT) for financial support, and the National Innovation Agency (NIA), Thailand for project code C48-52. Financial support has been granted by Rachadapisek Sompoch Endowment, Chulalongkorn University, Thailand.

She would like to thank Associate Professor Dr Joao Maia who gave valuable advice and discussion on the research including a financial support during carrying out the experiments in department of Macromolecular Science and Engineering, Case Western Reserve University, Cleveland, Ohio, USA.

She would like to thank all professors and friends at The Petroleum and Petrochemical College, Chulalongkorn University for giving her helps, good time and good memories.

Thus far, finally, she wishes to express her gratitude to her family for their love, understanding, encouragement, and for being a constant source of her inspiration.

TABLE OF CONTENTS

	PAGE	
Title Page	i	
Abstract (in English)	iii	
Abstract (in Thai)	iv	
Acknowledgements	v	
Table of Contents	vi	
List of Tables	xi	
List of Figures	xv	
List of Schemes	xxiii	
CHAPTER		
I	INTRODUCTION	1
II	LIERATURE REVIEW	4
	2.1 Mulch Film	4
	2.2 Polymer Matrix Composite (PMC)	9
	2.3 Biodegradable Filler: Natural Fiber	19
	2.4 Plasticization	30
	2.5 Crosslinking	37
III	EXPERIMENTAL	47
	3.1 Materials	47
	3.2 Methods	47
	3.3 Characterizations	53
	3.4 Overview of Research	57

CHAPTER		PAGE
IV	PREPARATION AND CHARACTERIZATION OF PLA FILLED WITH PEANUT SHELL AS COMPOSITES	59
	4.1 Abstract	59
	4.2 Introduction	59
	4.3 Experimental	61
	4.4 Results and Discussion	65
	4.5 Conclusion	76
	4.6 Acknowledgement	77
	4.7 References	78
V	THERMO-MECHANICAL BEHAVIOR OF PEANUT SHELL/PLA COMPOSITE MODIFIED BY POLYETHYLENE GLYCOL	81
	5.1 Abstract	81
	5.2 Introduction	81
	5.3 Experimental	83
	5.4 Results and Discussion	85
	5.5 Conclusion	97
	5.6 Acknowledgment	98
	5.7 References	98
VI	THE EFFECT OF TRIACETIN ON THERMAL, MECHANICAL, AND BIODEGRADABLE PROPERTIES OF PEANUT SHELL/PLA COMPOSITE	101
	6.1 Abstract	101

CHAPTER		PAGE
	6.2 Introduction	101
	6.3 Experimental	102
	6.4 Results and Discussion	105
	6.5 Conclusion	116
	6.6 Acknowledgement	117
	6.7 References	117
VII	EFFECT OF PEANUT SHELL ON THERMAL, MECHANICAL, AND WATER VAPOR BARRIER PROPERTIES OF PLASTICIZED COMPOSITE FILMS	119
	7.1 Abstract	119
	7.2 Introduction	119
	7.3 Experimental	121
	7.4 Results and Discussion	124
	7.5 Conclusion	137
	7.6 Acknowledgement	138
	7.7 References	138
VIII	THERMAL BEHAVIORS AND MECHANICAL PROPERTIES OF PLA-BAGASSE COMPOSITE FILM	141
	8.1 Abstract	141
	8.2 Introduction	142
	8.3 Experimental	144
	8.4 Results and Discussion	146

CHAPTER	PAGE
8.5 Conclusion	160
8.6 Acknowledgement	162
8.7 References	162
IX	
RHEOLOGICAL AND THERMAL BEHAVIOR OF PLA MODIFIED BY CHEMICAL CROSSLINKING IN THE PRESENCE OF ETHOXYLATED BISPHENOL A DIMETHACRYLATES	165
9.1 Abstract	165
9.2 Introduction	166
9.3 Experimental	167
9.4 Results and Discussion	171
9.5 Conclusion	201
9.6 Acknowledgement	202
9.7 References	202
X	
DISCUSSION OF WHOLE RESEARCH	205
10.1 Comparing between Peanut shell/PLA Composites with Polyethylene Glycol (form chapter V) and Peanut shell/PLA Composites with Triacetin (form chapter VI)	205
10.2 Comparing between Bagasse/PLA Composite Films with Single and Double Plasticizers (form chapter VIII)	206

CHAPTER	PAGE
10.3 Comparing between Peanut shell/PLA Composite Film (form chapter VII) and Bagasse/PLA Composite Film (form chapter VIII)	207
10.4 Comparing between Polyethylene (PE), Black Biodegradable (PBAT), Polylactic Acid (PLA), and Peanut shell/PLA Composite Films with use as a Mulch Films	208
10.5 Comparing between Biocomposite, Plasticization, and Chemical Crosslinking Techniques	209
10.6 Processing Techniques	210
10.7 References	212
XI CONCLUSIONS AND RECOMMENDATIONS	214
11.1 Conclusions	214
11.2 Recommendations	215
REFERENCES	216
APPENDICES	222
Appendix A Stress–Strain Curves of Sample Films in Chapter VII	222
Appendix B Calculation Cost of Samples in Each Chapter	224
CURRICULUM VITAE	227

LIST OF TABLES

TABLE		PAGE
CHAPTER II		
2.1	Plastic mulch film can be divided into 3 main categories	4
2.2	Properties of mulch film: Agroplás [®] from Electro Plastic, Brazil	5
2.3	Chemical composition of some common natural fibers	21
2.4	Physico–mechanical properties of natural fibers	22
2.5	The composition of peanut shell fiber	28
CHAPTER III		
3.1	Properties and compositions of peanut shell and bagasse fiber	50
CHAPTER IV		
4.1	Composition of each formulation	62
4.2	Cooling time and cycle time of each sample	62
4.3	Thermal properties of the second heating scan and density of PLA and the composites	68
4.4	Mechanical properties of PLA and the composites	71
4.5	E' and E'' (MPa) of PLA and the composites	74
4.6	Summary of the properties of the composites	77

TABLE		PAGE
CHAPTER V		
5.1	Composition of each formulation	84
5.2	Thermal properties of plasticized composites	88
5.3	Weight loss of PLA, 30PNS, and plasticized composites	90
5.4	Mechanical properties of plasticized composites	93
5.5	E' and E'' (MPa) of PLA, 30PNS, and plasticized composites	96
5.6	Summary of the properties of plasticized composites	98
CHAPTER VI		
6.1	Composition of each formulation	103
6.2	Thermal properties of plasticized composites	108
6.3	Mechanical properties of plasticized composites	109
6.4	E' and E'' (MPa) of 30PNS and plasticized composites	112
6.5	Weight loss of PLA, 30PNS, and plasticized composites	114
6.6	Summary of the properties of plasticized composites	117
CHAPTER VII		
7.1	Material formulations and film thickness of each sample	122
7.2	E' and E'' (MPa) of PLA, plasticized PLAs, and plasticized composites	130

TABLE		PAGE
7.3	Thermal properties of PLA, plasticized PLAs, and plasticized composites	132
7.4	Summary of the properties of plasticized composite films	138
CHAPTER VIII		
8.1	Material formulations and thickness of each sample	145
8.2	E' and E'' (MPa) of PLA, plasticized PLA, and the composites	151
8.3	Glass transition temperature (T_g), cold crystallization temperature (T_{cc}), melting temperature (T_m), melt crystallization temperature (T_{mc}), cold crystallization enthalpy (ΔH_{cc}), melting enthalpy (ΔH_m), melt crystallization enthalpy (ΔH_{mc}), and crystallinity (χ_c) of PLA, plasticized PLA, and composites	157
8.4	Mechanical properties in machine (MD) and transverse (TD) direction of PLA, plasticized PLA, and composites	160
8.5	Summary of the properties of bagasse fiber/PLA composite films	162
CHAPTER IX		
9.1	Composition of each sample	168
9.2	G' and G'' values at gel point of samples	180

TABLE		PAGE
9.3	Thermal properties of PLA, DCP/PLA, and PLA/DCP/Bis-EMAs pellets	190
9.4	Thermal properties of 0.3D5B sample from compression molding at various condition	193
9.5	Thermo-mechanical properties of PLA, DCP/PLA, and DCP/PLA/Bis-EMAs	197
9.6	Mechanical properties of PLA, 0.3D1B, 0.3D3B, 0.3D5B, 0.3D7B, and 0.5D7B	201

CHAPTER X

10.1	Properties of the PNS/PLA composite with triacetin versus with PEG	206
10.2	Properties of composite films with single plasticizer versus with double plasticizers	207
10.3	The density, decomposition temperature, and aspect ratio of peanut shell and bagasse fiber	207
10.4	Properties of 10PNS10T film versus 10BAG10T film	208
10.5	Properties of mulch films which are PE, PBAT, PLA, PNS/PLA, and bagasse/PLA films	209
10.6	Properties of the sample from biocomposite, plasticization, and chemical crosslinking methods	210

LIST OF FIGURES

FIGURE		PAGE
CHAPTER II		
2.1	Biodegradable mulch films cycle, starting from raising the bed and applying herbicide in spring to harvesting and the disposal of the films in late fall, and associated degradation processes.	6
2.2	Pictures of the white biodegradable films during and after the growing season (Bar length equals 5 cm).	8
2.3	Pictures of the black biodegradable films during and after the growing season (bar length equals 5 cm).	8
2.4	(a) white biodegradable film, (b) black biodegradable film, and (c) control polyethylene film after 5 weeks in contact with soil.	9
2.5	Composite types.	10
2.6	The tortuosity for a diffusing penetrant upon filler in a polymer matrix.	24
2.7	Plasticizer polymer response based on lubricity model.	32
2.8	Gel model of plasticizers.	32
2.9	Free volume model of plasticizers.	33
2.10	Mechanistic model of plasticizers.	34
2.11	TTT cure diagram for unsaturated polyester resin cured with 1.5% of benzoyl peroxide as an initiator.	42

FIGURE		PAGE
2.12	Shear moduli as a function of time during crosslinking reaction.	44
CHAPTER III		
3.1	Morphological image of peanut shell.	48
3.2	FTIR spectrum of peanut shell.	48
3.3	Morphological image of bagasse fibers.	49
3.4	FTIR spectrum of bagasse fiber.	49
3.5	Preparation of peanut shell/PLA composite by using twin-screw extruder.	51
3.6	Dumbbell specimen for tensile testing.	51
3.7	Preparation of peanut shell/PLA composite films by using blown film extrusion.	52
3.8	Preparation of bagasse/PLA composite films by using blown film extrusion.	53
CHAPTER IV		
4.1	TGA and DTG curves of PNS, PLA, and the composites.	66
4.2	DSC thermograms of (a) first heating scan and (b) second heating scan of PLA and the composites.	68
4.3	Morphological images of (a) PNS at 0.4 k magnification, (b) PNS at 15 k magnification, (c) PLA, (d) 30PNS at 1 k magnification, and (e) 30PNS at 5 k magnification.	69
4.4	Stress-Strain curve of PLA and the composites.	71

FIGURE		PAGE
4.5	Temperature dependence of (a) E' , (b) E'' , and (c) $\tan \delta$ of PLA and the composites.	72
4.6	Relationship between weight loss and composting time of PLA and the composites.	75
CHAPTER V		
5.1	TGA and DTG curves of PLA, 30PNS, and plasticized composites.	86
5.2	DSC thermograms of (a) heating scan and (b) cooling scan of PLA, 30PNS, and plasticized composites.	86
5.3	Relationship between weight loss and composting time of PLA, 30PNS, and plasticized composites.	89
5.4	Morphological images of (a) 30PNS, (b) 30P2.5PEG, and (c) 30P12.5PEG.	91
5.5	Stress–Strain curve of PLA, 30PNS, and plasticized composite.	92
5.6	Temperature dependence of (a) E' , (b) E'' , and (c) $\tan \delta$ of PLA, 30PNS, and plasticized composites.	93
CHAPTER VI		
6.1	TGA and DTG curves of PLA, 30PNS, and plasticized composites.	106
6.2	DSC thermograms of (a) heating scan and (b) cooling scan of PLA, 30PNS, and plasticized composites.	107
6.3	Stress–Strain curves of plasticized composites.	109

FIGURE		PAGE
6.4	Temperature dependence of (a) E' , (b) E'' , and (c) $\tan \delta$ of PLA, 30PNS, and plasticized composites.	111
6.5	Relationship between weight loss and composting time of PLA, 30PNS, and plasticized composites.	113
6.6	Morphological images of (a) 30PNS, (b) 30P2.5TRI, (c) 30P7.5TRI, and (d) 30P12.5TRI.	115
6.7	Morphological images of 30P12.5TRI after degradation test: (a) 2.5 k magnification, and (b) 5 k magnification.	116
CHAPTER VII		
7.1	Temperature dependence of (a) E' , (b) E'' , and (c) $\tan \delta$ of PLA and plasticized PLAs.	126
7.2	Temperature dependence of (a) E' , (b) E'' , and (c) $\tan \delta$ of plasticized composites at 5 wt% PNS.	127
7.3	Temperature dependence of (a) E' , (b) E'' , and (c) $\tan \delta$ of plasticized composites at 10 wt% PNS.	128
7.4	Temperature dependence of (a) E' , (b) E'' , and (c) $\tan \delta$ of plasticized composites at 15 wt% PNS.	129
7.5	DSC thermograms of (a) PLA and plasticized PLAs, (b) plasticized composites at 5 wt% PNS, (c) plasticized composites at 10 wt% PNS, and (d) plasticized composites at 15 wt% PNS.	131
7.6	Morphology images of (a) 2.5T, (b) 5T, (c) 7.5T, and (d) 10T.	133
7.7	Morphology images of (a) 15P2.5T and (b) 15P10T.	133

FIGURE		PAGE
7.8	Mechanical properties of PLA, plasticized PLAs, and plasticized composites of (a) tensile strength in MD, (b) tensile strength in TD, (c) Young's modulus in MD, (d) Young's modulus in TD, (e) elongation at break in MD, and (d) elongation at break in TD.	135
7.9	WVP of PLA, plasticized PLAs, and plasticized composites.	136

CHAPTER VIII

8.1	Temperature dependence of (a) E' , (b) E'' , and (c) $\tan \delta$ of PLA, plasticized PLA, and composites.	150
8.2	FTIR spectra of bagasse, PLA, plasticized PLA, and composite films.	152
8.3	TGA and DTG curves of bagasse, PLA, plasticized PLA, and composites.	153
8.4	DSC thermograms of (a) first heating scan, (b) first cooling scan, and (c) second heating scan of PLA, plasticized PLA, and composites.	155
8.5	Morphological images of (a) bagasse, (b) 10BAG, (c) 10BAG10T, and (d) 10BAG10T10G.	158

CHAPTER IX

9.1	Gel fraction of DCP/PLA as a function of DCP content.	173
-----	---	-----

FIGURE		PAGE
9.2	Gel fraction of chemical crosslinked PLA as a function of DCP content of (a) at room temperature and (b) after Soxhlet extraction.	174
9.3	Images of PLA, DCP/PLA, and DCP/PLA/Bis-EMAs pellets.	174
9.4	G' and G'' as a function of time of PLA and DCP/PLA at 150 °C.	175
9.5	G' and G'' as a function of time of 0.1DCP/PLA/Bis-EMAs at 150 °C.	176
9.6	G' and G'' as a function of time of 0.3DCP/PLA/Bis-EMAs at 150 °C.	176
9.7	G' and G'' as a function of time of 0.5DCP/PLA/Bis-EMAs at 150 °C.	177
9.8	Tan δ as a function of time of (a) DCP/PLA, (b) 0.1DCP/PLA/Bis-EMAs, (c) 0.3DCP/PLA/Bis-EMAs, and (d) 0.5DCP/PLA/Bis-EMAs at 150 °C.	177
9.9	G' and G'' as a function of time of 0.3D5B at 150 °C, 155 °C, and 160 °C.	180
9.10	Gel time as a function of DCP content at 150 °C.	181
9.11	Variations of (a) G' and (b) η^* as a function of angular frequency at 190 °C of DCP/PLA.	182
9.12	Variations of (a) G' and (b) η^* as a function of angular frequency at 190 °C of Bis-EMAs/PLA.	183
9.13	Variations of (a) G' and (b) η^* as a function of angular frequency at 190 °C of 0.1DCP/PLA/Bis-EMAs.	183

FIGURE		PAGE
9.14	Variations of (a) G' and (b) η^* as a function of angular frequency at 190 °C of 0.3DCP/PLA/Bis-EMAs.	184
9.15	Variations of (a) G' and (b) η^* as a function of angular frequency at 190 °C of 0.5DCP/PLA/Bis-EMAs.	185
9.16	cole-cole plot at 190 °C of (a) DCP/PLA, (b) 0.1DCP/PLA/Bis-EMAs, (c) 0.3DCP/PLA/Bis-EMAs, and (d) 0.5DCP/PLA/Bis-EMAs.	186
9.17	TGA thermograms of (a) DCP/PLA, (b) 0.1DCP/PLA/Bis-EMAs, (c) 0.3DCP/PLA/Bis-EMAs, and (d) 0.5DCP/PLA/Bis-EMAs.	187
9.18	DSC thermograms of (a) DCP/PLA, (b) 0.1DCP/PLA/Bis-EMAs, (c) 0.3DCP/PLA/Bis-EMAs, and (d) 0.5DCP/PLA/Bis-EMAs pellets.	188
9.19	The plot of T_g of 0.3D5B sample from compression molding at various temperature and time.	191
9.20	DSC thermograms of 0.3D5B sample of (a) 180 °C, (b) 190 °C, and (c) 200 °C.	192
9.21	Temperature dependence of (a) E' and $\tan \delta$, and (b) E'' of PLA and DCP/PLA.	194
9.22	Temperature dependence of (a) E' and $\tan \delta$, and (b) E'' of 0.1DCP/PLA/Bis-EMAs content.	195
9.23	Temperature dependence of (a) E' and $\tan \delta$, and (b) E'' of 0.3DCP/PLA/Bis-EMAs.	195
9.24	Temperature dependence of (a) E' and $\tan \delta$, and (b) E'' of 0.5DCP/PLA/Bis-EMAs content.	196

FIGURE		PAGE
9.25	Morphological images of (a) PLA, (b) 0.1D1B, (c) 0.1D5B, (d) 0.3D1B, (e) 0.3D5B, (f) 0.5D1B, and (g) 0.5D5B.	198
9.26	Stress–strain curves of PLA, 0.3D1B, 0.3D3B, 0.3D5B, 0.3D7B, and 0.5D7B samples	200

LISTS OF SCHEMES

SCHEME		PAGE
CHAPTER II		
2.1	PLA chemical structure.	15
2.2	Reaction schemes to produce PLA.	15
2.3	Hydrolysis of the ester linkages of PLA.	16
2.4	Structures of (a) Cellulose and (b) Lignin.	20
2.5	Structural formulae of multifunctional crosslinking agents.	39
2.6	Structural of Bis-EMAs.	40
2.7	One possibility of reaction scheme for chemical crosslinking of TAIC between two PLA molecules.	45
CHAPTER IX		
9.1	Formations of chain scission and crosslinking structure of PLA in the presence of DCP.	171
9.2	The possibility of chemical crosslinking between Bis-EMAs and PLA.	172

CHAPTER I

INTRODUCTION

Plant cultivation and crop protection are a critical issue in agriculture. The consumption of plastic mulch films, in agriculture poses a major environmental problem due to high molecular weight and hydrophobic properties of non-degradable plastics, such as polyethylene (PE) film. This lends the plastic mulch films high chemical stability, requiring about 100 years for its complete decomposition (Bilck, Grossmann et al. 2010). This is because plastic mulch films have been used increasingly by farmers to cultivate and protect crops. The requirement properties of mulch films are opacity (for weed control), weathering resistance appropriate to the service life, control soil temperature, limit soil erosion, and reduce water consumption. For example, the properties of PE mulch film have tensile strength ~25.8 MPa, elongation at break ~336.0 %, Young's modulus ~40.1 MPa, and water vapor permeability $\sim 0.01049 \times 10^{-6}$ g/m.Pa.day. The disadvantage of PE mulch films is not typically recycled, since they are often soiled and wet. Therefore, all of them end up in the landfill. Biodegradable mulch films offer one way of reducing the source of environmental pollution. It can be disposed directly into the soil or into a composting system at the end of their lifetime. Residual breakdown products of biodegradable mulch film after the cultivation period should not be toxic or persist in the environment, and should be completely mineralized into carbon dioxide or methane, water and biomass by means of soil micro-organisms in a reasonable time frame (Scarascia-Mugnozza, Schettini et al. 2006).

Polylactic acid or PLA is a biodegradable plastic, derived from renewable resources such as corn, starch, tapioca products, and sugarcane. Although PLA exhibited its advantages including processability, biocompatibility, biodegradability, and mechanical properties over other conventional materials (Suryanegara, Nakagaito et al. 2009). Those advantages of PLA are an interesting to choose for fabricating mulch film in this research. Nonetheless, the most important factors that prevent PLA from being commercially and widely used are its brittleness, high cost, and low thermal stability compared to commercial plastics such as PE (Hemvichian, Nagasawa et al. 2009). And the degradation rate of PLA is slow depending on the

environmental conditions and thickness of materials. From a structural point of view, this work focuses on three techniques, compounding (biocomposite), plasticization, and chemical crosslinking, as proposed solutions to overcome the aforementioned shortcomings associated with PLA.

Compounding is one of the most convenient and practical techniques used to modify properties and expand applications of PLA. Compounding PLA with natural fiber, as called “biocomposite or green composite”, has been proposed to reduce cost and improve both tensile strength and Young’s modulus of PLA. Natural fibers provide reinforcement properties at low cost, low density, high strength, and stiffness (Tao, Yan et al. 2009). Moreover, the addition of natural fiber into PLA enhanced the biodegradation of PLA–composites. Commonly, composites of PLA reinforced with natural fibers include cotton, hemp, kenaf, flax, and ramie have been prepared and studied (Graupner, Herrmann et al. 2009). Surprisingly, there is no literature examining the used of peanut shell and bagasse fiber as reinforcement PLA–composites. They are a substantial and low–priced agricultural by–product that is normally discarded and incinerated. In addition, peanut shell provides nitrogen (~2.63%) which is a good source of fertilizer for the crop production. This result agrees with other research, they found that fertilizer nutrient from peanut shell are nitrogen (1.19%), phosphorus (0.10%), and potassium (0.51%) (Verasan, Sae-jiew et al. 2014). And bagasse fiber played an important role in widespread engineering applications due to a good reinforcement. Thus the fabrications of mulch films from peanut shell/PLA and bagasse fiber/PLA composites are interesting.

The flexibility of PLA must be improved for the requirement of mulch film properties. Therefore, plasticization is the one method which commonly added to promote flexibility and processability. Previous researcher studied on plasticized PLA with various low molecular weight plasticizers such as citrate esters, triacetin, polyethylene glycol, glycerol, and partial fatty acid esters were aimed at modifying its inherent brittle behavior (Li and Huneault 2007). The choice of plasticizer used as a modifier for PLA has to be biodegradable, non–toxic, and non–volatile, with a relatively low molecular weight to produce the desired increase of the toughness value. Typically, amounts ranging from 10 %wt to 20 %wt of plasticizers are required to provide both a substantial reduction of glass transition temperature and

adequate mechanical properties. The addition of plasticizer over 20-30% (depending on plasticizer) into PLA leads to a phase separation. The plasticization is thus limited by the amount of plasticizer to be blended with PLA. The additions of plasticizer shows increase crystallization rate and elongation at break while decrease glass transition temperature and modulus. The best plasticizer for PLA is a triacetin because it has a solubility parameter in relation with PLA ($\delta = 21.42 \text{ MPa}^{1/2}$), resulting in a good compatibility between PLA and triacetin (Murariu, Ferreira et al. 2008). Polyethylene glycol (PEG) shows improvement in crystallization process of PLA (Byun, Kim et al. 2010). In the case of glycerol, it improves processibility while it does not affect glass transition temperature of PLA (Martin and Averous 2001). Thus triacetin, PEG, and glycerol are considered to choose for plasticizing PLA in this research.

Moreover, the thermal stability of PLA must be improved. Many techniques use to enhance this property of PLA, which are polymerization, graft copolymerization, and chain extender (Ogliaria, Ely et al. 2008, Yang, Wu et al. 2008). These techniques provide a high molecular weight PLA. Hence PLA has high molecular weight; it can be enhanced thermal stability. Chemical crosslinking is another technique utilized to improve thermal stability of PLA. This technique provides the network structure of PLA (Yang, Wu et al. 2008). The network structure can be retarded chain mobility and also increased thermal stability of PLA. This technique is economically advantageous because it was carried out in the melt state via extrusion process with only low amounts of crosslinking agent and no extra purification step and special apparatus were necessary.

The purpose of this research was to prepare PLA filled with natural fiber together with plasticizers as the composites by the melt mixing. The effects of natural fiber and plasticizer on mechanical, thermal, thermo-mechanical, morphological, and biodegradable properties were investigated. As a consequently, the composite films were fabricated by blown film extrusion. The composite films were determined barrier properties and discussed for processing and application as a mulch film. In addition, PLA have been further induced crosslinking structure via extrusion, aiming at studying thermal and rheological properties.

CHAPTER II

LITERATURE REVIEW

2.1 Mulch Film

Mulch film is loose film laid at ground level around crops to control soil temperature, limit soil erosion, reduce water consumption, deliver nutrients, and suppress weeds. Mulch films are generally made from LDPE, LLDPE or a blend and vary in thickness from 10 to 80 microns depending on the crop and the required service life (Cabot Corporation 2008). They are mainly transparent or black, but can also be white, black/white or colored (mainly to attract or repel certain insects). The lifetime of an agricultural mulch film varies considerably (e.g., months to years) depending on its application and the environmental conditions (Finkenstadta and Tisserat 2010).

Table 2.1 Plastic mulch film can be divided into 3 main categories

Standard	Premium	Special
- 30 – 40 microns	- 60 – 80 microns	- 15 – 50 microns
- one season service life	- up to 5 year's service life	- up to 3 year's service life
- fruit and vegetables	- vines and amenity plants	- specialist crops or for extended life

For black, white and black/white mulch films, the key performance requirements are opacity (for weed control), weathering resistance appropriate to the service life, and mechanical properties. The properties of the mulch film are shown in Table 2.2.

Table 2.2 Properties of mulch film: Agroplás® from Electro Plastic, Brazil (Bilck, Grossmann *et al.* 2010)

Film properties	Nominal value (SI)			Test method
	polyethylene film	black biodegradable film	White biodegradable film	
Film thickness (μm)	25.0 \pm 1.0	218.0 \pm 22.0	123.0 \pm 12.0	-
Young's modulus (MPa)	10.9 \pm 0.4	40.1 \pm 5.8	48.6 \pm 4.0	ASTM D822
Tensile strength (MPa)	25.8 \pm 8.4	6.1 \pm 1.6	8.4 \pm 1.1	ASTM D822
Elongation at break (%)	336.0 \pm 159.0	530.0 \pm 102.0	537.0 \pm 89.0	ASTM D822
Water vapor permeability ($\times 10^{-6}$) (g/m.Pa.day)	0.01049 \pm 0.0012	2.5 \pm 0.11	2.29 \pm 0.46	ASTM E96-01

As the use of plastic mulch film continues to increase in the agricultural industry, there are several major concerns about using mulch films which are the costs of removal and disposal of the used plastics and environmental issues. Most of the used mulch films are not typically recycled, since they are often soiled and wet, which make them difficult to recycle; therefore, mostly all of them end up in the landfill. To solve these problems, the use of biodegradable mulch films seems to be a promising solution because the films can degrade right in the field; therefore, the costs of removal and disposal will disappear, and the amount of waste ending up in landfills can be avoided (Garthe and Kowal 1993, Kijchavengkul, Auras *et al.* 2008).

2.1.1 Biodegradable Mulch Films

There are two main degradation mechanisms which may be considered for biodegradable mulch films:

2.1.1.1 *Photodegradation*

Photodegradation is the degradation process due to the exposure of films to certain amount of solar radiation. As a consequence of this exposure, the films become more brittle, with cracks, tears, holes, occurring before finally disintegrating into small flakes.

2.1.1.2 Biodegradation

Biodegradation, however, is a degradation process resulting from the action of naturally occurring microorganisms such as bacteria, fungi, and algae.

Appropriate degradation mechanisms must be triggered for biodegradable mulch films to work.

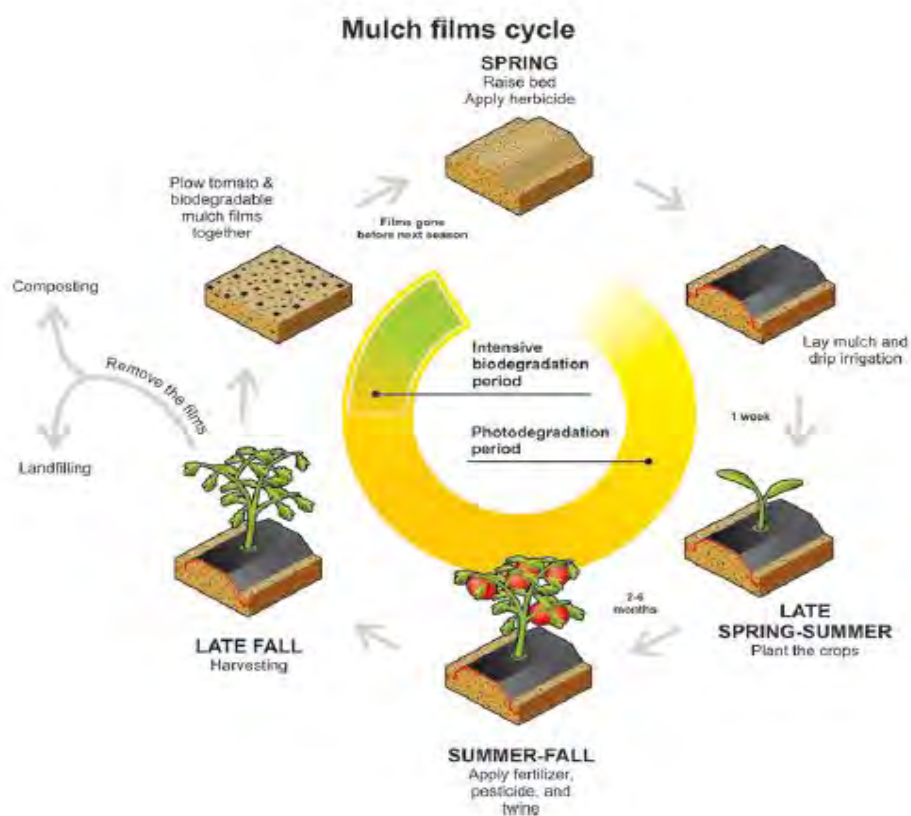


Figure 2.1 Biodegradable mulch films cycle, starting from raising the bed and applying herbicide in spring to harvesting and the disposal of the films in late fall, and associated degradation processes (Kijchavengkul, Auras *et al.* 2008)..

According to Figure 2.1, in the photodegradation period, factors affecting the photodegradation rate are categorized as: (1) formulation and quality of the film, (2) season, (3) geographical region, (4) amount of solar radiation and day length, (5) cloud cover, and (6) sun angle. In the biodegradation period, factors affecting biodegradation rate are categorized as: (1) the exposure conditions, including moisture, pH, temperature, and aerobic or anaerobic conditions of the soil, and (2) the polymer characteristic, such as polymer structure and chain flexibility, crystallinity, molecular weight, copolymer composition, thickness, size, and shape of the exposed film (Kijchavengkul, Auras *et al.* 2008).

Kijchavengkul *et al.* (2008) studied the use of new biodegradable films in agriculture under open field conditions. Three biodegradable mulch films made from modified biodegradable polyester of different thicknesses and colors (black and white) and a conventional low density polyethylene (LDPE) mulch film were used to cover the beds of tomato plants. Changes in physical appearance of the films were recorded as well as changes in their mechanical, optical, and physical properties. Once tomato harvest was completed, the conventional LDPE mulch film was removed and all the tomato plants were cut using a mower. The biodegradable mulch films were plowed into the soil. After the biodegradable films photodegraded, crosslink formation occurred within the films which promoted brittleness. Titanium dioxide, an additive used to produce white color in the films, catalyzed the photodegradation, while carbon black used for black color stabilized the photodegradation. In the Figure 2.2, the white films started to degrade after two weeks while it took about eight weeks for the black films to significantly degrade. Figure 2.3 showed that the black biodegradable film seems to be a more promising alternative as a mulch film because of the comparable yields and weed suppression ability to conventional mulch film.



Figure 2.2 Pictures of the white biodegradable films during and after the growing season (Bar length equals 5 cm).



Figure 2.3 Pictures of the black biodegradable films during and after the growing season (bar length equals 5 cm).

Victoria *et al.* (2010) reported the successful preparation of Osage orange wood fiber (OO)/PLA composite for use in agricultural mulch film. The PLA/OO mechanical properties were comparable to existing mulch film products and had the advantage of being completely biodegradable through a single growing season. The mechanical properties of PLA–OO composites were evaluated in dry and wet conditions. Higher concentration and larger particle sizes of OO generally had a greater effect on the mechanical properties especially the modulus. Crystallinity of the PLA was significantly higher at 25% OO fill corresponding to a smaller continuous polymer phase. Moreover, PLA–OO mulch films will provide

weed barrier and control soil erosion, as well as allowing the controlled release of the OO phytochemical components for additional protection.

Bilck *et al.* (2010) (Bilck, Grossmann *et al.* 2010) reported develop black and white biodegradable films by extrusion from cassava starch and poly(butylene adipate-co-terephthalate) (PBAT) blends to use as mulching film in strawberry production. In the Figure 2.4, the white and black biodegradable film started to present cracks after five weeks on the ground. No changes were observed in the control polyethylene film. White film showed cracks as early as in the first two weeks, and black film, after eight weeks. Moreover, weed growth was observed in beds covered with white film due to its transparency. The PBAT film showed small cracks in the structure five weeks after being laid onto the ground and, eight weeks afterwards, the maximum tensile strength, elongation at break and water sorption were reduced due to variations in temperature, humidity and solar radiation, which led to its biodegradation, crosslinking and photo- and biodegradation. However, these changes in the film structure did not influence the quality and amount of the fresh produce.



Figure 2.4 (a) white biodegradable film, (b) black biodegradable film, and (c) control polyethylene film after 5 weeks in contact with soil.

2.2 Polymer Matrix Composite (PMC)

Polymer matrix composites (PMCs) are comprised of a variety of short or continuous fibers bound together by a polymer matrix. The PMC is designed so that the mechanical loads to which the structure is subjected in service are supported by

the reinforcement. The function of the matrix is to bond the fibers together and to transfer loads between them. The reinforcement may consist of particles, whiskers, fibers, or fabrics, as shown in Figure 2.5.

PMCs are often divided into two categories: reinforced plastics, and advanced composites. The distinction is based on the level of mechanical properties (usually strength and stiffness); however, there is no unambiguous line separating the two. Reinforced plastic are relatively inexpensive. Advanced composites have been in use for only about 15 years, primarily in the aerospace industry, have superior strength and stiffness, and are relatively expensive.

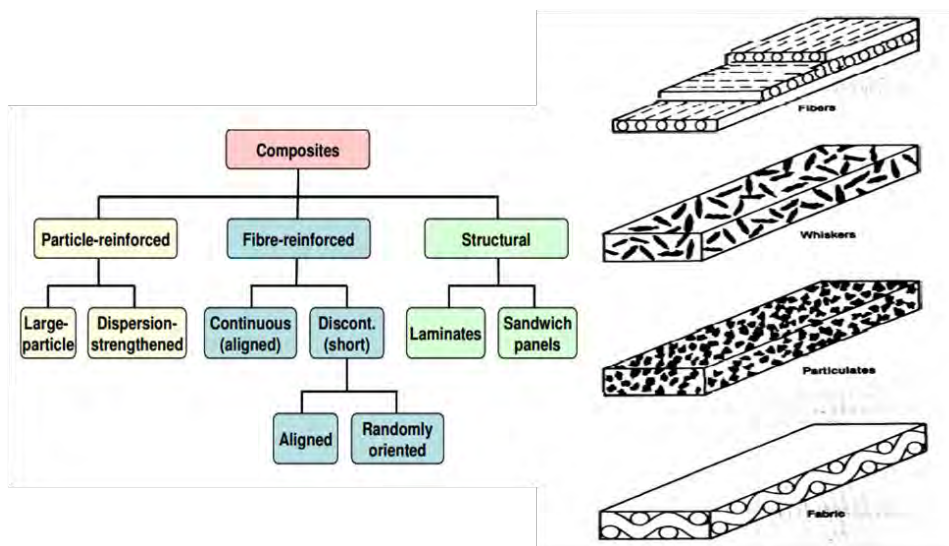


Figure 2.5 Composite types.

The properties of PMC depend on matrix, reinforcement, and interphase. Consequently, there are many variables to consider when designing a PMC. These include not only the types of matrix and reinforcement but also their relative proportions, geometry of reinforcement, and nature of interphase. Each of these variables must be carefully controlled to produce a structural material optimized for the conditions for which it is to be used.

The use of continuous-fiber reinforcement confers a directional character, called an isotropy, to the properties of PMCs. PMCs are the strongest when stressed parallel to direction of fibers (0° , axial, or longitudinal direction) and the weakest

when stressed perpendicular to fibers (90°, transverse direction). In practice, most structures are subjected to complex loads, necessitating the use of fibers oriented in several directions (e.g., 0°, ± 45°, 90°).

When discontinuous fibers or particles are used for reinforcement, the properties tend to be more isotropic because these reinforcements tend to be randomly oriented (Design).

The modified rule of mixture is often used to predict the tensile strength of PMC by assuming a perfect interfacial bond between fibers and matrix. The formula of the modified rule of mixtures is given by:

$$\sigma_{cu} = \chi_1 \chi_2 V_f \sigma_{fu} + V_m \sigma_m \quad (2.1)$$

Where χ_1 and χ_2 are fiber orientation and fiber length factors, respectively. The product of χ_1 and χ_2 , i.e. $\chi_1 \chi_2$, is a fiber efficiency factor for the strength of the composite. σ_{cu} and σ_{fu} are ultimate strength of the composite and fiber, respectively; V_f and V_m denote volume fraction of fiber and matrix; and σ_m is matrix stress at the failure of the composite (Fu and Lauke 1996).

2.2.1 For Particulate Composites

The addition of particles to a polymer can effectively enhance the stiffness of polymer matrix. The upper bound of elastic modulus of a particulate composite can be predicted by:

$$E_{c1} = E_p V_p + E_m (1 - V_p) \quad (2.2)$$

Where E_{c1} is the modulus of particulate composite, E_p is the modulus of particles, E_m is the modulus of polymer matrix, and V_p is the particle volume fraction. And a lower bound of the elastic modulus of particulate composite can be predicted by:

$$E_{c1} = E_p E_m / [E_p (1 - V_p) + E_m V_p] \quad (2.3)$$

The real value of the elastic modulus of particulate composite falls between the predicted values by Eqs. (2.2) and (2.3).

For simplicity and without loss of accuracy, an approximate method, i.e. the modified rule of mixtures can be used to predict the elastic modulus of particulate composites.

$$E_{cl} = \chi_p E_p V_p + E_m (1 - V_p) \quad (2.4)$$

Where χ_p is particle reinforcing factor for the modulus of particulate composite (value between 0 and 1).

2.2.2 For Short Fiber Composites

For aligned short fiber composites, the longitudinal modulus, E_{ll} , depends on fiber aspect ratio, $L/(2r_f)$ in which L is fiber length and r_f is radius of fiber. Based on Cox's shear-lag model, E_{ll} , is given by:

$$E_{ll} = E_f \left[1 - \frac{\tanh(\beta L / 2)}{\beta L / 2} \right] V_f + E_m (1 - V_f) \quad (2.5)$$

Where V_f is fiber volume fraction and E_f is elastic modulus of fiber. β is given by:

$$\beta = \left[\frac{2G_m}{E_f r_f^2 \ln(R / r_f)} \right]^{1/2} \quad (2.6)$$

Where G_m is shear modulus of matrix and R is mean separation of fibers normal to their length.

For a hexagonal fiber packing arrangement,

$$\ln \frac{R}{r_f} = \frac{1}{2} \ln \left(\frac{2\pi}{\sqrt{3}V_f} \right) \quad (2.7)$$

For a square packing arrangement,

$$\ln \frac{R}{r_f} = \frac{1}{2} \ln \left(\frac{\pi}{V_f} \right) \quad (2.8)$$

The transverse modulus and the in-plane shear modulus, E_{22} and G_{12} , are given below:

$$E_{22} = E_m (1 + 2\eta_1 V_f) / (1 - \eta_1 V_f) \quad (2.9)$$

$$G_{12} = G_m (1 + \eta_2 V_f) / (1 - \eta_2 V_f) \quad (2.10)$$

Where

$$\eta_1 = (E_f / E_m - 1) / (E_f / E_m + 2) \quad (2.11)$$

$$\eta_2 = (G_f / G_m - 1) / (G_f / G_m + 1) \quad (2.12)$$

Where G_f is shear modulus of fibers (Fu, Xu et al. 2002).

2.2.3 Biocomposite or Green Composite

Biocomposites (biodegradable composites) consist of biodegradable polymers as the matrix material and biodegradable fillers, usually biofibers (e.g. lignocelluloses fibers). Since both components are biodegradable, the composite as the integral part is also expected to be biodegradable (Averousa and Boquillon 2004).

2.2.3.1 *Biodegradable Polymers: Sources and Classification*

Biodegradable polymers can be classified in four categories depending on the synthesis and on the sources:

- Polymers from biomass such as the agro-polymers from agro-resources;

- (I) Polysaccharides, e.g., starches (wheat, potatoes, maize) ligno-cellulosic products (wood, straws) and others (pectins, chitosan/chitin, gums).
- (II) Protein and lipids, e.g., animals (casein, whey, collagen/gelatin), and plants (zein, soya, and gluten).
- Polymers obtained by microbial production, e.g., polyhydroxyalkanoates (PHA) such as poly(hydroxybutyrate) (PHB) and poly(hydroxybutyrate cohydroxyvalerate (PHBv).
- Polymers chemically synthesized using monomers obtained from agro-resources, e.g., poly(lactic acid) (PLA)
- Polymers whose monomers and polymers are both obtained by chemical synthesis from fossil resources, e.g., polycaprolactones (PCL), polyesteramides (PEA), aliphatic co-polyesters (PBSA) and aromatic co-polyesters (PBAT).

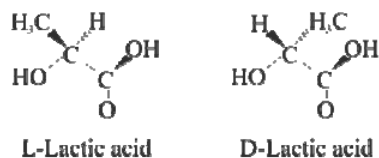
2.2.3.2 *Poly(lactic Acid)*

Poly(lactic acid) or polylactide (PLA) is a thermoplastic aliphatic polyester derived from renewable resources, such as corn starch, tapioca products or sugarcane. The fermentation of those renewable resources is produced lactic acid. The PLA chemical structure (Scheme 2.1) significantly depends on the way the technological process of polymerization of a monomer, i.e., lactide (LA), was performed. Scheme 2.2 shows the reaction to produce PLA. As a result, different forms of PLA may be obtained. These are as follows:

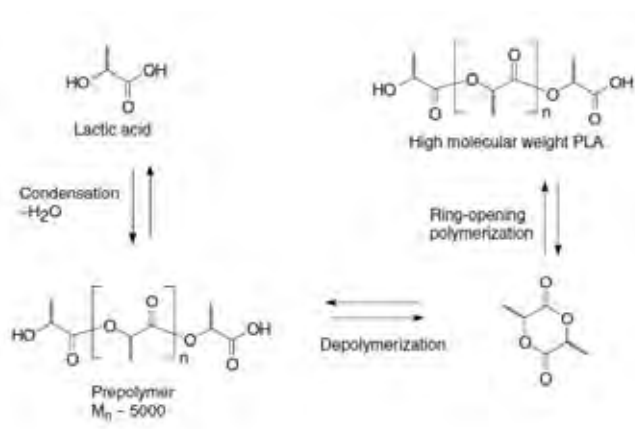
L(+)-PLA, where each monomeric unit of a PLA macromolecule shows a specific rotation L.

D(-)-PLA, where each monomeric unit of a PLA macromolecule shows a specific rotation D

L,D PLA, where monomeric units of a PLA macromolecule show both specific rotations (either L or D).



Scheme 2.1 PLA chemical structure.



Scheme 2.2 Reaction schemes to produce PLA.

2.2.3.3 PLA Physical Properties

The physical characteristics of high molecular weight PLA are to a great extent dependent on its transition temperatures for common qualities such as density, heat capacity, mechanical, and rheological properties. In the solid state, PLA can be either amorphous or semicrystalline, depending on the stereochemistry and thermal history. For amorphous PLA, the glass transition (T_g) determines the upper use temperature for most commercial applications. For semicrystalline PLA, both the T_g ($\sim 58^\circ\text{C}$) and melting point (T_m), $130\text{-}230^\circ\text{C}$ (depending on structure) are important for determining the use temperatures across various applications. Both of these transitions, T_g and T_m , are strongly affected by overall optical composition, primary structure, thermal history, and molecular weight. Above T_g amorphous PLA transition from glassy to rubbery and will behave as a viscous fluid upon further heating. Below T_g , PLA behaves as a glass with the ability to creep until cooled to its

accelerated by acids or bases and is dependent on moisture content and temperature. Article dimensions, crystallinity, and blends will affect the rate of degradation. PLA products rapidly degrade in both aerobic and anaerobic composting conditions.

2.2.3.5 Applications and Performance

Since PLA is an environmentally friendly polymer that can be designed to controllably biodegrade, it is ideally suited for many applications in the environment where recovery of the product is not practical, such as agricultural mulch films and bags. Composting of post-consumer PLA items is also a viable solution for many PLA products. However, the large growth seen for PLA in many applications does not depend upon the biodegradability of the material.

PLA resins can be tailor-made for different fabrication processes, including injection molding, sheet extrusion, blow molding, thermoforming, film forming, or fiber spinning. The key is controlling certain molecular parameters in the process such as branching, D-isomer content, and molecular weight distribution. The ability to selectively incorporate L-, D-, or meso-lactide stereoisomers into the polymer backbone allows PLA to be tailored for specific applications. The ease of incorporation of various defects into PLA allows for control of both crystallization rate and ultimate crystallinity.

Films are the second largest application area for PLA. Again, the ability to modify the crystallization kinetics and physical properties for a broad range of applications by D- or meso-comonomer incorporation, branching, and molecular weight change makes PLA extremely versatile. Films are transparent when stress crystallized and have acceptance by customers for food contact. PLA films can be prepared by the blown double bubble technology or preferably, cast-tempering. Cast-tempered films have very low haze, excellent gloss, and gas (O₂, CO₂, and H₂O) transmission rates desirable for consumer food packaging. PLA films also have superior dead fold or twist retention for twist wrap packaging (Henton, Gruber *et al.* 2005).

Tsuji *et al.* (1999) studied films of 1:1 blend and films non-blended were prepared from poly(L-lactic acid) (PLLA) and poly(D-lactic acid) (PDLA) with a solution casting method. The result showed the T_g of blend films is 58 °C higher than that for non-blended films with M_w in the range 5x10⁴-1x10⁵,

where predominant stereocomplexation occurs in the blend films. Moreover, T_m of stereocomplex crystallites of blend films has a maximum at M_w of around 1×10^5 , while T_m of homo-crystallites monotonously increases with the increasing M_w . This suggests that the crystalline thickness of the stereocomplex crystallites in blend films becomes the highest at M_w of around 1×10^5 . The enthalpy of melting for stereocomplex crystallites in 1:1 blend films was higher than that of homo-crystallites when M_w of polymers was below 2×10^5 , while this relationship was reversed when M_w increased to 1×10^6 .

Anderson *et al.* (2006) studied melt blending procedure was developed for the preparation of PLLA/PDLA stereocomplex crystallites dispersed in a PLLA matrix. The result showed the T_m of the PLLA homopolymer is present around $173.8 \text{ }^\circ\text{C}$, while the stereocomplex T_m , around $215.8 \text{ }^\circ\text{C}$. The area of the melting endotherm for the stereocomplex decreased as the amount of PDLA in the blend decreased showing that the initial composition of the blend can be used to control the amount of stereocomplex in the final material. The blends with the intermediate molecular weight, 3 wt% of the 14 kg mol/K PDLA, stood out as having the highest nucleation efficiencies and smallest half-time values, indicating that there may be an optimum molecular weight of the PDLA for stereocomplex nucleating agents. All of the blends containing the stereocomplex showed more significant improvements in the crystallization rate of PLLA compared to talc.

Yokohara *et al.* (2008) studied structure and properties for binary blends composed of PLA and poly(butylene succinate) (PBS) by an internal batch mixer. It found that PLA and PBS are immiscible in the molten state and the blends exhibit phase-separated structure. The addition of PBS enhances the crystallization of PLA because PBS droplets act as crystallization nuclei. In addition, the enhancement of the storage modulus due to the cold crystallization of PLA is shifted to lower temperature by blending PBS. This phenomenon indicates that PBS accelerates cold crystallization of PLA.

Ren *et al.* (2009) studied biodegradable binary and ternary blends of thermoplastic starch (TPS), PLA, and poly(butylene adipateco-terephthalate) (PBAT) give excellent properties when small amount of compatibilizer (anhydride functionalized polyester) is added. It showed that as PBAT content

increased, the value of the storage modulus (E') of the blends decreased, which indicated that the blends with less PBAT content were more elastic than those with more PBAT content. The T_g showed a slight decrease with increasing PBAT content. In addition, the vicat softening temperature (VST) increased with the PBAT content. It is because PBAT has higher VST than PLA.

Chang *et al.* (2011) studied the effects of poly(3-hydroxybutyrate) (PHB) on crystalline morphology of stereocomplex capacity of PLLA and PDLA were prepared using solvent-mixing, followed with film-casting. The neat stereocomplexed PLA (sc-PLA) exhibited T_g around 40 °C, and T_m at about 221 °C. The PHB/sc-PLA blend showed crystallization growth of sc-PLA in blends is hindered by presence of PHB and final morphology of the sc-PLA complexes is altered. The less perfect lamellae of sc-PLA formed in blends induced by the increase of PHB content in blends or higher T_c . In addition, the sc-PLA in blends melt-crystallized at 170 °C, show coexistence of feather-like and wedge-like spherulites. The concentration and/or distribution of the PHB (amorphous diluents) at the crystal growth front corresponding to variation of the slopes of spherulitic growth rates is a factor which results in the different orientation of sc-PLA lamellae in blends.

2.3 Biodegradable Filler: Natural Fiber

2.3.1 Fiber Source

The plants, which produce natural fibers, are classified as primary and secondary depending on their utilization. Primary plants are those grown for their fiber content while secondary plants are plants in which the fibers are produced as a by-product. Jute, hemp, kenaf, and sisal are examples of primary plants. Pineapple, oil palm and coir are examples of secondary plants.

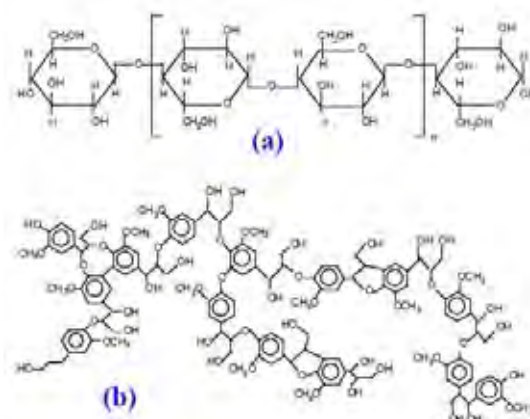
2.3.2 Fiber Types

There are six basic types of natural fibers. They are classified as follows: bast fibers (jute, flax, hemp, ramie and kenaf), leaf fibers (abaca, sisal and

pineapple), seed fibers (coir, cotton and kapok), core fibers (kenaf, hemp and jute), grass and reed fibers (wheat, corn and rice) and all other types (wood and roots).

2.3.3 Structure and Chemical Composition

Climatic conditions, age and the degradation process influence not only the structure of fibers, but also the chemical composition. The major chemical component of a living tree is water. However, on dry basis, all plant cell walls consist mainly of sugar based polymers (cellulose, hemicellulose) that are combined with lignin with lesser amount of extractives, protein, starch and inorganics. The chemical components are distributed throughout the cell wall, which is composed of primary and secondary wall layers. The chemical composition varies from plant to plant, and within different parts of the same plant. Moreover, All the natural reinforcing fibers are lingo-cellulosic in nature the principal component being cellulose and lignin (Scheme 2.4). The contents of cellulose and lignin vary from each bio-fiber to another. Table 2.3 shows the range of the average chemical constituents for a wide variety of plant types.



Scheme 2.4 Structures of (a) Cellulose and (b) Lignin.

Table 2.3 Chemical composition of some common natural fibers

Fiber	Cellulose (wt%)	Hemicellulose (wt%)	Lignin (wt%)	Waxes (wt%)
Bagasse	55.2	16.8	25.3	–
Bamboo	26–43	30	21–31	–
Flax	71	18.6–20.6	2.2	1.5
Kenaf	72	20.3	9	–
Jute	61–71	14–20	12–13	0.5
Hemp	68	15	10	0.8
Ramie	68.6–76.2	13–16	0.6–0.7	0.3
Abaca	56–63	20–25	7–9	3
Sisal	65	12	9.9	2
Coir	32–43	0.15–0.25	40–45	–
Oil palm	65	–	29	–
Pineapple	81	–	12.7	–
Curaua	73.6	9.9	7.5	–
Wheat straw	38–45	15–31	12–20	–
Rice husk	35–45	19–25	20	14–17
Rice straw	41–57	33	8–19	8–38

2.3.4 Properties of Natural Fibers

The properties of natural fibers differ among cited works, because different fibers were used, different moisture conditions were present, and different testing methods were employed. The natural fiber reinforced polymer composites performance depends on several factors, including fibers chemical composition, cell dimensions, microfibrillar angle, defects, structure, physical properties, and mechanical properties, and also the interaction of a fiber with the polymer. In order to expand the use of natural fibers for composites and improved their performance, it is essential to know the fiber characteristics. Mechanical properties of natural fibers can be influenced by many factors. Such as either fiber bundles or ultimate fiber is being tested. Table 2.4 presents the important physico-mechanical properties of commonly used natural fibers.

Table 2.4 Physico–mechanical properties of natural fibers

Fiber	Tensile strength (MPa)	Young's modulus (GPa)	Elongation at break (%)	Density [g/cm ³]
Abaca	400	12	3–10	1.5
Bagasse	290	17	–	1.25
Bamboo	140–230	11–17	–	0.6–1.1
Flax	345–1035	27.6	2.7–3.2	1.5
Hemp	690	70	1.6	1.48
Jute	393–773	26.5	1.5–1.8	1.3
Kenaf	930	53	1.6	–
Sisal	511–635	9.4–22	2.0–2.5	1.5
Ramie	560	24.5	2.5	1.5
Oil palm	248	3.2	25	0.7–1.55
Pineapple	400–627	1.44	14.5	0.8–1.6
Coir	175	4–6	30	1.2
Curaua	500–1150	11.8	3.7–4.3	1.4

2.3.4.1 Reinforcement Properties in a Composite Material

The role of the reinforcement in a composite material is fundamentally one of increasing the mechanical properties of the neat resin system. All of the different fibers used in composites have different properties and so affect the properties of the composite in different ways.

However, individual fibers or fiber bundles can only be used on their own in a few processes such as filament winding. For most other applications, the fibers need to be arranged into some form of sheet, known as a fabric, to make handling possible. Different ways for assembling fibers into sheets and the variety of fiber orientations possible lead to there being many different types of fabrics, each of which has its own characteristics. The mechanical properties of the reinforcing fibers are considerably higher than those of un–reinforced resin systems. The mechanical properties of the fiber/resin composite are dominated by the contribution of fiber to the composite. The four main factors that govern the fiber's contribution are:

1. The basic mechanical properties of the fiber itself.
2. The surface interaction of fiber and resin (the interface).
3. The amount of fiber in the composite (Fiber Volume Fraction).
4. The orientation of the fibers in the composite.

The surface interaction of fiber and resin is controlled by the degree of bonding that exists between the two. This is heavily influenced by the treatment given to the fiber surface.

Basic Properties of Fibers and Other Materials: The manufacturing process used largely governs the amount of fiber in the composite. However, reinforcing fabrics with closely packed fibers will give higher Fiber Volume Fractions (FVF) in a laminate than will those fabrics which are made with coarser fibers, or which have large gaps between the fiber bundles. Fiber diameter is an important factor here with the more expensive smaller diameter fibers providing higher fiber surface areas, spreading the fiber/matrix interfacial loads. As a general rule, the stiffness and strength of a laminate will increase in proportion to the amount of fiber present. However, above about 60-70% FVF (depending on the way in which the fibers pack together) although tensile stiffness may continue to increase, the laminate's strength will reach a peak and then begin to decrease due to the lack of sufficient resin to hold the fibers together properly.

Finally, since reinforcing fibers are designed to be loaded along their length, and not across their width, the orientation of the fibers creates highly direction-specific properties in the composite. This anisotropic feature of composites can be used to good advantage in designs, with the majority of fibers being placed along the orientation of the main load paths. This minimizes the amount of parasitic material that is put in orientations where there is little or no load (Gurit(UK) Jun 11, 2013).

Knowledge about fiber length and width is important for comparing different kinds of natural fibers. A high aspect ratio (length/width) is very important in cellulose based fiber composites as it give an indication of possible strength properties. The fiber strength can be an important factor in selecting a specific natural fiber for a specific application. Changes in the physical properties can be due to differences in fiber morphology. Major differences in structure such as density, cell wall thickness, length and diameter result in differences in physical properties (Faruk, Bledzki *et al.* 2012).

2.3.4.2 Barrier Properties

The transport properties are known to be strongly influenced by tortuous path altering factors including shape and aspect ratio of the filler, degree of exfoliation or dispersion, filler loading and orientation, adhesion to the matrix, moisture activity, filler-induced crystallinity, polymer chain immobilization, filler-induce solvent retention, degree of purity, porosity and size of the permeant (Sanchez-Garcia and Lagaron 2010).

Moreover, the presence of impermeable crystalline fibers is thought to increase the tortuosity or detour factor in the materials leading to slower diffusion processes and, hence, to lower permeability. To enhance barrier properties to gases and vapors the filler should be less permeable or impermeable and have optimum dispersion and a high aspect ratio (filler length/thickness ratio).

The model strives to predict the observed permeability based strictly on tortuosity arguments. The presence of filler (spherical, plate, cylindrical, etc.) introduces a tortuous path for a diffusing penetrant. The reduction of permeability arises from the longer diffusive path that the penetrants must travel in the presence of the filler. The tortuosity factor (τ) is defined as the ratio of the actual distance (d') that a penetrant must travel to the shortest distance (d) that it would have traveled in the absence of the filler and is expressed in terms of the length (L), width (W), and volume fraction of the sheets (ϕ_s) as (Bharadwaj 2001)

$$\tau = \frac{d'}{d} = 1 + \frac{L}{2W} \phi_s \quad (2.13)$$

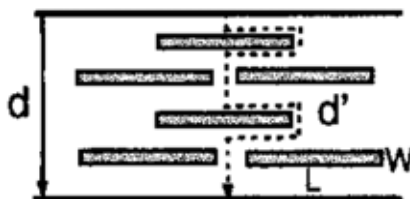


Figure 2.6 The tortuosity for a diffusing penetrant upon filler in a polymer matrix.

In addition, the mechanical and degradable properties of PLA can be much improved by natural fibers at lower cost. The potential advantages of using natural fiber have been well documented such as environmental friendliness as well as health and safety factors (Yu, Ren *et al.* 2010).

The study of mechanical and thermal properties of the natural fiber/PLA composites

Huda *et al.* (2006) examined the effect of reinforcing recycled newspaper (RNCF) on the thermal and mechanical properties of PLA/recycled newspaper fiber composites. The results indicated that the addition of fibers increased the thermal stability of the composites compared to neat PLA. The heat deflection temperature of the PLA/RNCF composites was found to be comparable to that of the glass fiber–reinforced PLA composites. It can be seen that the addition of 30 wt% RNCF increased the tensile strength of virgin PLA from 62.9 MPa to 67.9 MPa, which indicates that the stress is expected to transfer from the PLA polymer matrix to the stronger fibers. From the DMA results, incorporation of the fibers gave rise to a considerable increase of the storage modulus (stiffness) and to a decrease of the tan delta values. These results demonstrate the reinforcing effect of RNCF on PLA matrix.

Bax *et al.* (2008) studied the impact and tensile properties of PLA/Cordenka and PLA/flax composites. The result showed that the mechanical properties of the composites improved with a rising fiber mass content of 10 up to 30%. The flax/PLA and cordenka/PLA composites clearly differed in their impact strength. It is apparent that the impact strength of the PLA/flax composites increases with increasing fiber mass proportion. But the highest value is still 31% lower than the value for pure PLA. Moreover, the impact strength of Cordenka/PLA composites increase significantly and reach a maximum value of 72 kJ/m² at a fiber mass ratio of 30% which is approximately 4.5 times higher than the value for pure PLA.

Bledzki *et al.* (2009) studied PLA biocomposites with abaca fiber. It can be observed that the addition of 30 wt% of abaca fiber enhanced both modulus and tensile strength by factor 2.40 and 1.20, respectively. The Charpy A–notch impact resistance of PLA/abaca could be improved by factor 2.4. The dynamic mechanical analysis showed that incorporation of fiber reinforcement

causes a decrease in polymer chains mobility. The storage modulus of PLA-based composites remained much higher than of unreinforced PLA. The glass transition temperature derived from loss modulus characterizes with a slight shift to higher temperatures, if compared to PLA matrix.

Graupner *et al.* (2009) reported influence of different natural fibers (cotton, hemp, and kenaf) on the mechanical properties of PLA composites. The results showed that hemp and kenaf fiber bundles have the highest Young's modulus and the best potential as reinforcement for stiff composites. Moreover, cotton fibers have the higher elongation at break. In case of the composites, they reported that kenaf and hemp/PLA composites provided very high tensile strength and Young's modulus while cotton/PLA composite showed good impact strength. Their characteristics varied markedly depending on the characteristics of the raw fibers and fiber bundles and fiber used.

Tao *et al.* (2009) studied the preparation of ramie and jute fiber as reinforcement for PLA composite. The results showed that the mechanical properties of the PLA composite increase with the addition of fiber firstly and then decrease when the content of fibers is over 30 wt%. Furthermore, the mechanical properties of ramie/PLA composite are higher than those of jute/PLA composite because the strength of ramie fiber is higher than that of jute fiber.

The study of biodegradable properties of the natural fiber/PLA composites

Shogren *et al.* (2003) studied biodegradation of starch/poly(lactic acid)/poly(hydroxyester-ether) composite bars in soil. The results showed that the rates of weight loss increased in the order pure PLA (0%/year) <starch/PLA (0-15%/year) <starch/PHEE/PLA (4-50%/year) and increased with increasing starch and PHEE contents. Weight losses were due to starch only with the degradation proceeding from outside to inside along a narrow zone. It would be expected that the PLA in such a porous bar would, however, eventually biodegrade and fragment more quickly due to increased surface area and accessibility to microbes, especially for thinner specimens.

Ochi (2008) described the cultivation of kenaf and application to biodegradable composite materials. The unidirectional kenaf/PLA composites

showed tensile and flexural strengths of 223 MPa and 254 MPa, respectively. Moreover, tensile and flexural strength and elastic modulus of the kenaf fiber-reinforced composites increased linearly up to a fiber content of 50%. The biodegradability of kenaf/PLA composites was examined for four weeks using a garbage-processing machine. The tensile strength rapidly decreased from week 1 to week 2. After composting for four weeks, the strength gradually declined to 10%. The decrease in strength results from the degradation of polymerization of the cellulose in the kenaf fibers. Experimental results showed that the weight of composites decreased 38% after four weeks of composting.

Wu *et al.* (2009) studied the biodegradability of composite materials composed of PLA and green coconut fiber (GCF). Blends containing maleic anhydride-grafted PLA with GCF (PLA-g-MA/GCF) were studied. The composite was subject to biodegradation tests in a *Burkholderia cepacia* BCRC 14253 compost. The bacterium completely degraded both the PLA and the PLA-g-MA/GCF composite films. The PLA-g-MA/GCF (10 wt% GCF) was more easily degraded than pure PLA. Moreover, larger pores were apparent on the PLA-g-MA/GCF composite at 9 and 15 days, indicating that a higher level of destruction. Weight loss of the PLA-g-MA/GCF composite was also accelerated compared with that of PLA, exceeding 68% after 21 days. These results clearly indicate that the addition of GCF enhances the biodegradability of the composite.

Pradhan *et al.* (2010) studied compostability and biodegradation of PLA-wheat straw and PLA-soy straw composites in simulated composting bioreactor (ASTM D5338). The rate of degradation of composites is clearly higher than only PLA. This indicates that the enhancement of degradation may be due to the presence of readily degradable natural biomass in the composites and due to reduced average molecular weight of the PLA. The composites of PLA with untreated soy and wheat straw have been clearly demonstrated to be compostable products. This observation increases the possibility of adopting some modified or treated biomass in the composites as any loss of degradation that may occur due to the modification of the biomass can be leveraged with the priming/favorable effects observed due to the presence of readily degradable components of the biomass. This strategy can help satisfy the 90% degradation

requirements for the modified substrate components in a compostable plastic composite in 180 days.

2.3.5 Peanut Shell (*Arachis Hypogaea L.*)

Peanuts, also called groundnuts, ground-peas, earthnuts, pindar, jar-nut and manila-nut, are the pea-like fruit from the *Arachis hypogaea* plant, which is part of the bean family. There are several varieties of peanuts throughout the world.

Peanut shell is a waste material from processing of peanuts. It is an abundant and inexpensive agricultural by-product. Most of this agricultural by-product is arbitrarily discarded or set on fire. These disposals must result in environmental pollution. Indeed, some of them are burned to generate energy and used for animal feed. The potential application of peanut shell can produce natural fiber-based composites for ceiling, wall covering panels, and fiberboard manufacturers (Akgu and Tozluoglu 2008, Fasina 2008). The chemical composition of peanut shells is 8.2% protein, 28.8% lignin, 37.0% cellulose and 2.5% carbohydrate (Harrell 2010). Peanut shell is a good source of nitrogen fertilizer. A comparison between peanut shell and other crop residues, such as cereal straw and cotton carpel, indicated that peanut shell had higher lignin content, while holocellulose content was higher than cereal straw but lower than cotton carpel (Akgu and Tozluoglu 2008). The composition of peanut shell which use in this work was shown in Table 2.5.

Table 2.5 The composition of peanut shell

C (%)	H (%)	N (%)
40.22	5.55	2.63

Moreover, peanut shell is one of the potential adsorbent materials. It can be utilized for dye removal as it can also bring unlimited number of economic and environmental benefits to the industrial wastewater treatment. So natural peanut shell or modified peanut shell has been used as an adsorbent in removing heavy

metals and dyes from solutions (Song, Zou *et al.* 2011). There have been several reports that peanut shells can be converted into activated carbon and used to absorb various metal ions (cadmium, copper, lead, nickel, and zinc) and organic compounds (Wilson, Yang *et al.* 2006).

2.3.6 Bagasse Fiber

Bagasse fiber is a by-product of the sugar cane industry whose role is sugar, rum or biofuel production. This industry is located in the tropical and sub-tropical regions of the world where sugar cane (scientific name *Saccharum officinarum*) is cultivated. Sugar cane bagasse is the leftover after crushing of the stalk to extract the sugar cane juice from which sugar is obtained by evaporation and crystallization, and rum and ethanol which is used as biofuel, are obtained by fermentation. The bagasse/stalk ratio by mass is around 30%. Bagasse makes a sugar mill more than self-sufficient in energy; the surplus bagasse can be used as animal feed, in paper manufacture, or as fibers to replace asbestos in a cement matrix (Bilba and Arsene 2008). Bagasse is comprised of cellulose (46.0%), hemicellulose (24.5%), lignin (19.95%), fat and waxes (3.5%), ash (2.4%), silica (2.0%) and other elements (1.7%).

Stael *et al.* (2001) studied the impact behavior of chopped bagasse/polyethylene-co-vinyl acetate (EVA) composites. The results show that the incorporation of chopped bagasse produces a strong decrease in the impact strength. The brittle behavior associated with the composites with higher volume fractions could be attributed to the inhibition of the deformation capacity of EVA matrix due to the presence of the much stiffer bagasse material. Moreover, the impact strength was independent of the bagasse size, but varied with the volume fraction. As a function of the volume fraction it was shown that the mechanical performance of bagasse-EVA composites could be tailored to reproduce the behavior of wood-based particle boards.

Cao *et al.* (2006) studied the mechanical properties of biodegradable composites reinforced with bagasse fiber before and after alkali treatments. The results show that both the tensile and impact strength of the untreated bagasse fiber composites increased with increase in fiber content to an optimum fiber content of

65% only. Composites of 1% NaOH solution treated fibers showed maximum improvement. Approximately 13% improvement in tensile strength, 14% in flexural strength and 30% in impact strength had been found, respectively. SEM micrographs revealed that the fibers after the alkali treatment became finer due to the dissolution of the hemicellulose and increased aspect ratio, which resulted in a better fiber–matrix adhesion.

Cerqueira *et al.* (2011) studied mechanical behavior of polypropylene reinforced sugarcane bagasse fibers composites. The results show that the chemical modification of cellulose fibers from sugarcane bagasse was successfully accomplished and it was verified that effectively improves the tensile, flexural and impact strength in comparison to the polymer pure. Composites show tensile modulus compared to the PP. It was observed an increase of 45% impact strength. This fact can be explained by good interface between fibers–matrix.

2.4 Plasticization

Plasticizers are important classes of low molecular weight and non–volatile compounds that are widely used in polymer industries as additives. The primary role of such substances is to improve the flexibility and processability of polymers by lowering the second order transition temperature, the glass transition temperature (T_g). The council of the IUPAC (International Union of Pure and Applied Chemistry) defined a plasticizer as “a substance or material incorporated in a material (usually a plastic or elastomer) to increase its flexibility, workability, or distensibility”. These substances reduce the tension of deformation, hardness, density, viscosity and electrostatic charge of a polymer, at the same time as increasing the polymer chain flexibility, resistance to fracture and dielectric constant. Other properties are also affected, such as degree of crystallinity, optical clarity, electric conductivity, fire behavior and resistance to biological degradation, amongst other physical properties (Vieira, Silva *et al.* 2011).

2.4.1 Plasticizer Classification

Plasticizers can be either defined as external or internal. External plasticizers are low volatile substances that are added to polymers. In this case, plasticizer molecules interact with polymer chains, but are not chemically attached to them by primary bonds and can, therefore, be lost by evaporation, migration or extraction. On the other hand, internal plasticizers are inherent parts of the polymer molecules and become part of the product, which can be either co-polymerized into the polymer structure or reacted with the original polymer. Internal plasticizers generally have bulky structures that provide polymers with more space to move around and prevent polymers from coming close together. Therefore, they soften polymers by lowering the T_g and, thus, reducing elastic modulus. For both types, although more pronounced for internal plasticizers, a strong temperature dependence of material properties is observed. The benefit of using external plasticizers, compared to internal ones, is the chance to select the right substance depending on the desired product properties (Rahman and Brazel 2004).

Plasticizers can also be classified as primary and secondary. If a polymer is soluble in a plasticizer at a high concentration of the polymer, it is said to be a primary plasticizer. This type of plasticizers are used as the sole plasticizer or as the main element of the plasticizer, they should gel the polymer rapidly in the normal processing temperature range and should not exude from the plasticized material. Secondary plasticizers, on the other hand, have lower gelation capacity and limited compatibility with the polymer, they are typically blended with primary plasticizers, to improve product properties or reduce the cost (Vieira, Silva *et al.* 2011).

2.4.2 Plasticizer Model

There are four models that describe the effects of plasticizers:

1. Lubricity Model

The lubricity model states that plasticizer acts as a lubricant between polymer molecules. As a polymer is flexed, it is believed their molecules glide back and forth with the plasticizer providing the gliding planes. The model assumes a polymer macromolecules have, at the most, very weak bonds away from their crosslinked sites.

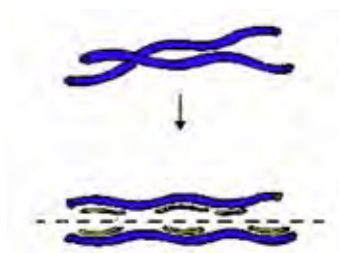


Figure 2.7 Plasticizer polymer response based on lubricity model.

2. Gel model

The Gel model of plasticization starts with a model of the polymer molecules in a three dimensional structure. The stiffness of polymer results from a gel of weak attachments at intervals along polymer chains. These points of gel are close together, thus, permitting little movement. Gel sites might be result of Van der Waals forces, hydrogen bonding, or crystalline structure. The Gel sites can interact with plasticizer, thus, separating a gel site of the adjacent polymer chains. The plasticizer by its presence separates a polymer chains allowing the polymer molecules to move more freely.

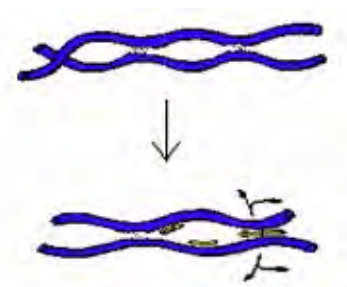


Figure 2.8 Gel model of plasticizers.

3. The Free Volume Model

The free volume Model is very involved with low-temperature flexibility. For any polymer the simplest explanation may be stated as the difference between observed volume at absolute zero and volume measured at a selected temperature. Addition of plasticizer to a polymer increases free volume of system. Likewise, free volume increases with rising temperature. An important application of

the model to external plasticization has been to clarify a lowering of the glass transition temperature of a compound by plasticizer. Plasticizers, because of their small molecular size compared to polymers, assist with greater polymer mobility. This is attributed to increased free volume until temperature at which polymer–plasticizer mixture freezes.

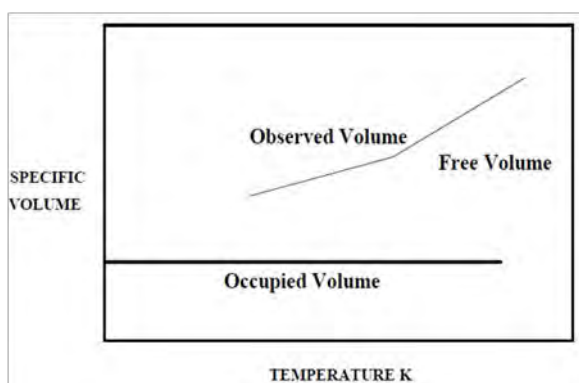


Figure 2.9 Free volume model of plasticizers.

4. The Mechanistic Model

The mechanistic model of plasticization (also referred to as salvation-desolvation equilibrium) supplements other three models previously discussed. This model can be depicted as having some resemblance to gel model. The essential difference is that in gel model, plasticizer stays attached to a site along polymer chain, whereas, the mechanistic model states plasticizer can move from one polymer location to another.

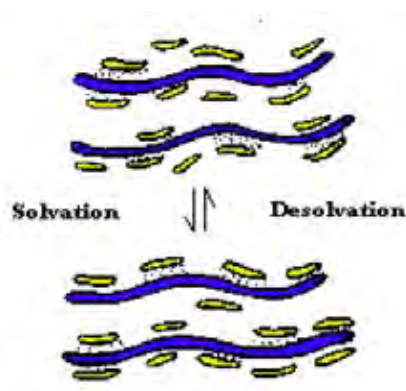


Figure 2.10 Mechanistic model of plasticizers.

2.4.3 Compatibility

If plasticizer–polymer compatibility is correct, the two materials will form a homogeneous mixture during processing and once cured, the plasticizer will remain in the compound upon cooling and resting at low temperature. From a practical standpoint, it is only necessary that the compatibility be observed at a plasticizer quantity suitable to produce the desired effect. To achieve a high degree of plasticizer compatibility, it is generally necessary that the plasticizer and polymer have approximately the same polarity. The ability to achieve and maintain compatibility with the polymer depends on the same factors that govern the behavior of simpler organic solvents and solutes. The thermodynamic basis for such interactions is expressed by *Hildebrand solubility parameters*, defined as the square root of cohesive energy density. Plasticizer compatibility with an amorphous polymer (or the amorphous phase of a partially crystalline polymer), δ , normally requires values that do not differ by more than + 1.5 (cal./cc). Solubility parameters for both polymers and plasticizers are conveniently calculated by the additive method of Small, who derived individual parameters for various atoms and groups in the molecules (HallStar).

Plasticizers are generally chosen on the basis of the following criteria:

- Compatibility of a plasticizer with a given polymer.
- Processing characteristics.

- Desired thermal, electrical and mechanical properties of the end product.
- Resistance to water, chemicals, solar radiation, weathering, dirt, microorganisms.
- Effect of plasticizer on rheological properties of polymer.
- Toxicity.
- Volume–cost analysis.

Attempts have been made to improve the processability, flexibility, and ductility of PLA is the use of plasticizers as for glassy polymers in the plastics industry. The choice of plasticizers to be used as modifiers for PLA is limited by the requirement of the application. Only non–toxic substances approved for food contact can be considered as plasticizing agents in food packaging materials. The plasticizer should be compatible with PLA and stable at the elevated temperature used during processing. The PLA/plasticizer blends should be stable over time because the migration of the plasticizer to the surface could be a source of contamination of the food or beverage in contact with the packaging or may possibly regain the initial brittleness of pure PLA.(Lemmouchi, Murariu *et al.* 2009).

In the past decade, a large amount of research was devoted to the plasticization of PLA to produce flexible films. Candidates included polyethylene glycol (PEG), citrate esters, glycerol, glyceryl triacetate, glucosemonoesters, (partially) fatty acid esters, lactide monomer, lactic acid oligomers, etc. have been widely attempted to plasticize PLA.

Up to the present time, Martin *et al.* (2001) studied the preparation of PLA was plasticized with various biocompatible plasticizers (10 and 20 %wt of glycerol, citrate ester, polyethylene glycol, oligomeric lactic acid). The results showed that the elongation at break increased with increasing plasticizer content, indicating that the properties of PLA can be changed from rigid to ductile. While, this was contrary to Young's modulus which decreased as the concentration of plasticizer increased. Thermal analyses demonstrated that oligomeric lactic acid (OLA) and polyethylene glycol (PEG) gave the best results. The glass transition temperature decreased from 58 to 12 °C and 18 °C for 20 wt% of PEG and OLA, respectively. Moreover, glycerol was found to be the least efficient plasticizer.

Oksman *et al.* (2003) reported the mechanical properties of plasticized PLA and PLA/flax composites. The triacetin was used as a plasticizer for PLA/flax composites. The result showed that the tensile stress decreased with increase in triacetin content. Moreover, the addition of 5 %wt triacetin in PLA shows the best impact strength. Higher triacetin content does not show any positive effect on Charpy impact strength of the PLA/flax composites.

Pillin *et al.* (2006) reported the use of poly(1,3-butanediol) (PBOH), dibutyl sebacate (DBS), acetyl glycerol monolaurate (AGM), and polyethylene glycol (PEG) as a plasticizers for PLA fabrication process. It was important to note that plasticizers blended with PLA decreased the glass transition temperature (T_g) and modified the melting and crystallization characteristics. The PEG is the most efficient for the T_g reduction and its clearly appears that for compositions higher than 20% of plasticizer, all the blends present a limit of miscibility and the T_g reaches a plateau value. With the most efficiency of the use PLA, only 20 wt% of PEG was successfully applied, whereas 30 wt% of the other plasticizers can be used. Nevertheless, the PLA blended to PEG become very brittle as a function of plasticizer content and molecular weight. So, PEG induces a decrease in cohesion of these materials that were shown by a very low stress at break. The more efficient plasticizers are PBOH, AGM, and DBS that give mechanical properties that can be consistent with soft packaging applications.

Piorkowska *et al.* (2006) studied the use of polypropylene glycol (PPG) as a plasticizer of PLA. They found that the plasticization decreased T_g which was reflected in a lower yield stress and improve elongation at break. The elongation at break was increased with the increase of plasticizer content. The crystallization in blends was accompanied by a phase separation facilitated by an increase of plasticizer content in the amorphous phase and by annealing of blends at crystallization temperature. The PLA/PPG (Mw 1000 g/mol) blends the phase separation was the most intense which facilitated plastic deformation of the blends and enabled to achieve the elongation at break 90–100% for 10 and 12.5 %wt PPG content in spite of relatively high T_g of PLA rich phase of the respective blends, 46.1–47.6 °C.

Murariu *et al.* (2008) studied PLA/CaSO₄ composites toughened with low molecular weight plasticizers ((bis(2-ethylhexyl) adipate (DOA) and glyceryl triacetate (triacetin–GTA)) and polymeric ester-like plasticizers. The result showed that the addition of up to 10 wt% plasticizer into these highly filled compositions can trigger a fourfold increase of the impact strength with respect to the compositions without any modifier, cold crystallization properties and a significant decrease of their glass transition temperature. In addition, the best impact performances up to fourfold increase of impact strength (Izod), were obtained by addition of GTA, whereas the polymeric plasticizers lead to PLA composites characterized by better thermal stability and higher tensile strength properties. It is also important to point out that the highest mechanical properties are obtained for the GTA with the best solubility parameter in relation to PLA (GTA). Another point is that the more important decrease of tensile strength recorded using DOA is not surprisingly due to its limited miscibility with PLA and to presence of DOA inclusions that should weaken this composition.

2.5 Crosslinking

Crosslinking is the formation of chemical links between molecular chains to form a three-dimensional network of connected molecules. The establishment of chemical bonds between polymer molecule chains may be accomplished by heat, vulcanization, irradiation or the addition of a suitable chemical agent. Crosslinking restricts chains from sliding past one another and generates elasticity in an amorphous polymer. It makes a polymer more resistant to heat, light, and other physical agencies, giving it a high degree of dimensional stability, mechanical strength, and chemical and solvent resistance. The effects of crosslinking on the physical properties of the polymers are primarily influenced by the degree of crosslinking, the regularity of the network formed, and the presence and absence of crystallinity in the polymer. For crystalline polymers there may be a reduction in crystallinity with a low degree of crosslinking as it hinders chain orientation, and the polymer may become softer, more elastic, and have a lower melting point. Crosslinking changes the local molecular packing and leads to a decrease in free

volume. This is reflected in an enhancement of glass transition temperature. Improvement in creep behavior also results from crosslinking as it restricts the viscous flow (Bhattacharya, Rawlins *et al.* 2009)

Advantages of crosslinking:

- | | |
|-------------------------------------|--|
| 1. Higher tensile strength | 7. Improved fluid resistance |
| 2. Improved abrasion/cut through | 8. Slightly better flame resistance |
| 3. Better crush resistance | 9. No change of electrical |
| 4. Solder iron resistance | 10. Negligible change in thermal stability |
| 5. Better over load characteristics | 11. Decrease in flexibility |
| 6. Resistance to stress cracking | 12. Improved high temperature mechanicals |

2.5.1 Chemical Crosslinking

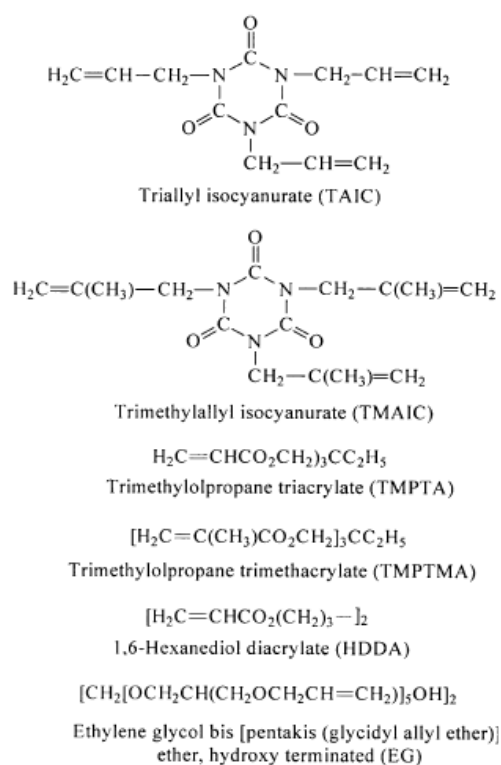
Chemical crosslinking is another possible way to introduce crosslinking structures. Some chemical reactions between the crosslinking agent and the polymer chains can be initiated by chemical treatments without irradiation, and modified materials with different gel fraction and crosslinking density for further processing of products can be obtained (Yang, Wu *et al.* 2008)

The chemical methods, peroxide induced crosslinking, which has been widely applied through the addition of small amount of peroxide during extrusion. By reactive extrusion peroxides decompose forming free radicals. These radicals present in polymer matrix can promote chain scission, branching, crosslinking or any combination of the three. These reactions will influence physical properties such as melt viscosity, crystallinity, glass transition temperature, melting temperature, tensile and impact strengths (Żenkiewicz, Rytlewski *et al.* 2010). For example, the crosslinking structures could be effectively introduced to PLA by initiation of dicumyl peroxide (DCP) in the presence of small amount of crosslinking agent (triallyl isocyanurate), and crosslinked PLA with significantly improved thermal stability and enhanced tensile strength (Yang, Wu *et al.* 2009).

2.5.2 Crosslinking Agent

The thermal stability of PLA can be significantly improved by the chemical crosslinking of PLA containing suitable concentration of various

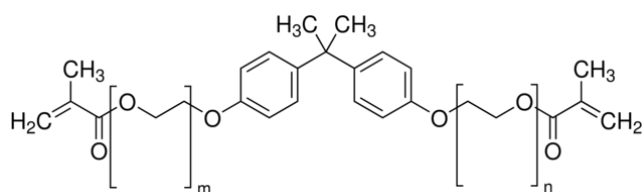
crosslinking agents such as TAIC, TMAIC and TMPTA. Scheme 2.5 lists structural formulae of prominent crosslinking agents for PLA. These agents all have multifunctional groups, which can react with polymer chains to form crosslinks (Galagan, Hsu *et al.* 2010).



Scheme 2.5 Structural formulae of multifunctional crosslinking agents.

2.5.3 Ethoxylated Bisphenol A Dimethacrylates (Bis-EMAs) Molecular Weight = 376

The use of resin adhesives containing low shrinkage crosslinking monomers such as ethoxylated bisphenol A dimethacrylates also facilitates the placement of resin composite restorations preventing excessive stress of contraction subsequent.



Scheme 2.6 Structural of Bis-EMAs.

Bis-EMAs can be used as a crosslinking agent and chain extender at the same time and a highly effective crosslinker. It can be carried out with conventional peroxides or irradiation. The resulting polymers have improved mechanical properties, as well as improved chemical and high temperature resistance (Ogliari, Ely *et al.* 2008)

2.5.4 Measurement of Gel Fraction

Gel fraction was measured by the weight remaining after dissolving the sample in chloroform using the following eq. 2.14

$$Gel\ fraction = \left(\frac{W_g}{W_0} \right) \times 100 \quad (2.14)$$

Where W_0 is initial weight (dry), W_g is the remaining weight (dry gel component) of the crosslinked sample after dissolving in chloroform at room temperature for 24 h.

2.5.5 Time Temperature Transformation (TTT) Diagram

For processing purposes, the gel points represents the state beyond which the material no longer flows and is therefore incapable of being processed. Gelation does not involve any change in the curing process (the reaction rate is unmodified), and therefore cannot be detected by techniques sensitive to chemical reaction, such as differential scanning calorimetry (DSC). However, the mechanical and viscoelastic properties of the reaction medium do change during gelation, which can therefore be detected by methods based on changes in these properties. It is generally accepted that gelation occurs at a fixed conversion value which is

independent of the curing temperature and depends on the functionality, reactivity, and stoichiometry of the reactive species. Vitrification is understood as a change from the liquid or rubbery state to the glassy state due to an increase in both crosslinking density and the molecular weight of the material during the curing process.

This transformation occurs when the T_g of the material coincides with the curing temperature. As of this moment, curing within the glassy state becomes extremely slow and the reactive process changes from chemical control to control by diffusion. The different states the material can pass through during the curing process can be represented in the time-temperature-transformation (TTT) diagram. For the construction of the TTT diagram it is necessary to know the curing kinetics up to when the material vitrifies and also the gel time (t_{gel}) and vitrification time (t_{vit}). Three characteristic temperatures exist in the TTT diagram: T_{g0} , the glassy transition temperature of the material without crosslinking; $_{gel}T_g$, the lowest curing temperature which allows material to gel before it vitrifies, which coincides with the curing temperature at which the material gels and vitrifies simultaneously; and $T_{g\infty}$, the highest glassy transition temperature, or lowest temperature at which complete curing can be achieved. Below T_{g0} the material does not crosslink. Between T_{g0} and $_{gel}T_g$ the liquid resin reacts until the glassy transition temperature coincides with the curing temperature; at this moment vitrification begins and the reaction changes to control by diffusion. Between $_{gel}T_g$ and $T_{g\infty}$, the material first gels and then vitrifies when $T_c = T_g$. Above $T_{g\infty}$ the material is completely cured and remains in the rubbery state after gelling. Figure 2.11 shows the example of TTT diagram of unsaturated polyester resin. The TTT diagram can be described with the Arrhenius equation:

$$\ln t = A + E/RT. \quad (2.15)$$

Where t is time, A is Arrhenius constant, E is the activation energy, R is the universal gas constant, and T is temperature (Ramis and Salla 1997, Zhang, Yi *et al.* 2008).

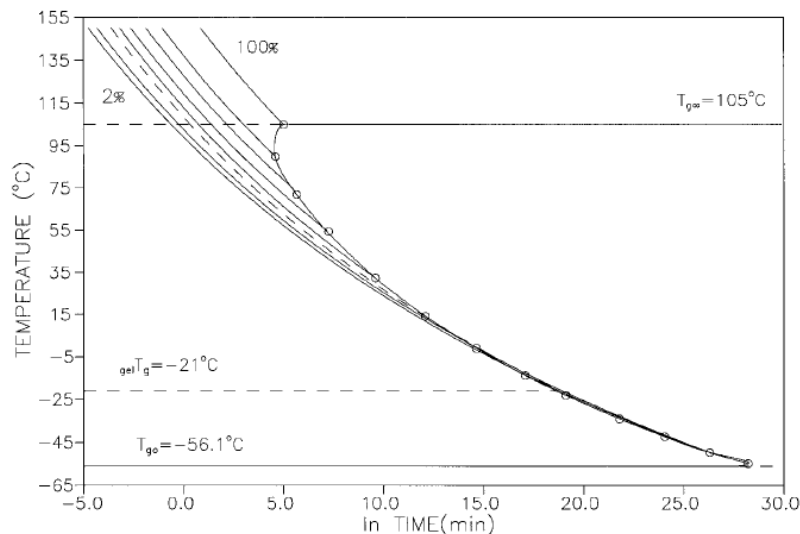


Figure 2.11 TTT cure diagram for unsaturated polyester resin cured with 1.5% of benzoyl peroxide as an initiator.

2.5.6 Crosslinking Polymer at The Gel Point

2.5.6.1 *Linear Viscoelasticity and Oscillatory Shear Experiments.*

When oscillatory shear measurements are performed in the linear viscoelastic regime, the storage modulus G' (elastic response) and loss modulus G'' (viscous behavior) are independent of the strain amplitude.

An oscillatory shear experiment, which is exposed to a sinusoidal strain (γ) at an angular frequency of ω will respond with a gradual approach to a steady sinusoidal stress (σ)

$$\gamma = \gamma_0 \sin \omega t \quad (2.16)$$

$$\sigma = \gamma_0 (G'(\omega) \sin \omega t + G''(\omega) \cos(\omega t)) \quad (2.17)$$

From this type of experiment the storage modulus G' , the loss modulus G'' and the dynamic viscosity $\eta' = G''/\omega$ can be determined. These are generally represented in terms of the elastic G' , viscous G'' , and complex shear modulus G^* :

$$G' \propto \sin \omega t, G'' \propto \cos \omega t, G^* = (G'^2 + G''^2)^{1/2} \quad (2.18)$$

$$\text{Loss tangent: } \tan \delta = \frac{G''}{G'} \text{ (measure of damping)} \quad (2.19)$$

2.5.6.2 Theoretical Models for Linear Viscoelasticity

In the linear viscoelastic regime (small strain values) the viscoelastic properties of the incipient gel can be described by the gel equation ($-\infty < t' < t$).

$$m(t) = S \int_{-\infty}^t (t-t')^n \gamma(t') dt' \quad (2.20)$$

When m = the shear stress

$\gamma(t')$ = the rate of deformation of the sample

S = the gel strength parameter (depends on the crosslinking density and the molecular chain flexibility)

n = the relaxation exponent

For incipient gels G' and G'' are expected to obey power laws in frequency: $G' \sim G'' \sim \omega^n$

The gel point of a chemical gel can be determined by observation of a frequency independent value of $\tan \delta$ versus time or versus temperature for a thermoreversible gel.

An alternative method is to plot against temperature the apparent viscoelastic exponents n' and n'' obtained from the frequency dependence of G' and G'' at each temperature of measurement and observing a crossover where $n' = n'' = n$.

2.5.6.3 The Behavior at The Gel Point of Crosslinking Polymer

Crosslinking polymers undergo phase transition from liquid to solid at critical extent of reaction. This phenomenon is called gelation. The polymer is said to be at the gel point (GP) if its steady shear viscosity is infinite and its

equilibrium modulus is zero. Several processes may contribute to this transition besides the connecting of molecular strands by chemical crosslinking: physical entanglements between the macromolecular strands, vitrification as the glass transition temperature rises with increasing extent of reaction, phase separation of the reaction components or products, and crystallization (Winter and Chambon 1986).

To determine the gel point during a crosslinking reaction, the complex moduli are measured as a function of time as shown in Figure 2.12. At early times, both of moduli are low and the elastic portion G' is much smaller than the viscous portion G'' . This is characteristic of a polymer liquid at low frequencies. The presence of a small elastic contribution well before the critical gel point is due to the stretching of the polymers under deformation and potentially physical entanglements between the polymers. As the crosslinking reaction progresses, the molecular weight of the polymers increases, increasing both the viscosity and relative contribution of the elastic modulus G' . Longer polymers have longer relaxation times and more entanglements. At a time known as the cross-over point, the elastic modulus becomes larger than the viscous modulus. As the reaction progresses to completion, the elastic and viscous moduli approach their equilibrium values. Stiffer gels will have a higher elastic modulus and a smaller phase angle δ . In the limit of a very stiff gel, the viscous contribution may be negligible (Grillet, Wyatt *et al.* 2012).

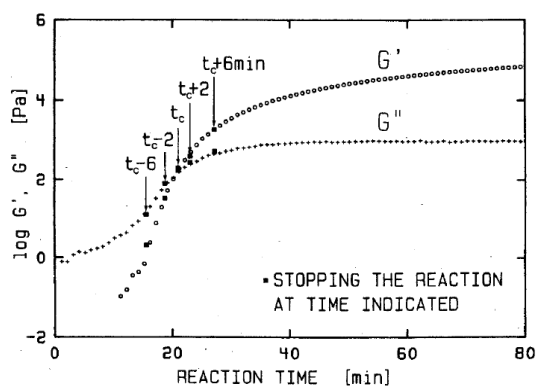
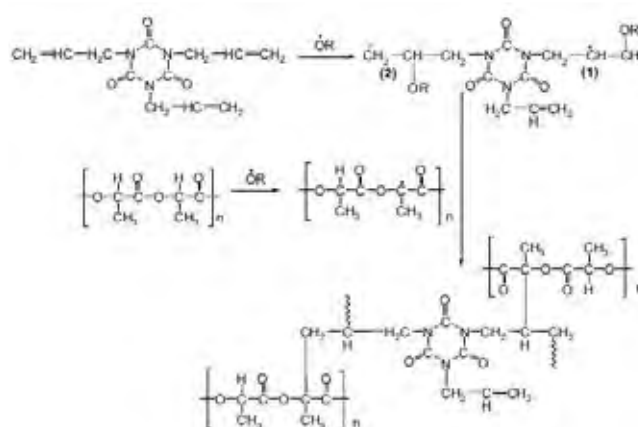


Figure 2.12 Shear moduli as a function of time during crosslinking reaction.

Yang *et al.* (2008) studied thermal and mechanical properties of chemical crosslinked PLA. Crosslinking was introduced via chemical treatment of the melt by adding small amounts of crosslinking agent triallyl isocyanurate (TAIC) and dicumyl peroxide (DCP) as seen in Scheme 2.7. The results showed that the crosslinking of PLA started at a low content of either TAIC or DCP, resulting in a decrease of crystallinity and a significant improvement of the thermal degradation initiation and completion temperatures, which indicated better thermal stability than neat PLA. Crosslinking was also responsible for the improved tensile modulus and tensile strength.



Scheme 2.7 One possibility of reaction scheme for chemical crosslinking of TAIC between two PLA molecules.

Quynh *et al.* (2007) studied crosslinked PLA have been produced by radiation modification in the presence of a suitable crosslinker (TAIC). The results showed that the properties of crosslinked samples are governed by crosslinking density and these improvements seemed to increase with radiation dose. The melting and crystallinity peaks of crosslinked PLA decreased with the radiation dose and seemed to be non-crystalline. These decreases may be caused by reduction of degree of crystallization of polymer chains suggested that the molecular chains were crosslinked in the amorphous state. The crosslinking structure formed in irradiated samples of PLA containing TAIC resulted in a significant improvement of their mechanical properties.

Changgang et al. (2009) studied the effects of dicumyl peroxide (DCP) at low concentrations on initiating crosslinking of polylactide (PLA) by melt blending. The results showed that the crosslink rate of the blends increased with DCP content increasing. The PLA gel with 0.73 wt% of DCP appeared obvious crystallization behavior and a new crystalline structure may be formed as DCP was 1.4 wt%. And it was also found that the exothermal peak temperature of PLA gel decreased with increasing DCP content except for the gel with 1.4 wt% of DCP. It also has been inferred by rheology analysis that the blend may be the structure of gel or 3D network. Comparing to PLA melt, the G' and G'' for the PLA with 1.1 wt% DCP were higher than PLA and increased with the frequencies increasing. The G' was enhanced and higher than G'' at whole frequencies, meanwhile, the G' showed a “plateau” at low frequency. The results indicated that the PLA with 1.1 wt% DCP had a strong gel–3D network structure.

Young Shin et al. (2010) studied the rheological and thermal properties of the PLA modified by electron beam irradiation in the presence of glycidyl methacrylate (GMA). In the case of irradiated virgin PLA, η^* and G' seriously decreased with increasing irradiation dose and were much lower than those of virgin PLA due to the chain scission. However, the chain scission was suppressed and branching was enhanced by introducing the GMA. It was confirmed that a branching or a chain scission reaction was more dominant than a crosslinking reaction from the very low gel fraction in all tested samples. Compared to virgin PLA, irradiated PLA with 3 phr GMA had a η^* of about 10 times higher and G' of 100 times higher than those of virgin PLA at 0.1 rad/s because of long chain branched structure. Gel fraction measurement revealed that chain scission and branching was more dominant than crosslinking.

CHAPTER III EXPERIMENTAL

3.1 Materials

PLA grade 4043D ($\rho = 1.25 \text{ g/cm}^3$, $\delta = 21.42 \text{ MPa}^{1/2}$, MFI = 2.60 g/10min, and $T_m = 210 \text{ }^\circ\text{C}$) was purchased from Nature-Work LLC. Peanut shell (PNS) was ground to 5-100 μm with the moisture content of $5.10 \pm 0.11\%$. Bleached bagasse fibers (treated with H_2O_2 and ClO_2 to reduce lignin content and to lighten the fibers) from Biodegradable Packaging for Environment Co., Ltd. were ground and sieved into powder (30-200 μm , $6.34 \pm 0.22 \%$ moisture content) before use. Plasticizers i.e. triacetin with a 99% purity ($M_w \approx 218 \text{ g/mol}$, $\delta = 22.00 \text{ MPa}^{1/2}$, and $\rho = 1.15 \text{ g/cm}^3$) was purchased from Sigma-Aldrich, polyethylene glycol ($M_w \approx 400 \text{ g/mol}$, $\delta = 20.2 \text{ MPa}^{1/2}$, and $\rho = 1.124 \text{ g/cm}^3$) was purchased from Fluka Analytical and glycerol, analytical grade ($M_w \approx 92 \text{ g/mol}$, $\delta = 17.7 \text{ MPa}^{1/2}$, and $\rho = 1.25 \text{ g/cm}^3$), purchased from Ajak Finechem Pty Ltd. Antioxidants i.e. Irganox 1010 ($\rho = 1.15 \text{ g/cm}^3$ and $T_m = 110\text{-}125 \text{ }^\circ\text{C}$) and QUENT 68 ($T_m = 185 \text{ }^\circ\text{C}$) were purchased from Global Connections Public Co. Ltd. Dicumyl peroxide (DCP) with a 99% purity was used as a radical initiators and Bisphenol A ethoxylate dimethacrylate (Bis-EMAs) with $M_w = 376 \text{ g/mol}$ was used as a crosslinking agent, were purchased from Sigma-Aldrich.

3.2 Methods

3.2.1 Preparation of Natural Fibers (Peanut Shell and Bagasse Fiber)

3.2.1.1 Preparation of Peanut Shell

Peanut shells were finely ground by PFI mill and pass through the sieve of 100 mesh size. Then peanut shells were dried in an oven at $80 \text{ }^\circ\text{C}$ for 24 h before compounding. The peanut shell is the particulate matter seen in Figure 3.1. It is estimated that the average size is 5-100 μm . Table 3.1 shows properties and compositions of peanut shell.

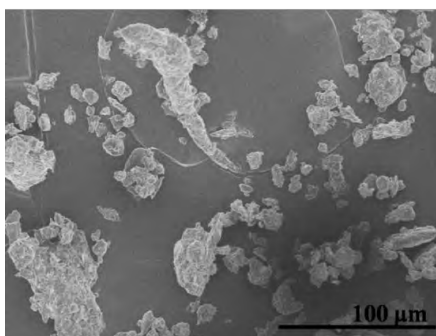


Figure 3.1 Morphological image of peanut shell.

The FTIR spectrum of Peanut shell (Figure 3.2) shows a broad absorbance band centered around 3450 cm^{-1} which is assigned to the hydrogen-bonded hydroxyl groups (O–H). Other interesting absorption bands found at 1638 cm^{-1} , bands at 1452 cm^{-1} , 1322 cm^{-1} , 1060 cm^{-1} , and 891 cm^{-1} are assigned to C=C aromatic stretching vibration of lignin (partly bleached), C–H bending from $-\text{CH}_2$, and $-\text{CH}_3$ groups, cellulose linkages, and β -glycosidic linkage, respectively.

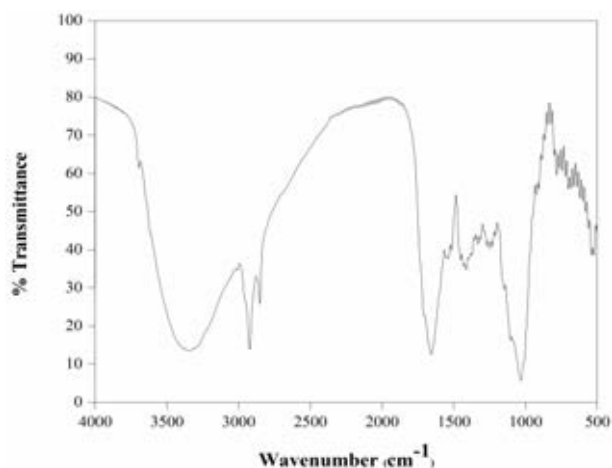


Figure 3.2 FTIR spectrum of peanut shell.

3.2.1.2 Preparation of Bagasse Fiber

Bagasse fibers were treated with H_2O_2 and ClO_2 to reduce lignin content and to lighten the fibers. Then bagasse fibers were finely ground by PFI mill and pass through the sieve of 100 mesh size. Bagasse fibers were dried in an oven at

80 °C for 24 h before compounding. Bagasse fiber is composed of many fibrils as seen in Figure 3.3. It is estimated that the average size of the bagasse fibers is 10-30 μm in diameter and 100-200 μm in length (aspect ratio \approx 6.67-10.29). The density is about 1.74 g/cm^3 . Table 3.1 show properties and compositions of bagasse fiber.

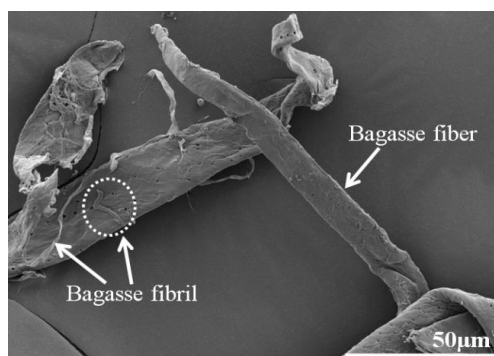


Figure 3.3 Morphological image of bagasse fiber.

Figure 3.4 shows spectrum of bagasse fiber. It shows a broad absorbance band centered around 3462 cm^{-1} which is assigned to the hydrogen-bonded hydroxyl groups (O-H). The absorption bands found at 1642 cm^{-1} , 1450 cm^{-1} , 1374 cm^{-1} , 1051 cm^{-1} , and 890 cm^{-1} are assigned to C=C aromatic stretching vibration of lignin (partly bleached), C-H bending from $-\text{CH}_2$, and $-\text{CH}_3$ groups, cellulose linkages, and β -glycosidic linkage, respectively.

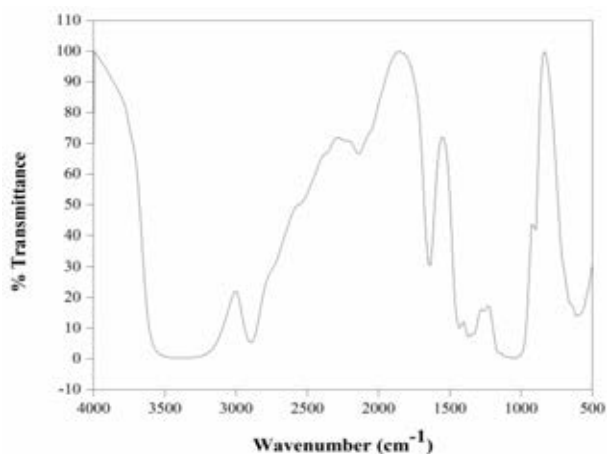


Figure 3.4 FTIR spectrum of bagasse fiber.

Table 3.1 Properties and compositions of peanut shell and bagasse fiber

Properties	Peanut shell	Bagasse fiber	Method
Density (g/cm ³)	1.63	1.74	-
Aspect ratio	2.52-5.16	6.67-10.29	-
Alpha–Cellulose (%)	37.68	75.40	TAPPI T 203 cm-09
Holocellulose (%)	54.56	99.09	Wise et al. 1946
Lignin (%)	29.03	0.34	TAPPI T 222 cm-11
Water retention (%)	5.19±0.11	6.34±0.22	ISO 14487
Protein (%)	9.29	-	-
Carbohydrate (%)	21.82	-	-
Oil (%)	0.92	-	-

3.2.2 Preparation of PNS/PLA Composites by Using Twin–Screw Extruder

The PLA pellets and peanut shell were dried at 60 °C for 24 h before processing. PLA and peanut shell were mixed with plasticizers and antioxidants. All melt blending were performed using a LABTECH (type LHFS1–271822) corotating twin–screw extruder with L/D ratio 40 (D = 20 mm, and L = 800 mm) as seen in Figure 3.5. The temperature profile was maintained in the range 120-180 °C from the feed throat to the die and the rotational speed was fixed at 40 rpm.

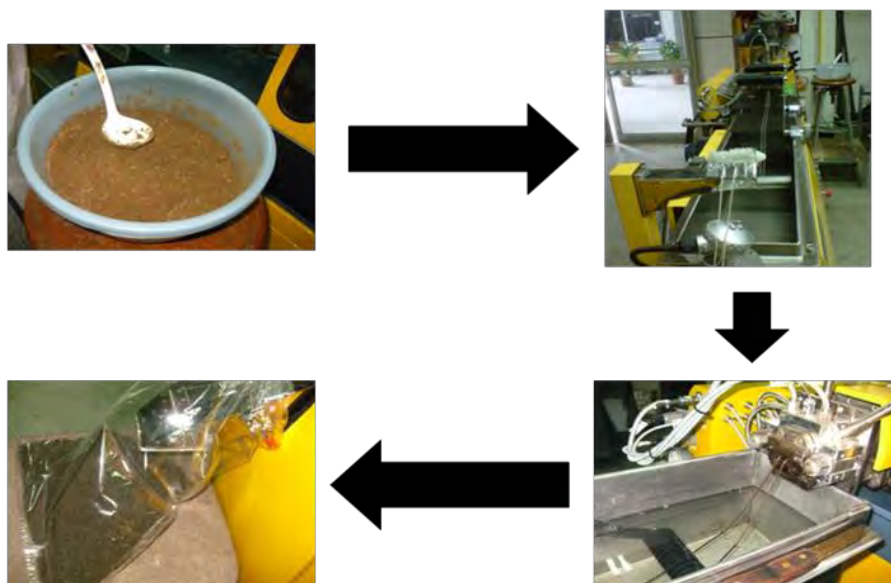


Figure 3.5 Preparation of peanut shell/PLA composite by using twin-screw extruder.

3.2.3 Preparation of PNS/PLA Composite by Using Injection Molding

The compounding pellets were injected into dumbbell specimen for tensile testing (Figure 3.6) was produced using an injection machine (Battenfeld), and the operating temperature was used in the range 150-160°C with an injection pressure 6.5 bar at screw speed 160 rpm. The mold temperature was conducted at 30-40 °C, the cooling time was used 30-45 s, and cycle time was used 30-60 s.



Figure 3.6 Dumbbell specimen for tensile testing.

3.2.4 Preparation of PNS/PLA Composite Film by Using Blown Film Extrusion

The composite films were produced using a LABTECH (model LTE20–30) single–screw extruder with $L/D = 40$ ($D = 20$ mm, and $L = 800$ mm) and annular die with outer diameter of 70 mm and inner diameter of 68.5 mm are shown in Figure 3.7. The operating temperature of blown film extrusion was operated in the range of 140–180 °C and the rotational speed was fixed at 60 rpm with the blow up ratio of 2:1.

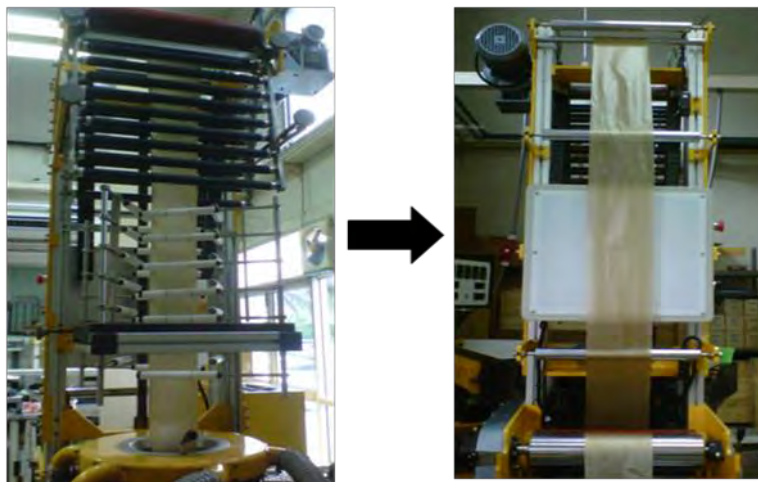


Figure 3.7 Preparation of peanut shell/PLA composite films by using blown film extrusion.

3.2.5 Preparation of Bagasse/PLA Composite Film by Using Blown Film Extrusion

The bagasse/PLA composite films were produced using a LABTECH (model LTE20–30) single–screw extruder with $L/D = 40$ ($D = 20$ mm, and $L = 800$ mm). The operating temperature of blown film extrusion (Figure 3.8) was operated in the range of 140–160 °C and the rotational speed was fixed at 60 rpm with the blow up ratio of 2:1.



Figure 3.8 Preparation of bagasse/PLA composite films by using blown film extrusion.

3.2.6 Preparation of Chemical Crosslinked PLA by Using Twin-Screw Extruder

PLA samples containing different concentrations of Bis-EMAs (1, 3, 5, and 7 phr) and DCP (0.1, 0.2, 0.3, 0.4, and 0.5 phr) were mixed in a corotating twin-screw extruder with an L/D ratio of 40 (LABTECH type LHFS1-271822). The temperature profile was maintained in the range of 140-190 °C from the feed throat to the die and the rotational speed was fixed at 10 rpm.

The rheological and thermo-mechanical testing specimens were prepared by compression molding (Wabash, model V50H-18-CX) for 5 min at 200 °C and subsequently cooled under pressure by water circulation through the plates.

3.3 Characterizations

3.3.1 Differential Scanning Calorimeter (DSC)

Differential Scanning Calorimeter was performed using a Perkin-Elmer DSC 822 under N₂ atmosphere. The samples were heated from 20 °C to 200 °C at heating rate of 10 °C/min and held at 200 °C for 5 min (1st run), then they were cooled to 20 °C at heating rate of 10 °C/min and reheated under the same

conditions (2nd run). The glass transition temperature (T_g), cold crystallization temperature (T_{cc}), and melting temperature (T_m) of each specimens were recorded from the second run. Degree of crystallization (χ_c) was calculated as:

$$\chi_c = \frac{\Delta H_m - \Delta H_{cc}}{\Delta H_{m0} \times w} \times 100 \quad (3.1)$$

ΔH_m is the enthalpy of melting, ΔH_{cc} is the enthalpy of cold crystallization, ΔH_{m0} is enthalpy of melting for 100% crystalline PLA sample, taken as 93 J/g, w is the weight fraction of PLA in the composite.

3.3.2 Thermogravimetric Analyzer (TGA)

Thermogravimetry analysis was carried out in TGA Q5 TA under a nitrogen flow (100 ml/min). The samples were measured from 30 °C to 700 °C with a heating rate of 10 °C/min. The decomposed temperature is the temperature at maximum rate of mass loss (T_{max}), of DTG curve were evaluated.

3.3.3 Tensile Tests

Tensile tests were performed using the Instron Universal Testing Machine (4206) with the crosshead speed of 50 mm/min. The specimens were prepared according to the ASTM D638 standard. Izod impact testing was performed according to ASTM D256 (notched type), and the impact strength was measured using the ZWICK 5113 Pendulum Impact Tester with the pendulum load of 21.6 J. The ten samples were used to characterize each material and their average values are reported.

Tensile testing was carried out using Universal Testing Machine (Lloyd LRX) with a 500 N load cell at crosshead speed of 50 mm/min according to ASTM D822. The film samples were prepared by cut into rectangular with a width of 10 mm, a length of 100 mm, and a thickness of 80-180 μ m. The ten samples were used to characterize each material and their average values are reported.

3.3.4 Dynamic Mechanical Analyzer (DMA)

The dynamic mechanical analysis (DMA) was performed using EPLEXOR 100N in tension mode. The sample dimensions with length of 40 mm, width of 10 mm and thickness of 1 mm were used. The measurements were carried out at a constant frequency of 1 Hz, strain amplitude of 0.1%, and a temperature range of 0-140 °C with a heating rate of 2 °C/min.

3.3.5 Biodegradability Testing

The composites bars (40×30×3 mm) were buried in sandy soil (pH 4.6-4.8) approximately 3 cm deep and put in the oven to investigate the biodegradability for 8 weeks. The temperature and moisture were kept constant at 60 ± 5 °C and 10-30 %RH. After removal from sandy soil, samples were gently washed with water and equilibrated at ambient temperature for 1 day. Samples were weighed weekly for 8 weeks. The weight loss was evaluated using the following equation:

$$\text{weight loss (\%)} = \{(w_0 - w_1) / w_0\} \times 100 \quad (3.2)$$

where w_0 and w_1 are the sample weights before and after the biodegradation tests, respectively.

3.3.6 Morphological Observation

The material microstructure was examined using a field emission scanning electron microscope (HITACHI S4800) with an acceleration voltage of 5 kV. The freeze-fractured ends of specimens were sputtering coated (HITHACHI E-1010) with a thin layer of platinum prior to analysis.

3.3.7 Water Vapor Permeability (WVP)

Water Vapor Permeability (WVP) of the films was measured by using the ASTM E96-01 standard method (ASTM, 2001b). The film was cut into 90 mm x 90 mm pieces and each piece was put onto cup which was filled 20 g of silica gel (desiccant) to produce a 0% RH under the film. Film was placed in between the cap

and the ring cover of each cup sealed with paraffin. The cups were placed in desiccators containing saturated $(\text{Mg}(\text{NO}_3)_2 \cdot 6\text{HNO}_3)$ solution (50 ± 3 %RH), which were maintained in 25 °C. The RH gradient was 50:0 (%RH outside: %RH inside the cup). The cups were weighted (± 0.0001 g) until the change of weight became stable. The amount of water permeated through the films was determined from the weight gain of the cups. The water vapor transmission rate (WVTR) and water vapor permeability (WVP) were triplicated and calculated according to:

$$\text{WVTR} = \Delta w / \Delta t \cdot A \quad (3.3)$$

$$\text{WVP} = \text{WVTR} / L \cdot \Delta p \quad (3.4)$$

Where WVTR is in $\text{g}/\text{h} \cdot \text{m}^2$, $\Delta w/\Delta t$ is rate of water gain in g/h , A is the exposed area of the film in m^2 , L is the mean thickness of film specimens in m , and Δp is the difference in partial water vapor pressure between the two sides of film specimens in Pa . The water vapor pressure on the high-stream side of the film was 2.34 kPa (i.e., saturated water vapor pressure at 20 °C), while the low-stream side is assumed to be zero.

3.3.8 Rheological Measurement

The rheological properties were measured using Anton Paar Rheometer. The measurement was run using parallel plate ($d = 25$ mm) and the gap was set at 1 mm. The samples were loaded between parallel plates and melted at 190 °C for 2 min before compressed. Frequency sweeps between 0.1 - 100 rad/s were carried out at 5% strain which is the linear viscoelastic region of the measured samples.

3.3.9 Gel Fraction

Gel fraction was measured by the weight remaining after dissolving the sample in chloroform using the following eq. 3.6

$$Gel\ fraction = \left(\frac{W_g}{W_0} \right) \times 100 \quad (3.6)$$

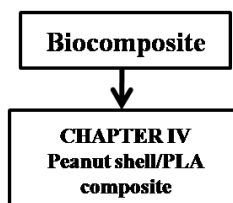
Where W_0 is initial weight (dry), W_g is the remaining weight (dry gel component) of the crosslinked sample after dissolving in chloroform at room temperature for 24 h.

Sohxlet extraction: the gel contents of the crosslinked samples were determined by extracting the soluble fraction with boiling chloroform (61-62 °C) for 2 h in a sohxlet extractor (SER 148).

3.4 Overview of Research

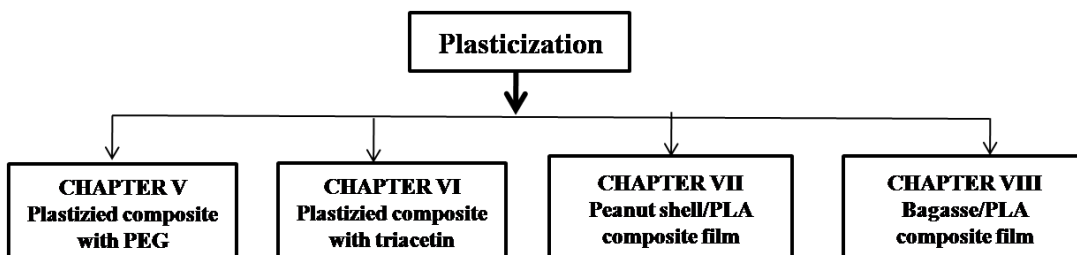
3.4.1 Biocomposite

- To improve the mechanical and biodegradable properties of PLA by adding peanut shell



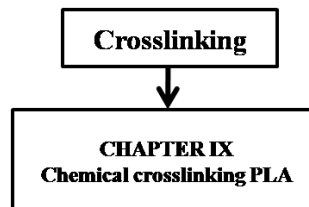
3.4.2 Plasticization

- To improve the flexibility and processibility of the composites and the composite films by adding plasticizers



3.4.3 Chemical Crosslinking

- To improve the thermal properties of PLA by adding crosslinking agent



CHAPTER IV

PREPARATION AND CHARACTERIZATION OF PLA FILLED WITH PEANUT SHELL AS COMPOSITES

4.1 Abstract

Peanut shell fiber (PNS) was combined with polylactic acid (PLA) to form biocomposites. The biocomposites, with up to 40 %wt PNS, were prepared using a twin-screw extruder. The effect of PNS content on the thermal, mechanical, thermo-mechanical, morphological, and biodegradable properties was studied. The results showed that the addition of PNS caused a reduction of the melting temperature as well as the decomposition temperature. The morphological study showed poor interfacial adhesion between the PNS and PLA matrix. The mechanical properties revealed that the maximum tensile strength and Young's modulus were at a 30 %wt PNS loading and decreased as more PNS was incorporated into the PLA matrix. The impact strength decreased with an increase in PNS content. Moreover, the addition of PNS showed significantly improvement of the storage modulus of PLA at high temperature (>80 °C). The presence of PNS enhanced the biodegradability of the biocomposites.

4.2 Introduction

Nowadays, the entitlement of environmental pollution is important issue leading to minimization of consumption and decreasing waste of non-degradable plastics such as polyethylene and polypropylene. To overcome this issue, bioplastics or biomaterials are used as alternative materials. Among those materials, biocomposites made from natural fibers and biodegradable polymers, which have been interested to replace the non-degradable plastics because they are completely decomposed under environmental conditions or composting system.

Natural fibers are used as reinforcement in biocomposites. They are composed of cellulose, hemicelluloses, lignin, etc. The amount of cellulose content in natural fibers affects directly on mechanical properties of the biocomposites. From

literature point of views, the use of natural fibers with high cellulose content, such as flax (71.00 wt%), hemp (70.20-74.70 %wt), jute (61.00-71.50 %wt), kenaf (31.00-39.00 %wt), and ramie (68.60-76.20 %wt), can enhance the mechanical properties of biocomposites [1, 2]. Surprisingly, there is no literature reporting about the use of peanut shell (PNS) as reinforcement biocomposites. Peanut shell (PNS), a natural fiber, is a waste product from the processing of peanuts. It is a substantial and low-priced agricultural by-product that is normally burned to generate energy or used for animal feed. The chemical composition of PNS is composed of cellulose (37.68 %wt), hemicelluloses (16.88 %wt), lignin (29.03 %wt), and oil (0.92 %wt). In addition, the potential applications of PNS can produce composites for ceilings, wall covering panels, as well as fiberboard manufacture [3, 4]. Therefore, the development of PNS as a reinforcement-based biocomposite is becoming a viable option.

Poly(lactic acid) (PLA), one type of biodegradable thermoplastic derived from renewable resources—corn, starch, tapioca product, and sugarcane bagasse—is considered an alternative biodegradable polymer in biocomposites [5]. According to Bax et al. [6], cordenka reinforced PLA at a fiber mass proportion of 30 %wt showed high impact strength and tensile strength, while a biocomposite made from PLA and flax showed high Young's modulus. Supported by Chen et al. [7], the addition of 30 %wt sugar beet pulp into the PLA biocomposite resulted in increasing modulus but drastically reduced yield strength and elongation. Ochi [8] found that the tensile and flexural strength of kenaf fiber reinforced PLA biocomposites increased linearly to 50 %wt kenaf fiber. Moreover, Han et al. reported that the flexural modulus of kenaf/PLA biocomposite increased with kenaf fiber up to 40 %wt [9]. The improvement of mechanical properties of the PLA biocomposites with ramie and jute fibers, up to 30 %wt, was shown in the study of Tao et al. [10]. Jang et al. [11] studied coconut fiber reinforced PLA biocomposites which showed an increase in the tensile strength and Young's modulus with increasing weight fractions of coconut fiber.

In the present time, the biodegradable property is the one reason that has attracted many researchers to produce biocomposites and to study their biodegradation in various conditions. Teramoto et al. [12] studied the biodegradation

of abaca fiber/PLA biocomposites in soil that showed 10% weight loss after 60 days. Ochi [8] found that mass of kenaf/PLA biocomposites decreased 38% within 4 weeks in a garbage-processing machine. In a *Burkholderia cepacia* BCRC 14253 compost, coconut fiber/maleic anhydride-grafted PLA was degraded over 92% after 21 days that has been reported by Wu et al. [13]. Pradhan et al. [14] found that wheat straw/PLA and soy straw/PLA biocomposites were degraded 90% in the composting bioreactor after 70 days. Banana fiber/PLA biocomposites showed 80-100% degradation within 25 days in bacterial medium as reported by Jandas et al. [15].

In the current study, PNS/PLA biocomposites were fabricated by twin-screw extrusion followed by injection molding. The influence of PNS content on the thermal, mechanical, thermo-mechanical, and morphological properties of the biocomposites has been investigated. Furthermore, the effect of PNS content on biodegradable properties was evaluated and discussed.

4.3 Experimental

4.3.1 Materials

Polylactic acid (PLA), 4043D grade ($\rho = 1.25 \text{ g/cm}^3$ and $T_m = 210 \text{ }^\circ\text{C}$), was purchased from Nature-Work LLC. Peanut shell (PNS) was ground to 5-100 μm (aspect ratio = 2.52-5.16) with a moisture content of $5.19 \pm 0.11\%$ and $\rho = 1.63 \text{ g/cm}^3$. The compositions of peanut shell are cellulose (37.68 %wt), hemicelluloses (16.88 %wt), lignin (29.03 %wt), and oil (0.92 %wt). Irganox 1010 ($\rho = 1.15 \text{ g/cm}^3$ and $T_m = 110\text{-}125 \text{ }^\circ\text{C}$) and Quent 68 ($T_m = 185 \text{ }^\circ\text{C}$) from Ciba Specialty Chemicals, were used as stabilizers.

4.3.2 Sample Preparation

The PLA pellets and PNS were dried at $60 \text{ }^\circ\text{C}$ for 24 h before processing. The PLA and PNS, at 10, 20, 30, 40 %wt, were mixed with 0.5 phr of each stabilizer (Irganox 1010 and Quent 68). All melt blending was performed using a LABTECH (type LHFS1-271822) corotating twin-screw extruder with an L/D ratio of 40 ($D = 20 \text{ mm}$, and $L = 800 \text{ mm}$). Table 4.1 summarizes the composition of each formulation. The temperature profile was maintained in the range of $120 \text{ }^\circ\text{C}$ to $170 \text{ }^\circ\text{C}$ from the feed throat to the die, with the rotational speed was fixed at 40 rpm.

Table 4.1 Composition of each formulation

Material				Code
Peanut shell (wt%)	PLA (wt%)	Antioxidant (phr)		
		Irganox 1010	QUENT 68	
0	100	0.5	0.5	PLA
10	90	0.5	0.5	10PNS
20	80	0.5	0.5	20PNS
30	70	0.5	0.5	30PNS
40	60	0.5	0.5	40PNS

The compounding pellets were injected into dumbbell specimen for tensile testing was produced using an injection machine (Battenfeld), and the operating temperature was 150 °C to 160 °C with an injection pressure of 6.5 bar at a screw speed of 160 rpm. The mold temperature was conducted at 30 °C to 40 °C. Table 4.2 shows the cooling time and cycle time of each formulation.

Table 4.2 Cooling time and cycle time of each sample

Sample	Cooling time (s)	Cycle time (s)
PLA	30	45
10PNS	30	45
20PNS	30	45
30PNS	30	45
40PNS	45	60

4.3.3 Characterization

4.3.3.1 *Thermogravimetric Analyzer (TGA)*

Thermogravimetric analysis was carried out with a TGA Q5 TA under a nitrogen flow (100 ml/min). The samples were measured from 30 °C to

500 °C with a heating rate of 10 °C/min. The decomposition temperature and temperature at maximum rate of mass loss (T_{\max}), of derivative thermogravimetric curve (DTG) were evaluated.

4.3.3.2 Differential Scanning Calorimeter (DSC)

Differential scanning calorimeter was performed using a Perkin–Elmer DSC 822 under N_2 atmosphere. The samples were heated from 10 °C to 200 °C at a heating rate of 10 °C/min and held at 200 °C for 5 min (1st run), then they were cooled to 10 °C at a heating rate of 10 °C/min and reheated under the same conditions (2nd run). The glass transition temperature (T_g), cold crystallization temperature (T_{cc}), and melting temperature (T_m) of each specimens was recorded from the second run. The degree of crystallization (χ_c) was calculated as:

$$\chi_c = \frac{\Delta H_m - \Delta H_{cc}}{\Delta H_{m0} \times w} \times 100 \quad (4.1)$$

Where ΔH_m is the enthalpy of melting, ΔH_{cc} is the enthalpy of cold crystallization, ΔH_{m0} is enthalpy of melting for the 100% crystalline PLA sample, taken as 93 J/g, w is the weight fraction of PLA in the composite [16].

4.3.3.3 Morphological Observation

The material microstructure was examined using a field emission scanning electron microscope (FE–SEM; HITACHI S4800) with an acceleration voltage of 5 kV. The freeze–fractured ends of specimens were sputtering coated (HITHACHI E–1010) with a thin layer of platinum prior to analysis.

4.3.3.4 Tensile Tests

Tensile tests were performed using an Instron Universal Testing Machine (4206) with a crosshead speed of 50 mm/min. The specimens were prepared according to ASTM D638 standard.

Impact testing was performed according to ASTM D256 (notched type), and the impact strength was measured using the ZWICK 5113 pendulum impact tester with a pendulum load of 21.6 J. Ten samples were used to characterize each material and average values were reported.

4.3.3.5 Dynamic Mechanical Analyzer (DMA)

Dynamic mechanical analysis (DMA) was performed using an EPLEXOR 100N in tension mode. The sample dimensions with a length of 40 mm, width of 10 mm, and thickness of 3 mm were used. The measurements were carried out at a constant frequency of 1 Hz, strain amplitude of 0.1%, and a temperature range of 0 °C to 120 °C, with a heating rate of 2 °C/min.

4.3.3.6 Biodegradability Testing

The composite bars (40×30×3 mm) were buried in a pan of approximately 3 cm of sandy soil (pH 4.6-4.8) and put in the oven to investigate biodegradability. The temperature and moisture were kept constant at 60 ± 5 °C and 10-30 %RH. After removal from the sandy soil, samples were gently washed with water and equilibrated at ambient temperature for 1 day. The samples were weighed weekly for 8 weeks. The weight loss was evaluated using the following equation:

$$\text{weight loss (\%)} = \{(w_0 - w_1) / w_0\} \times 100 \quad (4.2)$$

where w_0 and w_1 are the sample weights before and after the biodegradation tests, respectively.

4.3.3.7 Density Tests

The sample pellets were measured the density by using ultracycnometer (ultracycnometer 1000 version 2.5) under helium flow.

$$\rho_{comp} = \rho_f V_f + \rho_m (1 - V_f) \quad (4.3)$$

Where ρ_{comp} is the density of composite, ρ_f and ρ_m are the density of fiber and matrix, respectively. V_f is the volume fraction of fiber.

4.4 Results and Discussion

4.4.1 Thermogravimetry

Figure 4.1 shows the thermogravimetric (TG) and derivative thermogravimetric (DTG) curves of PLA and the biocomposites. The decomposed temperature is the temperature at the maximum rate of mass loss (T_{\max}), or DTG curve. Considering the thermogram of PNS, a three-step transition is found where the first mass loss gradually occurs at ~ 100 °C, which contributes to a loss of moisture content of ~ 5 %wt. The second transition is associated with the hemicelluloses together with extractive residue decomposition at T_{\max} of ~ 264.3 °C. The third transition is associated with the cellulose at T_{\max} of ~ 339.5 °C and a char residue content of 32.1 %wt. The PLA sample shows a single transition at T_{\max} of ~ 357.5 °C and has higher decomposition temperature than the PNS. Moreover, the biocomposites are lower decomposition temperature than that of PLA because moisture in the PNS can encourage chain scission of the PLA ester bonds [17]. Since hydrolysis of PLA chains influenced by moisture as well as temperature, it is possible to accelerate the degradation of PLA. Thus an increase of PNS content resulted in a decrease of T_{\max} of the biocomposites, which is due to a large amount of hydrolyzed PLA chains together with low thermal stability of PNS.

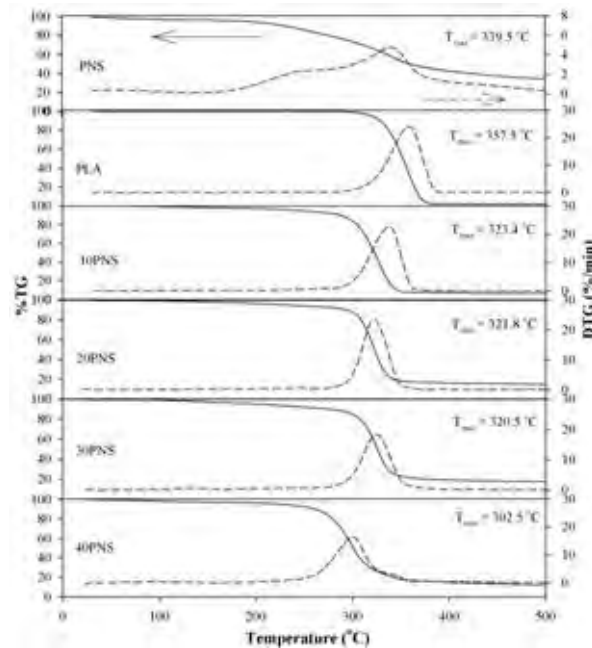


Figure 4.1 TGA and DTG curves of PNS, PLA, and the composites.

4.4.2 Density Tests

The results reveal that the density values of PLA and PNS are 1.25 g/cm^3 and 1.63 g/cm^3 , respectively. It was found that density of the biocomposites increased from 1.25 g/cm^3 to 1.35 g/cm^3 when the addition of PNS into PLA up to 30 %wt, as seen in Table 4.3. In the case of adding PNS over 30 %wt, the density decreased to 1.28 g/cm^3 (40PNS sample). In addition, the biocomposites show that the theoretical density has the same value as the experimental density except 40PNS sample (Table 4.3). For 40PNS sample, the experimental density is 1.28 g/cm^3 while the theoretical density is 1.37 g/cm^3 . This indicated that volume increases about 4.77% since the density is inversely proportional to the volume. It can be noted that PNS is a major factor effect on moisture absorption in the biocomposites. So, the increasing PNS content means that increase of moisture content in the biocomposites leads to accelerate biodegradation due to hydrolysis of PLA chains [18]. Thereby, the moisture loss from PNS can induce porous or void structures in the biocomposite (as seen in FE–SEM result). It can be confirmed that the increase in volume causes by the presence of void in the biocomposite resulting in a reduction of density.

4.4.3 Crystallization and Melting Behavior of The Composites

Figure 4.2(a) and Table 4.3 show the first heating scan of PLA and the biocomposites. The results demonstrate that the biocomposites show slightly lower T_g than that of PLA. This implies that the hydrolytic degradation of PLA chains causes by moisture content in PNS. Perhaps another reason is a small amount of oil content in PNS (0.92 %wt) quietly effect on T_g leading to plasticizing effect. Moreover, it can be seen that 10PNS and 20PNS samples show two melting peaks and also observe cold crystallization peak, while 30PNS and 40PNS samples show one melting peak and cold crystallization peak disappear. Hence, cold crystallization can induce new crystalline of PLA during heating, which show possibly two melting peaks. The behavior to form two melting peaks reported that lamellar was rearranged during crystallization and the low-temperature peak (T_{m1}) formed the cold crystalline, while the high-temperature peak (T_{m2}) formed the original crystalline [16, 19].

Figure 4.2(b) and Table 4.3 show the second heating scan of PLA and the biocomposites. It was found that the T_g of the biocomposites did not change with increasing PNS up to 30 %wt when compared to PLA. Notably, the 40PNS sample shows a reduction of T_g . This result can be explained as moisture losses in PNS that hydrolyzes the PLA chains during the first heating scan, which finally generate some short chains of PLA in the system such as lactic acid, oligomers, and other water soluble products [20]. As a result of this, their short chains can act as plasticizer to increase chain mobility during the second heating resulting in a decreasing of T_g . In addition, the biocomposites have lower T_{cc} and T_m than that of PLA. A similar effect has also been observed in other PLA biocomposites [21]. The biocomposites show lower T_{cc} (~87-109 °C) than that of PLA (128 °C). The T_{cc} of the biocomposites also decreased with increasing PNS content because PNS facilitated the crystallization process of PLA. The T_m of the biocomposites shows two peaks and T_m does not change with increasing PNS content (except 40PNS sample). Moreover, the crystallinity of the biocomposites increased when compared to PLA, which indicates that PNS is an effective nucleating agent for PLA. The crystallinity of the biocomposites increased with PNS content up to 30 %wt. The addition of PNS at 40

%wt shows decrease in crystallinity due to the presence of many void structures in the sample as mentioned in the density result.

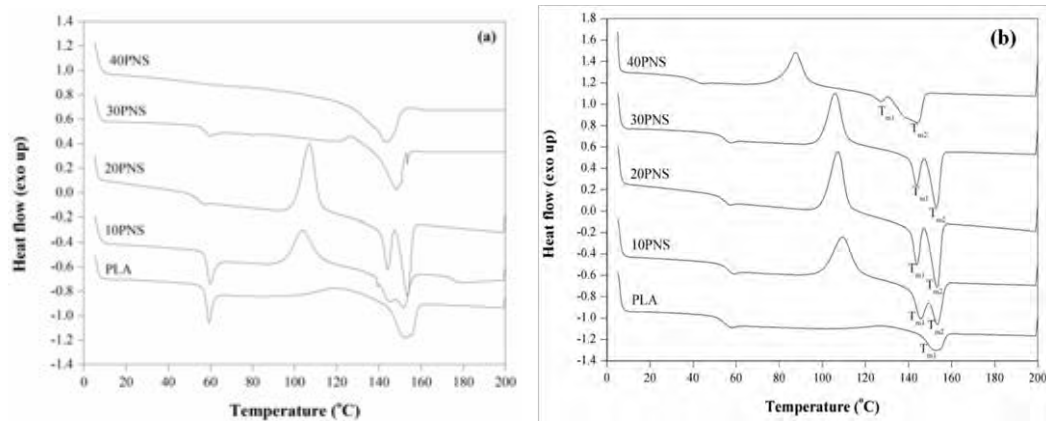


Figure 4.2 DSC thermograms of (a) first heating scan and (b) second heating scan of PLA and the composites.

Table 4.3 Thermal properties of the second heating scan and density of PLA and the composites

Sample	T_g (°C)	T_{cc} (°C)	ΔH_{cc} (J/g)	$T_{m1}; T_{m2}$ (°C)	ΔH_m (J/g)	χ_c (%)	Density (g/cm ³)	
							Theory	Experiment
PLA	51.1	128.4	4.6	152.7	8.3	3.98	1.25	1.25
10PNS	51.9	109.3	23.9	145.4; 153.4	28.1	5.02	1.27	1.25
20PNS	51.1	107.2	25.2	143.9; 153.3	30.0	6.45	1.31	1.31
30PNS	51.7	105.9	22.1	143.8; 153.1	28.0	9.06	1.34	1.35
40PNS	36.0	87.6	18.5	127.5; 144.1	21.4	5.19	1.37	1.28

4.4.4 Morphology Properties

The morphology of PNS, PLA, and 30PNS is observed by FE-SEM, images shown in Figure 4.3. The PNS is the particulate matter seen in Figure 4.3a and Figure 4.3b. It is estimated that the average size is 5–100 μm and aspect ratio of 2.52–5.16. The PNS shows roughness on the surface and agglomeration. The PLA sample reveals a smooth and uniform fractured surface containing some cracking

(Figure 4.3c). In Figure 4.3d, the PNSs are in good distribution in the PLA matrix, which suggests that processing under high shear rate improves the distribution of the PNS. Moreover, several voids occurring on the surface of the composites are due to the moisture losses from PNS during the processing. Figure 4.3e shows that PNS has pulled out and aggregated in the PLA matrix indicating poor adhesion between the PNS and PLA matrix.

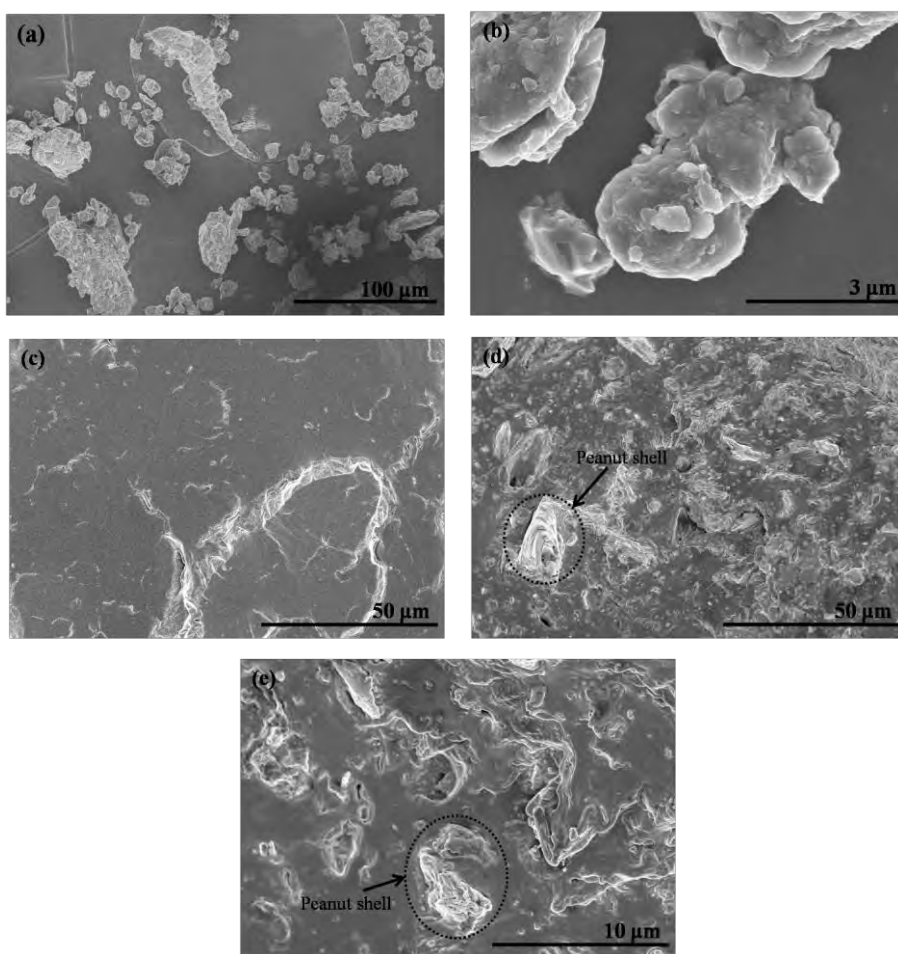


Figure 4.3 Morphological images of (a) PNS at 0.4 k magnification, (b) PNS at 15 k magnification, (c) PLA, (d) 30PNS at 1 k magnification, and (e) 30PNS at 5 k magnification.

4.4.5 Mechanical Properties

Stress–strain curves and mechanical values of PLA and the biocomposites are shown in Figure 4.4 and Table 4.4, respectively. PLA has greater tensile strength than that of the biocomposites (except 30PNS). For the 10-20 %wt PNS loading, the tensile strength did not improve when compared to PLA because a low amount of PNS content was not adequate to transfer stress effectively. Moreover, the results show that both tensile modulus and strength of the biocomposites improved when increasing PNS up to 30 %wt, while the elongation at break decreased. This suggests that the contribution of crystallinity to enhance strength and Young's modulus in the biocomposites agreed well with degree of crystallization as seen in DSC results (Table 4.3). The incorporation of 30 %wt PNS content improved the modulus of PLA from 1,858.53 MPa to 2,261.42 MPa and the tensile strength increased from 64.32 MPa to 67.02 MPa, while the elongation at break decreased from 10.09% to 6.51%. The maximum tensile strength was at 30 %wt short fiber loading and decreased as more fiber was incorporated into the matrix, also reported by Ibahim et al [22]. It can be noted that Young's modulus of PLA increased by adding PNS, whereas an increase of tensile strength indicated that there was good stress transfer from the matrix to PNS. However, higher PNS content did not improve either tensile strength or modulus in the biocomposites due to agglomeration and poor dispersion of PNS in the PLA matrix. Tao et al. also had the same finding in which the addition of fibers decreased the mechanical properties of biocomposites [10]. Furthermore, the many voids in the sample are also the defect to decrease the mechanical properties.

The notched izod impact strength of PLA and the biocomposites is shown in Table 4.4. When compared with PLA, the impact strength of the biocomposites is reduced. This suggests that the presence of PNS can induce the point of stress and initiate cracking in PLA matrix. In addition, the impact strength of the biocomposites decreased with an increase of PNS content because more PNSs have possibly high agglomerations, which are the weak points starting to crack and then the biocomposite easily to failure.

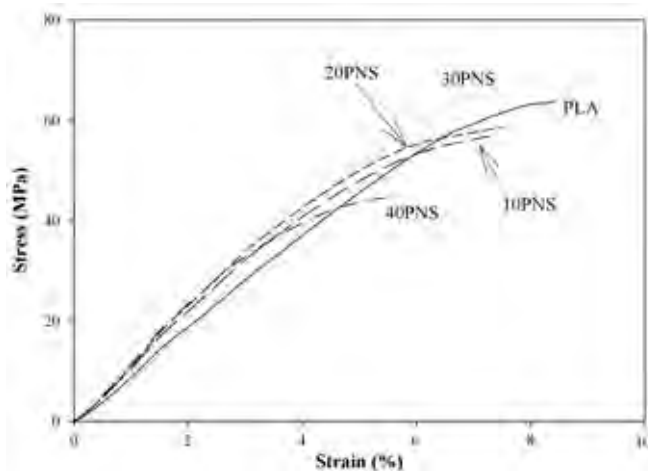


Figure 4.4 Stress–Strain curves of PLA and the composites.

Table 4.4 Mechanical properties of PLA and the composites

Sample	Tensile strength (MPa)	Young's modulus (MPa)	Elongation at break (%)	Impact testing (kJ/m ²)
PLA	64.32±1.50	1858±20	10.09±9.52	9.10±0.29
10PNS	59.21±1.12	2106±53	7.83±1.09	8.40±0.50
20PNS	64.34±0.73	2188±57	7.01±0.67	7.60±0.83
30PNS	67.02±0.46	2261±31	6.51±0.63	7.60±0.20
40PNS	55.48±1.83	1946±117	5.89±1.92	6.10±1.61

4.4.6 Thermo-Mechanical Properties

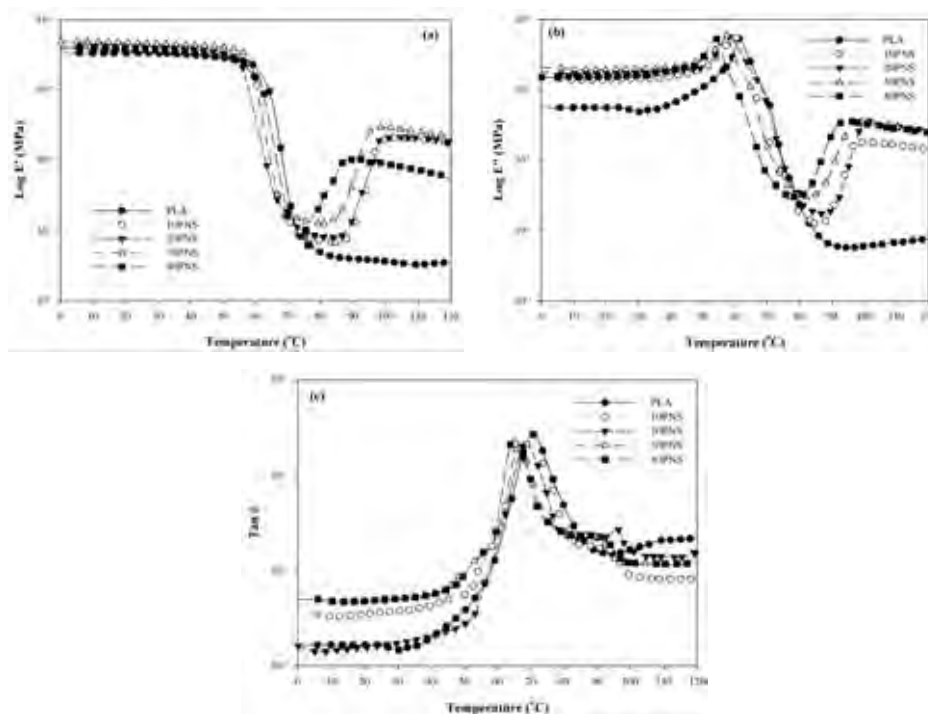


Figure 4.5 Temperature dependence of (a) E' , (b) E'' , and (c) $\tan \delta$ of PLA and the composites.

Figure 4.5(a) and Table 4.5 show the effect of temperature on storage modulus (E'), which relates directly to the stiffness of the biocomposites. At ambient temperature, the E' of the biocomposite is higher than that of PLA. This result suggests that the improvement in the stiffness is due to the addition of PNS into PLA matrix. It should be noted that the E' of the biocomposites increased with an increasing PNS content up to 30 %wt. This agrees well with the modulus results obtained from the mechanical testing (Table 4.4). In the glass transition region, PLA and the biocomposites showed an abrupt drop in the E' . As the temperature increased, the E' of the biocomposites showed an abrupt increase. This change in the E' is attributed to cold crystallization since it happened at a temperature close to the cold crystallization temperature. The biocomposites achieved cold crystallization at ~ 87 - 109 °C, while PLA's cold crystallization appeared at ~ 128 °C (small broad peak), as

observed in DSC results (Table 4.3). At 100 °C, the biocomposites displayed higher the E' when compared to PLA, which suggest that the presence of PNS can induce early cold crystallization. PNS induced PLA crystallization and strongly improved the E' of PLA. This result confirms that the adding PNS into the PLA matrix enhances the rigidity of PLA. Moreover, the E' of the biocomposites at 120 °C was still higher than that of PLA. This means that the biocomposites can bear loads at higher temperatures more efficiently than that of PLA because of greater rigidity and easier cold crystallization before the melting stage.

Figure 4.5(b) and Table 4.5 show the loss modulus (E''), or ability of the material to dissipate energy, which is related to viscosity. The biocomposites reveal a slightly higher magnitude peak of the E'' when compared to PLA. This suggests that that addition of PNS promotes high viscosity, which produces more dissipation energy. This means that the biocomposites are more difficult to process when compared to PLA. Moreover, the E'' of the biocomposites slightly shifts to a lower temperature with a higher loss modulus value when PNS content increased. As the temperature increased, the E'' was largely reduced.

The ratio of E'' to E' is measured as a loss factor, or $\tan \delta$, as observed in Figure 4.5(c). Since $\tan \delta$ represents the T_g of the material, The T_g of the biocomposites shows shift to a lower temperature than that of PLA and the T_g trend is in agreement with DSC results, as shown in Figure 4.2 and Table 4.3. Moreover, the damping reveals that the molecular motion of PLA is greater when compared to the biocomposites. The limited molecular motion in the biocomposites agrees well to the stiffness due to the presence of PNS and a developed crystalline structure.

Table 4.5 E' and E'' (MPa) of PLA and the composites

sample	T _g from Tan δ	30 °C		100 °C		120 °C	
		E'	E''	E'	E''	E'	E''
PLA	70.80	3326.74±31.24	48.31±4.21	3.66±0.64	0.60±0.04	3.54±1.02	0.76±0.03
10PNS	66.70	3775.17±43.75	142.34±5.53	195.34±6.56	17.66±2.64	170.24±7.56	13.71±0.53
20PNS	66.60	3889.70±34.54	178.50±3.64	204.91±10.04	35.94±2.54	173.83±6.03	26.99±1.45
30PNS	63.50	4558.92±20.53	197.75±8.67	284.61±8.57	33.99±5.08	213.66±10.11	25.51±0.63
40PNS	59.90	3653.78±54.24	158.13±5.67	84.61±9.34	31.96±7.35	83.66±11.49	24.56±1.59

4.4.7 Biodegradation Study

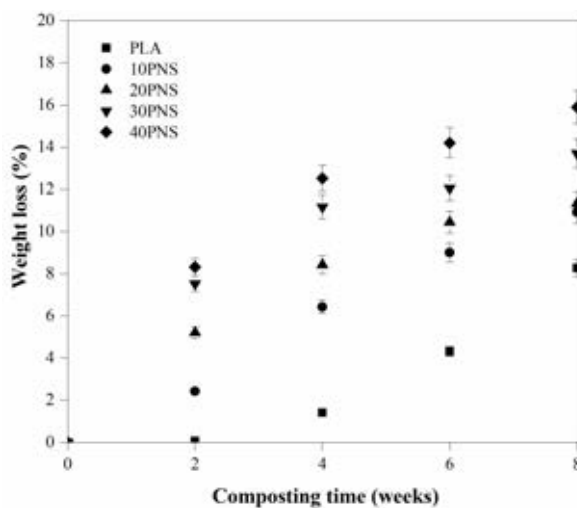


Figure 4.6 Relationship between weight loss and composting time of PLA and the composites.

The biodegradability of PLA and the biocomposites is illustrated in Figure 4.6. The biocomposites have clearly higher weight loss than that of PLA. The biodegradability of the biocomposites is ~10-16% within 8 weeks of composting in soil at 60 °C. The weight loss increased with PNS content because the PNS can absorb moisture during composting and then the moisture accelerated the hydrolysis of PLA chains. The principal of PLA degradation, the first state is usually hydrolyzed the PLA chains, and the second state is the degradation by microorganisms in soil starting from the surface to the interior of the sample [20, 23]. The order of biodegradation can be determined as follows: 40PNS>30PNS>20PNS>10PNS>PLA. The result clearly indicates that the addition of PNS enhanced the biodegradation of the biocomposites. Similar study of biodegradation of other biocomposites has been reported [14].

4.5 Conclusion

This study prepared PLA filled with PNS as the biocomposites. It revealed that the amount of PNS strongly affected both thermal and mechanical properties of the biocomposites in comparison to PLA. The TGA results revealed that the biocomposites had less heat stability than PLA. The DSC results demonstrated that PNS can act as a nucleating agent for cold crystallization of PLA. Moreover, the crystallinity of the biocomposites increased and led to enhancement in modulus. While, the biocomposites had slightly lower thermal properties (T_g , T_{cc} , T_m) than that of PLA. The density of the biocomposites increased with the addition of PNS into PLA up to 30 %wt. The experimental density of the biocomposites was the same as the theoretical density except the 40PNS sample. In addition, the morphology exhibited poor adhesion between the PNS and PLA matrix, with an aggregation of PNS in the biocomposites. The mechanical properties of the biocomposites increased with the addition of PNS firstly, and then decreased when the PNS loading was over 30 %wt. The biocomposites were higher the E' than that of PLA. When increasing temperature beyond T_g , the E' abruptly increased suggesting cold crystallization occurred. Moreover, the biodegradation study revealed that PNS enhanced the biodegradability of the biocomposites. The properties of the composites were summarized in Table 4.6.

Table 4.6 Summary of the properties of the composites

Properties		Decrease	Increase
Thermal properties (T_d, T_g, T_{cc}, T_m)		-	
Mechanical properties	Tensile strength		++
	Young's modulus		+++
	Elongation at break	--	
	Impact strength	--	
Thermo-mechanical properties	Storage modulus		+++
	Loss modulus		+++
Biodegradabation study			+++

Note: The symbols, that increase from high to low, are +++, ++, and +, respectively.

The symbols, that decrease from high to low, are ---, --, and -, respectively.

In Table 4.6, It can be seen that the elongation at break and impact strength of the composites did not improve, and further improve these properties by plasticization method as discussed in Chapter V and VI.

4.6 Acknowledgement

Financial support has been granted by National Research Council of Thailand (NRCT).

4.7 References

- [1] F.L. Digabel and L. Averous, "Effects of lignin content on the properties of lignocellulose-based biocomposites," Carbohydrate Polymers, vol. 66, pp. 537-545, 2006.
- [2] K. Goda and Y. Cao, "Research and development of fully green composites reinforced with natural fibers," Journal of Solid Mechanics and Materials Engineering, vol. 1, pp. 1073-1084, 2007.
- [3] O.O. Fasina, "Physical properties of peanut hull pellets," Bioresource Technology, vol. 99, pp. 1259-1266, 2008.
- [4] M. Akgu and A. Tozluoglu, "Utilizing peanut husk (*Arachis hypogaea* L.) in the manufacture of medium-density fiberboards," Bioresource Technology, vol. 99, pp. 5590-5594, 2008.
- [5] L.-T. Lim, R. Auras, and M. Rubino, "Processing technologies for poly(lactic acid)," Progress in Polymer Science, vol. 33, pp. 820-852, 2008.
- [6] Bax, B. and J. Mussig, "Impact and tensile properties of PLA/Cordenka and PLA/flax composites," Composites Science and Technology, vol. 68, pp. 1601-1607, 2008.
- [7] F. Chen, L. Liu, P.H. Cooke, K.B. Hicks, and J. Zhang, "Performance enhancement of poly(lactic acid) and sugar beet pulp composites by improving interfacial adhesion and penetration," Industrial & Engineering Chemistry Research, vol. 47, pp. 8667-8675, 2008.
- [8] S. Ochi, "Mechanical properties of kenaf fibers and kenaf/PLA composites," Mechanics of Materials, vol. 40, pp. 446-452, 2008.
- [9] S.O. Han, , M. Karevan, I.N. Sim, M.A. Bhuiyan, Y.H. Jang, J. Ghaffar, and K. Kalitzidou, "Understanding the reinforcing mechanisms in kenaf fiber/PLA and kenaf/PP composites: a comparative study," International Journal of Polymer Science, vol. 2012, pp. 8, 2012.

- [10] Y. Tao, L. Yan, and R. Jie, "Preparation and properties of short natural fiber reinforced poly(lactic acid) composites," Transaction of Nonferrous Metals Society of China, vol. 19, pp. 651-655, 2009.
- [11] J.Y. Jang, T.K. Jeong, H.J. Oh, J.R. Youn, and Y.S. Song, "Thermal stability and flammability of coconut fiber reinforced poly(lactic acid) composite," Composites: Part B, vol. 43, pp. 2434-2438, 2012.
- [12] N. Teramoto, K. Urata, K. Ozawa, and M. Shibata, "Biodegradation of aliphatic polyester composites reinforced by abaca fiber," Polymer Degradation and Stability, vol. 86, pp. 401-409, 2004.
- [13] C.S. Wu, "Renewable resource-based composites of recycled natural fibers and maleated polylactide bioplastic: Characterization and biodegradability," Polymer Degradation and Stability, vol. 94, pp. 1076-1084, 2009.
- [14] R. Pradhan, M. Misra, L. Erickson, and A. Mohanty, "Compostability and biodegradation study of PLA-wheat and PLA-soy straw based green composites in simulated composting bioreactor," Bioresource Technology, vol. 101, pp. 8489-8491, 2010.
- [15] P.J. Jandas, S. Mohanty, S.K. Nayak, and H. Srivastava, "Effect of surface treatments of banana fiber on mechanical, thermal, and biodegradability properties of PLA/banana fiber biocomposites," Polymer Composites, DOI 10.1002/pc.21165, pp. 1689-1700, 2011.
- [16] K.Y. Lee, J.J. Blaker, and A. Bismarch, "Surface functionalisation of bacterial cellulose as the route to produce green polylactide nanocomposites with improved properties," Composites Science and Technology, vol. 69, pp. 2724-2733, 2009.
- [17] Y.Q. Zhao, H.Y. Cheung, K.T. Lau, C.L. Xu, D.D. Zhao, and H.L. Li, "Silkworm silk/poly(lactic acid) biocomposites: Dynamic mechanical, thermal and biodegradable properties," Polymer Degradation and Stability, vol. 95, pp. 1978-1987, 2010.
- [18] H.-Y. Cheung, K.T. Lau, Y.F. Pow, Y.Q. Zhao, and D. Hui, "Biodegradation of a silkworm silk/PLA composite," Composites: Part B, vol. 41, pp. 223-228, 2010.

- [19] O. Martin, and L. Averous, "Poly(lactic acid): plasticization and properties of biodegradable multiphase systems," Polymer, vol. 42, pp. 6209-6219, 2001.
- [20] B.S. Ndazi and S. Karlsson, "Characterization of hydrolytic degradation of polylactic acid/rice hulls composites in water at different temperatures," Express Polymer Letters, vol 5, no.2, pp. 119-131, 2011.
- [21] M.D. Sanchez-Garcia, E. Gimenez, and J.M. Lagaron, "Morphology and barrier properties of solvent cast composites of thermoplastic biopolymers and purified cellulose fibers," Carbohydrate Polymers, vol. 71, pp. 235-244, 2008.
- [22] N.A. Ibrahim, W.M.Z.W. Yunus, M. Othman, K. Abdan, and K.A. Hadthon, "Poly(Lactic Acid) (PLA)-reinforced kenaf bast fiber composites: The effect of triacetin," Journal of Reinforced Plastics and Composites, vol. 29, pp. 1099-1111, 2010.
- [23] Y.X. Wang, L. Wang, M. Zhang, X.L. Wang, and Y.Z. Wang, "Biodegradation behavior of P(3HB, 4HB)/PLA blends in real soil environments," Polymer Testing, vol. 32, pp. 60-70, 2013.

CHAPTER V
THERMO-MECHANICAL BEHAVIOR OF PEANUT SHELL/PLA
COMPOSITE MODIFIED BY POLYETHYLENE GLYCOL

5.1 Abstract

Green composites were prepared from peanut shell (PNS) and polylactic acid (PLA) plasticized with polyethylene glycol (PEG) in order to improve thermo-mechanical properties. The added PEG in the composites showed improvement of PLA molecular mobility as seen by the reduction of glass transition, cold crystallization, and melting temperature. Moreover, plasticized composite showed decrease the decomposition temperature when compared to unplasticized composite. The morphological study of plasticized composites revealed good dispersion of PNS in the PLA matrix. The thermo-mechanical properties showed the enhancement of PLA performance at high temperature use by the incorporation of PNS together with PEG due to cold crystallization at a high temperature which improved storage modulus. The tensile strength and Young's modulus of plasticized composites decreased while the elongation at break and impact strength increased with the increasing PEG content. The added PEG into the composites showed improvement of the biodegradability.

5.2 Introduction

Due to an ever increasing demand for plastics, numerous types of biodegradable material have been developed from natural resources in order promote environmental friendly products. Polylactic acid (PLA) is the most popular bioplastic derived from renewable resources which available used for packaging materials. However, it is brittleness limited its application. The plasticization is the one method of modifying PLA which can be altered the brittleness. Several plasticizers have been used in PLA such as triacetin, glycerol, citrate esters, and partial fatty acid esters, as well as polyethylene glycol. Polyethylene glycol (PEG) was used as plasticizer for PLA in this study. According to the literature, Sheth et al. [1] found that the blending

of PLA and PEG were miscible blends in the compositions less than 50/50. The tensile strength of PLA/PEG blends was decreased with the increasing PEG content. Martin et al. [2] studied the thermal properties of plasticized PLA with various plasticizers compared to PLA showed that PEG can be regarded as the most efficient plasticizer of PLA. These results were also found in Kulinski et al. [3] as reported about plasticized PLA with PEG mentioned that the loading PEG decreased the glass transition temperature (T_g) and increased the ability of PLA chains to cold crystallization. Supported by Byun et al., [4] the incorporation of PEG into PLA decreased T_g and enhanced the elongation at break causes reducing in brittleness.

Furthermore, in order to develop PLA-based composites or green composite has been become attractive in recent year. Commonly, the composites of PLA reinforced with natural fibers include cotton, hemp, kenaf, flax, as well as ramie have been prepared and studied [5]. Surprisingly, there is not literature examining the used of peanut shell/PLA composites. Peanut shell (PNS), a natural fiber material, is composed of cellulose, lignin, protein, and carbohydrates[6]. It can used to produce green composites for ceilings, wall covering panels, as well as fiberboard manufacture [7, 8]. Considerable effort has been modified green composites by blending with PEG. Masirek et al. [9] studied the plasticization of hemp/PLA composites with PEG decreased the modulus with the increasing PEG content in PLA amorphous phase. Qu et.al [10] found that the added PEG into the PLA/cellulose nanofibrils composites showed increase in the tensile strength and elongation because PEG improved the intermolecular interaction between hydrophobic PLA and hydrophilic cellulose nanofibrils. The improvement of the toughness of PLA/starch composites by adding PEG shown in the study of Wang et al. [11].

Previously, our research group has prepared PNS/PLA composites. The results showed that the improvement of tensile strength and modulus of the composites with the addition of PNS was up to 30 %wt. Therefore, the PNS content of 30 %wt was chosen to prepare PLA/PNS composites together with PEG by the melt mixing process. The effects of PEG content on thermal, thermo-mechanical, mechanical, morphological, as well as biodegradable properties of the composites were investigated.

5.3 Experimental

5.3.1 Materials

PLA, grade 4043D ($\rho = 1.25 \text{ g/cm}^3$, $\delta = 21.42 \text{ MPa}^{1/2}$, and $T_m = 210 \text{ }^\circ\text{C}$), was purchased from Nature-Work LLC. PNS ($\rho = 1.63 \text{ g/cm}^3$) was ground to 5-100 μm (aspect ratio=2.52-5.16) with a moisture content of 5.19 ± 0.11 . PEG ($M_w \approx 400 \text{ g/mol}$, $\delta = 20.2 \text{ MPa}^{1/2}$, and $\rho = 1.124 \text{ g/cm}^3$) was purchased from Fluka Analytical. Irganox 1010 and Quent 68 from Ciba Specialty Chemicals were used as antioxidants.

5.3.2 Sample Preparation

Preparation of plasticized composites were performed using a LABTECH (type LHFS1-271822) corotating twin-screw extruder with an L/D ratio of 40 ($D = 20 \text{ mm}$, and $L = 800 \text{ mm}$). PLA and PNS were mixed with PEG and antioxidants (Irganox 1010 and Quent 68). Table 5.1 reveals the composition of each formulation. The temperature profile was maintained in the range of $120 \text{ }^\circ\text{C}$ to $170 \text{ }^\circ\text{C}$ from the feed throat to the die, and the rotational speed was fixed at 40 rpm.

The tensile specimens were produced using an injection machine (Battenfeld), and the operating temperature was $150 \text{ }^\circ\text{C}$ to $160 \text{ }^\circ\text{C}$ with an injection pressure of 6.5 bar at a screw speed of 160 rpm. The mold temperature was conducted at $30 \text{ }^\circ\text{C}$ to $40 \text{ }^\circ\text{C}$, the cooling time was 45 s, and cycle time was used 60 s.

Table 5.1 Composition of each formulation

Material					Code
Peanut shell (wt%)	PLA (wt%)	PEG (phr)	Antioxidants (phr)		
			Irganox	QUENT	
			1010	68	
-	100	-	0.5	0.5	PLA
30	70	-	0.5	0.5	30PNS
30	70	2.5	0.5	0.5	30P2.5PEG
30	70	5.0	0.5	0.5	30P5PEG
30	70	7.5	0.5	0.5	30P7.5PEG
30	70	10.0	0.5	0.5	30P10PEG
30	70	12.5	0.5	0.5	30P12.5PEG

5.3.3 Characterizations

The thermal properties were carried out by differential scanning calorimeter (DSC; Perkin-Elmer DSC 822) and thermogravimetric analyzer (TGA; Q5 TA) with a heating rate of 10 °C/min under nitrogen flow. The biodegradable properties were evaluated weight weekly during the 8 weeks using the following equation:

$$weight\ loss\ (\%) = \{(w_0 - w_1) / w_0\} \times 100 \quad (5.1)$$

where w_0 and w_1 are the sample weights before and after the biodegradation tests, respectively. The sample bars (40×30×3 mm) were buried in sandy soil (pH 4.6-4.8) and put in the oven at 60 ± 5 °C and 10-30 %RH. The morphological properties were examined using a field emission scanning electron microscope (FE-SEM; HITACHI S4800) with an acceleration voltage of 5 kV. The tensile properties were carried out using an Instron Universal Testing Machine (4206) with a crosshead speed of 50 mm/min according to ASTM D638 and the impact strength was measured using the ZWICK 5113 pendulum impact tester with a pendulum load of 21.6 J according to

ASTM D256 (notched type). The thermo–mechanical properties was performed using an EPLEXOR 100N in tension mode carried out at a constant frequency of 1 Hz, strain amplitude of 0.1%, and a temperature range of 0 °C to 120 °C, with a heating rate of 2 °C/min.

5.4 Results and Discussion

5.4.1 Thermogravimetry

Figure 5.1 shows the decomposed temperature at the maximum rate of mass loss (T_{\max}), or DTG curve of PLA, unplasticized composite (30PNS), and plasticized composites. It is obvious that T_{\max} of plasticized composites is lower than that of unplasticized composite due to the presence of plasticizer. Moreover, the decomposition temperature of plasticized composites also slightly decreased with the increasing PEG content. As a reported by Hassouna et al. [12], the thermal stability of PLA decreased which is due to the addition of PEG because the initial decomposition temperature of PEG is lower than PLA.

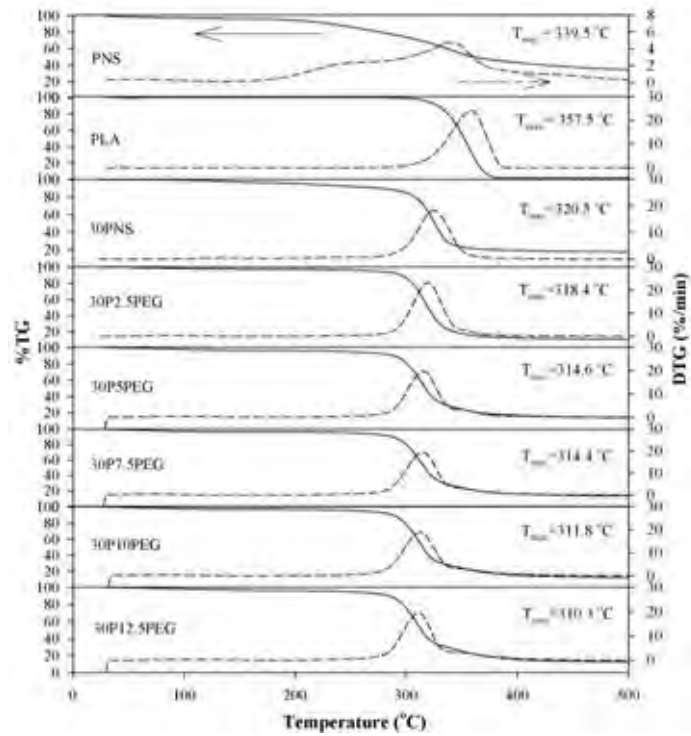


Figure 5.1 TGA and DTG curves of PLA, 30PNS, and plasticized composites.

5.4.2 Crystallization and Melting Behavior of Plasticized Composites

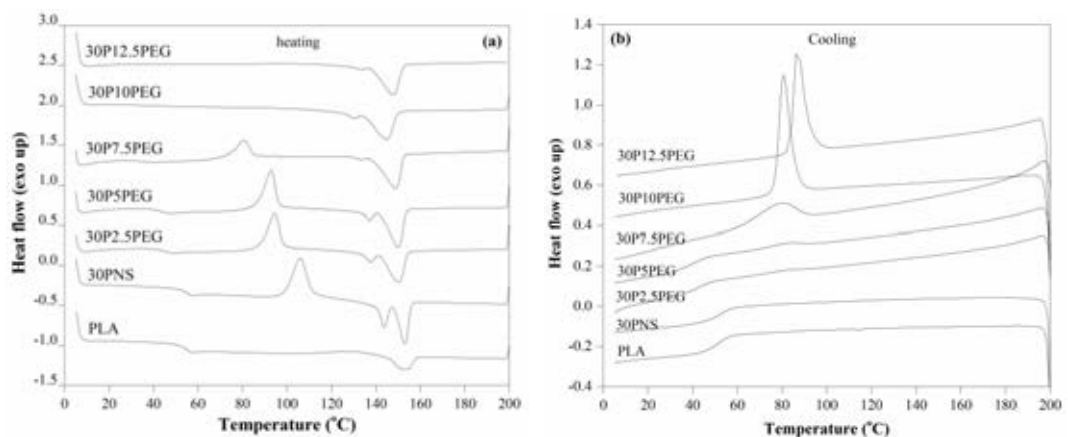


Figure 5.2 DSC thermograms of (a) heating scan and (b) cooling scan of PLA, 30PNS, and plasticized composites.

DSC thermograms of PLA, 30PNS, and plasticized composites are shown in Figure 5.2 and Table 5.2. Plasticized composites are characterized by the glass transition temperature (T_g) values between 30 °C and 40 °C, significantly decreased when compared to unplasticized composite and PLA ($T_g \sim 51$ °C). The results show that T_g of plasticized composites decreased with increasing PEG content due to the plasticizing effect. The cold crystallization temperature (T_{cc}) of plasticized composites (~ 80 °C– 94 °C) is lower than that of unplasticized composite (~ 105 °C) indicates that the improvement of chain motion increased the ability of PLA chains to crystallize. The increasing PEG content shifts the T_{cc} peak to a lower temperature. This can be explain that the increasing chain mobility at low temperature associated with the higher T_g depression [13]. Interestingly, the plasticized composites still show two melting peaks(T_m) and shift to a lower temperature when compared to unplasticized composite. It well known that the low–melting peak formed cold crystalline and high–melting peak formed original crystalline which corresponding to the imperfect crystal structures and perfect crystal structures, respectively. This behavior demonstrated by Qin et al [14]. It results also associate with other research findings where the increasing amount of plasticizer resulted in decrease the T_m and presence two peaks [15]. Moreover, the T_m of plasticized composites slightly decreased with increasing PEG content. This suggests that the addition of PEG decreased the crystal sizes due to the reducing of melting peak.

During the cooling scans as seen in Figure 5.2b, the melt crystallization temperature (T_{mc}) of plasticized composites occurs at high plasticizer content (7.5 %wt–12.5 %wt). The T_{mc} of plasticized composites increased with increasing PEG content. It indicates that high plasticizer enhanced the chain motion and reorientation of PLA chain to crystallization. This means that PLA chains had time to rearrangement for crystallization due to the increasing free volume. The increasing chain motion improved the crystallization rate as found in study of Yu et.al [16]. The influence of plasticizer on crystallization behavior of PLA blend is also reported by Ahmed et.al [17]. Moreover, the crystallization of PLA depends on the cooling rates, nucleation density, and annealing time.

Especially at 10 %wt–12.5 %wt PEG content, the T_g and T_{cc} are absent while the T_{mc} is appear, resulted in plasticized composites are highly

crystalline after cooling scan. Since PLA crystals are reorganize into more perfect crystal structures during heating scan because the imperfect crystal structures are able to occur during previous cooling scan [18, 19]. This phenomenon has effect on the melting temperature. It can be observed that the low-melting peak of plasticized composites at 10 %wt-12.5 %wt PEG content showed clearly small and close to merge into one melting peak which shifted to lower temperature. This phenomenon is also observed by Ke et. al [20]. The results can be concluded that plasticized composites behave like a semi-crystalline polymer at low PEG content and transformed into more crystalline polymer at high PEG content.

The crystallinity of plasticized composites largely increased from 4.52% to 46.03% when compared to unplasticized composite. This means that the additive, particularly plasticizer, improved the ability of the PLA matrix to crystallize.

Table 5.2 Thermal properties of plasticized composites

Sample	T _g (°C)	T _{cc} (°C)	ΔH _{cc} (J/g)	T _{m1} ; T _{m2} (°C)	ΔH _m (J/g)	χ _c (%)	T _{mc} (°C)	ΔH _{mc} (J/g)
PLA	51.1	128.4	4.6	152.7	8.3	3.98	-	-
30PNS	51.7	105.87	23.06	143.80; 153.08	26.00	4.52	-	-
30P2.5PEG	40.9	94.39	19.52	137.45; 150.23	26.26	10.61	-	-
30P5PEG	39.0	92.92	21.02	137.08; 149.97	27.40	10.29	-	-
30P7.5PEG	30.7	80.70	10.15	133.32; 148.56	23.41	21.89	79.08	9.34
30P10PEG	-	-	-	132.21; 145.91	27.24	46.03	80.62	22.10
30P12.5PEG	-	-	-	133.57; 148.12	24.98	43.17	87.08	20.03

$$\chi_c = \frac{\Delta H_m - \Delta H_{cc}}{\Delta H_{m0} \times w} \times 100, \Delta H_{m0} \text{ is enthalpy of melting for 100\% crystalline PLA}$$

sample, taken as 93 J/g, w is the weight fraction of PLA in the composite [21].

5.4.3 Biodegradation Study

Figure 5.3 and Table 5.3 show the weight loss of PLA, 30PNS, and plasticized composites. The weight loss of plasticized composites is slightly higher than that of unplasticized composite. This indicates that the incorporation of PEG enhanced the degradation due to the loosening of intermolecular interaction. Moreover, the rate of degradation of plasticized composites slightly increased with increasing PEG content. It can be explained that an increasing PEG content resulted in an enormous plastically deformed polymer on the surfaces [22].

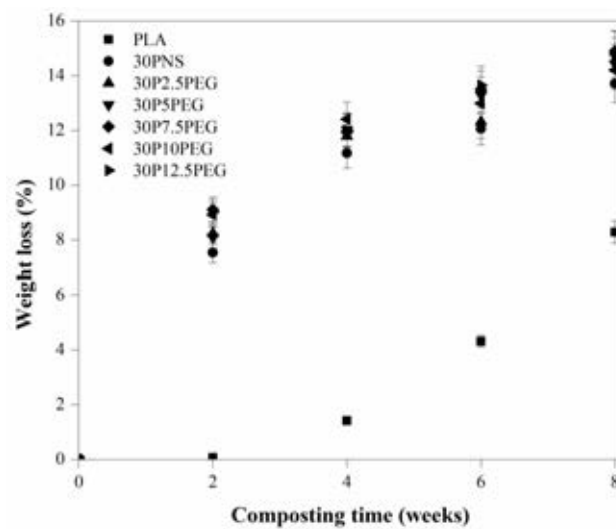


Figure 5.3 Relationship between weight loss and composting time of PLA, 30PNS, and plasticized composites.

Table 5.3 Weight loss of PLA, 30PNS, and plasticized composites

Sample	Weight loss (%)			
	2 week	4 week	6 week	8 week
PLA	0.08±0.01	1.42±0.07	4.32±0.22	8.28±0.41
30PNS	7.53±0.38	11.17±0.56	12.06±0.60	13.71±0.69
30P2.5PEG	8.24±0.41	11.79±0.58	12.32±0.62	14.87±0.74
30P5PEG	8.09±0.40	12.03±0.60	13.29±0.66	14.43±0.72
30P7.5PEG	9.10±0.46	12.45±0.59	13.50±0.67	14.90±0.75
30P10PEG	8.92±0.44	12.91±0.62	13.59±0.64	14.20±0.71
30P12.5PEG	9.02±0.45	12.01±0.60	13.65±0.68	14.65±0.73

5.4.4 Morphology Properties

The fractured surfaces of unplasticized composite and plasticized composites show many PNSs pull out with relatively clean fiber surface and aggregate in PLA matrix that is an indication of poor adhesion between them as seen in Figure 5.4. However, the good dispersion of PNSs in the PLA matrix is observed in plasticized composites. This suggests that the addition of PEG improved the dispersion of PNS during the mixing. Interestingly, the size of agglomerated PNS in plasticized composites is smaller than that of unplasticized composite. This observation indicates that the loading of PEG tend to further improved the dispersion state and reduced the agglomeration of PNS in the related composition.

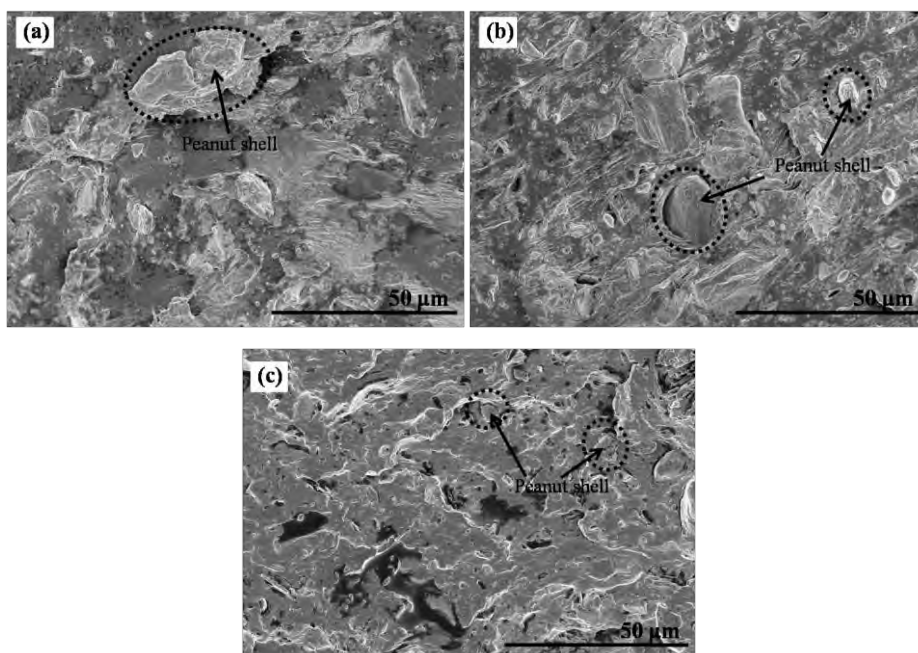


Figure 5.4 Morphological images of (a) 30PNS, (b) 30P2.5PEG, and (c) 30P12.5PEG.

5.4.5 Mechanical Properties

The effect of PEG on the composites on the mechanical properties is revealed in Figure 5.5 and Table 5.4. Plasticized composites show lower tensile strength and Young's modulus than that of unplasticized composite. This can be explained that plasticizer reduced the intermolecular forces between the polymer chains, resulted in soften and more flexible material. The results show that the tensile strength and Young's modulus of plasticized composites are decreased with increasing PEG content. On the other hand, it can be seen that the elongation at break of plasticized composites increased with increasing PEG content, which increases the ability of the material deformation. This results also found in Byun et al [4]. They reported that the addition of PEG increased elongation at break and decreased the tensile strength by reducing T_g . The increasing PEG content enhanced the chain mobility which allows more chain to crystalline. This contributes to a large amount of crystallinity increases the chain drawing. As a reported by Kulinski et al [3], the mechanism of plastic deformation in semi-crystalline PLA is associated with the

deformation of amorphous phase follow by strain-induced crystallization. It can be seen that the plasticized composites appear the yield point since the yield point associated with a deformation of ductile polymers in the solid state. Plastic flow takes place beyond yielding, accompanied by chain orientation of crystalline lamellae into the form of parallel microfibrils [23].

The notched izod impact strength of plasticized composites is also shown in Table 5.4. The impact strength of plasticized composites increased when compared to unplasticized composite. It can be seen that the impact strength of plasticized composites increased with PEG content. The higher loading of plasticizer into the composite resulted in improved the toughness because plasticizer improved the dispersion of PNSs in PLA matrix (as seen in FE-SEM result, Figure 5.4).

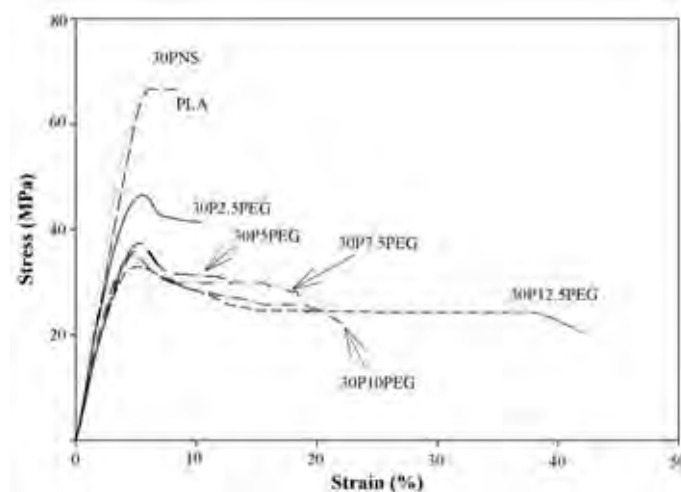


Figure 5.5 Stress-Strain curve of PLA, 30PNS, and plasticized composite.

Table 5.4 Mechanical properties of plasticized composites

Sample	Tensile strength (MPa)	Young's modulus (MPa)	Elongation at break (%)	Impact testing (kJ/m ²)
PLA	64.32±1.50	1858±20	10.09±9.52	9.10±0.29
30PNS	67.02±0.46	2261±31	6.51±0.63	7.60±0.20
30P2.5PEG	45.78±0.32	2003±42	12.36±0.78	9.10±1.43
30P5PEG	35.65±0.50	1587±38	18.87±2.06	10.60±2.10
30P7.5PEG	32.24±0.94	1495±29	21.89±2.25	12.20±1.93
30P10PEG	30.33±0.58	1326±45	25.43±1.37	15.90±2.49
30P12.5PEG	29.21±1.07	1224±76	40.89±2.01	20.50±1.09

5.4.6 Thermo-Mechanical Properties

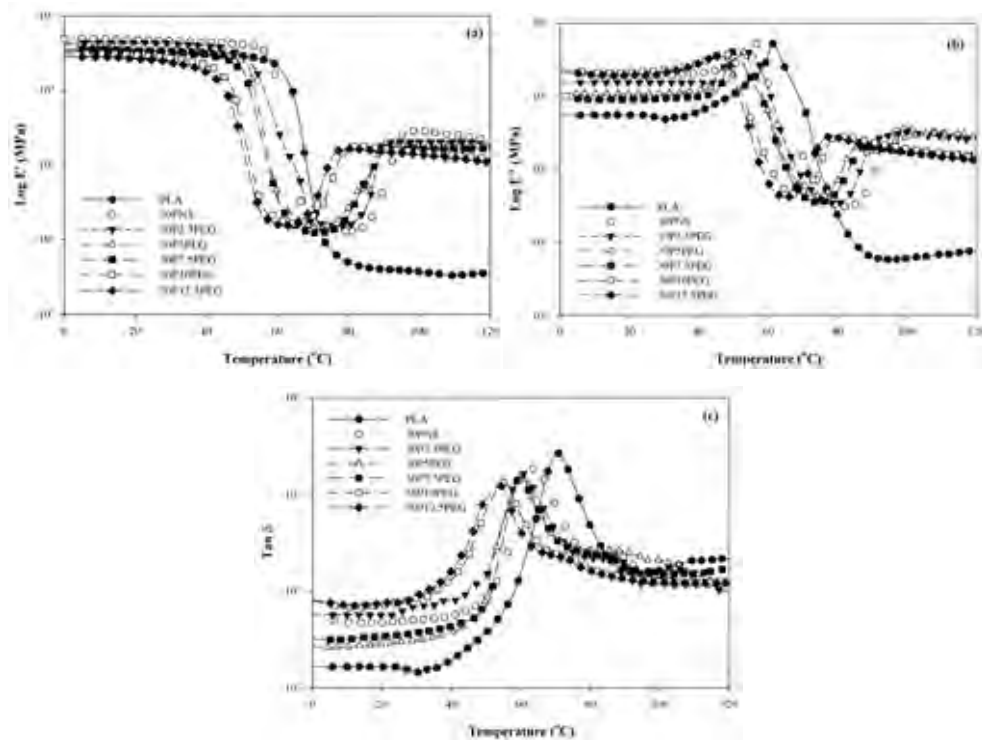


Figure 5.6 Temperature dependence of (a) E' , (b) E'' , and (c) $\tan \delta$ of PLA, 30PNS, and plasticized composites.

Figure 5.6a and Table 5.5 show the storage modulus (E') of PLA, 30PNS, and plasticized composites. At 30 °C, the E' of plasticized composites decreased compared to unplasticized composite due to the plasticizing effect. Moreover, the E' of plasticized composites is decreased with increase of PEG content. This result also agreed well with the modulus from the mechanical testing (Table 5.4). In addition, it can be noted that as the temperature increased near to the transition region, the sharp drop of the E' of all samples is presented. At higher plasticizer concentration, the E' starts earlier dropping due to a high local plasticization of the composites.

At 80 °C, plasticized composites at 10-12.5 %wt PEG content show E' higher than that of 2.5-7.5 %wt PEG content and unplasticized composite. As the temperature increase up to 100 °C, the E' of plasticized composites at 2.5-7.5 %wt PEG content become increase compared to 10-12.5 %wt PEG content. This contributed to the cold crystallization, as observed in DSC results (Table 5.2), improved the rigidity at high temperature. Especially the plasticized composites at 10-12.5 %wt PEG content are not seen the cold crystallization by DSC testing but it is detected by DMA testing.

However, unplasticized composite is still higher storage modulus than plasticized composites at high temperature (>100 °C). The advantage of plasticized composites is the development of modulus at earlier temperature than unplasticized composite, while the limiting temperature of plasticized composites is melting temperature which shows lower than that of unplasticized composite. Thus the applications of materials depend on the range of temperature usage which is limited by the melting temperature. In general, the E' of all samples is decreased with the increasing temperature.

Figure 5.6b and Table 5.5 show the loss modulus (E'') which is related to viscosity. The E'' peak of plasticized composites is lower than that of unplasticized composite. It can be suggested that the presence of PEG decreased the viscosity. This means that the addition of plasticizer into the composites can be processed easier than unplasticized composite. Moreover, the E'' peaks of plasticized composites are broader than that of unplasticized composite. This can be indicated that the

broadening of the E'' peak due to a wider distribution of PLA chain mobility. The broadening of the E'' peak has also been reported by Li et al [13].

The $\tan \delta$ which is related to T_g as observed in Figure 5.6c. $\tan \delta$ shows similar results as DSC (see Figure 5.2 and Table 5.2); T_g of plasticized composites are lower than that of unplasticized composite. The increasing PEG content shows reducing T_g of the composites.

Moreover, the damping showed that the molecular motion of unplasticized composite is higher than that of plasticized composites. The molecular motion of plasticized composites improved because of the presence of plasticizer.

Table 5.5 E' and E'' (MPa) of PLA, 30PNS, and plasticized composites

Sample	T _g	at 30 °C		at 80 °C		at 100 °C	
		E'	E''	E'	E''	E'	E''
PLA	70.80	3326.74±31.24	48.31±4.21	4.92±1.03	2.40±1.94	3.66±0.64	0.60±0.04
30PNS	63.50	4558.92±20.53	197.75±8.67	12.91±3.40	3.32±0.63	284.61±8.57	33.99±5.08
30P2.5PEG	60.70	4290.90±94.53	154.19±10.43	15.94±7.64	3.47±1.52	205.56±10.53	31.81±4.65
30P5PEG	59.80	3583.23±53.63	109.69±12.53	26.67±8.03	7.06±2.21	185.07±12.54	27.50±2.59
30P7.5PEG	58.80	3186.24±74.86	103.99±7.43	29.54±4.58	7.01±3.09	165.02±11.56	17.61±3.06
30P10PEG	54.80	2709.46±53.78	228.78±11.43	177.04±15.30	26.42±5.39	147.18±8.53	19.33±7.30
30P12.5PEG	54.30	2302.31±32.70	213.60±16.04	165.94±10.54	26.85±8.40	136.73±13.29	17.62±6.32

5.5 Conclusion

In this study, plasticized composites were prepared using plasticizer, PEG. Plasticized composites showed lower thermal properties than that of unplasticized composite and PLA. The crystallinity of plasticized composites was improved, suggested that PEG enhanced the ability of the PLA matrix to crystallize. The TGA results revealed that plasticized composites showed less heat stability. The lower decomposition temperature of plasticized composites indicated the poorer intermolecular interaction caused by plasticizing effect. Biodegradation study revealed that the weight loss of plasticized composites was slightly increased with increasing PEG content. Moreover, the morphology showed that the addition of PEG tends to further improve the dispersion state and reduced the agglomeration of PNS in the composites. For the mechanical testing, the tensile strength and Young's modulus of plasticized composites decreased while the elongation at break and impact strength increased with increasing PEG content. The storage and loss modulus of plasticized composites were decreased when compared to unplasticized composite. Thus plasticized composites had better processability than unplasticized composite. Moreover, plasticized composites showed storage modulus in the range of 136 MPa-205 MPa at 100 °C which was able to use at high temperature application. The properties of plasticized composites were summarized in Table 5.6

Table 5.6 Summary of the properties of plasticized composites

Properties		Decrease	Increase
Thermal properties (T_d, T_g, T_{cc}, T_m)		--	
Mechanical properties	Tensile strength	--	
	Young's modulus	--	
	Elongation at break		+++
	Impact strength		++
Thermo-mechanical properties	Storage modulus	--	
	Loss modulus	--	
Biodegradabation study			+

Note: The symbols, that increase from high to low, are +++, ++, and +, respectively.

The symbols, that decrease from high to low, are ---, --, and -, respectively.

5.6 Acknowledgement

Financial support has been granted by National Research Council of Thailand (NRCT).

5.7 References

- [1] Sheth, M., et al., Biodegradable Polymer Blends of Poly(lactic acid) and Poly(ethylene glycol). Journal of Applied Polymer Science, 1997. 66: p. 1495-1505.
- [2] Martin, O. and L. Averous, Poly(lactic acid): plasticization and properties of biodegradable multiphase systems. Polymer, 2001. 42: p. 6209-6219.
- [3] Kulinski, Z. and E. Piorkowska, Crystallization, structure and properties of plasticized poly(L-lactide). Polymer, 2005. 46: p. 10290-10300.

- [4] Byun, Y., Y.T. Kim, and S. Whiteside, Characterization of an antioxidant polylactic acid (PLA) film prepared with α -tocopherol, BHT and polyethylene glycol using film cast extruder. Journal of Food Engineering, 2010. 100: p. 239-244.
- [5] Graupner, N., A.S. Herrmann, and J. Müssig, Natural and man-made cellulose fibre-reinforced poly(lactic acid) (PLA) composites: An overview about mechanical characteristics and application areas. Composites: Part A, 2009. 40: p. 810–821.
- [6] Harrell, Design for Sustainable Development Spring 2010.
- [7] Fasina, O.O., Physical properties of peanut hull pellets. Bioresource Technology, 2008. 99: p. 1259–1266.
- [8] Akgu, M. and A. Tozluoglu, Utilizing peanut husk (*Arachis hypogaea* L.) in the manufacture of medium-density fiberboards. Bioresource Technology, 2008. 99: p. 5590–5594.
- [9] Masirek, R., et al., Composites of Poly(L-lactide) with Hemp Fibers: Morphology and Thermal and Mechanical Properties. Journal of Applied Polymer Science, 2007. 105: p. 255-268.
- [10] Qu, P., et al., Nanocomposites of poly(lactic acid) reinforced with cellulose nanofibrils. Bioresources, 2010. 5(3): p. 1811-1823.
- [11] Wang, J., W. Zhai, and W. Zheng, Poly(Ethylene Glycol) Grafted Starch Introducing a Novel Interphase in Poly(Lactic Acid)/Poly(Ethylene Glycol)/Starch Ternary Composites. Journal of Polymers and the Environment, 2012. 20: p. 528-539.
- [12] Hassouna, F., et al., New approach on the development of plasticized polylactide (PLA): Grafting of poly(ethylene glycol) (PEG) via reactive extrusion. European Polymer Journal, 2011.
- [13] Li, H. and M.A. Huneault, Effect of nucleation and plasticization on the crystallization of poly(lactic acid). Polymer, 2007. 48: p. 6855-6866.
- [14] Qin, L., et al., Mechanical and thermal properties of poly(lactic acid) composites with rice straw fiber modified by poly(butyl acrylate). Chemical Engineering Journal, 2011. 166: p. 772-778.

- [15] Byun, Y., Y.T. Kim, and S. Whiteside, Characterization of an antioxidant polylactic acid (PLA) film prepared with α -tocopherol, BHT and polyethylene glycol using film cast extruder. Journal of Food Engineering, 2010. 100: p. 239–244.
- [16] Yu, L., et al., Cold Crystallization and Postmelting Crystallization of PLA Plasticized by Compressed Carbon Dioxide. Journal of Polymer Science: Part B: Polymer physics, 2008. 46: p. 2630-2636.
- [17] Ahmed, J., et al., Thermal and Rheological Properties of L-Polylactide/Polyethylene Glycol/Silicate Nanocomposites Films. Journal of Food Science, 2010. 75: p. 97-108.
- [18] Frone, A.N., et al., Morphology and thermal properties of PLA-cellulose nanofibers composites. Carbohydrate Polymers, 2013. 91: p. 377-384.
- [19] Hu, Y., et al., Crystallization and phase separation in blends of high stereoregular poly(lactide) with poly(ethylene glycol). Polymer, 2003. 44: p. 5681-5689.
- [20] Ke, T. and X. Sun, Melting Behavior and Crystallization Kinetics of Starch and Poly(lactic acid) Composites. Journal of Applied Polymer Science, 2003. 89: p. 1203-1210.
- [21] Lee, K.-Y., J.J. Blaker, and A. Bismarck, Surface functionalisation of bacterial cellulose as the route to produce green polylactide nanocomposites with improved properties. Composites Science and Technology, 2009. 69: p. 2724-2733.
- [22] Ibrahim, N.A., et al., Poly(Lactic Acid) (PLA)-reinforced Kenaf Bast Fiber Composites: The Effect of Triacetin. Journal of Reinforced Plastics and Composites, 2010. 29: p. 1099-1111.
- [23] Seguela, R. and F. Rietsch, Double yield point in polyethylene under tensile loading. Journal of Materials Science Letters, 1990. 9: p. 46-47.

CHAPTER VI

THE EFFECT OF TRIACETIN ON THERMAL, MECHANICAL, AND BIODEGRADABLE PROPERTIES OF PEANUT SHELL/PLA COMPOSITE

6.1 Abstract

Plasticized composites were prepared from peanut shell (PNS) and polylactic acid (PLA) together with triacetin. Plasticized composites showed reduction of glass transition, cold crystallization, and melting temperature. Moreover, plasticized composites were decreased the decomposition temperature when compared to unplasticized composite. The morphological study of plasticized composites revealed good dispersion of PNS in the PLA matrix. The thermo-mechanical properties showed the enhancement of PLA performance at high temperature use by the incorporation of PNS together with triacetin due to cold crystallization at a high temperature which improved storage modulus. The tensile strength and Young's modulus of plasticized composites decreased while the elongation at break and impact strength increased with the increasing triacetin content. The biodegradability was improved due to the presence of triacetin.

6.2 Introduction

Biodegradable materials have wide potential in many applications which are packaging, automotives, furniture, and medical devices. PLA is the most promising biodegradable material which is a good biodegradability, biocompatibility, and good mechanical properties [1, 2]. However, PLA are brittle and slow degradation rate and it is therefore necessary to use plasticizers to enhance the toughness.

Natural fibers are widely used to improve the degradable properties of PLA. Several researchers studied the degradation of natural fiber/PLA composites. Shogrena et al. [3] reported that the starch/PLA/poly(hydroxyester-ether) composites were degraded 4-50% within 1 year in soil. The weight loss of the composites was due to starch only with the degradation proceeding from outside to inside. According to Ochi [4] showed that kenaf/PLA composites were biodegraded because the mass

decreased 38% in a garbage-processing machine within 4 weeks. Pradhan et al. [5] found that wheat straw/PLA and soy straw/PLA composites were degraded 90% in the composting bioreactor after 70 days. The enhancement in degradation of those composites was due to the presence of natural biomass. Wu et al. [6] studied that the blends containing maleic anhydride-grafted PLA and green coconut fiber were degraded larger than 92% after 21 days in a *Burkholderia cepacia* BCRC 14253 compost.

This work was to prepare the peanut shell/PLA composites together with triacetin by the melt mixing process. The effects of triacetin content on thermal, thermo-mechanical, mechanical, morphological, as well as biodegradable properties were investigated.

6.3 Experimental

6.3.1 Materials

Polylactic acid, grade 4043D ($\rho = 1.25 \text{ g/cm}^3$, $\delta = 21.42 \text{ MPa}^{1/2}$, and $T_m = 210 \text{ }^\circ\text{C}$), was purchased from Nature-Work LLC. Peanut shell was ground to 5-100 μm with a moisture content of $5.19 \pm 0.11 \%$. Triacetin with a 99% purity ($M_w \approx 218 \text{ g/mol}$, $\delta = 22.00 \text{ MPa}^{1/2}$, and $\rho = 1.15 \text{ g/cm}^3$) was purchased from Sigma-Aldrich. Irganox 1010 and Quent 68 from Ciba Specialty Chemicals, were used as stabilizers.

6.3.2 Sample Preparation

Preparation of plasticized composites were performed using a LABTECH (type LHFS1-271822) corotating twin-screw extruder with an L/D ratio of 40 ($D = 20 \text{ mm}$, and $L = 800 \text{ mm}$). PLA and PNS were mixed with triacetin and antioxidants (Irganox 1010 and Quent 68). Table 6.1 reveals the composition of each formulation. The temperature profile was maintained in the range of $120 \text{ }^\circ\text{C}$ to $170 \text{ }^\circ\text{C}$ from the feed throat to the die, and the rotational speed was fixed at 40 rpm.

The tensile specimens were produced using an injection machine (Battenfeld), and the operating temperature was $150 \text{ }^\circ\text{C}$ to $160 \text{ }^\circ\text{C}$ with an injection

pressure of 6.5 bar at a screw speed of 160 rpm. The mold temperature was conducted at 30-40 °C, the cooling time was 45 s, and cycle time was used 60 s.

Table 6.1 Composition of each formulation

Material					Code
Peanut shell (wt%)	PLA (wt%)	triacetin (phr)	Antioxidants (phr)		
			Irganox 1010	QUENT 68	
-	100	-	0.5	0.5	PLA
30	70	-	0.5	0.5	30PNS
30	70	2.5	0.5	0.5	30P2.5TRI
30	70	5.0	0.5	0.5	30P5TRI
30	70	7.5	0.5	0.5	30P7.5TRI
30	70	10.0	0.5	0.5	30P10TRI
30	70	12.5	0.5	0.5	30P12.5TRI

6.3.3 Characterization

6.3.3.1 *Thermogravimetric Analyzer (TGA)*

Thermogravimetric analysis was carried out with a TGA Q5 TA under a nitrogen flow (100 ml/min). The samples were measured from 30 °C to 500 °C with a heating rate of 10 °C/min. The decomposition temperature and temperature at maximum rate of mass loss (T_{max}), of derivative thermogravimetric curve (DTG) were evaluated.

6.3.3.2 *Differential Scanning Calorimeter (DSC)*

Differential scanning calorimeter was performed using a Perkin–Elmer DSC 822 under N₂ atmosphere. The samples were heated from 10 °C to 200 °C at a heating rate of 10 °C/min and held at 200 °C for 5 min (1st run), then they were cooled to 10 °C at a heating rate of 10 °C/min and reheated under the same conditions (2nd run). The glass transition temperature (T_g), cold crystallization

temperature (T_{cc}), and melting temperature (T_m) of each specimens was recorded from the second run. The degree of crystallization (χ_c) was calculated as:

$$\chi_c = \frac{\Delta H_m - \Delta H_{cc}}{\Delta H_{m0} \times w} \times 100 \quad (6.1)$$

Where ΔH_m is the enthalpy of melting, ΔH_{cc} is the enthalpy of cold crystallization, ΔH_{m0} is enthalpy of melting for the 100% crystalline PLA sample, taken as 93 J/g, w is the weight fraction of PLA in the composite [7].

6.3.3.3 Morphological Observation

The material microstructure was examined using a field emission scanning electron microscope (FE-SEM; HITACHI S4800) with an acceleration voltage of 5 kV. The freeze-fractured ends of specimens were sputtering coated (HITHACHI E-1010) with a thin layer of platinum prior to analysis.

6.3.3.4 Tensile Tests

Tensile tests were performed using an Instron Universal Testing Machine (4206) with a crosshead speed of 50 mm/min. The specimens were prepared according to ASTM D638 standard.

Izod impact testing was performed according to ASTM D256 (notched type), and the impact strength was measured using the ZWICK 5113 pendulum impact tester with a pendulum load of 21.6 J. Ten samples were used to characterize each material and average values were reported.

6.3.3.5 Dynamic Mechanical Analyzer (DMA)

Dynamic mechanical analysis (DMA) was performed using an EPLEXOR 100N in tension mode. The sample dimensions with a length of 40 mm, width of 10 mm, and thickness of 3 mm were used. The measurements were carried out at a constant frequency of 1 Hz, strain amplitude of 0.1%, and a temperature range of 0 °C to 120 °C, with a heating rate of 2 °C/min.

6.3.3.6 Biodegradability Testing

The composite bars (40×30×3 mm) were buried in a pan of approximately 3 cm of sandy soil (pH 4.6-4.8) and put in the oven to investigate

biodegradability. The temperature and moisture were kept constant at 60 ± 5 °C and 10-30 %R.H. After removal from the sandy soil, samples were gently washed with water and equilibrated at ambient temperature for 1 day. The samples were weighed weekly during the 8 weeks. The weight loss was evaluated using the following equation:

$$\text{weight loss (\%)} = \{(w_0 - w_1) / w_0\} \times 100 \quad (6.2)$$

where w_0 and w_1 are the sample weights before and after the biodegradation tests, respectively.

6.4 Results and Discussion

6.4.1 Thermogravimetry

Figure 6.1 shows the TG and DTG curves of 30PNS and plasticized composites. It is obvious that T_{\max} of plasticized composites are lower than that of 30PNS due to the presence of triacetin. The decomposition temperature of plasticized composites also decreased with the increasing triacetin content. It can be noted that addition of high amount of triacetin characterized by high volatility can lead to an important decreased the thermal stability of the materials [8].

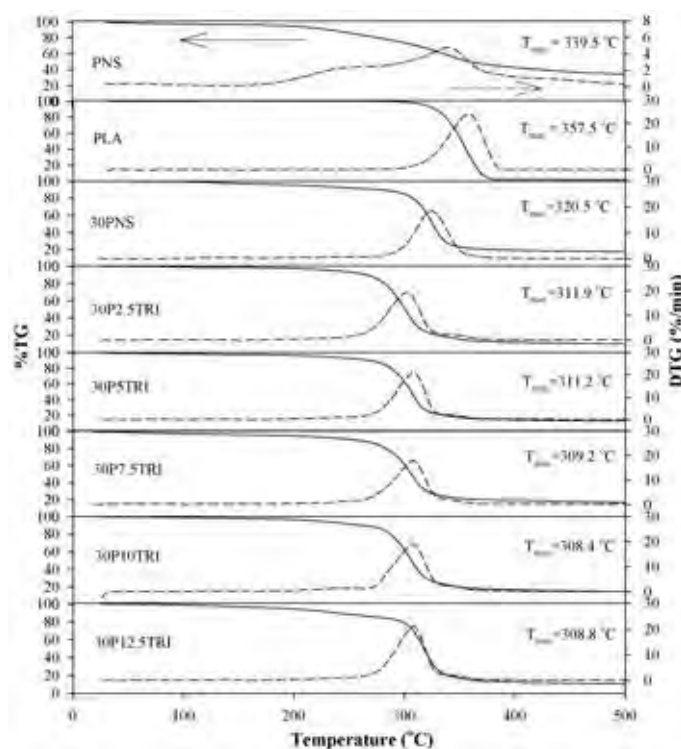


Figure 6.1 TGA and DTG curves of PLA, 30PNS, and plasticized composites.

6.4.2 Crystallization and Melting Behavior of Plasticized Composites

DSC thermograms of the second heating scan of PLA, 30PNS, and plasticized composites are shown in Figure 6.2a and Table 6.2. The results also show that T_g of plasticized composites decreases with increasing triacetin content indicates that the addition of triacetin enhances segmental mobility of PLA chains. The DSC thermograms from heating scans of plasticized composites reveal T_g , T_{cc} , and T_m which are shift to lower temperature when compared to PLA. The T_{cc} of plasticized composites (~ 72 °C- 81 °C) are lower than that of unplasticized composite (~ 105 °C), suggests that the increasing chain mobility increases slightly the ability of PLA chains to crystallize. The higher triacetin content is shift the cold crystallization peak to a lower temperature. This can be associated to two different phenomena. The first one is the increase chain mobility at low temperature associates with the larger T_g depression. This T_g reduction enables crystallization to start at an earlier temperature upon heating. A second phenomenon is the reduced crystallization induction period due to the presence of crystalline nuclei already form during the cooling process [9].

During the cooling scans, the melt crystallization temperature (T_{mc}) of plasticized composites occurs at high triacetin content (7.5 %wt-12.5 %wt) as seen in Figure 6.2b. The T_{mc} for plasticized composites increased with increasing plasticizer content. It indicates plasticizer enhances crystallization in the composites. This influence of plasticizer on crystallization behavior of PLA blend was also reported by Ahmed et.al [10]. The crystallinity of plasticized composites increased when compared to PLA.

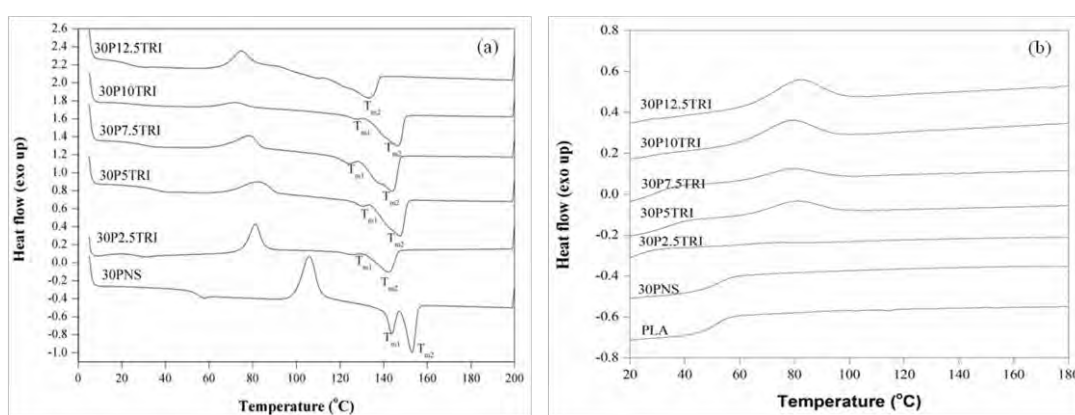


Figure 6.2 DSC thermograms of (a) heating scan and (b) cooling scan of PLA, 30PNS, and plasticized composites.

Table 6.2 Thermal properties of plasticized composites

sample	T _g (°C)	T _{cc} (°C)	ΔH _{cc} (J/g)	T _{m1} ;T _{m2} (°C)	ΔH _m (J/g)	χ _c (%)	T _{mc} (°C)	ΔH _{mc} (J/g)
PLA	51.1	128.4	4.6	152.7	8.3	3.98	-	-
30PNS	51.73	105.87	23.06	143.80; 153.08	26.00	4.52	-	-
30P2.5TRI	21.33	81.21	12.91	125.13; 142.24	17.46	6.99	-	-
30P5TRI	29.83	81.96	11.94	130.21; 147.44	30.18	28.02	-	-
30P7.5TRI	24.37	78.30	9.82	123.88; 143.79	34.41	37.77	78.91	5.71
30P10TRI	20.90	72.14	4.06	126.93; 146.53	25.10	32.32	78.89	11.07
30P12.5TRI	18.39	74.63	13.08	133.31	25.30	18.77	80.91	7.10

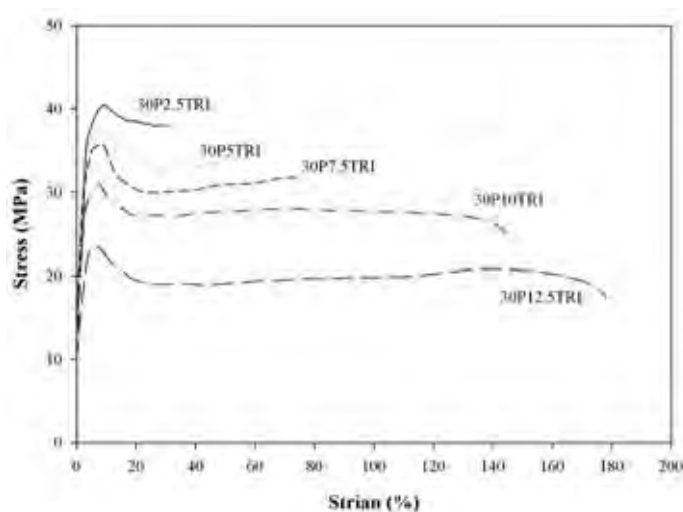
6.4.3 Mechanical Properties

Table 6.3 and Figure 6.3 show mechanical properties of PLA, 30PNS, and plasticized composites. Plasticized composites are poorer tensile strength and Young's modulus than unplasticized composite. The results show that the tensile strength and Young's modulus of plasticized composites decreases with the increasing triacetin content. This can be explained that plasticizer decreased the intermolecular forces among the polymer chains, resulted in a softened and more flexible material. On the other hand, the enhancement in elongation at break is obtained for plasticized composites with triacetin because triacetin is the best solubility parameter in relation to PLA [8].

The notched izod impact strength of plasticized composites is shown in Table 6.3. Toughness is the major factor controlling the impact strength. By compared to unplasticized composite, the impact strength of plasticized composites is increased. It can be seen that the impact strength of plasticized composites increased with triacetin content. The higher loading of plasticizer into the composites resulted in an increase of the toughness because the dispersion of peanut shell in PLA matrix was improved (as seen in FE–SEM result).

Table 6.3 Mechanical properties of plasticized composites

sample	Tensile strength (MPa)	Young's modulus (Mpa)	Elongation at break (%)	Impact testing (kJ/m ²)
PLA	64.32±1.50	1858±20	10.09±9.52	9.10±0.29
30PNS	67.02±0.46	2261±31	6.51±0.63	7.60±0.20
30P2.5TRI	40.74±0.84	1948±63	28.89±1.51	15.30±1.59
30P5TRI	36.08±2.50	1645±82	40.66±1.68	23.10±1.75
30P7.5TRI	32.83±1.13	1523±87	72.40±2.16	28.50±2.47
30P10TRI	26.20±1.11	1107±50	157.02±2.20	34.40±1.95
30P12.5TRI	15.10±0.25	653±44	271.60±2.51	38.20±1.39

**Figure 6.3** Stress–Strain curves of plasticized composites.

6.4.4 Thermo–Mechanical Properties

Figure 6.4a and Table 6.4 show the E' as a function of temperature for 30PNS and plasticized composites. At ambient temperature, the E' of plasticized composites is lower than that of 30PNS sample due to the plasticizing effect. The results clearly show that as the temperature increases near to the glass transition temperature, the sharp drop of the E' of all sample is presented. At higher triacetin

content, the E' starts earlier dropping due to a high local plasticization. The sudden increase of the E' as a result of PLA cold crystallization, as observed in DSC results. At 100 °C, E' of unplasticized composite is 284 MPa while those of plasticized composites are lower than 200 MPa. The developed E' of plasticized composites becomes lower and declines more with increasing temperature.

Figure 6.4b and Table 6.4 show the temperature dependence of the E'' or ability of the material to dissipate energy, which is related to viscosity. The E'' of unplasticized composite is rather high suggesting high viscosity. The E'' of plasticized composites shifts to lower a temperature compared to unplasticized composite. Moreover, the peaks of plasticized composites were broader and lower than those of unplasticized composite. This broadening peak of the E'' indicated a wider distribution in the range of PLA chain mobility. The E'' peak broadening has also been reported by Li et al [9]. This also suggests that the adding triacetin into the composites can be processed easier than unplasticized composite.

The ratio of E'' to E' is measured as a loss factor, or $\tan \delta$, as observed in Figure 6.4c. $\tan \delta$ shows similar results as DSC (see Figure 6.2 and Table 6.2); T_g of plasticized composites is lower than that of 30PNS. The increasing triacetin content shows reducing of T_g . Moreover, the damping reveals that the molecular motion of unplasticized composite is lower than that of plasticized composites. The molecular motions of plasticized composites improved due to the presence of triacetin.

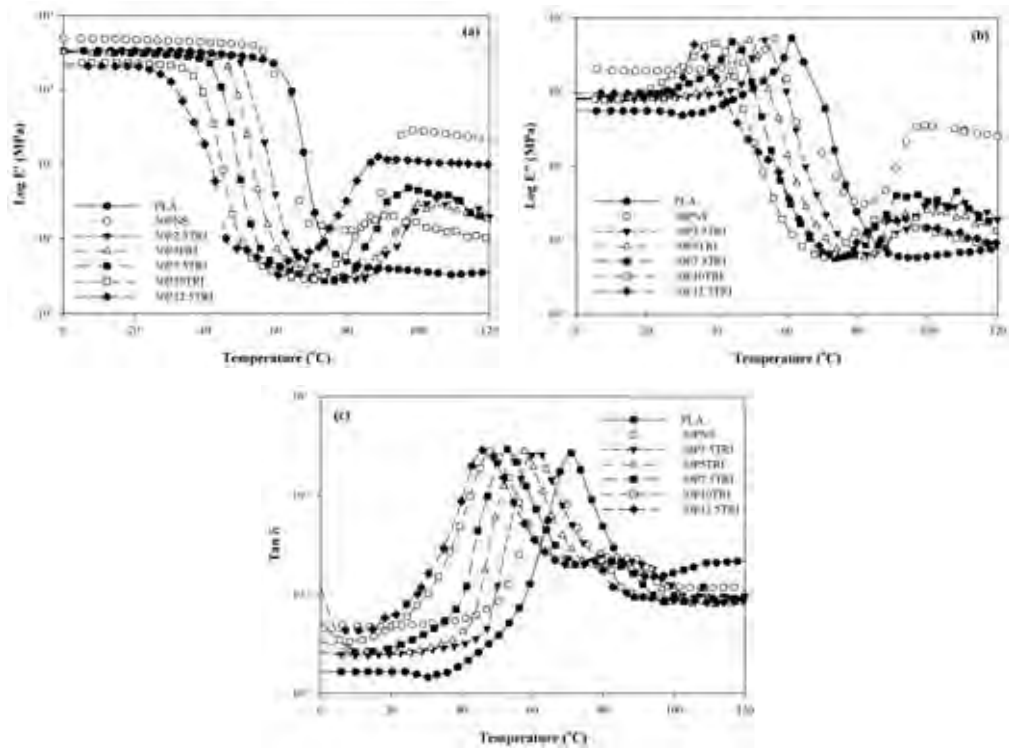


Figure 6.4 Temperature dependence of (a) E' , (b) E'' , and (c) $\tan \delta$ of PLA, 30PNS, and plasticized composites.

Table 6.4 E' and E'' (MPa) of 30PNS and plasticized composites

sample	T _g	at 30 °C		at 100 °C		at 120 °C	
		E'	E''	E'	E''	E'	E''
PLA	70.80	3326.74±31.24	48.31±4.21	4.92±1.03	2.40±1.94	3.66±0.64	0.60±0.04
30PNS	63.50	4558.92±20.53	197.75±8.67	284.61±8.57	33.99±5.08	213.66±10.11	25.51±2.63
30P2.5TRI	62.60	3158.90±49.65	84.41±10.43	23.54±6.39	2.85±0.49	18.14±4.12	1.69±0.43
30P5TRI	57.60	3079.86±54.40	83.78±6.42	29.27±7.40	2.50±0.65	16.86±6.30	1.36±0.41
30P7.5TRI	52.80	2956.14±64.77	116.27±8.39	34.72±7.54	3.37±0.42	18.05±5.20	1.61±0.69
30P10TRI	47.70	2136.58±53.87	219.89±14.29	16.76±8.56	1.44±0.57	8.59±2.64	0.84±0.53
30P12.5TRI	39.80	1271.11±63.68	159.75±11.45	107.19±3.95	1.45±0.65	7.19±14.43	0.90±0.56

6.4.5 Biodegradation Study

Figure 6.5 and Table 6.5 illustrate the biodegradability of plasticized composites within 8 weeks of composting in soil at 60 °C. The weight loss of plasticized composites is slightly higher than that of unplasticized composite. This indicates that the incorporation of plasticizer enhanced the degradation due to the loosening of intermolecular interaction. In addition, the rate of degradation of plasticized composites is slightly increased with triacetin content. It can be explained that an increase of plasticizer content resulted in a large amount of plastically deformed polymer on fracture surfaces [11].

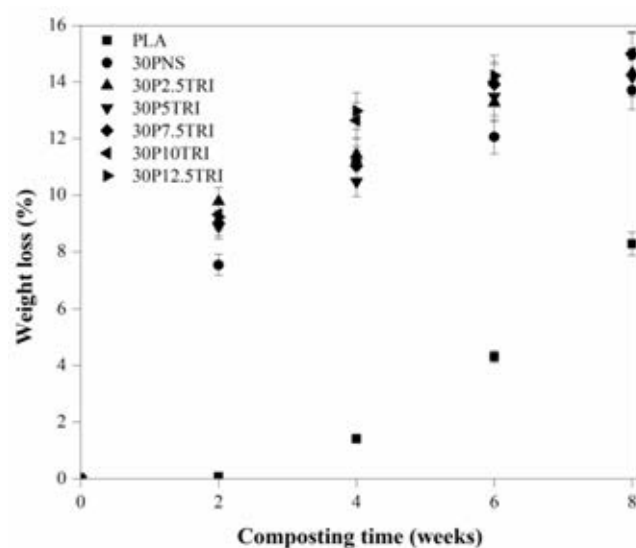


Figure 6.5 Relationship between weight loss and composting time of PLA, 30PNS, and plasticized composites.

Table 6.5 Weight loss of PLA, 30PNS, and plasticized composites

sample	Weight loss (%)			
	2 week	4 week	6 week	8 week
PLA	0.08±0.01	1.42±0.07	4.32±0.22	8.28±0.41
30PNS	7.53±0.38	11.17±0.56	12.06±0.60	13.71±0.69
30P2.5TRI	8.78±0.49	10.43±0.57	13.27±0.66	14.33±0.72
30P5TRI	8.89±0.44	10.48±0.52	13.49±0.67	14.18±0.71
30P7.5TRI	9.01±0.45	11.04±0.55	13.92±0.69	14.98±0.75
30P10TRI	9.32±0.47	12.65±0.63	14.01±0.70	15.03±0.75
30P12.5TRI	9.23±0.46	12.98±0.65	14.23±0.71	14.99±0.76

6.4.6 Morphology Properties

The morphologies of the fractured surfaces of unplasticized composite and plasticized composites are investigated by FE-SEM. Figure 6.6a shows the fractured surface of unplasticized composite with many peanut shells pulled out with relatively clean fiber surface and aggregated in PLA matrix that was an indication of poor adhesion between them. However, the good dispersion of peanut shell in the PLA matrix is observed in plasticized composites (Figure 6.6b-6.6d). This suggests that the addition of triacetin improved the dispersion of peanut shell under high shear rate during processing. Interestingly, the size of agglomerated peanut shell in the plasticized composites is smaller than that of unplasticized composite. This observation seems to indicate that the addition of plasticizer tend to further improved the dispersion state and reduced the agglomeration of peanut shell in the related composition.

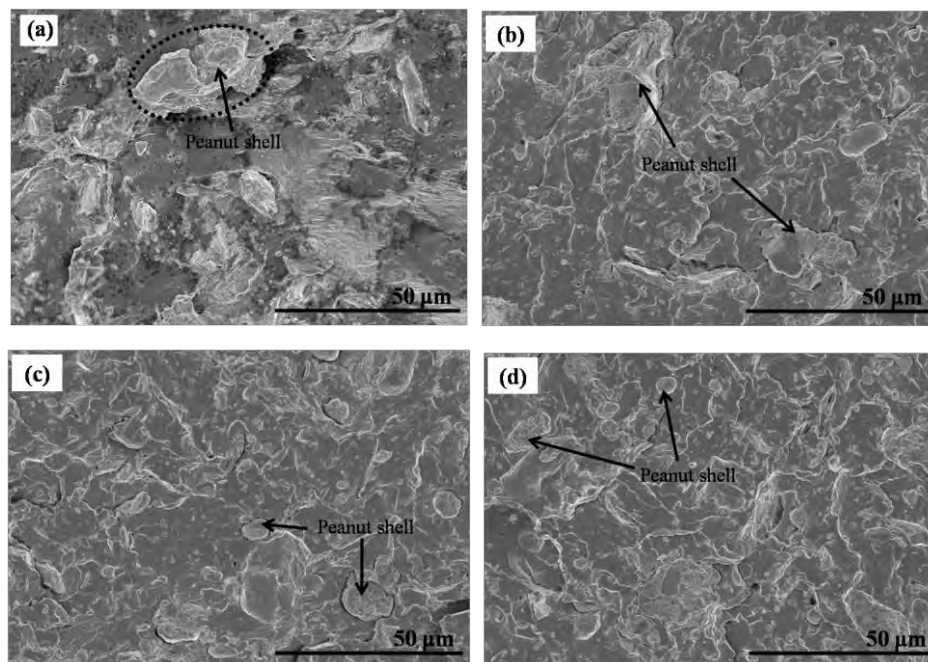


Figure 6.6 Morphological images of (a) 30PNS, (b) 30P2.5TRI, (c) 30P7.5TRI, and (d) 30P12.5TRI.

Figure 6.7 shows the morphology of the fractured surface of 30P12.5TRI after composting test for 8 weeks. The appearance of crack and void structure on the surface suggested the degradation of some peanut shell. Within the zone of degradation, partially degraded peanut shell can be visualized, suggests that removal of peanut shell is due to microbial action in soil rather than physical removal (i.e. fibers popping out). Similar result of biodegradation of starch/PLA/poly(hydroxyester-ether) composites in soil has been reported [3]. Moreover, the biodegradation of the samples occur near the interface between peanut shell and matrix.

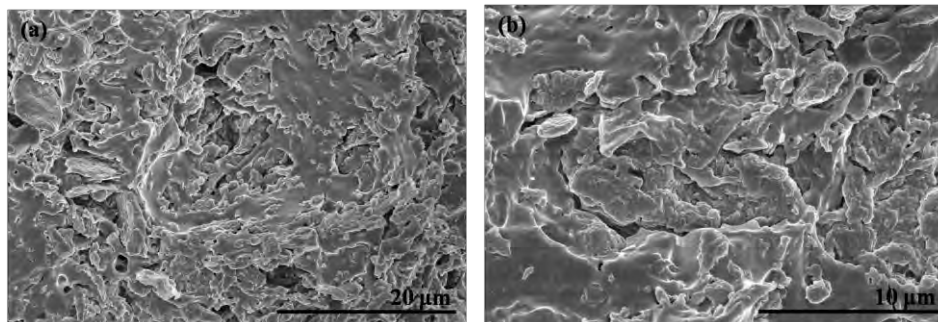


Figure 6.7 Morphological images of 30P12.5TRI after degradation test: (a) 2.5 k magnification, and (b) 5 k magnification.

6.5 Conclusion

In this work, plasticized composites were prepared using triacetin as a plasticizer. Plasticized composites were lower thermal properties than that of unplasticized composite and PLA. The crystallinity of plasticized composites improved, suggests that triacetin enhanced the ability of the PLA matrix to crystallize. The TGA results showed that plasticized composites were decreased the decomposition temperature when compared to unplasticized composite. The lower decomposition temperature of plasticized composites indicated the poorer intermolecular interaction caused by plasticizing effect. Biodegradation study revealed that the weight loss of plasticized composites slightly increased with increase in triacetin content. Moreover, the morphology showed that the addition of triacetin tends to further improve the dispersion state and reduce the agglomeration of PNS in the composites. The tensile strength and Young's modulus of plasticized composites decreased while the elongation at break and impact strength increased with increasing triacetin content. The storage and loss modulus of plasticized composites were decreased when compared to unplasticized composite. Thus plasticized composites were better processability than unplasticized composite. The properties of plasticized composites were summarize in Table 6.6.

Table 6.6 Summary of the properties of plasticized composites

Properties		Decrease	Increase
Thermal properties (T_d, T_g, T_{cc}, T_m)		--	
Mechanical properties	Tensile strength	--	
	Young's modulus	--	
	Elongation at break		+++
	Impact strength		++
Thermo-mechanical properties	Storage modulus	--	
	Loss modulus	--	
Biodegradabation study			+

Note: The symbols, that increase from high to low, are +++, ++, and +, respectively.

The symbols, that decrease from high to low, are ---, --, and -, respectively.

6.6 Acknowledgement

Financial support has been granted by National Research Council of Thailand (NRCT).

6.7 References

- [1] Tao, Y., L. Yan, and R. Jie, Preparation and properties of short natural fiber reinforced poly(lactic acid) composites. Transactions of Nonferrous Metals Society of China, 2009. 19: p. 651–655.
- [2] Yang, S.L., et al., Thermal and mechanical properties of chemical crosslinked polylactide (PLA). Polymer Testing, 2008. 27: p. 957–963.
- [3] Shogrena, R.L., et al., Biodegradation of starch/polylactic acid/poly(hydroxyester-ether) composite bars in soil. Polymer Degradation and Stability, 2003. 79: p. 405–411.

- [4] Ochi, S., Mechanical properties of kenaf fibers and kenaf/PLA composites. Mechanics of Materials, 2008. 40: p. 446–452.
- [5] Pradhan, R., et al., Compostability and biodegradation study of PLA-wheat straw and PLA-soy straw based green composites in simulated composting bioreactor. Bioresource Technology, 2010. 101: p. 8489–8491.
- [6] Wu, C.S., Renewable resource-based composites of recycled natural fibers and maleated polylactide bioplastic: Characterization and biodegradability. Polymer Degradation and Stability, 2009. 94: p. 1076–1084.
- [7] Lee, K.Y., J.J. Blaker, and A. Bismarch, Surface functionalisation of bacterial cellulose as the route to produce green polylactide nanocomposites with improved properties. Composites Science and Technology, 2009. 69: p. 2724–2733.
- [8] Murariu, M., et al., Polylactide (PLA)–CaSO₄ composites toughened with low molecular weight and polymeric ester-like plasticizers and related performances. European Polymer Journal, 2008. 44: p. 3842–3852.
- [9] Li, H. and M.A. Huneault, Effect of nucleation and plasticization on the crystallization of poly(lactic acid). Polymer, 2007. 48: p. 6855–6866.
- [10] Ahmed, J., et al., Thermal and Rheological Properties of L-Polylactide/Polyethylene Glycol/Silicate Nanocomposites Films. Journal of Food Science, 2010. 75: p. 97–108.
- [11] Ibrahim, N.A., et al., Poly(Lactic Acid) (PLA)-reinforced Kenaf Bast Fiber Composites: The Effect of Triacetin. Journal of Reinforced Plastics and Composites, 2010. 29: p. 1099–1111.

CHAPTER VII
EFFECT OF PEANUT SHELL ON THERMAL, MECHANICAL, AND
WATER VAPOR BARRIER PROPERTIES OF PLASTICIZED COMPOSITE
FILMS

7.1 Abstract

Plasticized PLA and plasticized composite films from peanut shell (PNS) and polylactic acid (PLA) were prepared with triacetin as a plasticizer. The results showed that the addition of triacetin into PLA (plasticized PLAs) improved PLA molecular mobility as seen by the reduction of glass transition, cold crystallization, and melting temperatures. Furthermore, the thermo–mechanical properties revealed the improvement of PLA performance at high temperature by the addition of PNS together with triacetin. The morphological study of plasticized composites showed poor interfacial adhesion between PNS and PLA matrix. However, the increasing triacetin content improved the distribution of PNS in PLA matrix. The tensile strength and Young’s modulus of plasticized PLAs decreased while the elongation at break increased with the increasing triacetin content. The adding PNS into plasticized PLAs showed enhancement of Young’s modulus. The water vapor permeabilities of plasticized PLA and plasticized composite films were lower than that of PLA film.

Keyword: composite film, polylactic acid, peanut shell, triacetin, water vapor permeability

7.2 Introduction

The plastic materials are critically issue in waste management and environmental pollution. The consumption of plastic materials poses a major environmental problem due to non–degradable plastics, such as polyethylene. This lends the plastic materials high chemical stability, requiring about 100 years for its complete decomposition [1]. This is because plastic have been used increasing for selected applications which are packaging bags and films [2]. To overcome the

environmental pollution, the biodegradable plastics offer one way of decreasing this problem because it can be disposed directly into the soil or into a composting system at the end of their lifetime.

Poly(lactic acid) or PLA is a biodegradable plastic which derived from renewable resources. PLA is widely used in packaging application because it has many advantages including processability, biocompatibility, as well as biodegradability [3]. However, the brittleness and poor barrier properties have limited their packaging application. Firstly, the use of plasticizer can be enhanced the toughness of materials. Several researches have been modified PLA properties by plasticization method. Oksman et al. [4] reported that the addition of triacetin showed the enhancement of elongation at break of PLA and flax/PLA composites. Ren et al. [5] studied plasticized PLA with triacetin and oligomeric poly(1,3-butylene glycol adipate) which used as a multiple plasticizers. The results showed that the elongation at break increased with the increasing plasticizers while the tensile strength was decreased. Murariu et al. [6] studied plasticized PLA with low molecular weight ester-like plasticizers. They found that the improvement in mechanical performance is obtained from 20 wt% glyceryl triacetate or triacetin. In the same year, Murariu et al. [7] studied plasticized CaSO₄/PLA with triacetin. The result showed that the addition of 10 wt% triacetin into CaSO₄/PLA showed the highest ultimate elongation. The elongation at break of PLA and kenaf/PLA composites increased with the increasing triacetin content, but the tensile strength and stiffness were reduced as reported by Ibrahim et al. [8]. Mansor et al. [9] found that the flexural strength and elongation at break of starch/PLA plasticized with 5 wt% triacetin. Harmaen et al. [10] reported that the addition of 5 wt% triacetin showed decreasing in tensile strength and modulus of oil palm empty fruit bunch/PLA composites.

In addition, the water vapor barrier properties of PLA can be enhanced by the addition of natural fibers which increased the tortuosity for water molecules pathway to go through the thickness of materials [11]. The using natural fibers have the advantages e.g. biodegradability, high strength, low density, and low cost. Numerous researches have been studied on the synthetic fibers such as cellulose nanowhiskers and cellulose nanocrystals. For example, Sanchez-Garcia et al. [12] studied that the addition of 3 wt% cellulose nanowhiskers into PLA was reduced

water permeability up to 82%. The reduction of 34% in water permeability were obtained for the cast films containing 1 wt% of surfactant–modified cellulose nanocrystals as reported by Fortunati et al. [11]. Lexmeshwar et al. [13] also found that the water vapor transmission rate slightly decreased when the content of modified cellulose increased.

Due to the synthetic fibers higher cost, the natural fiber, peanut shell, is interested as an alternative material in order to improved barrier properties of PLA. Peanut shell is an inexpensive agricultural by–product from processing peanuts which consists of 37.0% cellulose, 28.8% lignin, 8.2% protein, and 2.5% carbohydrate [14].

This work was to fabricate PLA–peanut shell composite films by blown film extrusion. The effect of triacetin and peanut shell contents on the mechanical, thermal, thermo–mechanical, barrier, and morphological properties were investigated.

7.3 Experimental

7.3.1 Materials

PLA grade 4043D ($\rho = 1.25 \text{ g/cm}^3$ and $T_m = 210 \text{ }^\circ\text{C}$) was purchased from Nature–Work LLC. Peanut shell was ground to $5\mu\text{m}$ – $100 \mu\text{m}$ with the moisture content of 5%. Triacetin with a 99% purity ($M_w \approx 218 \text{ g/mol}$ and $\rho = 1.15 \text{ g/cm}^3$) was purchased from Sigma–Aldrich. Irganox 1010 and Quent 68 from Ciba Specialty Chemicals were used as stabilizers.

7.3.2 Sample preparation

Preparation of plasticized PLAs and plasticized composites were performed using a LABTECH (type LHFS1–271822) corotating twin–screw extruder with an L/D ratio of 40 ($D = 20 \text{ mm}$, and $L = 800 \text{ mm}$). PLA and peanut shell (5, 10, and 15 wt%) were mixed with triacetin (2.5, 5, 7.5, and 10 phr), and 0.5 phr stabilizers (Irganox 1010 and QUENT 68). Table 7.1 summarizes the composition of each formulation. The temperature profile was maintained in the

range of 120 °C-160 °C from the feed throat to the die and the rotational speed was fixed at 40 rpm.

The PLA-based composite films were produced using a LABTECH (model LTE20–30) single-screw extruder with L/D = 40 (D = 20 mm, and L = 800 mm). The operating temperature of blown film extrusion was operated in the range of 140 °C-160 °C and the rotational speed was fixed at 60 rpm with the blow up ratio of 2:1. The film thickness of each sample is shown in Table 7.1.

Table 7.1 Material formulations and film thickness of each sample

Materials				Code	Film thickness
Peanut shell (wt%)	PLA (wt%)	Triacetin (phr)	Stabilizers (phr)		(μm)
-	100	-	-	PLA	80.23 \pm 5.32
-	100	2.5	0.5	2.5T	82.53 \pm 4.32
-	100	5.0	0.5	5T	82.23 \pm 6.32
-	100	7.5	0.5	7.5T	80.85 \pm 5.34
-	100	10.0	0.5	10T	80.39 \pm 4.94
5	95	2.5	0.5	5P2.5T	112.53 \pm 8.59
5	95	5.0	0.5	5P5T	115.94 \pm 5.64
5	95	7.5	0.5	5P7.5T	114.20 \pm 8.45
5	95	10.0	0.5	5P10T	114.45 \pm 5.85
10	90	2.5	0.5	10P2.5T	134.30 \pm 3.75
10	90	5.0	0.5	10P5T	134.05 \pm 9.32
10	90	7.5	0.5	10P7.5T	145.34 \pm 5.33
10	90	10.0	0.5	10P10T	140.12 \pm 6.32
15	85	2.5	0.5	15P2.5T	143.59 \pm 6.43
15	85	5.0	0.5	15P5T	145.93 \pm 4.74
15	85	7.5	0.5	15P7.5T	152.02 \pm 4.76
15	85	10.0	0.5	15P10T	148.52 \pm 9.43

7.3.3 Characterizations

Dynamic mechanical analysis (DMA) was performed using EPLEXOR 100N in tension mode. The measurements were carried out at a constant frequency of 1 Hz, strain amplitude of 0.1%, and a temperature range of 0 °C-120 °C with a heating rate of 2 °C/min.

Differential Scanning Calorimeter (DSC) was performed using a Perkin–Elmer DSC 822 under N₂ atmosphere. The film samples were heated from 10 °C to 200 °C at heating rate of 10 °C/min. Degree of crystallization (χ_c) was calculated as:

$$\chi_c = \frac{\Delta H_m - \Delta H_{cc}}{\Delta H_{m0} \times w} \times 100 \quad (7.1)$$

ΔH_m is the enthalpy of melting, ΔH_{cc} is the enthalpy of cold crystallization, ΔH_{m0} is enthalpy of melting for 100% crystalline PLA sample, taken as 93 J/g, w is the weight fraction of PLA in the composite [15].

Morphological analysis was examined using a field emission scanning electron microscope (FE–SEM, HITACHI S4800) with an acceleration voltage of 5 kV. The freeze–fractured ends of specimens were sputtering coated (HITHACHI E–1010) with a thin layer of platinum prior to analysis.

The mechanical properties were carried out using a Universal Testing Machine (Lloyd) with a 500 N load cell at a crosshead speed of 50 mm/min according to ASTM D822. The film samples were prepared by cut into rectangular with a width of 10 mm, and a length of 100 mm. The ten samples were used to characterize each material and their average values are reported.

Water Vapor Permeability (WVP) of film samples was measured accordance with ASTM E96–01 method. Film samples were cut into 90x90 mm pieces and each piece was put onto the cup which was filled 20 g of silica gel (0 %R.H.). The film–covered cups were placed in desiccators containing saturated (Mg(NO₃)₂.6HNO₃ solution at 25 °C and 50 ± 3 %R.H. The relative humidity gradient was 50:0 (%R.H. outside: %R.H. inside the cup). The water vapor

transmission rate (WVTR) and water vapor permeability (WVP) were calculate according to:

$$\text{WVTR} = \Delta w / \Delta t \cdot A \quad (7.2)$$

$$\text{WVP} = \text{WVTR} / L \cdot \Delta p \quad (7.3)$$

Where $\Delta w / \Delta t$ is rate of water gain (g/h), A is the exposed area of the film (m^2), L is the mean thickness of film specimens (m), and Δp is the difference partial water vapor pressure between the two sides of film specimens (Pa). The water vapor pressure on the high-stream side of film is 2.34 kPa (i.e., saturated water vapor pressure at 20 °C), while the low-stream side is assumed to be zero.

7.4 Results and Discussion

7.4.1 Dynamic Mechanical Properties

Figure 7.1(a) and Table 7.2 show the storage modulus (E') of PLA and plasticized PLAs. At ambient temperature, the E' of plasticized PLAs is lower than that of PLA due to the plasticizing effect. It can be seen that the E' decreases with the increasing triacetin content. Furthermore, the results clearly show that as temperature increased near to the glass transition temperature (T_g), the sharp drop of the E' . When triacetin is increased, the E' of plasticized PLAs is dropped earlier less than PLA. Further increasing temperature to ~90 °C, the developed E' of plasticized PLAs reveals the sudden increasing as a result of PLA cold crystallization, as observed in DSC results (Table 7.3). This explains that triacetin can induce PLA cold crystallization which improved the modulus of plasticized PLAs ~30 MPa while PLA did not increase in modulus.

Figure 7.1(b) and Table 7.2 show the loss modulus (E''), or ability of the material to dissipate energy, which is related to viscosity. The E'' of plasticized PLAs is slightly lower than that of PLA. This suggests that triacetin reduced the viscosity of PLA. It means that plasticized PLAs can be processed easier than that of

PLA. The increasing triacetin content shifts the E'' to lower temperature with lower value. As temperature increased, the E'' reduced largely.

The ratio of E'' to E' is measured as a loss factor, or $\tan \delta$ is observed in Figure 7.1(c). Since $\tan \delta$ can represent T_g of the material, T_g of plasticized PLAs is lower than that of PLA and their T_g trend is agreement with DSC results (Figure 7.5 and Table 7.3). The damping shows that the molecular motion of PLA is higher than that of plasticized PLAs. It suggests that the increasing triacetin content improved the molecular motion of PLA.

Figure 7.2(a)-7.4(a), and Table 7.2 show the E' of plasticized composites at 5 wt%, 10 wt%, and 15 wt% PNS, respectively. At 30 °C, the E' of plasticized composites is decreased with the increasing triacetin content. Plasticized composites are higher the E' than that of plasticized PLAs due to the presence of PNS. When PNS content is increased leading to improve the E' as can seen in Table 7.2. This result suggests that the addition of PNS improved the rigidity of the materials because of the stiffness of PNS. Furthermore, the results clearly show that as temperature increased near to the T_g , the drop of the E' from ~2.75 GPa-3.87 GPa down to ~17 MPa-30 MPa for all plasticized composites. As the increasing temperature, the E' of plasticized composites became increase because the cold crystallization improved the modulus of materials. It can be noted that plasticized composites are earlier cold crystallization than that of plasticized PLAs. This clarifies that the addition of PNS together with triacetin can strongly induce PLA cold crystallization. At 100 °C, the E' of plasticized composites at 5 %wt, 10 %wt, and 15 %wt of PNS are ~21 MPa-55 MPa, ~20 MPa-62 MPa, and ~38 MPa-98 MPa, respectively. This explains that plasticized composites at 15 wt% PNS is still greater the E' at high temperature than that of plasticized composites at 5 wt% PNS. This means that plasticized composites at 15 wt% PNS have a better temperature resistance when compared to plasticized composites at 5 wt% PNS.

Figure 7.2(b)-7.4(b) and Table 7.2 show the E'' of plasticized composites. Plasticized composites are also shifted the E'' to lower temperature with lower value when triacetin was increased. In addition, plasticized composites at 15 wt% PNS are higher the E'' than plasticized composites at 5 wt% PNS as seen in Table 7.2. When compared with plasticized PLAs, the E'' of plasticized composites is

increased. This suggests that the adding PNS into plasticized PLAs is more difficult to process due to the increase in viscosity.

Tan δ is observed in Figure 7.2(c)-7.4(c). T_g from Tan δ peak shows similar results as DSC (see Figure 7.5 and Table 7.3); T_g of plasticized composites is reduced with increasing triacetin. The damping reveals that the molecular motion of plasticized composites at 5 %wt PNS is the greatest while the molecular motion of plasticized composites at 15 %wt PNS is the lowest. The limited molecular motion in plasticized composites agrees well to the stiffness because of the presence of PNS and the developed crystalline.

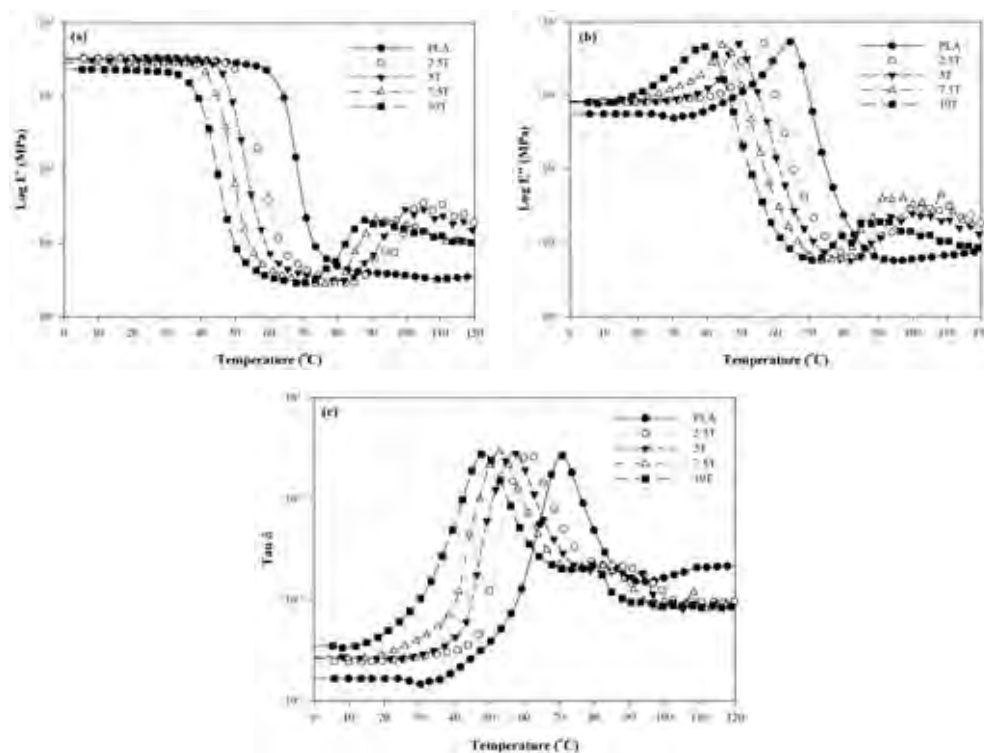


Figure 7.1 Temperature dependence of (a) E' , (b) E'' , and (c) $\tan \delta$ of PLA and plasticized PLAs.

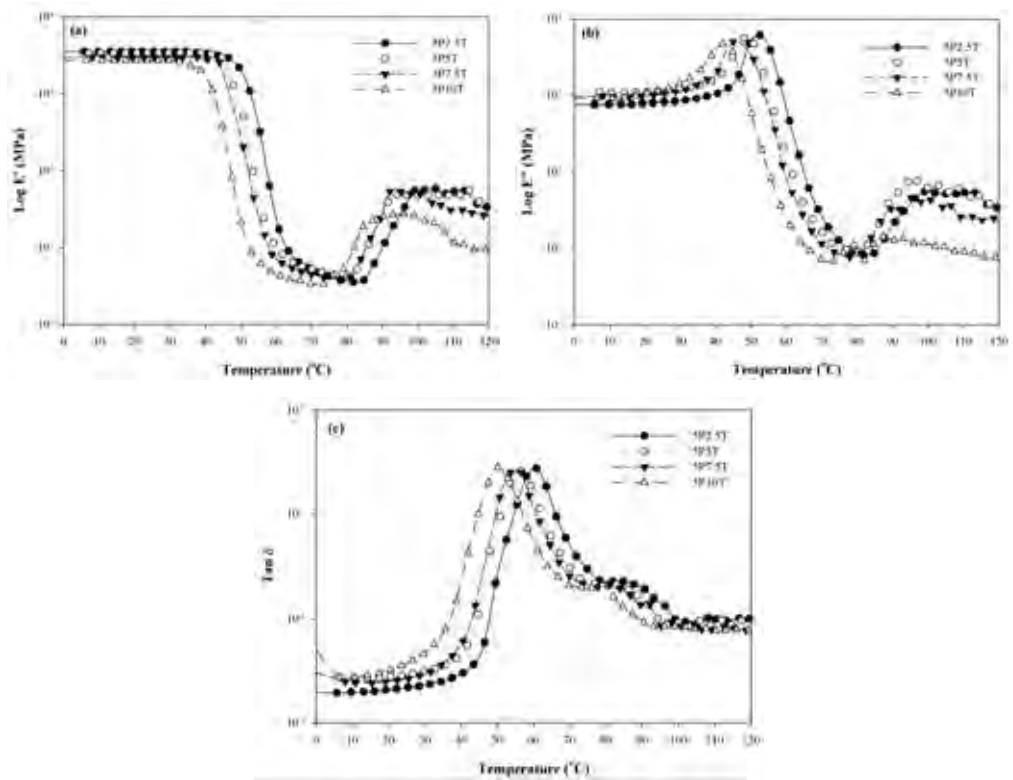


Figure 7.2 Temperature dependence of (a) E' , (b) E'' , and (c) $\tan \delta$ of plasticized composites at 5 wt% PNS.

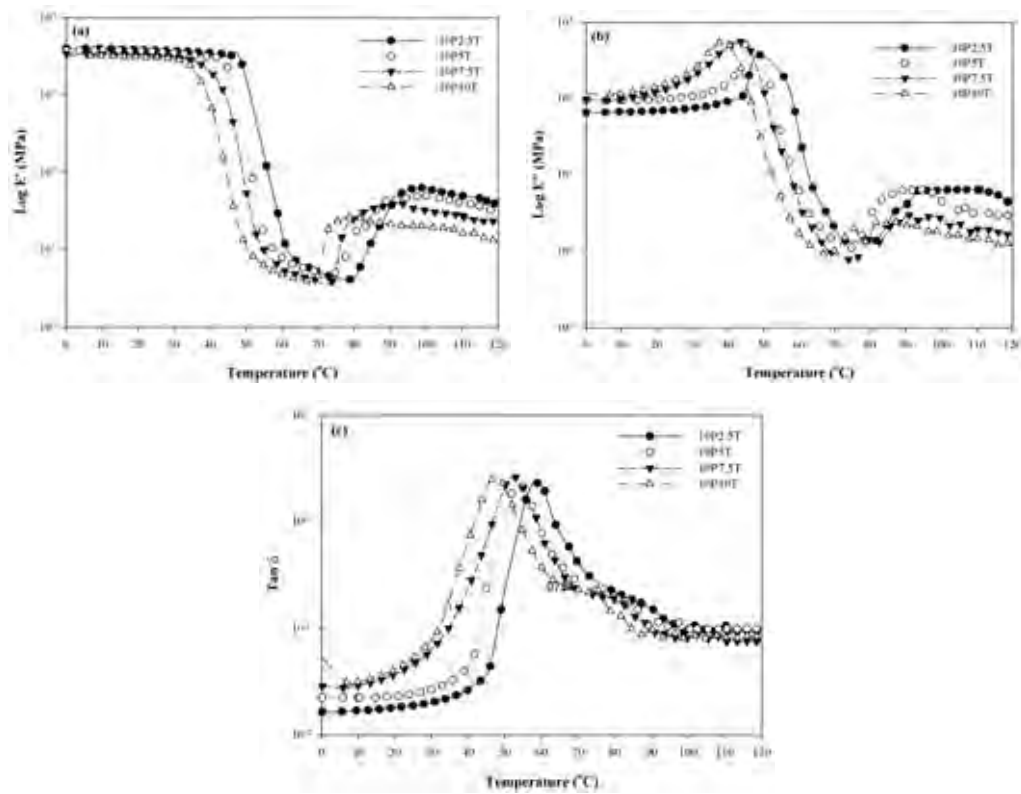


Figure 7.3 Temperature dependence of (a) E' , (b) E'' , and (c) $\tan \delta$ of plasticized composites at 10 wt% PNS.

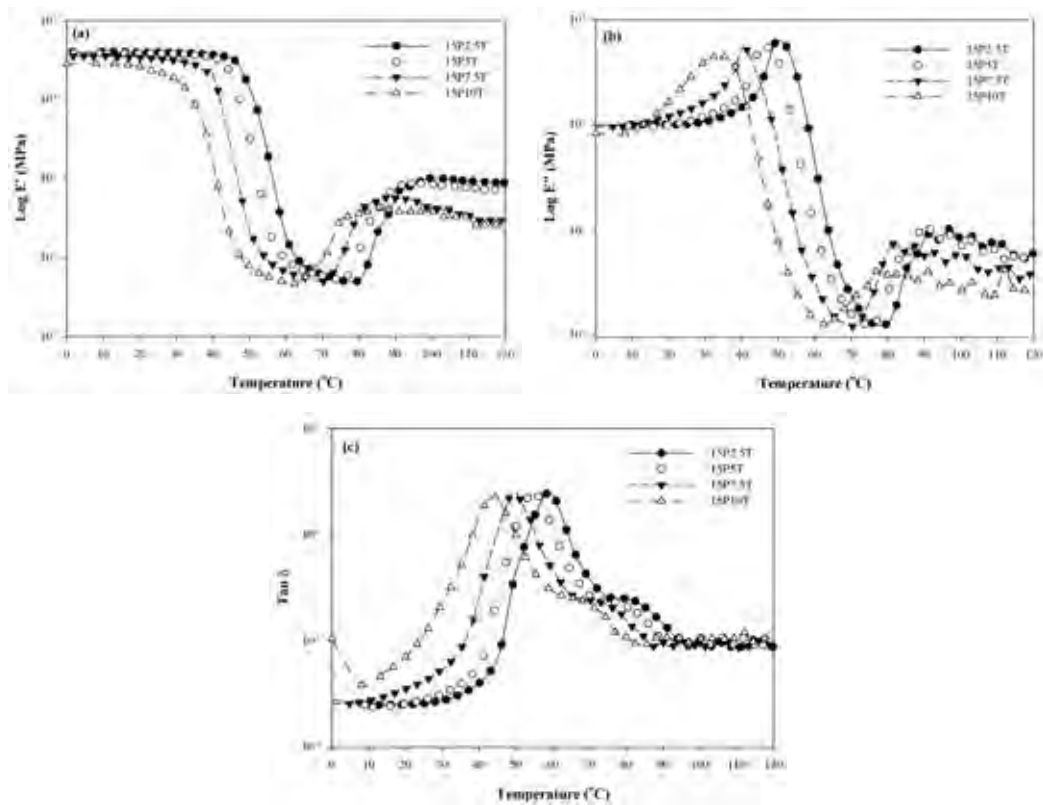


Figure 7.4 Temperature dependence of (a) E', (b) E'', and (c) tan δ of plasticized composites at 15 wt% PNS.

Table 7.2 E' and E'' (MPa) of PLA, plasticized PLAs, and plasticized composites

Sample	T _g from Tan δ	at 30 °C		at 100 °C		at 120 °C	
		E'	E''	E'	E''	E'	E''
PLA	70.80	3326.74±194	48.30±10.42	3.66±0.14	0.60±0.11	3.53±1.49	0.76±0.21
2.5T	62.60	3123.30±105	86.63±9.42	29.46±1.53	2.89±0.52	18.14±3.20	1.69±0.03
5T	57.60	3079.86±103	88.78±12.43	29.27±2.53	2.50±0.11	16.86±5.50	1.36±0.11
7.5T	52.80	2804.04±240	116.27±16.36	25.05±5.21	3.37±0.83	10.24±3.68	1.16±0.43
10T	47.70	2136.58±184	219.89±21.43	22.76±4.20	1.44±0.21	9.88±6.29	0.75±0.45
5P2.5T	60.80	3537.83±135	86.45±11.43	55.28±4.98	5.49±0.84	38.71±6.30	3.52±0.40
5P5T	56.50	3376.21±150	119.95±15.34	47.98±6.20	6.16±0.65	30.28±8.49	4.00±0.67
5P7.5T	53.60	3003.87±158	118.45±12.53	40.89±6.58	4.27±0.12	20.19±5.78	2.22±0.53
5P10T	50.10	2753.23±209	140.72±14.39	21.75±5.25	1.15±0.44	8.24±5.29	0.74±0.65
10P2.5T	58.80	3690.45±184	75.71±10.09	62.94±6.27	6.33±0.45	38.60±6.20	3.88±0.26
10P5T	54.70	3468.82±159	114.42±16.32	49.59±8.40	4.52±0.35	30.59±7.04	2.94±0.74
10P7.5T	52.80	3017.68±219	178.30±19.54	39.36±6.29	2.77±0.76	23.36±9.21	1.66±0.64
10P10T	46.50	2804.88±154	211.24±12.50	20.19±6.93	1.86±0.13	10.19±7.45	1.26±0.25
15P2.5T	58.30	3874.21±175	107.94±15.38	98.64±2.32	8.49±0.62	85.64±4.44	4.77±0.46
15P5T	56.10	3780.48±140	116.74±20.04	82.78±9.34	7.10±0.61	62.75±2.79	4.19±0.79
15P7.5T	48.10	3111.21±125	160.17±14.55	41.09±3.69	5.78±0.42	30.14±6.30	3.79±0.22
15P10T	44.40	2884.12±168	387.11±21.42	38.32±7.73	2.67±0.52	26.50±8.46	2.08±0.78

7.4.2 Crystallization and Melting Behavior

Figure 7.5 and Table 7.3 show the DSC thermograms of PLA, plasticized PLAs, and plasticized composites. In Figure 7.5(a), the results show that plasticized PLAs are lower T_g than that of PLA. The T_g of plasticized PLAs decreased with the increasing triacetin content. This explains that triacetin enhances the chain mobility of PLA. Interestingly, the addition of triacetin induced cold crystallization temperature (T_{cc}). This behavior suggests that plasticizer enhanced the segmental mobility of PLA chains and decreased the intermolecular forces between them which can easily promote PLA crystallization. This result was also found in Martin et al [16]. The T_{cc} and melting temperature (T_m) of plasticized PLAs are decreased with the increasing triacetin content. It can be noted that triacetin decreased the melting point of PLA, which provided an ease of process.

DSC thermograms of plasticized composites are shown in Figure 7.5(b)-7.5(d) and Table 7.3. The T_g of plasticized composites is slightly decreased with increasing triacetin. Moreover, the T_{cc} of plasticized composites is shifted toward to lower temperatures when PNS is increased. This reveals that the presence of PNS facilitated the crystallization process of PLA. The T_m of plasticized composites did not significantly change with the increasing PNS content.

The crystallinity of plasticized PLAs increased when compared to PLA. This means that triacetin improved the ability of PLA matrix to crystallize. When compared with plasticized PLAs, the adding PNS into plasticized PLAs did not significantly improve the crystallinity. Moreover, plasticized composites are slightly increased the crystallinity with the increasing PNS which suggests that PNS can act as a nucleating agent.

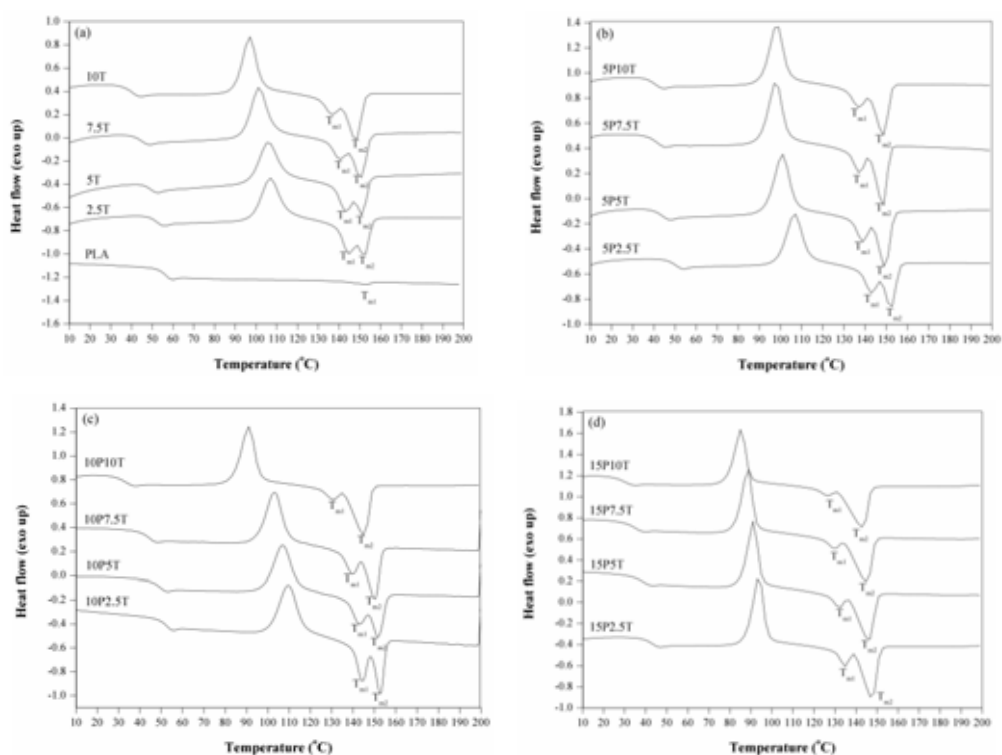


Figure 7.5 DSC thermograms of (a) PLA and plasticized PLAs, (b) plasticized composites at 5 wt% PNS, (c) plasticized composites at 10 wt% PNS, and (d) plasticized composites at 15 wt% PNS.

Table 7.3 Thermal properties of PLA, plasticized PLAs, and plasticized composites

Sample	T _g (°C)	T _{cc} (°C)	ΔH _{cc} (J/g)	T _{m1} ; T _{m2} (°C)	ΔH _m (J/g)	χ _c (%)
PLA	54.3	-	-	154.2	1.2	1.3
2.5T	48.5	107.1	15.7	144.9; 152.8	18.3	2.9
5T	45.3	105.1	16.0	141.9; 150.9	21.8	6.6
7.5T	40.6	101.1	17.4	139.9; 150.7	23.0	6.5
10T	35.5	97.1	18.1	136.8; 148.7	26.2	9.7
5P2.5T	46.2	107.1	18.0	143.7; 152.8	20.6	3.1
5P5T	39.8	101.1	18.9	138.5; 148.8	22.6	4.4
5P7.5T	36.9	97.0	20.1	135.4; 148.8	24.1	4.9
5P10T	28.2	98.1	19.5	137.0; 148.7	23.8	5.4
10P2.5T	48.5	109.7	23.6	144.3; 152.8	26.5	3.6
10P5T	44.9	106.8	22.0	142.7; 151.7	25.7	4.7
10P7.5T	40.1	103.2	23.8	139.8; 150.2	28.1	5.6
10P10T	28.2	91.0	24.4	130.5; 144.7	29.9	7.3
15P2.5T	41.9	93.1	26.0	137.5; 146.7	32.3	8.3
15P5T	38.5	91.1	25.7	134.5; 146.6	32.1	8.6
15P7.5T	35.3	89.1	27.4	131.0; 144.7	34.5	9.8
15P10T	26.3	85.0	29.2	130.0; 142.7	33.8	6.5

7.4.3 Morphology Properties

The morphology of plasticized PLAs is shown in Figure 7.6. The fracture surfaces of plasticized PLAs did not show phase separation. This suggests that triacetin is compatible with PLA matrix. It can be observed that the increasing triacetin content showed rougher surface. In Figure 7.6(d), the some cracks are obvious. This explains that the higher loading triacetin can occur the formation of cracks or voids due to strongly decreasing the intermolecular forces between PLA chains. As reported by Ibrahim et.al [8], an increasing plasticizer content resulted in a large amount of plastically deformed polymer on fracture surfaces.

Fig. 7.7 shows the morphology of plasticized composites. In Figure 7.7(a)-7.7(b), the results show that the good distribution of PNS in the PLA matrix

are observed, suggest that triacetin improved the distribution of PNS under high shear rate during processing. When compared with 15P10T sample (Figure 7.7(b)), it is clearly seen that PNS are better distribution than 15P2.5T sample (Figure 7.7(a)). This explains that the increasing triacetin content improved the dispersion of PNS. In general, plasticizers have also been reported to reduce the viscosity of polymer and improve the dispersion of fiber in the PLA matrix [17, 18].

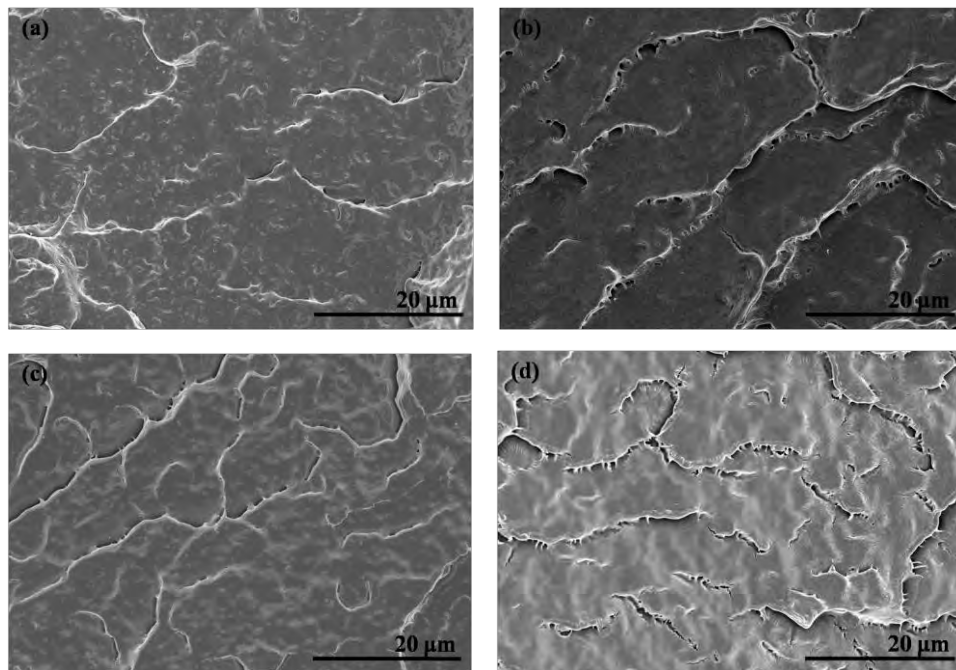


Figure 7.6 Morphology images of (a) 2.5T, (b) 5T, (c) 7.5T, and (d) 10T.

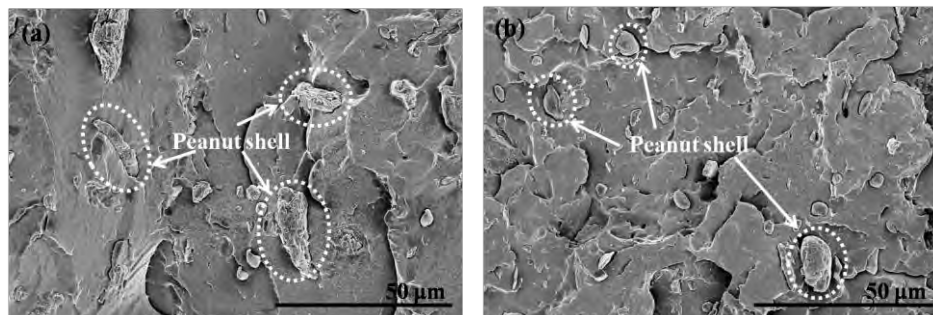


Figure 7.7 Morphology images of (a) 15P2.5T and (b) 15P10T.

7.4.4 Mechanical Properties

Figure 7.8 reveals the mechanical properties of films in both machine (MD) and transverse (TD) directions. The tensile strength, Young's modulus, and elongation at break of all samples in MD are higher than TD. Plasticized PLAs show a decrease in tensile strength and Young's modulus in MD and much more in TD while increase in the elongation at break. This suggests that triacetin decreased the intermolecular between PLA chains and the increase in triacetin content loosen more intermolecular interaction. In the case of plasticized composites, the tensile strength and Young's modulus are significantly decreased in MD rather than in TD compared to those of PLA and plasticized PLAs. This suggests that the increasing PNS decreased tensile strength because the adhesion between PNS and PLA matrix became poor (as seen in FE-SEM results). However, the Young's modulus of plasticized composites increased while the elongation at break decreased with increase in PNS content. The mechanical improvement is occurred in MD than in TD, suggests that the orientation of PNS and PLA crystalline are mainly happened in MD.

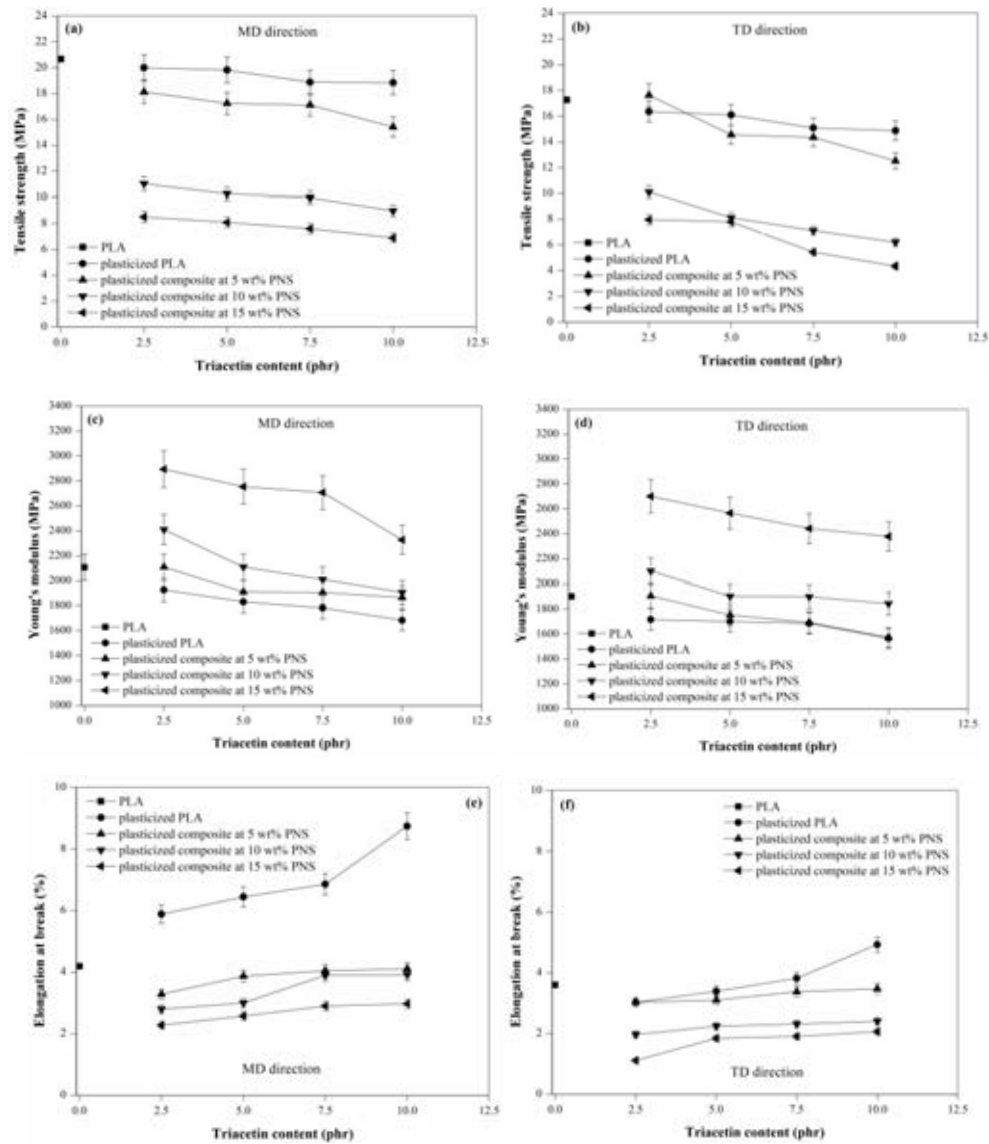


Figure 7.8 Mechanical properties of PLA, plasticized PLAs, and plasticized composites of (a) tensile strength in MD, (b) tensile strength in TD, (c) Young's modulus in MD, (d) Young's modulus in TD, (e) elongation at break in MD, and (f) elongation at break in TD.

7.4.5 Water Vapor Permeability (WVP)

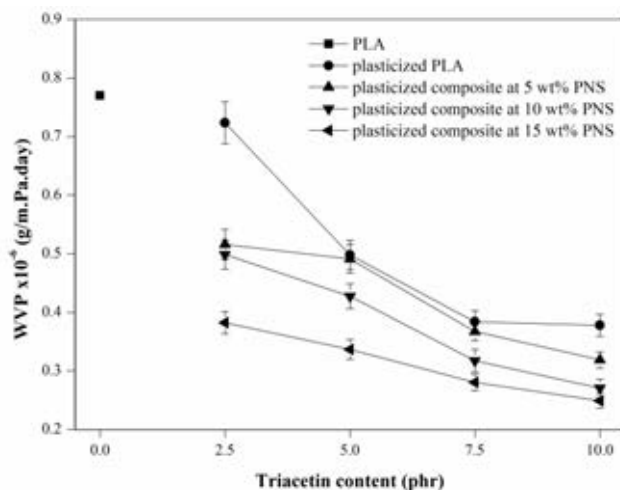


Figure 7.9 WVP of PLA, plasticized PLAs, and plasticized composites.

Figure 7.9 shows WVP data of PLA, plasticized PLA, and plasticized composite films. The WVP of PLA is 0.77×10^{-6} g/m.Pa.day while plasticized PLAs are ~ 0.37 g/m.Pa.day- 0.72×10^{-6} g/m.Pa.day under 0 %R.H.-33 %R.H. gradient. The results show that plasticized PLAs are lower WVP than that of PLA. This indicates that the addition of triacetin improved the barrier properties to water. It can be seen that the incorporation of triacetin increased the crystallinity of PLA (as seen in DSC results), leads to enhance barrier properties. In the case of plasticized composites, the WVP decreased with the increasing PNS content. This suggests that the presence of PNS is thought to increase the tortuous path in the films resulted in reducing the permeability [19]. In addition, the additions of PNS can as a nucleating agent to increase the crystallinity which also decreases the permeability. This means that low WVP of plasticized composites which decreased moisture loss. These results are in good agreement with previous studies by Fortunati et al [11]. The lowest reduction in WVP is observed in the case of adding 15 wt% PNS (~ 0.24 g/m Pa day- 0.38×10^{-6} g/m Pa day).

7.5 Conclusion

This work revealed that plasticized PLA and plasticized composite films were produced by blown film extrusion. The storage and loss modulus of plasticized PLAs decreased with the increasing triacetin content ensuring the plasticizing effect. On the other hand, the storage and loss modulus of plasticized composites were increased with PNS content. When increasing temperature beyond T_g , there was an event that the storage modulus abruptly increased suggesting cold crystallization to occur. The addition of triacetin brought down T_g of PLA and plasticized composites. Thus the increasing triacetin improved the processibility by reduced melting point. The crystallinity of plasticized composites was improved suggesting triacetin together with PNS enhanced the ability of the PLA matrix to crystallize. The morphological properties showed the poor adhesion between PNS and PLA matrix in plasticized composites. However, the increasing triacetin improved distribution of PNS in PLA matrix. The mechanical properties informed that plasticized PLAs and plasticized composites were better mechanical properties in MD than TD. The increasing triacetin content decreased tensile strength and Young's modulus while the elongation at break of plasticized PLAs was increased. Moreover, plasticized composites revealed that the tensile strength decreased while the modulus increased with PNS content. The results showed that plasticized PLAs were lower water vapor permeability than that of PLA. The adding PNS into plasticized PLAs improved the barrier properties to water because the presence of PNS was thought to increase the tortuosity. One property of much film was reduced the water consumption. The composite films showed a decrease in WVP which can use as a much film. Table 7.4 summarizes properties of plasticized composite films.

Table 7.4 Summary of the properties of plasticized composite films

Properties		Decrease	Increase
Thermal properties (T_d, T_g, T_{cc}, T_m)		--	
Mechanical properties	Tensile strength	--	
	Young's modulus	--	
	Elongation at break		++
Thermo-mechanical properties	Storage modulus	--	
	Loss modulus	--	
Water vapor permeability		---	

Note: The symbols, that increase from high to low, are +++, ++, and +, respectively.

The symbols, that decrease from high to low, are ---, --, and -, respectively.

7.6 Acknowledgement

Financial support has been granted by National Research Council of Thailand (NRCT).

7.7 References

- [1] Bilck, A.P., M.V.E. Grossmann, and F. Yamashita, Biodegradable mulch films for strawberry production. Polymer Testing, 2010. 29: p. 471–476.
- [2] Copinet, A., et al., Effects of ultraviolet light (315 nm), temperature and relative humidity on the degradation of polylactic acid plastic films. Chemosphere, 2004. 55: p. 763–773.
- [3] Suryanegara, L., A.N. Nakagaito, and H. Yano, The effect of crystallization of PLA on the thermal and mechanical properties of microfibrillated cellulose-reinforced PLA composites. Composites Science and Technology, 2009. 69: p. 1187–1192.

- [4] Oksman, K., M. Skrifvars, and J.-F. Selin, Natural fibre as reinforcement in polylactic acid (PLA) composites. Composites Science and Technology, 2003. 63: p. 1317–1324.
- [5] Ren, Z., L. Dong, and Y. Yang, Dynamic Mechanical and Thermal Properties of Plasticized Poly(lactic acid). Journal of Applied Polymer Science, 2006. 101: p. 1583–1590.
- [6] Murariu, M., et al., Polylactide (PLA) designed with desired end-use properties: 1. PLA compositions with low molecular weight ester-like plasticizers and related performances. Polymers for advanced technologies, 2008. 19: p. 636–646.
- [7] Murariu, M., et al., Polylactide (PLA)-CaSO₄ composites toughened with low molecular weight and polymeric ester-like plasticizers and related performances. European Polymer Journal, 2008. 44: p. 3842–3852.
- [8] Ibrahim, N.A., et al., Poly(Lactic Acid) (PLA)-reinforce Kenaf Bast Fiber Composites: The Effect of Triacetin. Journal of Reinforced Plastics and Composites, 2010. 29(7): p. 1099–1111.
- [9] Mansor, M.K., et al., Effect of Triacetin on The Mechanical Properties, Morphology and Water Absorption Of Poly(Lactic Acid)/Tapioca Starch Composites. Malaysian Polymer Journal, 2011. 6(2): p. 165–175.
- [10] Harmaen, A.S., et al., Effect of Triacetin on Tensile Properties of Oil Palm Empty Fruit Bunch Fiber-Reinforced Polylactic Acid Composites. Polymer-Plastics Technology and Engineering, 2013. 52: p. 400–406.
- [11] Fortunati, E., et al., Effects of modified cellulose nanocrystals on the barrier and migration properties of PLA nano-biocomposites. Carbohydrate Polymers, 2012. 90: p. 948–956.
- [12] Sanchez-Garcia, M.D. and J.M. Lagaron, On the use of plant cellulose nanowhiskers to enhance the barrier properties of polylactic acid. Cellulose, 2010. 17: p. 987–1004.
- [13] Laxmeshwar, S.S., et al., Preparation and properties of composite films from modified cellulose fibre-reinforced with PLA. Der Pharma Chemica, 2012. 4(1): p. 159–168.

- [14] Harrell, T., et al., Developing Peanut Shell Fuel Briquettes for Household Use in Malawi. Design for Sustainable Development, 2010.
- [15] Lee, K.Y., J.J. Blaker, and A. Bismarch, Surface functionalisation of bacterial cellulose as the route to produce green polylactide nanocomposites with improved properties. Composites Science and Technology, 2009. 69: p. 2724–2733.
- [16] Martin, O. and L. Averous, Poly(lactic acid): plasticization and properties of biodegradable multiphase systems. Polymer, 2001. 42: p. 6209–6219.
- [17] Li, H. and M.A. Huneault, Effect of nucleation and plasticization on the crystallization of poly(lactic acid). Polymer, 2007. 48: p. 6855–6866.
- [18] Teixeira, E.d.M., et al., Properties of thermoplastic starch from cassava bagasse and cassava starch and their blends with poly(lactic acid). Industrial Crops and Products, 2012. 37: p. 61–68.
- [19] Sanchez-Garcia, M.D., E. Gimenez, and J.M. Lagaron, Morphology and barrier properties of solvent cast composites of thermoplastic biopolymers and purified cellulose fibers. Carbohydrate Polymers, 2008. 71: p. 235–244.

CHAPTER VIII
THERMAL BEHAVIORS AND MECHANICAL PROPERTIES OF
PLA–BAGASSE COMPOSITE FILM

8.1 Abstract

Green composites were prepared from bagasse fiber and polylactic acid (PLA) together with a single (triacetin) and the double (triacetin and glycerol) plasticizers in order to improve PLA performance at high temperature use. The presence of plasticizer improved PLA molecular mobility as seen by the reduction of glass transition, cold crystallization, and melting temperatures. The double plasticizers brought down the melting temperature as well as the decomposition temperature when compared to a single plasticizer added in the PLA/bagasse composite. The morphological study of the composites showed poor interfacial adhesion between the bagasse fiber and PLA matrix. Moreover, thermo–mechanical properties revealed the improvement of PLA performance at high temperature use by the addition of bagasse fiber and plasticizers due to cold crystallization at a high temperature which developed high storage modulus. In other words, the bagasse fiber with a single plasticizer allowed PLA to develop high strength and modulus at room temperature while the bagasse fiber with the double plasticizers improved PLA modulus at a high temperature with more ductility and competitive tensile strength at room temperature. The tensile strength of both composite films was superior in machine direction suggesting that crystallization occurred in the machine direction during blown film extrusion.

Keywords: Polylactic acid · Bagasse fiber · Biocomposite · Plasticizer · Blown film extrusion

8.2 Introduction

Bagasse fiber, one of the effective biofiber materials which can be commonly derived from sugar production, is composed of hollow cellulose fibrils held together by lignin and hemicelluloses [1]. Many researchers have been extensively pressed to develop bagasse fiber for both industry and academia. It offered high stiffness, high strength as well as excellent thermal properties. In industry, the use of bagasse fiber played an important role in widespread engineering applications in various sectors like, automotive part, infrastructure, and manufacture of paper, board products, and as a fuel for the sugar factory [2, 3]. Furthermore, in order to encourage environmentally friendly policies, “Green composites” is widely entitled. The design of products and processes that minimize the use and generation of the hazardous substances must be preferably performed. From the structural point of view, in order to use bagasse fiber with higher efficiency, the push toward to develop bagasse fiber as reinforcement part based composite have been performed. Polylactic acid (PLA), one type of biodegradability thermoplastics derived from renewable resources such as corn, starch, tapioca products as well as sugarcane bagasse, is considered as an alternative green material [4]. Composites of PLA reinforced with biofibers including cotton, hemp, kenaf, flax, and ramie have been prepared and studied for their thermal and mechanical properties [5-8]. Biofibers have many advantages because they are cost effective, light weight, and a biodegradable material. The addition of these biofibers can alter the thermal behavior of PLA bulk properties, mostly by improving crystallization, especially cold crystallization and modulus of elasticity.

Up to the present time, several studies have been carried out to understand the thermal behavior of PLA-based composites. Bledzki *et al.* [9] found that PLA biocomposites with abacus fibers enhanced the glass transition temperature because the fibers restricted molecular movement. Suryanegara *et al.* [10] found that microfibrillated cellulose accelerates the crystallization of PLA. The improvement of heat resistance of the PLA composites with ramie and jute fibers shown in the study of Tao *et al.* [11] as the reinforcement of natural fiber prevented the deformation of the PLA-based composites. Moreover, the surface modification by chemical

treatment on ramie fibers, as performed by Yu *et al.* [7], resulted in improved thermal stability of the composites. Huda *et al.* [8] studied surface-treated kenaf fiber reinforced PLA composites which showed an enhancement of the thermal and mechanical properties.

Considerable effort has been made to improve the processability, flexibility and ductility of PLA-based composites by blending with plasticizers such as citrate esters, triacetin, poly(ethylene glycol), and glycerol [12, 13]. Triacetin and glycerol were used as plasticizers for PLA in this study. According to the literature, Ibrahim *et al.* [14] studied the effect of triacetin in PLA/kenaf biocomposites and they found the decrease in storage modulus and softening temperature for plasticized biocomposites. These phenomena were also found in Oksman *et al.* [6] as reported about the plasticized PLA/flax composites with triacetin. Murariu *et al.* [15] mentioned that the plasticized PLA/CaSO₄ composites with triacetin showed cold crystallization properties and a distinctly decrease of the glass transition temperature (T_g). Martin *et al.* [16] found that the increasing glycerol concentration reduced the melting temperature of PLA while had a negligible influence on the T_g of PLA. Supported by Wang *et al.*, [17] the glycerol plasticized starch/PLA composite did not influence the T_g . The green composites are valued for injection molding applications. However, PLA is primarily used for packaging and agricultural applications; film applications could be more relevant than the injection molded products. This work is the first to show that PLA-bagasse fiber composites can be fabricated into film and their mechanical properties can be improved, especially the modulus, for using at high temperatures.

Therefore, the purpose of this research work was to prepare PLA filled with bagasse fiber together with single (triacetin) and double (triacetin and glycerol) plasticizers as green composites by the melt mixing. The effect of a single and the double plasticizers on thermal properties was investigated. Furthermore, the composites were fabricated by blown film extrusion to produce green composite films. The thermo-mechanical, as well as tensile properties, were evaluated and discussed for processing and application.

8.3 Experimental

8.3.1 Materials

Poly(lactic acid) (PLA) grade 4042D from Nature-Work LLC was used. Bleached bagasse fibers (treated with H₂O₂ and ClO₂ to reduce lignin content and to lighten the fibers) from Biodegradable Packaging for Environment Co., Ltd. were ground and sieved into powder (5-200 μm, 10 %moisture content) before use. The plasticizers were triacetin (99%), purchased from Eastman and glycerol, analytical grade (MW ≈ 92 g/mol and ρ =1.25 g/cm³), purchased from Ajak Finechem Pty Ltd. Irganox 1010 and Quent 68 from Ciba Specialty Chemicals, were used as stabilizers.

8.3.2 Preparation of The Green Composite

Preparation of the PLA-based composites were performed using a LABTECH (type LHFS1-271822) corotating twin-screw extruder with an L/D ratio of 40 (D = 20 mm, and L = 800 mm). PLA and bagasse fiber (10 g) were mixed with 10 g triacetin, 10 g glycerol, and 0.5 g stabilizers (Irganox 1010 and QUENT 68). Table 8.1 summarizes the composition of each formulation. The temperature profile was maintained in the range of 120-160 °C from the feed throat to the die and the rotational speed was fixed at 40 rpm.

The PLA-based composite films were produced using a LABTECH (model LTE20-30) single-screw extruder with L/D = 40 (D = 20 mm, and L = 800 mm). The operating temperature of blown film extrusion was operated in the range of 140-160 °C and the rotational speed was fixed at 60 rpm with the blow up ratio of 2:1. The film samples were tested for mechanical properties. The thermo-mechanical testing specimens were prepared by compression molding (Wabash, model V50H-18-CX) for 25 min at 180 °C and subsequently cooled under pressure by water circulation through the plates. The thermo-mechanical properties were performed in tension mode using an EPLEXOR 100 N at a frequency of 1 Hz.

Table 8.1 Material formulations and thickness of each sample

Material	Code	Film thickness (μm)
10 g Bagasse, 90 g PLA, and 0.5 g of stabilizers (or 9.90 wt% Bagasse, 89.10 wt% PLA, and 0.49 wt% of stabilizers)	10BAG	146.20 \pm 7.33
10 g Triacetin, 90 g PLA, and 0.5 g of stabilizers (or 9.90 wt% Triacetin, 89.10 wt% PLA, and 0.49 wt% of stabilizers)	10T	85.02 \pm 5.20
10 g Triacetin, 10 g Glycerol, 90 g PLA, and 0.5 g of stabilizers (or 9.00 wt% Triacetin, 9.00 wt% Glycerol, 81.08 wt% PLA, and 0.45 wt% of stabilizers)	10T10G	80.30 \pm 4.75
10 g Bagasse, 90 g PLA, 10 g Triacetin, and 0.5 g of stabilizers (or 9.00 wt% Bagasse, 81.08 wt% PLA, 9.00 wt% Traiacetin, and 0.45 wt% of stabilizers)	10BAG10T	142.42 \pm 9.21
10 g Bagasse, 90 g PLA, 10 g Triacetin, 10 g Glycerol, and 0.5 g of stabilizers (or 8.26 wt% Bagasse, 74.38 wt% PLA, 8.26 wt% Triacetin, 8.26 wt% Glycerol, and 0.41 wt% of stabilizers)	10BAG10T10G	136.47 \pm 6.32

8.3.3 Characterization of The Green Composite Film

The chemical structures were analyzed by attenuated total reflection fourier transforms infrared spectroscopy (ATR–FTIR; Nicolet Nexus 670 FTIR). The thermal properties were carried out by differential scanning calorimeter (DSC; Perkin-Elmer DSC 822) and thermogravimetric analyzer (TGA; Q5 TA) with a heating rate of 10 °C/min under a nitrogen flow. The morphological properties were examined using a field emission scanning electron microscope (FE–SEM; HITACHI S4800) with an acceleration voltage of 5 kV. The mechanical properties were carried out using a Universal Testing Machine (Lloyd) with a 2500 N load cell at a crosshead speed of 50 mm/min according to ASTM D822.

8.4 Results and Discussion

The compounding of PLA and bagasse fiber was limited by the ability of the composites to be blown into a stable bubble. As a result, the maximum bagasse content that could be added to PLA was 10 g (~9 wt%). Bagasse fiber was rather bulky like other cellulose fibers, so they obtained film was rather stiff. It should be noted that all the composite films have to contain the plasticizer since the composite films without plasticizer are difficult to process. There were two composites used in this work; the bagasse/PLA composite with a single plasticizer (triacetin ~9 wt%) and one with the double plasticizers (triacetin and glycerol at ~8.26 wt% each). Table 8.1 lists the composition of each component for both composites. The composite with the double plasticizers shows a good processability compared to the composite with a single plasticizer. Evidently, the blown-film bubble fabricated from the double plasticizers is more stable than the latter one. It can be noted that the addition of glycerol improves the processability. The optimum plasticizer (single and double plasticizers) is thus a compromise between the process requirements and the desired material stiffness.

8.4.1 Thermo-Mechanical Properties

Figure 8.1(a) and Table 8.2 show the effect of temperature on storage modulus (E'), which relates directly to the stiffness of the composites. At ambient temperature, the E' of the composite without plasticizer (10BAG) is higher than that of PLA. This result suggests that the bagasse fiber can be used to reinforce PLA matrix. For plasticized PLA (both 10T and 10T10G), it shows lower E' than PLA due to the plasticizing effect. In the case of the composites, it is similarly seen that E' of the double plasticizers (10BAG10T10G) is lower than that of a single plasticizer (10BAG10T). This indicates that the softening is due to the addition of glycerol which is rather small molecule. The addition of a second plasticizer, glycerol decreases E' from 2,840 MPa (for 10BAG10T) to 2,430 MPa (see Table 8.2). This agrees well with the modulus results from the mechanical testing (Table 8.4). Although the modulus can be lowered by adding plasticizers, the composites are not

actually softened because their modulus values are still high (2,840 and 2,430 MPa as compared to the modulus of polyethylene mulch film, ~ 65 MPa but this range of modulus is applicable as thermoforming sheet) [18]. Furthermore, the results clearly show that as temperature increased near to the glass transition temperature, the sharp drop of the storage modulus from 2.5-3.0 GPa down to about 13 MPa or less happened around 60 °C (about the glass transition temperature) for PLA and 10BAG. When the plasticizer was added, the storage modulus dropped earlier about 40 °C to ~11-24 MPa for the plasticized PLA, and ~30-70 MPa for the composites, respectively. Especially, when both plasticizers were added, the storage modulus became the lowest and drop sooner than the others suggesting this double plasticized PLA was the softest compound. When bagasse fiber was added, both single and double plasticized PLA composites showed an increase in their storage moduli. It is noted that these storage moduli of the composites still abruptly dropped at the temperature closed to those of unfilled-plasticized PLA. So, it is summarized that the stiffness of the composites are strongly dependent on plasticizer rather than filler addition. Further increase of temperature to about 70 °C and more, as seen in the insert plot in Figure 8.1 (a), revealed the sudden increase of the storage modulus as a result of PLA cold crystallization, as observed in DSC results (Table 8.3). This clarifies that the bagasse fiber only can induce PLA cold crystallization (at rather high temperature 107 °C) which strongly improves the modulus of the 10BAG composite above 150 MPa while pure PLA does not show an increase in modulus. For example, at 100 °C, E' of PLA is 2.34 MPa while those of 10BAG, 10BAG10T, and 10BAG10T10G are greater than 100 MPa. This was also supported by DSC results (see Table 8.3). On the other hand, the single plasticizer can induce PLA cold crystallization earlier (at 90 °C) but less strong than bagasse fiber. The double plasticized PLA (10T10G) causes cold crystallization taken place at even lower temperature (80 °C). The composite with the double plasticizers shows that cold crystallization is well developed at lower temperature (~75 °C) than the composite with a single plasticizer (~87 °C). The developed storage modulus of the plasticized PLA or the composites becomes lower and declined more with increasing temperature for the double plasticizer than for the single plasticizer. This means that the composite with a single plasticizer has a greater temperature resistance than the

latter one. From Table 8.2, this suggests the cold crystallization of the composites with plasticizers at high temperature e.g. 100 °C was completed while the cold crystallization of the composite without plasticizer was partially occurred so the composites with plasticizers show higher rigidity (higher modulus) than that of the composite without plasticizer while E' at 120 °C of the composite without plasticizer become higher than the composites with plasticizers. In general, the E' decreases with increasing temperature, especially at a temperature higher than the glass transition temperature; however, the E' of the composites not only turn to increase at higher temperature beyond the glass transition region because of the presence of cold crystallization, but also retain their rigidity due to the development of a high modulus value until the melting temperature.

Figure 8.1(b) and Table 8.2 show the loss modulus (E''), or ability of the material to dissipate energy, which is related to viscosity. The E'' of PLA is rather low suggesting low viscosity (less dissipates energy). By adding either bagasse fiber or plasticizers at low temperature, the loss modulus is doubly enhanced. As temperature increased, the loss modulus reduced largely. Only bagasse fiber addition, the composite is not softened while the addition of plasticizer shifts the loss modulus to lower temperature with lower value. The double plasticized composite shows the lowest loss modulus at low temperature and lower than the single plasticized composite at high temperature. This also suggests that the double plasticizer in the composite can be processed easier than the composite with single plasticizer. The ratio of E'' to E' is measured as a loss factor, or $\tan \delta$, as observed in Figure 8.1(c) and Table 8.2. $\tan \delta$ shows similar results as DSC (see Figure 8.4 and Table 8.2); T_g of the composites are lower than that of PLA. The composite with a single plasticizer has a higher glass transition temperature than that of the composite with the double plasticizers. Moreover, its damping reveals that the molecular motion of PLA is the greatest while the motion of the composite with the double plasticizers is greater than that of the one with a single plasticizer. The limited molecular motion in the composites agrees well to the stiffness because of the presence of bagasse fiber and the developed crystalline.

Thus the bagasse/PLA composite with double plasticizers is better for processing into film although the film is rather stiff at room temperature due to

reinforcing effect of bagasse fiber. Furthermore, both plasticized composites are suitable enough to use at high temperature because the storage modulus at high temperature (>80 °C) is in the range of 100-160 MPa which is strong enough for mechanical application (although upon heating the plasticized composites may be softened to the storage modulus of 30-70 MPa around the glass transition temperature).

The results are useful for processing. Without plasticizers, the composite is rigid or difficult to process and possibly causes poor mixing. The plasticizers are needed to ease the processing by lowering the modulus. The double plasticized composite is a good compromise rather than the single plasticized composite; however, the high plasticizer amount may be inferior to the mechanical properties. Moreover, for application aspect, due to the high modulus of the obtained plasticized composites, they are probably good for use as thermoforming sheets rather than mulch films.

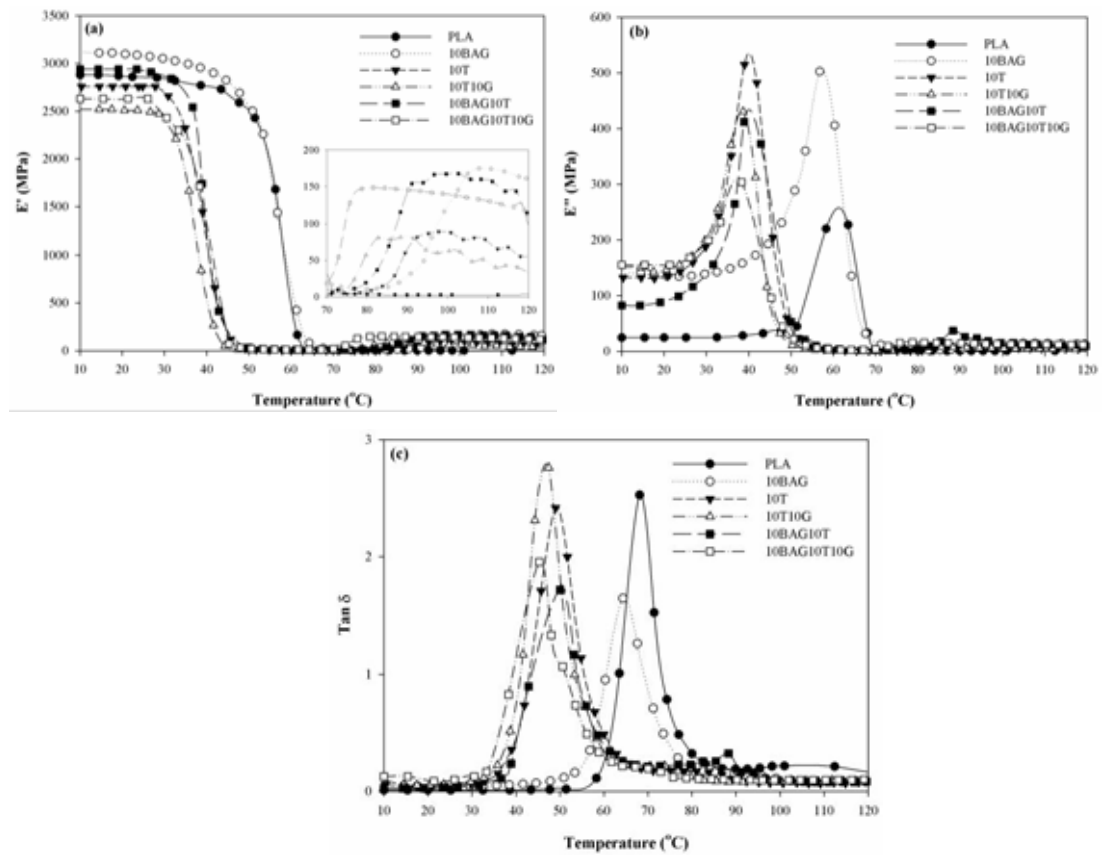


Figure 8.1 Temperature dependence of (a) E' , (b) E'' , and (c) $\tan \delta$ of PLA, plasticized PLA, and composites.

Table 8.2 E' and E'' (MPa) of PLA, plasticized PLA, and the composites

sample	T _g from Tan δ	30 °C		100 °C		120 °C	
		E'	E''	E'	E''	E'	E''
PLA	68.70	2820.21±20.02	42.25±2.53	2.34±0.86	0.58±0.05	8.47±1.21	4.12±0.92
10BAG	65.30	3052.89±32.16	138.37±6.47	115.46±6.03	12.59±0.13	156.54±8.54	12.68±0.43
10T	49.00	2658.73±26.42	187.18±8.46	87.72±4.53	6.10±0.53	57.05±7.47	4.02±0.65
10T10G	45.40	2372.48±21.40	199.42±7.67	62.81±5.25	5.17±0.68	33.05±4.67	3.01±0.44
10BAG10T	50.00	2840.20±18.32	155.62±4.90	167.26±8.43	15.01±0.86	113.78±7.54	9.39±0.64
10BAG10T10G	45.30	2430.71±22.84	198.98±5.36	137.55±5.34	12.92±0.50	117.28±9.50	11.59±0.13

8.4.2 Characterization of the Bagasse Fiber/PLA Composite Films

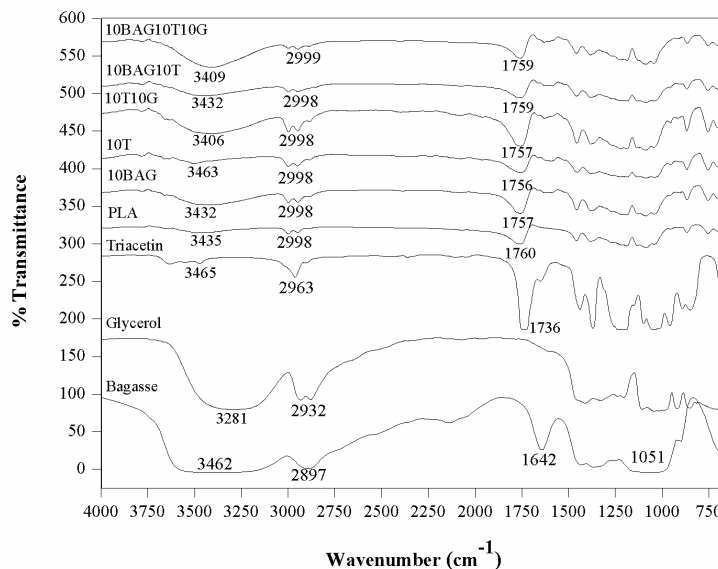


Figure 8.2 FTIR spectra of bagasse, PLA, plasticized PLA, and composite films.

Figure 8.2 shows FTIR spectra of bagasse fiber, PLA, plasticized PLA, and the composites film from ATR mode because the samples are rather opaque. The bagasse fiber shows a broad absorbance band centered around 3462 cm^{-1} which is assigned to the hydrogen-bonded hydroxyl groups (O–H) [19]. Other interesting absorption bands found at 1642 cm^{-1} , broad bands at 1450 cm^{-1} , 1374 cm^{-1} , 1051 cm^{-1} , and 890 cm^{-1} are assigned to C=C aromatic stretching vibration of lignin (partly bleached), C–H bending from $-\text{CH}_2$, and $-\text{CH}_3$ groups, cellulose linkages, and β -glycosidic linkage, respectively [20]. The PLA spectrum shows an obvious absorbance at 1760 cm^{-1} , 1458 cm^{-1} , 1383 cm^{-1} , $1189\text{--}1086\text{ cm}^{-1}$, 868 cm^{-1} , and 755 cm^{-1} which are assigned to the stretching vibration of the carbonyl group (C=O), C–H bending of $-\text{CH}_2$, and CH_3 , C–O stretching, crystalline phase, and amorphous phase, respectively [21]. In the case of both plasticized PLA films, there are an obvious absorbance at $\sim 3406\text{--}3432\text{ cm}^{-1}$ and $\sim 1756\text{--}1757\text{ cm}^{-1}$ corresponding to the O–H stretching and C=O stretching, respectively. These results indicate that the plasticized PLA (10T and 10T10G) exhibits the characteristic peaks of both PLA and plasticizers, of which does not significantly changes due to the physical interaction

[22]. In addition, the spectra of the composites with plasticizers exhibit broad peaks at $\sim 3400\text{ cm}^{-1}$ and $\sim 1597\text{ cm}^{-1}$ which are assigned to characteristic peaks of bagasse and also show peak at $\sim 1759\text{ cm}^{-1}$ which is assigned to characteristic peak of PLA. It is strongly confirmed that no chemical interaction occur between bagasse, PLA, and the plasticizers since no new characteristic peaks appear [23].

8.4.3 Thermogravimetry

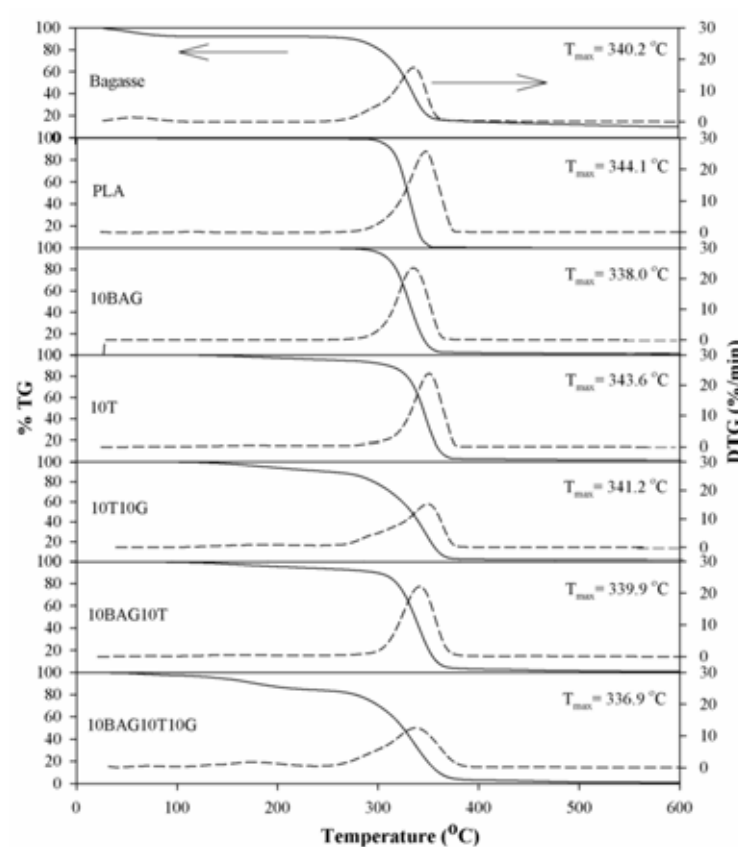


Figure 8.3 TGA and DTG curves of bagasse, PLA, plasticized PLA, and composites.

Figure 8.3 shows the thermogravimetric (TG) and derivative thermogravimetric (DTG) curves of bagasse fiber, PLA, plasticized PLA, and the composites. The decomposed temperature is the temperature at the maximum rate of mass loss (T_{max}), or DTG curve. Considering the thermogram of the bagasse fiber, a

two-step transition is found where the first mass loss gradually occurs ~ 100 °C, which contributes to the loss of moisture content of ~ 10 %wt. The second transition is associated with the cellulose decomposition at T_{\max} 340.2 °C. The char residue is about 10 %wt. Polylactic acid (PLA) has one transition in its chain decomposition at T_{\max} 344.1 °C. It is obvious that T_{\max} of the composite without plasticizer (10BAG) is lower than that of PLA which can be ascribed to low thermal stability of the bagasse fiber. However, moisture remained in the bagasse fiber which can encourage the ester bonds scission of PLA [24]. The plasticized PLA films (10T and 10T10G) show slight decrease of the decomposition temperature compared to that of PLA due to the volatilization of the plasticizers. For the 10BAG10T composite, single decomposition gradually occurs from 120 °C with T_{\max} 339.9 °C while two steps of mass loss are clearly seen in the 10BAG10T10G composite. The composite with double plasticizers (with glycerol that absorbs moisture) makes the first decomposition starting at a temperature lower than 100 °C [25]. Subsequently, the second step shows the decomposition of bagasse fiber together with PLA at ~ 120 -336 °C (T_{\max} 336.9 °C). It was not surprising to find that the decomposition temperature of the composite films is slightly lower than those of the starting materials due to the presence of plasticizers.¹⁵ The thermal stability of 10BAG10T is slightly higher than that of 10BAG10T10G. This is to note that the compatibility between bagasse fiber and PLA decrease in the presence of glycerol.

8.4.4 Crystallization and Melting Behavior

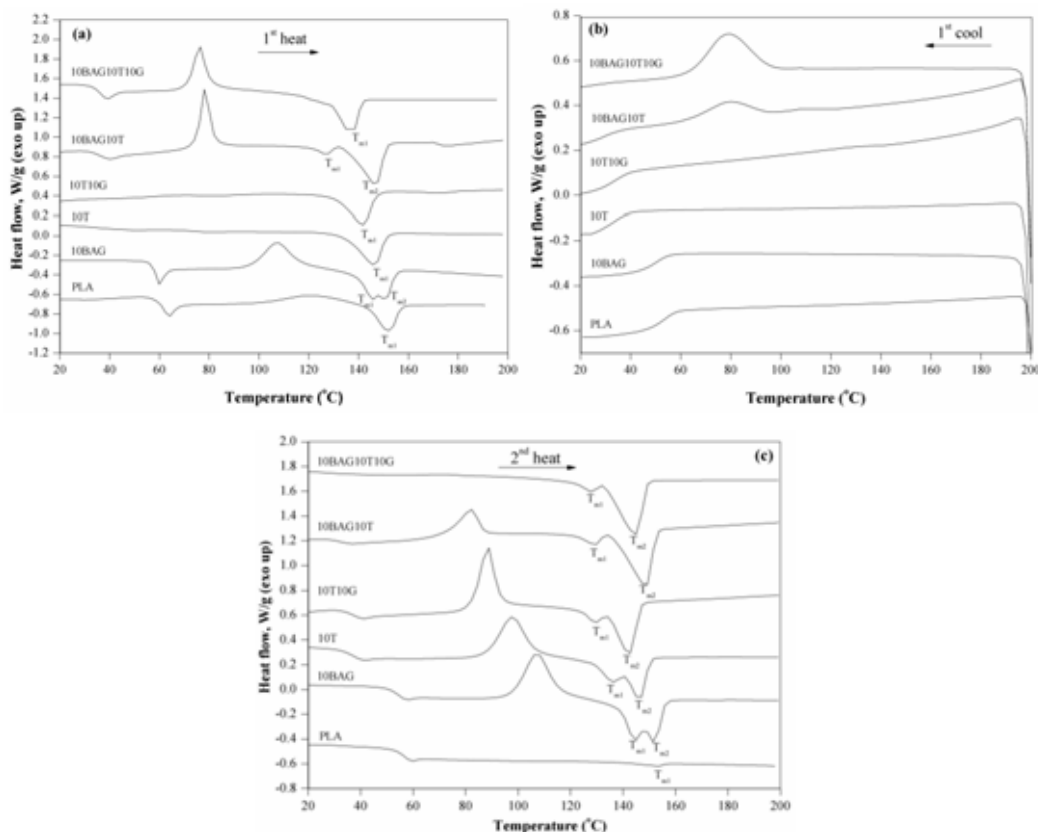


Figure 8.4 DSC thermograms of (a) first heating scan, (b) first cooling scan, and (c) second heating scan of PLA, plasticized PLA, and composites.

Figure 8.4 and Table 8.3 show the DSC thermogram of PLA where its glass transition temperature (T_g) and melting temperature (T_m) taken from the second heating were 54.3 °C (lower than that of the first heating scan) and 154.2 °C (with melting enthalpy ~ 1.2 J/g). The T_{cc} and T_m of the double plasticized PLA (10T10G) are lower than those of a single plasticizer (10T) while the T_g of both 10T10G and 10T are not different. This suggests that glycerol is a poor plasticizer for PLA [16]. However, glycerol shows a decreasing of the melting point of the material, which provides an ease of process. Interestingly, both bagasse fiber and plasticizers can induce PLA melt and cold crystallization at ~ 79 – 81 °C and 72 – 80 °C, found in both cooling and heating scans, respectively. The PLA melt crystallization is typically not

found during cooling even with plasticizers; bagasse fiber is therefore a very effective nucleating agent for PLA (a similar observation was also found in the microfibrillated cellulose/PLA composite) [10]. The crystallinity of the composites largely increases and the crystalline makes the composite films turn opaque white. However, T_g and T_m of the composites with plasticizers are lower than (T_g 28.2 °C for single plasticizer and less for double plasticizers; T_m ~129 °C, 149 °C for a single plasticizer and ~128 °C, 145 °C for the double plasticizers) those of the composite without plasticizer due to the plasticizing effect [15]. The plasticization enhances the segmental mobility of polymer chains and easily enables chain slippage to promote the craze formation since the plasticizer penetrates into the polymer chains and decreases the intermolecular forces between them. Moreover, this suggests that the composites can melt before PLA ($T_m = 154.2$ °C) or they cannot resist high temperature usage as compared to pure PLA or they can be used up to 120 °C, just below its first melting temperature.

Table 8.3 Glass transition temperature (T_g), cold crystallization temperature (T_{cc}), melting temperature (T_m), melt crystallization temperature (T_{mc}), cold crystallization enthalpy (ΔH_{cc}), melting enthalpy (ΔH_m), melt crystallization enthalpy (ΔH_{mc}), and crystallinity (χ_c) of PLA, plasticized PLA, and composites

Sample	First heating scan						First cooling scan		Second heating scan					
	T_g (°C)	T_{cc} (°C)	ΔH_{cc} (J/g)	$T_{m1};$ T_{m2} (°C)	ΔH_m (J/g)	χ_c (%)	T_{mc} (°C)	ΔH_{mc} (J/g)	T_g (°C)	T_{cc} (°C)	ΔH_{cc} (J/g)	$T_{m1};$ T_{m2} (°C)	ΔH_m (J/g)	χ_c (%)
PLA	60.2	122.0	20.2	153.1	29.1	31.3	-	-	54.3	-	-	154.2	1.2	1.3
10BAG	56.8	107.0	20.4	145.2; 151.4	23.0	27.8	-	-	50.5	107.1	26.0	144.3; 151.9	28.1	2.5
10T	40.2	-	-	146.9	21.2	25.6	-	-	32.4	97.6	24.6	136.1; 146.7	26.0	1.8
10T10G	-	-	-	142.4	21.1	28.0	-	-	32.4	88.4	22.3	129.3; 142.8	29.1	9.0
10BAG10T	32.0	80.0	18.0	127.4; 147.9	29.1	38.6	79.7	8.2	28.2	82.8	11.7	129.5; 149.5	22.6	14.5
10BAG10T10G	35.3	72.5	18.1	138.7	44.5	64.3	81.3	20.3	-	-	-	128.3; 145.4	31.7	45.8

$$\chi_c = \frac{\Delta H_m - \Delta H_{cc}}{\Delta H_{m0}} \times 100, \Delta H_{m0} \text{ is enthalpy of melting for 100\% crystalline PLA sample, taken as 93 J/g, } w \text{ is the weight fraction of}$$

PLA in the composite [26].

8.4.5 Morphological Properties

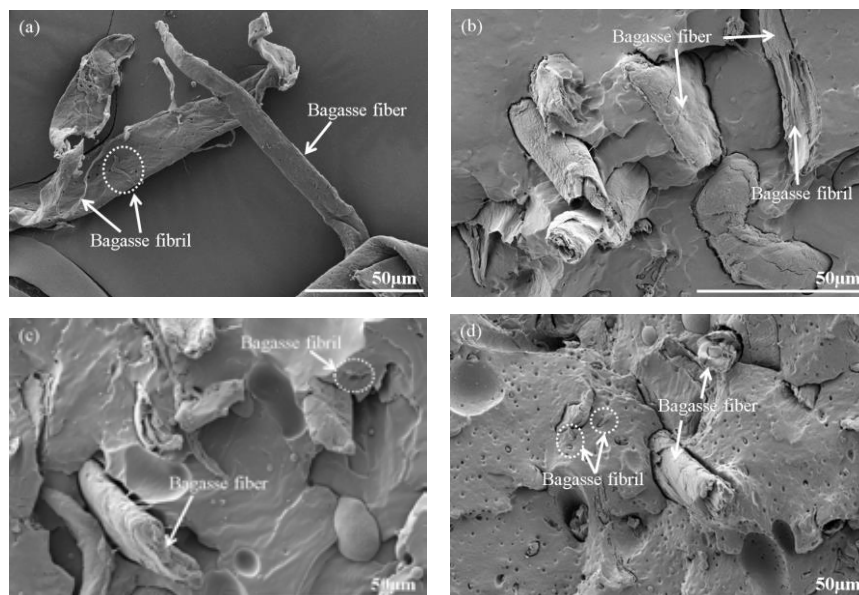


Figure 8.5 Morphological images of (a) bagasse, (b) 10BAG, (c) 10BAG10T, and (d) 10BAG10T10G.

The morphology of the bagasse fiber and the composites were observed by FE-SEM, which the images shown in Figure 8.5. Bagasse fiber is composed of many fibrils as seen in Figure 8.5(a). It is estimated that the average size of the bagasse fibers is 10-30 μm in diameter and 100-200 μm in length. In Figure 8.5(b), there are many bagasse fibers pulled out and aggregated in PLA matrix. The presence of voids around the fiber indicates poor adhesion between the bagasse fiber and PLA matrix. In Figure 8.5(c) and Figure 8.5(d), the good distribution of bagasse fibers and fibrils in the PLA matrix are observed, suggesting the plasticizers improve the distribution of the fibers under high shear rate during processing. Plasticizer has also been reported to decrease the viscosity and consequently increase the dispersion of fiber in the PLA matrix [27]. In Figure 8.5(c), it is clearly seen that the fibrils are implanted in PLA matrix while the Figure 8.5(d) shows the distribution of fibrils in tiny void. Several tiny voids occurring are due to the moisture loss from glycerol during the melt mixing. These results were also

found in Martin et al. [16] who reported that the plasticized starch/PLA with glycerol showed large and non-uniform holes. It should be noted that the addition of glycerol creates more defects that result in poor tensile strength.

8.4.6 Mechanical Properties

The green composite films produced by blown film extrusion were used for mechanical testing. Table 8.4 reveals the tensile properties of the films in both machine (MD) and transverse (TD) directions. Young's modulus of PLA in MD is almost twice of the modulus in TD while tensile strengths in both directions are not much different. This suggests the crystalline mainly align in MD. The plasticized PLA (10T and 10T10G) shows a decrease in tensile strength and Young's modulus in MD and much more in TD because the plasticizer decrease the intermolecular between PLA chains and more plasticizers loosen more intermolecular interaction (agreed well with thermal stability as seen in TGA results). The tensile strength and modulus of the 10BAG sample increase significantly in MD rather than in TD compared to that of PLA due to reinforcing effect. Besides the reinforcement of bagasse fiber, the contribution of crystallinity to enhance strength, elongation and Young's modulus is obvious when its amount is increased significantly as in both plasticized composite films. However, the mechanical improvement is occurred in MD than in TD. This suggests that the orientation of bagasse fiber and PLA crystalline are mainly happened in MD while the plasticizing effect overwhelms in TD. The plasticized PLA/bagasse fiber composites are very anisotropic. Although the composite with double plasticizers show poorer tensile strength and modulus, it has higher elongation at break than the one with single plasticizer. This contributes to higher crystallinity allowing more chain drawing and the increase in chain mobility due to the lowering of T_g , which agrees to the previous report by N. Wang et al [18]. They found that the elongation at break can be improved by the addition of glycerol. A higher amount of plasticizers, which are responsible for an increase in free volume, thus allow some additional mobility of polymer chain. In addition, the weak strength in TD also indicates that bagasse fiber cannot act to retard crack propagation and poor adhesion between the fiber and PLA matrix.

Table 8.4 Mechanical properties in machine (MD) and transverse (TD) direction of PLA, plasticized PLA, and composites

Sample	Fiber orientation	Tensile strength (MPa)	Elongation at break (%)	Young's Modulus (MPa)
PLA	MD	4.01±0.36	3.72±1.87	1000.32±186.06
	TD	3.50±0.21	2.08±0.18	615.25±62.12
10BAG	MD	6.99±0.45	1.95±1.50	1452.90±36.54
	TD	0.52±0.13	1.03±0.26	1207.74±52.37
10T	MD	3.11±0.50	7.33±0.94	892.24±66.01
	TD	2.06±0.29	5.02±0.35	210.42±105.00
10T10G	MD	1.89±0.84	9.12±0.79	620.75±21.93
	TD	0.72±0.09	6.84±0.20	174.02±84.56
10BAG10T	MD	6.73±0.81	2.73±0.26	1248.53±96.31
	TD	1.09±0.06	2.05±0.21	262.84±19.37
10BAG10T10G	MD	4.35±0.33	5.78±1.60	721.06±68.06
	TD	0.69±0.07	3.24±1.18	156.71±14.85

8.5 Conclusion

This work reveals that bagasse fiber and plasticizers strongly alter the crystallization behavior of PLA such that thermal stability and mechanical properties of the plasticized composites differ from those of pure PLA. The storage and loss moduli of PLA increased with the addition of bagasse fiber ensuring the reinforcement effect. On the other hand, they are reduced by the addition of single plasticizer, triacetin and even more decreased with the double plasticizers, triacetin and glycerol. Moreover, the plasticizer brought down T_g of PLA significantly. However, the single or double-plasticizer showed less effect on changing T_g of PLA. The single plasticized PLA/bagasse fiber composite showed improved storage modulus with higher T_g as compared to the double plasticized PLA/bagasse fiber

composite and the plasticized PLA. Thus the double-plasticized PLA/bagasse fiber composite is better processability than the single-plasticized one. When increasing temperature beyond T_g , (>70 °C) there was an event that the storage modulus abruptly increased suggesting cold crystallization to occur. The bagasse fiber had stronger reinforcement effect than the plasticizers while the plasticizer had strong decrease in T_g so, the double plasticized composite had lower T_g (45 °C) and storage modulus (>100 MPa) than the single-plasticized one (T_g 50 °C and $E' >150$ MPa). The effect of bagasse fiber and plasticizer on loss modulus and tan delta were mostly similar to the storage modulus. This suggests that although the double plasticized PLA/bagasse fiber composite is easier to process but its mechanical properties may be poorer than the single-plasticized one and both plasticized PLA/bagasse fiber composites can be used at high temperature. The plasticized PLA/bagasse fiber composite films are suitable for use as thermoforming sheet. FTIR results show the characteristics absorption peaks of bagasse fiber, plasticizers and PLA in the composites. TGA results reveals that with the plasticizers, the composites show less heat stability; they start to decompose at temperatures greater than 100 °C due to the loss of moisture and plasticizer decomposition, especially in the case of the double plasticizers where two transitions were observed. The lower decomposition temperature of the plasticized composites indicated the poorer intermolecular interaction caused by plasticizing effect. DSC results agree that either bagasse fiber or each plasticizer can act as nucleating agent for cold crystallization of PLA and the combination of bagasse fiber and plasticizers causes the melt crystallization of PLA. Thus the crystallinity of the plasticized PLA/bagasse fiber composites increases largely and contributes to enhance the mechanical properties. Besides, bagasse fiber and the plasticizers cause the appearance of two melting temperatures of PLA which are lower than PLA melting temperature. For the double plasticized composite, the first T_m at 128 °C and the second T_m at 148 °C are less than those of the single-plasticized composite (129 and 149 °C); the first melting was much smaller than the second one. This suggests the use of the plasticized composites at high temperature is limited upto 120 °C. The morphology shows the poor adhesion between bagasse fiber and PLA matrix and bagasse fiber aggregates in the un-plasticized composite. In addition, although the bagasse fiber distributed better in the plasticized

composites, the inferior structure of the double-plasticized composite with the tiny voids (from moisture removal of glycerol) contributes to the poorer mechanical properties than those of the single-plasticized composite. Tensile testing informs that the plasticized composites are anisotropic having better mechanical properties in MD than TD. As expected, the single-plasticized composite shows better mechanical properties than the double-plasticized composite mainly due to the loosening of intermolecular interaction.

Table 8.5 Summary of the properties of bagasse fiber/PLA composite films

Properties		Decrease	Increase
Thermal properties (T_d, T_g, T_{cc}, T_m)		--	
Mechanical properties	Tensile strength		+
	Young's modulus	-	
	Elongation at break		+
Thermo-mechanical properties	Storage modulus	-	
	Loss modulus	-	

Note: The symbols, that increase from high to low, are +++, ++, and +, respectively.

The symbols, that decrease from high to low, are ---, --, and -, respectively.

8.6 Acknowledgement

Financial support has been granted by the National Innovation Agency (NIA), Thailand for project code C48-52.

8.7 References

- [1] M.J. John and S. Thomas, *Carbohydr. Polym.* 71, 343 (2008).
- [2] M. Tewari, V. K. Singh, P. C. Gope, and A.K. Chaudhary, *J. Mat. Sci.* 3, 171 (2012).

- [3] Z. Huang, X. Liang, H. Hu, L. Gao, Y. Chen, and Z. Tong, Polym. Degrad. Stab. 94, 1737 (2009).
- [4] A.N. Nakagaito, A. Fujimura, T. Sakai, Y. Hama, and H. Yano, Compos. Sci. Technol. 69, 1293 (2009).
- [5] N. Graupner, A.S. Herrmann, and J. Müssig, Composites: Part A 40, 810 (2009).
- [6] K. Oksman, M. Skrifvars, and J.-K. Selin, Compos. Sci. Technol. 63, 1317 (2003).
- [7] T. Yu, J. Ren, S. Li, H. Yuan, and Y. Li, Composites: Part A 41, 499 (2010).
- [8] M.S. Huda, L.T. Drzal, A.K. Mohanty, and M. Misra, Compos. Sci. Technol. 68, 424 (2008).
- [9] A.K. Bledzki, A. Jazzkiewicz, and D. Scherzer, Composites: Part A 40, 404 (2009).
- [10] L. Suryanegara, A.N. Nakagaito, and H. Yano, Compos. Sci. Technol. 69, 1187 (2009).
- [11] Y. Tao, L. Yan, and R. Jie, Trans. Nonferrous Met.Soc. China 19, 651 (2009).
- [12] H. Li and M.A. Huneault, Polym. 48, 6855 (2007).
- [13] M.G.A. Vieira, M.A. Altenhofen da Silva, L. Oliveira dos Santos, and M.M. Beppu, Eur. Polym. J. 47, 254 (2011).
- [14] N.A. Ibrahim, W.M.Z.W. Yunus, M. Othman, K. Abdan, and K.A. Hadithon, J. Reinf. Plast. Compos. 29, 1099 (2010).
- [15] M. Murariu, A. Da Silva Ferreira, M. Pluta, L. Bonnaud, M. Alexandre, and P. Dubois, Eur. Polym. J. 44, 3842 (2008).
- [16] O. Martin and L. Averous, Polym. 42, 6209 (2001).
- [17] N. Wang, J. Yu, P.R. Chang, and X. Ma, Carbohydr. Polym. 71, 109 (2008).
- [18] J.W. Cho, K.S. Woo, B.C. Chun, and J.S. Park, Eur. Polym. J. 31, 1227 (2001).
- [19] S. Riyajan and I. Intharit, J. Elastomers Plast. 43, 513 (2011).
- [20] M. Nasar, A. Emam, M. Sultan, and A.A. Abdel Hakim, Indian J. Sci. Technol. 3, 207 (2010).
- [21] A. Copinet, C. Bertrand, S. Govindin, V. Coma, and Y. Couturier, Chemosphere 55, 763 (2004).
- [22] G. Zhang, J. Zhang, X. Zhou, and D. Shen, J. Appl. Polym. Sci. 88, 973 (2003).

- [23] M.K. Mansor, N.A. Ibrahim, W.M.Z.W. Yunus, and C.T. Ratnam, Malaysian Polym. J. 6, 165 (2011).
- [24] Y.Q. Zhao, H.Y. Cheung, K.T. Lau, C.L. Xu, D.D. Zhao, and H.L. Li, Polym. Degrad. Stab. 95, 1978 (2010).
- [25] B. Dou, V. Dupont, P.T. Williams, H. Chen, and Y. Ding, Bioresour. Technol. 100, 2613 (2009).
- [26] E. Fortunati, I. Armentano, Q. Zhou, A. Iannoni, E. Saino, L. Visai, and L.A. Berglund, Carbohydr. Polym. 87, 1596 (2012).
- [27] E.d.M. Teixeira, A.A.S. Curvelo, A.C. Correa, J.M. Marconcini, G.M. Glenn, and L.H.C. Mattoso, Ind. Crops. Prod. 37, 61 (2012).

CHAPTER IX
RHEOLOGICAL AND THERMAL BEHAVIOR OF PLA MODIFIED BY
CHEMICAL CROSSLINKING IN THE PRESENCE OF ETHOXYLATED
BISPHENOL A DIMETHACRYLATES

9.1 Abstract

Crosslinking structures of PLA can be effectively introduced into PLA by melt mixing using the initiation of dicumyl peroxide (DCP) in the presence of ethoxylated bisphenol A dimethacrylates (Bis-EMAs) which was used as a crosslinking agent. The results showed that the introduction of DCP into PLA above 3 phr increased storage modulus and complex viscosity when compared to PLA. DCP/PLA/ in the presence of various content showed the optimum of storage modulus and complex viscosity were at a 5 phr Bis-EMAs loading and decreased as more Bis-EMAs were incorporated into DCP/PLA. The thermal stability of DCP/PLA/Bis-EMAs did not change when compared to PLA. Moreover, the glass transition and cold crystallization of 0.3DCP/PLA/Bis-EMAs and 0.5DCP/PLA/Bis-EMAs increased with increasing Bis-EMAs content. The crystallinity of DCP/PLA and DCP/PLA/Bis-EMAs were lower than that of PLA. The thermo-mechanical properties revealed storage modulus and loss modulus of DCP/PLA/Bis-EMAs increased with increasing Bis-EMAs contents up to 5 phr.

Keywords: Polylactic acid, Ethoxylated bisphenol A dimethacrylates, Chemical crosslinking, Rheological properties

9.2 Introduction

Poly(lactic acid) (PLA) is a biodegradable polymer which has biocompatibility, biodegradability as well as superiority to mechanical properties over other conventional materials [1]. In general, it is widely used in various applications, which are packaging, medical device and textile, based on the environmental friendly materials. However, the poor thermal properties limited its applications. It is well known that the introduction of crosslinking structures is proved effective for enhancing the thermal properties of PLA materials.

The crosslinking structures of PLA were widely introduced by irradiation (γ -irradiation or electron beam irradiation) in the presence of various crosslinking agents e.g. triallyl isocyanurate (TAIC), trimethylallyl isocyanurate (TMAIC), trimethylolpropane triacrylate (TMPTA), and 1,6-Hexanediol diacrylate (HDDA) [2]. Many researchers found that TAIC has been proved to be a good crosslinking agent for PLA via irradiation method. According to Quynh et al. [3], they reported that the radiation dose of 30 kGy is the maximum to introduce PLLA crosslinking structure in the presence of 3 %wt TAIC. Mitomo et al. [2] also found that PLLA/3 %wt TAIC irradiated at 50 kGy showed typical heat stability above glass transition temperature.

The crosslinking structures of PLA can be formed by chemical crosslinking in the presence of a small amount of initiator and crosslinking agent via extrusion process [4]. In general, the crosslinking of PLA can be introduced by peroxides which were decomposed forming free radicals during the melt blending. Thus, these free radicals reacted with PLA chains which can obtain chain scission, branching, crosslinking, or combination of those three reactions. As reported by Zenkiewicz et al. [5], the addition of dicumyl peroxide (DCP) content up to 0.4 %wt into PLA increased the gel fraction of PLA to 93% which is desired for crosslinking. Further the increasing DCP content more than 0.4 %wt became decreasing the gel fraction of PLA to 82%, thus caused the undesired for crosslinking.

In addition, the rheological properties are important to understand the structure–property relationship in the blend. According to Changgang et al. [6] found that the addition of DCP into PLA was higher storage modulus and complex

viscosity than that of PLA at all frequency and gel-3D structure was formed. The complex viscosity and storage modulus of DCP/PLA blend increased with DCP content up to 0.5 %wt at low frequency because the incorporation of DCP can be introduced crosslinking structure between PLA chains have been reported in Huang et al. [7]. More recently, the crosslinking of PLA with DCP and crosslinking agents can form a gel structure as a reported by Yang et al. [8]. They found that the gel fraction of crosslinked PLA starts at 0.15 %wt TAIC and 0.2 %wt DCP and the increasing gel fraction resulted in developed the storage modulus in glassy state and improved thermal stability.

Therefore, this research work was to introduce crosslinking structures of PLA in the presence of small amounts of Bisphenol A ethoxylate dimethacrylate (Bis-EMAs) as a crosslinking agent and DCP via extrusion, aiming at improving the thermal and rheological properties. The effect of DCP and Bis-EMAs content on the rheological, thermal, thermo-mechanical, and morphological properties was investigated.

9.3 Experimental

9.3.1 Materials

Polylactic acid, grade 4043D ($\rho = 1.25 \text{ g/cm}^3$ and $T_m = 210 \text{ }^\circ\text{C}$), was purchased from Nature-Work LLC. Dicumyl peroxide (DCP) was used as a radical initiators and Bisphenol A ethoxylate dimethacrylate (Bis-EMAs) with $M_w = 376$ was used as a crosslinking agent, were purchased from Sigma-Aldrich.

9.3.2 Sample Preparation

PLA samples containing different concentrations of Bis-EMAs (1, 3, 5, and 7 phr) and DCP (0.1, 0.2, 0.3, 0.4, and 0.5 phr) were mixed in a corotating twin-screw extruder with an L/D ratio of 40 (LABTECH type LHFS1-271822). The temperature profile was maintained in the range of 140-190 $^\circ\text{C}$ from the feed throat to the die and the rotational speed was fixed at 10 rpm. Table 9.1 shows composition of each sample.

The rheological, thermo-mechanical, thermal (decomposition temperature), and morphological testing specimens were prepared by compression molding (Wabash, model V50H-18-CX) for 5 min at 200 °C and subsequently cooled under pressure by water circulation through the plates.

Table 9.1 Composition of each sample

DCP (phr)	Bis-EMAs (phr)	PLA (wt%)	Code
0	0	100	PLA
0.1	0	100	0.1DCP
0.2	0	100	0.2DCP
0.3	0	100	0.3DCP
0.4	0	100	0.4DCP
0.5	0	100	0.5DCP
0.1	1	100	0.1D1B
0.1	3	100	0.1D3B
0.1	5	100	0.1D5B
0.1	7	100	0.1D7B
0.3	1	100	0.3D1B
0.3	3	100	0.3D3B
0.3	5	100	0.3D5B
0.3	7	100	0.3D7B
0.5	1	100	0.5D1B
0.5	3	100	0.5D3B
0.5	5	100	0.5D5B
0.5	7	100	0.5D7B

9.3.3 Characterization

9.3.3.1 *Measurement of Gel Fraction*

- Dissolving sample pellet in chloroform at room temperature

Gel fraction was measured by the weight remaining after dissolving sample pellet in chloroform using the following eq. 9.1

$$\text{Gel fraction} = \left(\frac{W_g}{W_0} \right) \times 100 \quad (9.1)$$

Where W_0 is initial weight (dry), W_g is the remaining weight (dry gel component) of the crosslinked sample after dissolving in chloroform at room temperature for 24 h.

- Soxhlet extraction

The gel contents of the crosslinked samples (pellet) were determined by extracting the soluble fraction with boiling chloroform (61°C-62 °C) for 2 h in a soxhlet extractor (SER 148). The gel fraction was calculated using eq. 9.1.

9.3.3.2 Rheological Measurement

The rheological properties were measured using Anton Paar Rheometer. The measurement was run using parallel plate ($d = 25$ mm) and the gap was set at 1mm. The samples were loaded between parallel plates and melted at 190 °C for 2 min before compressed. Frequency sweep between 0.1-100 rad/s was carried out at 5% strain which is the linear viscoelastic region of the measured samples. Time sweep was performed at 150 °C for 7,200 sec and frequency of 1 Hz with a strain of 5 %.

9.3.3.3 Thermogravimetric Analyzer (TGA)

Thermogravimetric analysis was carried out with a TA Instruments (Q500 TGA) under a nitrogen flow (40 ml/min). The samples were measured from 30 °C to 600 °C with a heating rate of 10 °C/min. The decomposition temperature and temperature at maximum rate of mass loss (T_{\max}), of derivative thermogravimetric curve (DTG) were evaluated.

9.3.3.4 Differential Scanning Calorimeter (DSC)

Differential scanning calorimeter was performed using a Perkin–Elmer DSC 822 under N_2 atmosphere. The sample pellets were heated from

10 °C to 200 °C at a heating rate of 10 °C/min. The glass transition temperature (T_g), cold crystallization temperature (T_{cc}), and melting temperature (T_m) of each specimens was recorded from the second run. The degree of crystallization (χ_c) was calculated as:

$$\chi_c = \frac{\Delta H_m - \Delta H_{cc}}{\Delta H_{m0} \times w} \times 100 \quad (9.2)$$

Where ΔH_m is the enthalpy of melting, ΔH_{cc} is the enthalpy of cold crystallization, ΔH_{m0} is enthalpy of melting for the 100% crystalline PLA, taken as 93 J/g, w is the weight fraction of PLA in samples [9].

9.3.3.5 Dynamic Mechanical Analyzer (DMA)

Dynamic mechanical analysis (DMA) was performed using an EPLEXOR 100N in tension mode. The sample dimensions with a length of 40 mm, width of 10 mm, and thickness of 3 mm were used. The measurements were carried out at a constant frequency of 1 Hz, strain amplitude of 0.1%, and a temperature range of 10 °C to 120 °C, with a heating rate of 2 °C/min.

9.3.3.6 Morphological Observation

The material microstructure was examined using a field emission scanning electron microscope (FE-SEM; HITACHI S4800) with an acceleration voltage of 5 kV. The freeze-fractured ends of specimens were sputtering coated (HITACHI E-1010) with a thin layer of platinum prior to analysis.

9.3.3.7 Mechanical Testing

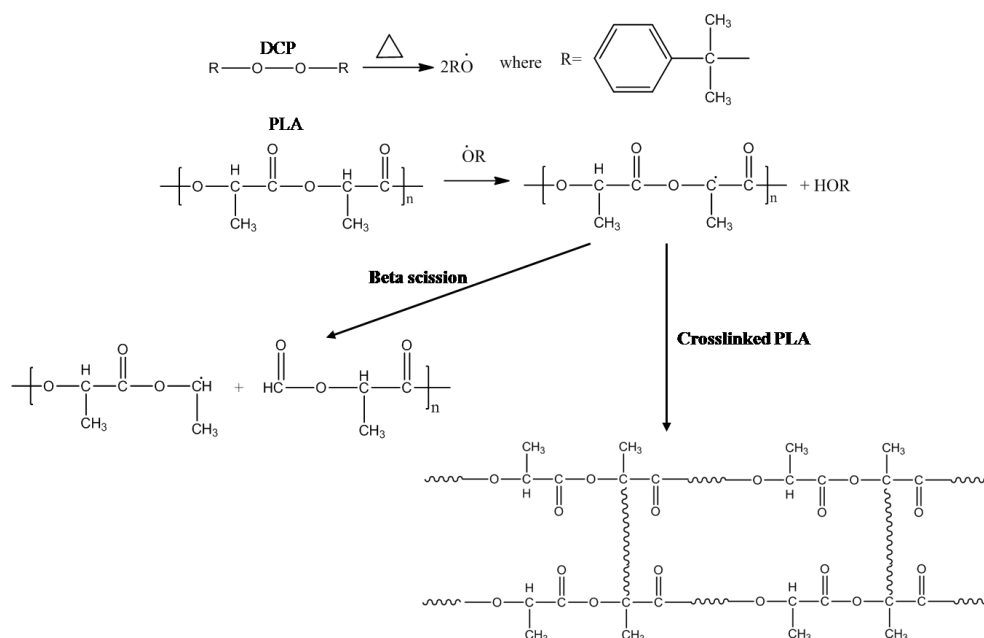
Tensile tests were performed using an Instron Universal Testing Machine (4206) with a crosshead speed of 50 mm/min. The specimens were prepared according to ASTM D638 standard.

Impact testing was performed according to ASTM D256 (notched type), and the impact strength was measured using the ZWICK 5113 pendulum impact tester with a pendulum load of 21.6 J.

9.4 Results and Discussion

9.4.1 Chemical Crosslinking Reaction of PLA

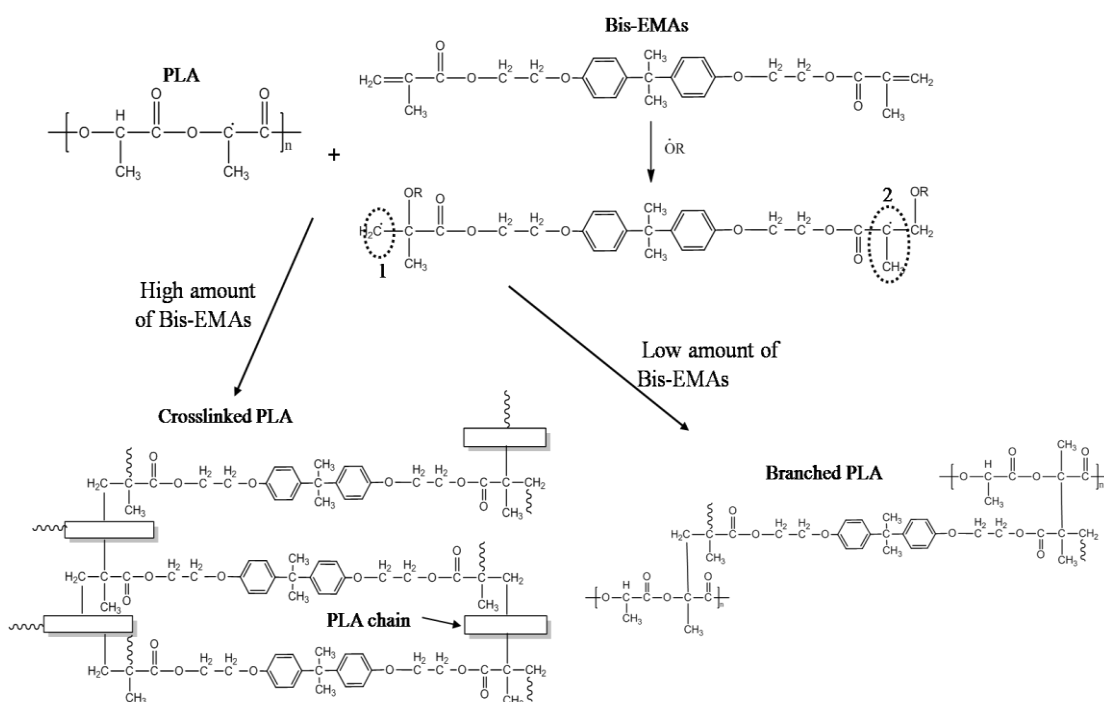
For DCP/PLA system, the introducing of DCP is decomposed into free radicals during extrusion and PLA is created radicals by the abstraction hydrogen with radicals from peroxide. Thus the radicals from PLA can be generated and reacted with themselves to forming the crosslinking structure as seen in Scheme 9.1. However, radicals can be created at the tertiary hydrogen atom positions on PLA chains which is the possible way to promote chain scission [10].



Scheme 9.1 Formations of chain scission and crosslinking structure of PLA in the presence of DCP.

The reaction of chemical crosslinking of PLA in the presence of Bis-EMAs (DCP/PLA/ Bis-EMAs) was shown in Scheme 9.2. The double bonds in Bis-EMAs are broken and created two possible way of radicals, which are usual way at position 1 and rare way at position 2. Then the radicals from Bis-EMAs reacted with radicals from PLA can be created the chemical crosslinking reaction as seen in Scheme 9.2. The two competitive reaction can be occurred which consisted of branched PLA and crosslinked PLA structure. The branched PLA obtained from the

loading low amount of Bis-EMAs while the crosslinked PLA obtained from the adding high amount of Bis-EMAs. At the same time, the combination of branching and crosslinking reaction can be occurred [11].



Scheme 9.2 The possibility of chemical crosslinking between Bis-EMAs and PLA.

9.4.2 Gel Fraction

Figure 9.1 shows the gel fraction of DCP/PLA. The result shows that gel fraction of DCP/PLA sample at room temperature condition are higher than that of sohxlet extraction. This is due to the solubility of sample increased with the increasing temperature. The gel fractions from room temperature condition and sohxlet extraction show the same tendency. Moreover, the gel fraction of DCP/PLA samples increased with the increasing DCP content. The values of gel fraction from room temperature condition are less than 60% which are corresponding to low amount of crosslinking structure.

Gel fraction of DCP/PLA/Bis-EMAs at room temperature condition and sohxlet extraction are shown in Figure 9.2(a) and Figure 9.2(b), respectively. It

can be seen that the gel fractions of DCP/PLA/Bis-EMAs are higher than that of DCP/PLA because the presence of Bis-EMAs as a crosslink agent effectively enhanced the crosslinking structure. The gel fractions from room temperature condition (< 90%) are also higher than sohxlet extraction (< 40%). A high value of gel fraction suggests that there is a higher possibility of crosslinking than that of branching and chain scission. In addition, the gel fractions of DCP/PLA/Bis-EMAs samples of both conditions increased with increasing Bis-EMAs up to 5 phr. Further increasing Bis-EMAs to 7 phr resulted in decrease the gel fraction. It can be explained that the loading of Bis-EMAs over 5 phr is generated a large amount of radicals led to degradation of PLA chains. This situation is undesired reaction for chemical crosslinking PLA in the presence of Bis-EMAs.

Figure 9.3 shows the sample pellets of PLA, DCP/PLA and DCP/PLA/Bis-EMAs. Gel is found in the crosslinking sample. PLA pellets did not observe gel. It can be seen that a high amounts of DCP and Bis-EMAs loading show high amount of gel content in the sample. This result agrees with the gel fraction. Since the gel increased that associated with increasing crosslinking structure, the sample pellets showed more opaque.

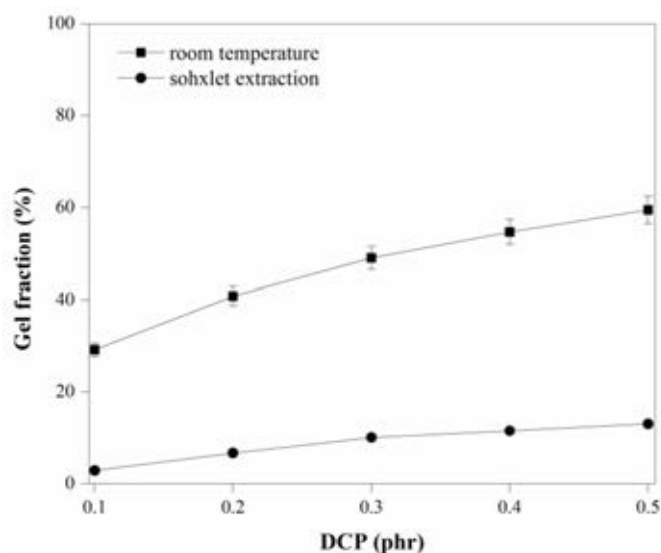


Figure 9.1 Gel fraction of DCP/PLA as a function of DCP content.

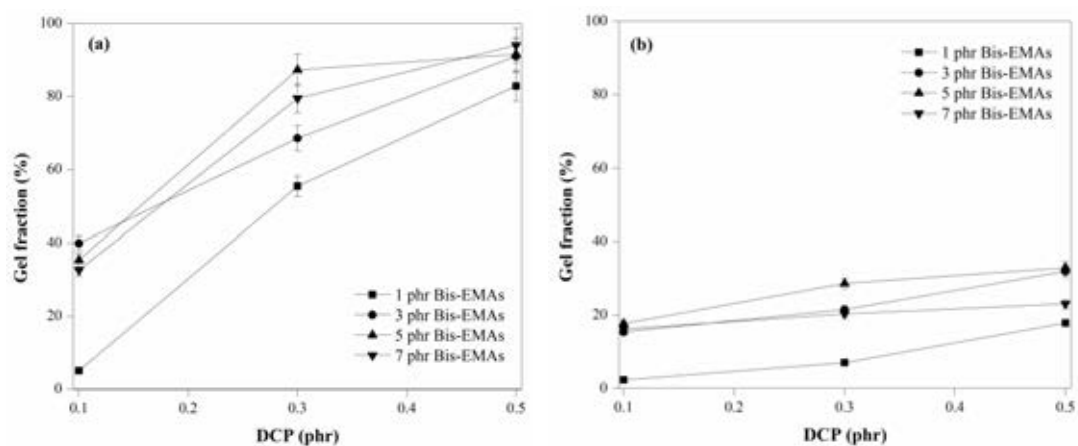


Figure 9.2 Gel fraction of chemical crosslinked PLA as a function of DCP content of (a) at room temperature and (b) after soxhlet extraction.

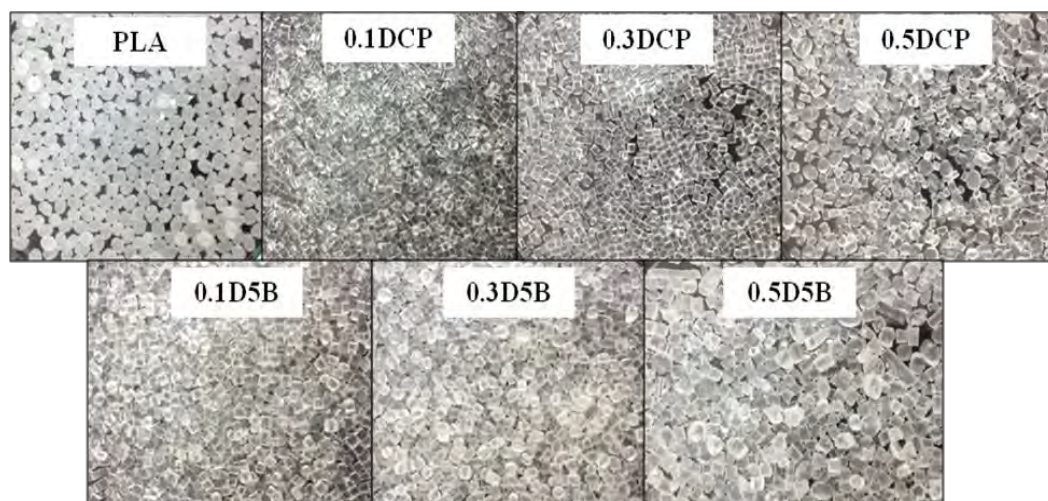


Figure 9.3 Images of PLA, DCP/PLA, and DCP/PLA/Bis-EMAs pellets.

9.4.3 Rheological Properties

9.4.3.1 Time Sweep

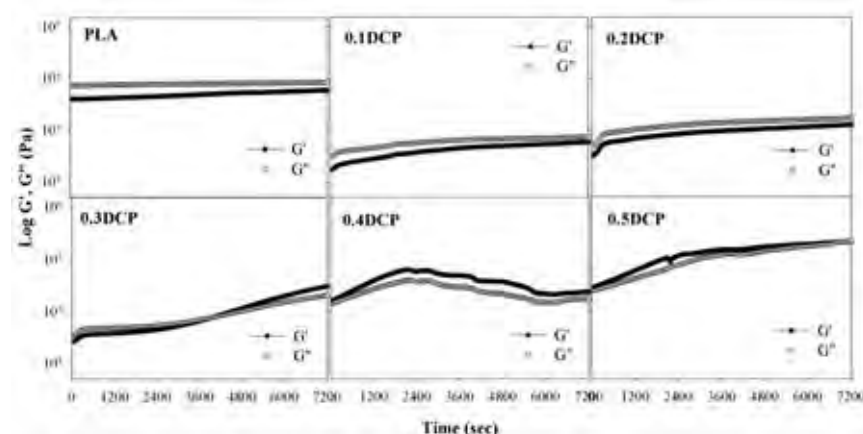


Figure 9.4 G' and G'' as a function of time of PLA and DCP/PLA at 150 °C.

Figure 9.4 shows the variation of the storage (G') and loss (G'') modulus versus time at 150 °C. The crossover between G' and G'' defines the gel point of a polymer chains form a three-dimensional network [12]. The results show that the G' and G'' of PLA are parallel and $G'' > G'$ is characteristics of polymer liquid. The addition of DCP at 3 phr observes the gel point (gel time~3940 s), indicates that the crosslinking reaction started at this point. At gel point, the $G'=G''$ is about 7,670 Pa. Above the gel point, the G' increased and reached a steady state value corresponding to the end of the crosslinking reaction. In the case of 0.1DCP and 0.2DCP samples, they did not observe the gel point. It can be suggested that the addition of DCP below 0.3 phr is not sufficient to promote radical reaction. At above 0.3 phr DCP, the G' and G'' are parallel and the G' is larger than the G'' due to the completion of crosslinking reaction.

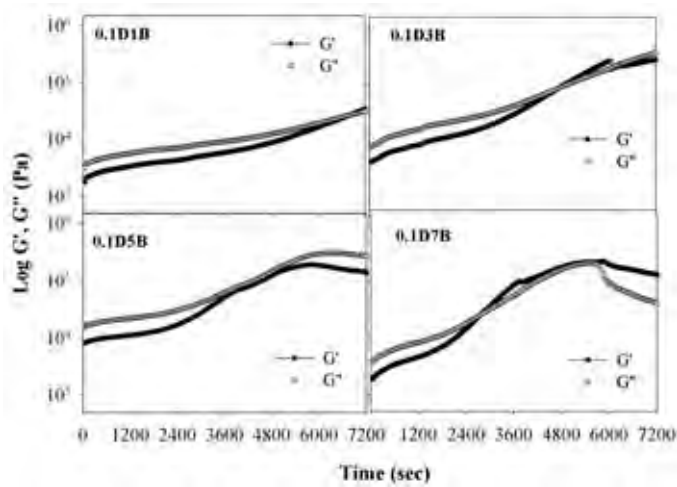


Figure 9.5 G' and G'' as a function of time of 0.1DCP/PLA/Bis-EMAs at 150 °C.

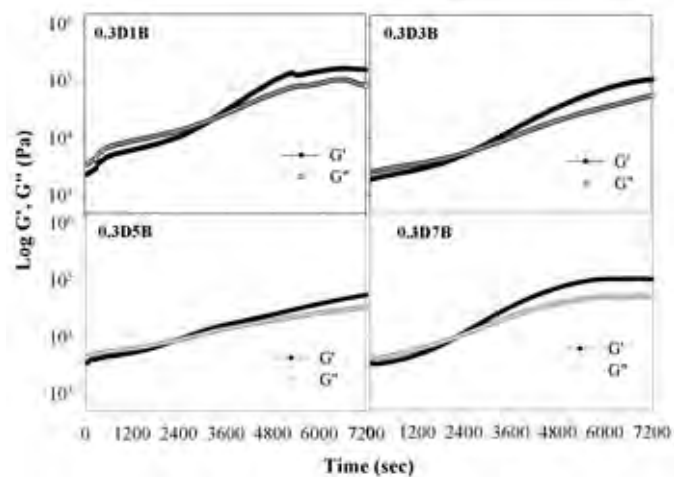


Figure 9.6 G' and G'' as a function of time of 0.3DCP/PLA/Bis-EMAs at 150 °C.

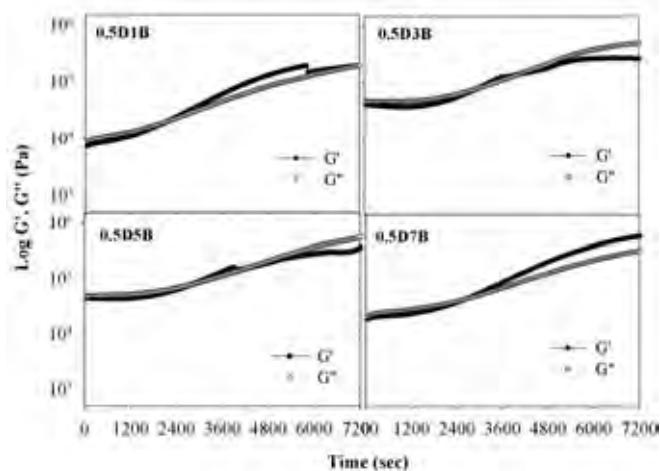


Figure 9.7 G' and G'' as a function of time of 0.5DCP/PLA/Bis-EMAs at 150 °C.

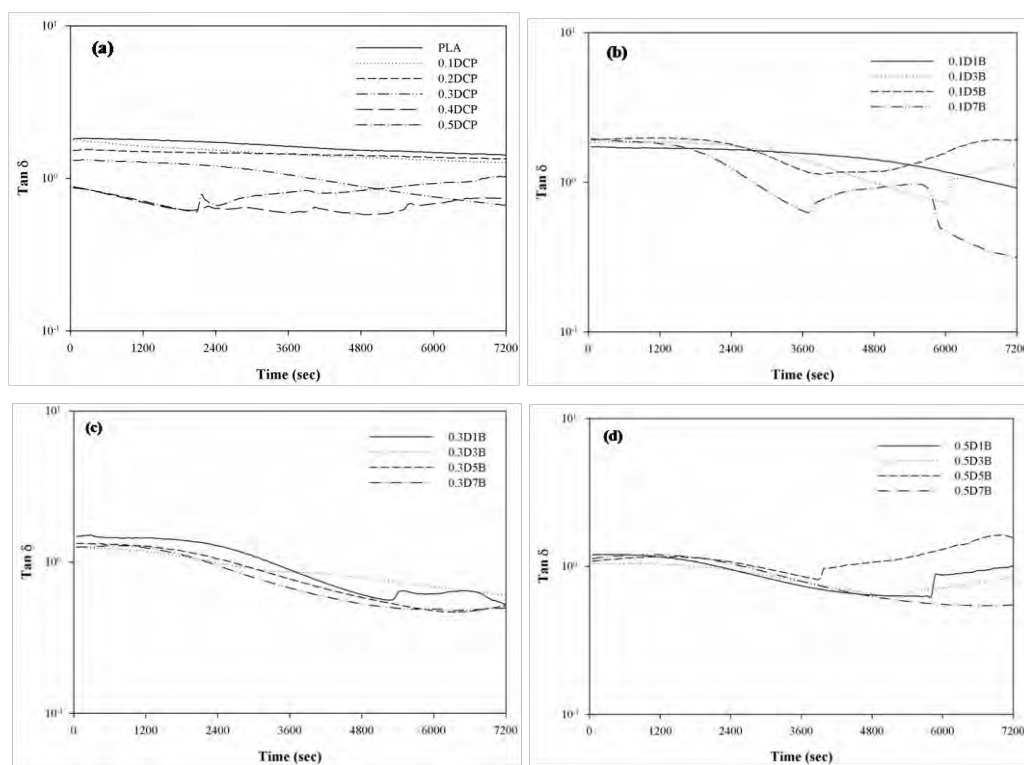


Figure 9.8 $\tan \delta$ as a function of time of (a) DCP/PLA, (b) 0.1DCP/PLA/Bis-EMAs, (c) 0.3DCP/PLA/Bis-EMAs, and (d) 0.5DCP/PLA/Bis-EMAs at 150 °C.

To determine the gel point during a crosslinking reaction of DCP/PLA/Bis-EMAs, the G' and G'' are measured as a function of time at 150 °C as

shown in Figure 9.5–9.7. At early times, all DCP/PLA/Bis–EMAs show that the elastic portion G' is much smaller than the viscous portion G'' . The presence of a small elastic contribution well before the critical gel point is due to the stretching of the polymer under deformation and potentially physical entanglements between the polymer chains.

Before gel point, DCP/PLA/Bis–EMAs show lower moduli than PLA. This suggests that DCP/PLA/Bis–EMAs are process easier than PLA. Since the samples before gel point are still in liquid state where viscous properties dominate [13].

As the reactions begin to gel and a crosslinked network is formed, both G' and G'' begin to increase; however, the rate of increase of G' is much higher than that of G'' since now the elastic properties dominate. At the gel point, the crossover point between G' and G'' values of 0.1DCP/PLA/Bis–EMAs are $\sim 26,300$ Pa– $93,600$ Pa and both G' and G'' values increase with an increase in Bis–EMAs up to 5 phr as seen in Table 9.2. The moduli values at gel point of 0.3DCP/PLA/Bis–EMAs and 0.5DCP/PLA/Bis–EMAs are $\sim 8,030$ Pa– $21,500$ Pa and $\sim 20,700$ Pa– $80,200$ Pa, respectively. The results of PLA show that the G' ($\sim 40,400$ Pa– $59,100$ Pa) and G'' ($\sim 73,000$ Pa– $84,200$ Pa) are parallel and $G'' > G'$. The crossover point between G' and G'' values of all DCP/PLA/Bis–EMAs samples decreased when compared to PLA. In the case of 0.3DCP/PLA/Bis–EMAs samples, both G' and G'' values ($\sim 8,030$ Pa– $21,500$ Pa) at gel point are higher than 0.3DCP/PLA ($7,670$ Pa). This suggests that the addition of Bis–EMAs is effectively crosslink agent to promote crosslinking structure due to improvement in moduli. In the case of 0.5DCP/PLA/Bis–EMAs samples, the addition of Bis–EMAs at 1 phr and 7 phr into 0.5DCP/PLA observes the gel point. Especially 0.5D3B and 0.5D5B samples are not clearly observed the cross over between G' and G'' but it is observed the nearest point between G' and G'' (at 2980 sec for 0.5D3B and 2730 sec for 0.5D5B). Moreover, 0.5DCP/PLA/Bis–EMAs shows higher the moduli at gel point than 0.3DCP/PLA/Bis–EMAs. This indicates that a large amount of DCP together with Bis–EMAs content obtained high moduli due to a large amount of network structure. At gel point, all DCP/PLA/Bis–EMAs samples are still lower both G' and G'' than PLA, which means that DCP/PLA/Bis–EMAs is still process easier than PLA.

As the crosslinking reaction progresses, elastic modulus G' is increased due to more entanglements of polymers. Both G' and G'' values above the gel point of all DCP/PLA/Bis-EMAs samples become higher than PLA. In the case of 0.1DCP/PLA/Bis-EMAs, G'' becomes higher than G' after the cross point, which suggests that small amount of crosslinking structure occurred and the sample has more part of viscous properties. For 0.3DCP/PLA/Bis-EMAs, the G' becomes larger than the G'' after gel point. Stiffer gels will have a higher G' . Moreover, 0.5DCP/PLA/Bis-EMAs show the highest moduli values and higher than 0.5DCP/PLA. Especially 0.5D3B and 0.5D5B samples show $G'' > G'$ over the time period measurement but it has the nearest value between G' and G'' , which are in the range of 2400 sec–4600 sec as seen in Figure 9.7. This case suggests that the combination of branching and crosslinking reaction can possibly occur.

Figure 9.8(a) shows $\tan \delta$ which is the ratio of G'' to G' or damping of PLA and DCP/PLA. The $\tan \delta$ reveals that the molecular motion of PLA is greater when compared to DCP/PLA. $\tan \delta$ values of 0.1DCP/PLA and 0.2DCP/PLA are clearly above 1, which indicated that G' and G'' crossing does not occur in the time period examined. For the 0.3DCP/PLA, the $\tan \delta$ value is slightly decreased as increase time and the value equal 1 when $G'=G''$ (gel point). In the case of 0.4DCP/PLA and 0.5DCP/PLA, the $\tan \delta$ values are below 1 due to $G' > G''$ over the time period measurement which is a characteristic of elastic material. Figure 9.8(b)–9.8(c) show $\tan \delta$ of DCP/PLA/Bis-EMAs samples. $\tan \delta$ of DCP/PLA/Bis-EMAs samples are above 1 when $G'' > G'$ (before gel point) and below 1 when $G' > G''$ (after gel point). This can be noted that the molecular motions of DCP/PLA/Bis-EMAs are restricted with the increasing G' . The $\tan \delta$ decreased with an increase in Bis-EMAs content. The limited molecular motion in the melt state of DCP/PLA/Bis-EMAs is due to crosslinking structure. So, the network structure provides stronger intermolecular forces and relatively greater resistance to flow. Moreover, the results show that DCP/PLA/Bis-EMAs are lower molecular motions than PLA.

Table 9.2 G' and G'' values at gel point of samples

Sample	G'=G'' (Pa) at gel point
0.3DCP	7,670
0.1D1B	26,300
0.1D3B	84,300
0.1D5B	93,600
0.1D7B	26,400
0.3D1B	21,500
0.3D3B	8,650
0.3D5B	8,030
0.3D7B	9,930
0.5D1B	20,700
0.5D3B	23,700 (at gel time~2980 sec)
0.5D5B	80,200 (at gel time~2730 sec)
0.5D7B	46,600

Note: 0.5D3B and 0.5D5B use the nearest point between G' and G'' to report.

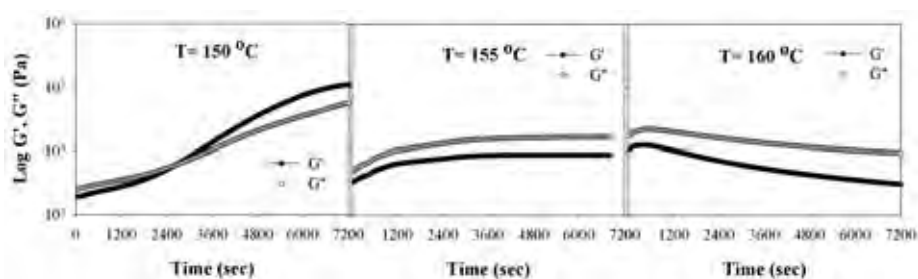


Figure 9.9 G' and G'' as a function of time of 0.3D5B at 150 °C, 155 °C, and 160 °C.

Figure 9.9 shows G' and G'' of 0.3D5B at various temperature. The results show that temperature at 150 °C has higher moduli (in the range of 10^4 – 10^5 Pa) than that of temperature at 155 °C and 160 °C (in the range of 10^3 – 10^4 Pa). It can be seen that the G' at 150 °C (after 2400 sec) has higher than the G''. While the

G'' become higher than the G' over the time period measurement when increase temperature to 155 °C and 160 °C. This suggests that the sample behaves like a viscous characteristic with increasing temperature. In view of the fact that the moduli are seriously effect on the processing and decrease with an increase temperature. At higher temperature, the connections between molecular chains became weaker because the molecules possessed higher energy than at lower temperature. As a result of this, the melted sample flowed more easily that why the crosslink sample can process at high temperature.

The gel times of DCP/PLA/Bis-EMAs decreased with increase DCP content as seen in Figure 9.10. The addition of Bis-EMAs decreases the gel time of the sample. Moreover, the gel time decreased with the increasing Bis-EMAs content. This confirmed that Bis-EMAs are effectively crosslinking agent to promote the crosslinking network of PLA. Moreover, a large amounts of DCP and Bis-EMAs loading show decrease in gel time.

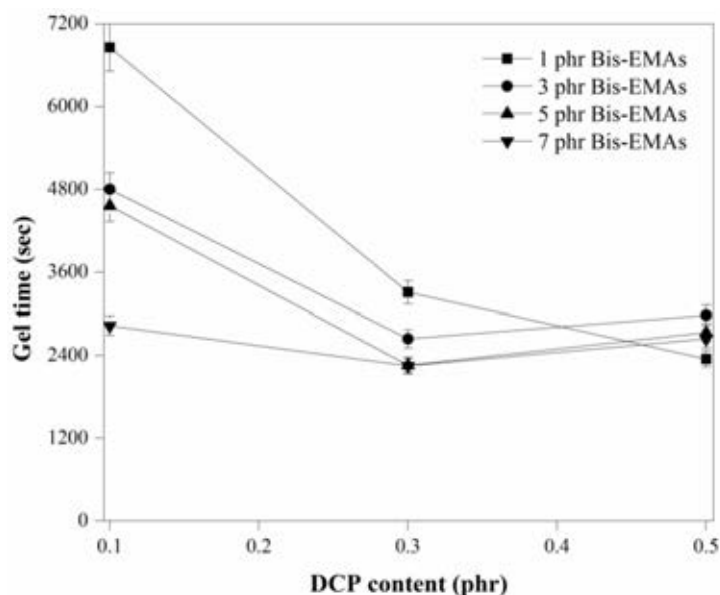


Figure 9.10 Gel time as a function of DCP content at 150 °C.

9.4.3.2 Frequency Sweep

The G' of PLA and DCP/PLA as a function of angular frequency at 190 °C are shown in Figure 9.11a. At low frequency, the introducing of

DCP into PLA more than 3 phr shows increase the G' when compared to PLA. This result suggests that the addition of DCP below 0.3 phr is not sufficient to promote radical reaction. The G' of DCP/PLA is increased with the increasing DCP content. It is well known that DCP can induce the crosslinking structure between PLA chains resulted in improve the interaction and entanglement of PLA chain. This result agree with Huang et al. [14]. They reported that the G' of DCP/PLA increased with DCP content up to 0.5 %wt at low frequency because the incorporation of DCP can be introduced crosslinking structure between PLA chains.

The complex viscosity (η^*) of PLA and DCP/PLA as a function of angular frequency at 190 °C are shown in Figure 9.11b. The η^* of DCP/PLA is increased with increasing DCP content. When compared with PLA, the η^* of DCP/PLA decreased when DCP content below 0.4 phr at low frequency. The η^* of PLA and DCP/PLA are decreased with increasing frequencies which are a shear thinning behavior or pseudoplastic fluid. Especially 0.4DCP and 0.5DCP are stronger pseudoplastic fluid than PLA.

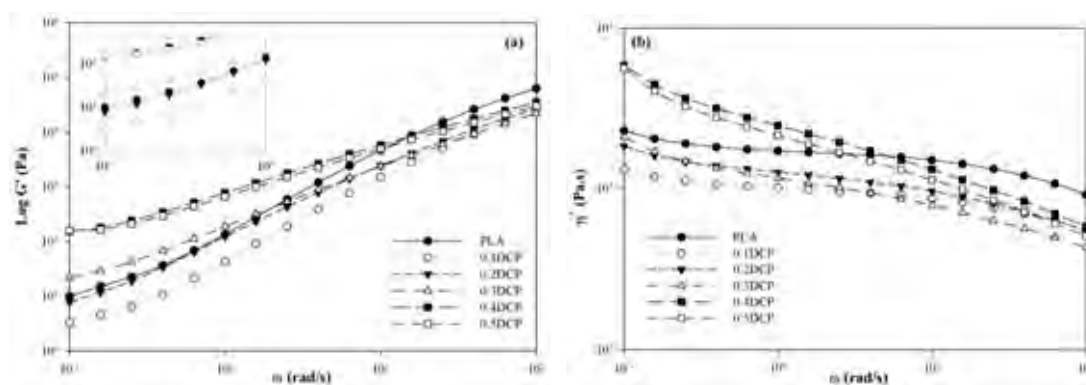


Figure 9.11 Variations of (a) G' and (b) η^* as a function of angular frequency at 190 °C of DCP/PLA.

The G' and η^* of PLA and Bis-EMAs/PLA as a function of angular frequency at 190 °C are shown in Figure 9.12. The G' and η^* of Bis-EMAs/PLA are lower than that of PLA. The G' and η^* decreased with the increasing Bis-EMAs content, implies that Bis-EMAs was not reacted with PLA chains to form the crosslinking structure, and acted as a role of plasticizer.

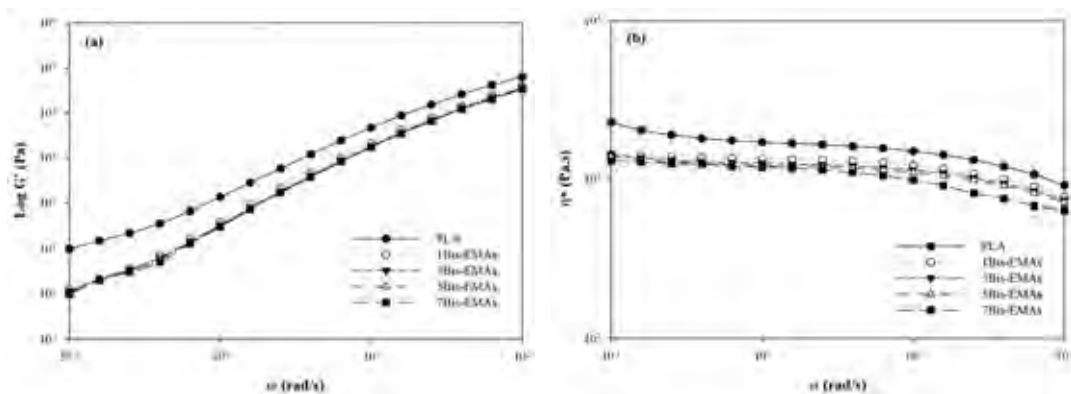


Figure 9.12 Variations of (a) G' and (b) η^* as a function of angular frequency at 190 °C of Bis-EMAs/PLA.

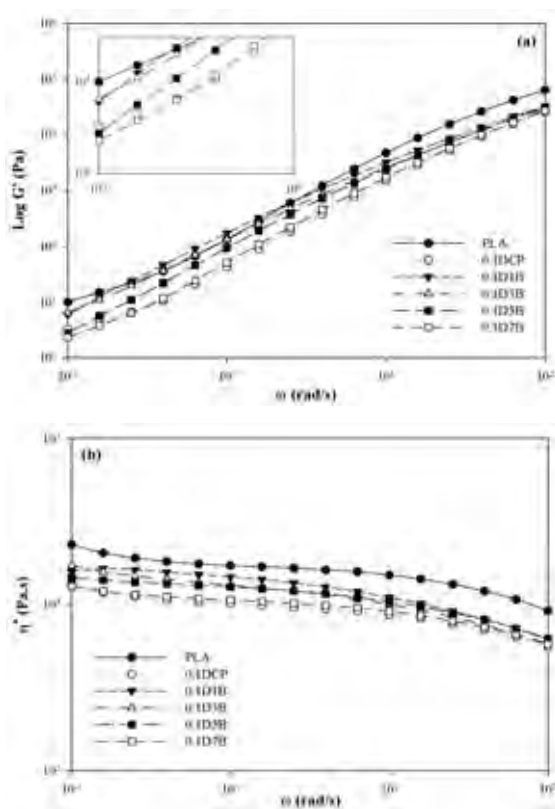


Figure 9.13 Variations of (a) G' and (b) η^* as a function of angular frequency at 190 °C of 0.1DCP/PLA/Bis-EMAs.

Figure 9.13a shows the G' of 0.1DCP/PLA/Bis-EMAs. It can be seen that 0.1DCP/PLA/Bis-EMAs show lower the G' than that of PLA. This is due to low amounts of radicals are generated which are not enough to promote crosslinking structure between PLA and Bis-EMAs. When compared to 0.1DCP/PLA, the addition of Bis-EMAs below 5phr increased the G' . As the increasing Bis-EMAs content, the G' is dramatically decreased. Figure 9.13b shows that 0.1DCP/PLA/Bis-EMAs are lower the η^* than that of PLA. The η^* also decreased with the increasing Bis-EMAs content. This case is not suitable reaction for chemical crosslinking PLA with Bis-EMAs.

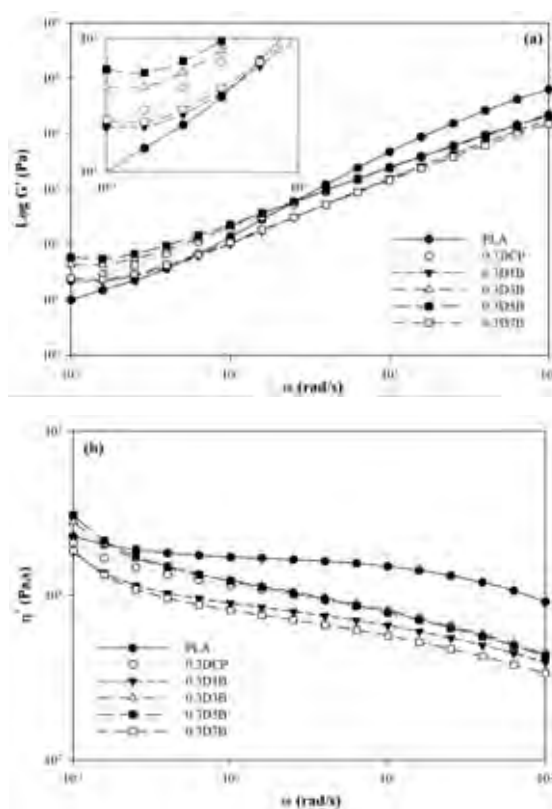


Figure 9.14 Variations of (a) G' and (b) η^* as a function of angular frequency at 190 °C of 0.3DCP/PLA/Bis-EMAs.

In Figure 9.14a, 0.3DCP/PLA/Bis-EMAs are higher the G' than that of PLA and 0.3DCP/PLA at low frequency. It can be seen that 0.3DCP/PLA/Bis-EMAs showed plateau G' at low frequencies (0.1 rad/s–0.3 rad/s). In the principle,

plateau G' is associated with chains entanglement or crosslinking structure in polymer melt [15]. The G' of 0.3DCP/PLA/Bis-EMAs is increased with the addition of Bis-EMAs up to 5 phr. The increasing G' means that enhanced the melt elasticity of material [16]. Further increasing Bis-EMAs over 5 phr resulted in decrease the G' . This result agrees with the decrease in gel fraction as seen in Figure 9.10. Consequently, the optimum of the G' is at 5 phr Bis-EMAs loading and decreases as more Bis-EMAs content. This concludes that the added Bis-EMAs at 5 phr are the best desired crosslinking reaction for 0.3DCP/PLA/Bis-EMAs. As seen in Figure 9.14b, 0.3DCP/PLA/Bis-EMAs at 3 phr and 5 phr of Bis-EMAs are higher η^* than that of PLA and 0.3DCP/PLA at low frequency. The η^* of 0.3DCP/PLA/Bis-EMAs is increased with the increasing Bis-EMAs up to 5 phr Bis-EMAs.

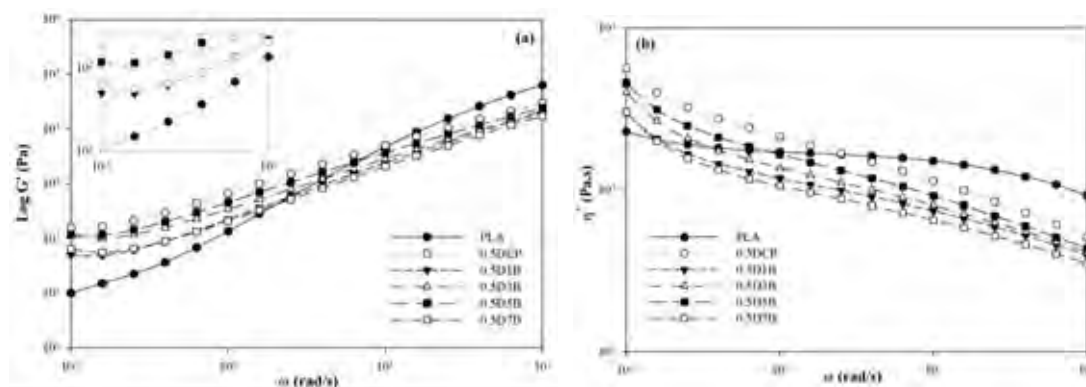


Figure 9.15 Variations of (a) G' and (b) η^* as a function of angular frequency at 190 °C of 0.5DCP/PLA/Bis-EMAs.

In the case of 0.5DCP/PLA with the various amounts of Bis-EMAs are shown in Figure 9.15a. The results show that the plateau G' of 0.5DCP/PLA/Bis-EMAs is higher than that of PLA but lower than that of 0.5DCP/PLA at low frequency. This can be proposed as two competitive reaction as seen in scheme 9.2. The adding at low amount of crosslinking agent can be created the chain branching while the high amount of crosslinking agent can be created the crosslinking structure [10]. It indicates that the combination of branching and crosslinking structures can be occurred in this case. At low frequency, the plateau G' increased with the increasing

Bis-EMAs up to 5 phr and further decreased when Bis-EMAs over 5 phr. The η^* of 0.5DCP/PLA/Bis-EMAs shows the tendency in agreement with G' as seen in Figure 9.15b.

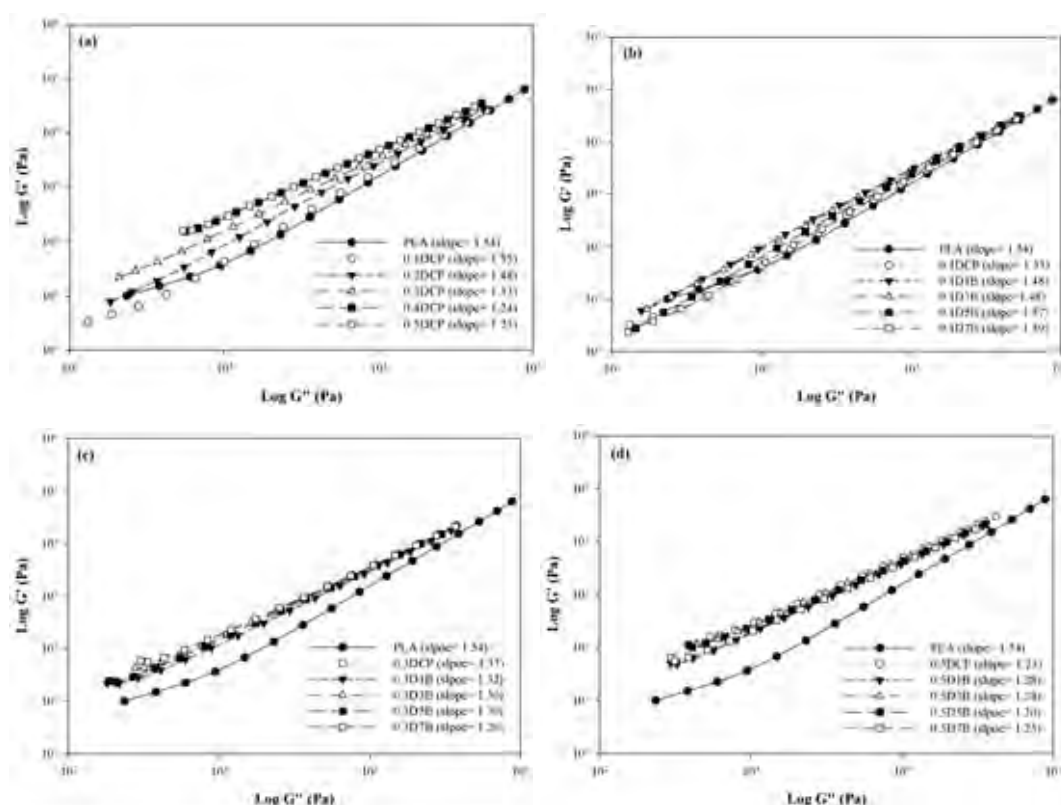


Figure 9.16 Cole–cole plot at 190 °C of (a) DCP/PLA, (b) 0.1DCP/PLA/Bis-EMAs, (c) 0.3DCP/PLA/Bis-EMAs, and (d) 0.5DCP/PLA/Bis-EMAs.

The Cole–Cole plot or log G' versus log G'' as shown in Figure 9.16 can represent the crosslinking, branching, and chain scission. In general, the slope of linear polymer from Cole–Cole plot is about 2 and dependent on the chain branching and crosslinking level [11, 17]. In Figure 9.16a, the results show that the slopes of DCP/PLA are lower than that of PLA. It can be concluded that the chain structure changes by the formation of crosslinking. As seen in Figure 9.16b, 0.1DCP/PLA with various Bis-EMAs does not significant change in slope due to a little crosslinking structure. In Figure 9.16c–9.16d, the slopes of crosslinked PLAs decreased with increasing Bis-EMAs content. Moreover, 0.5DCP/PLA with various

Bis-EMAs are lower the slopes than that of 0.3DCP/PLA with various Bis-EMAs. This means that increase in DCP and Bis-EMAs content are significant change the structure of PLA.

9.4.4 Thermogravimetry

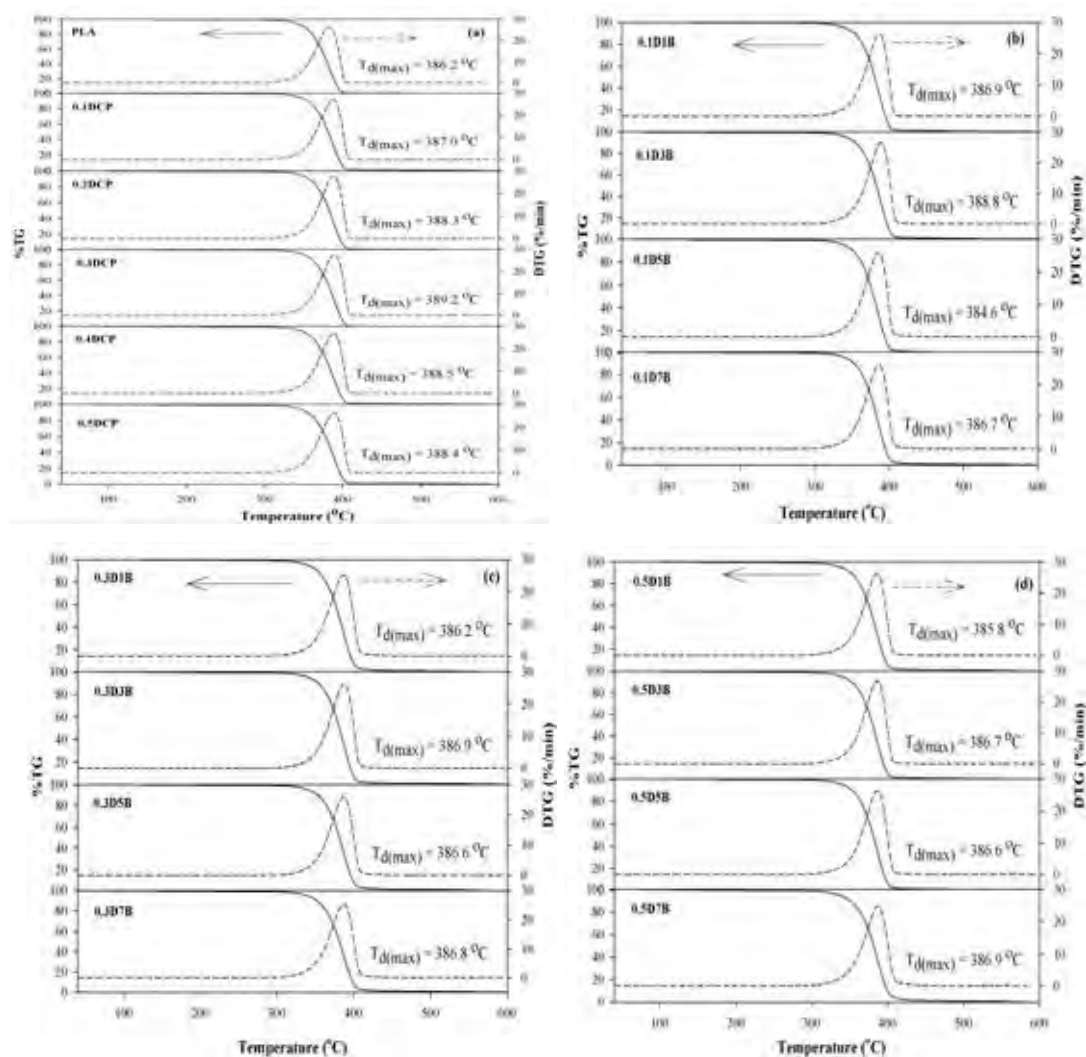


Figure 9.17 TGA thermograms of (a) DCP/PLA, (b) 0.1DCP/PLA/Bis-EMAs, (c) 0.3DCP/PLA/Bis-EMAs, and (d) 0.5DCP/PLA/Bis-EMAs.

Figure 9.17 shows the thermogravimetric (TG) and derivative thermogravimetric (DTG) curves of PLA, DCP/PLA, and DCP/PLA/Bis-EMAs. The decomposition temperature is the temperature at the maximum rate of mass loss

($T_{d(max)}$), or DTG curve. In Figure 9.17a, the decomposition temperatures of DCP/PLA are slightly higher than that of PLA. This can be ascribed to the introduction of DCP improves the thermal stability of PLA. In addition, the results of DCP/PLA/Bis-EMAs show one transition in its chain decomposition at $T_{max} \sim 386.5$ °C, which are similarly vale with PLA ($T_{max} \sim 386.2$ °C) as seen in Figure 9.17b–9.17d. However, the thermal stability of DCP/PLA/Bis-EMAs does not significantly change with increasing Bis-EMAs content.

9.4.5 Crystallization and Melting Behavior

9.4.5.1 Thermal Properties of PLA, DCP/PLA, and DCP/PLA/Bis-EMAs Pellets

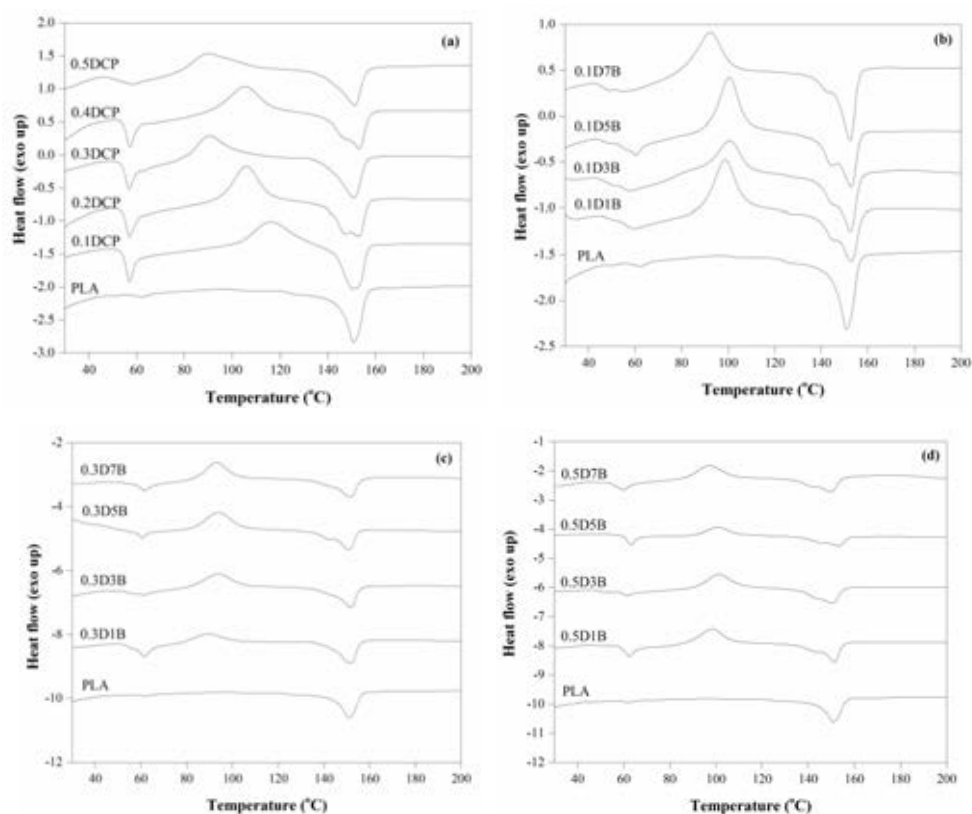


Figure 9.18 DSC thermograms of (a) DCP/PLA, (b) 0.1DCP/PLA/Bis-EMAs, (c) 0.3DCP/PLA/Bis-EMAs, and (d) 0.5DCP/PLA/Bis-EMAs pellets.

Figure 9.18a and Table 9.3 show the DSC thermograms of PLA and DCP/PLA. The T_g of DCP/PLA was slightly decreased when compared to PLA. The T_g and T_{cc} of DCP/PLA decreased with the increasing DCP content. This was due to the generation of high cumyloxy radical can encourage chain scission of PLA as seen in the scheme 9.1 [7].

Figure 9.18b shows the DSC thermograms of 0.1DCP/PLA/Bis-EMAs. T_g of 0.1DCP/PLA/Bis-EMAs pellet is lower than that of PLA. This case indicated that low amount of free radical was generated due to low DCP content. It expected that free Bis-EMAs were not reacted with PLA which can act as a plasticizer in this system. This result agreed with rheological properties of Bis-EMAs/PLA as seen in Figure 9.12. The T_{cc} and T_m of 0.1DCP/PLA/Bis-EMAs decreased with increasing Bis-EMAs content. Moreover, the T_m of 0.1DCP/PLA/Bis-EMAs exhibited two peaks compared to PLA resulted in two kinds of lamellae structure. This explained that the low-melting peak corresponding to less perfect crystal structure while the high-melting peak corresponding to more perfect crystal structure [18]. So, this case was not suitable to produce the crosslinking PLA.

Figure 9.18c and 9.18b show the DSC thermograms of 0.3DCP/PLA/Bis-EMAs and 0.5DCP/PLA/Bis-EMAs, respectively. The results demonstrated that T_g of both samples were slightly higher than PLA. It suggested that crosslinking structure decreased chain motion. The T_{cc} of both samples were shift to higher temperature with increase in Bis-EMAs content. This explained that the large molecular chain networks inhibited chain segment motion for crystallization. T_m of both samples did not change when compared to PLA.

The crystallinities of DCP/PLA/Bis-EMAs decreased when compared to PLA. Moreover, high amounts of DCP and Bis-EMAs content promoted a large crosslinking structure resulted in decreasing crystallinity, which obstructed the PLA chains for crystallization.

Table 9.3 Thermal properties of PLA, DCP/PLA, and PLA/DCP/Bis-EMAs pellets

Sample	T _g (°C)	T _{cc} (°C)	ΔH _{cc} (J/g)	T _{m1} ; T _{m2} (°C)	ΔH _m (J/g)	χ _c (%)
PLA	57.9	-	-	151.2	44.8	48.1
0.1DCP	55.5	115.6	31.2	151.9	41.9	11.5
0.2DCP	55.4	105.9	36.7	152.9	45.0	8.9
0.3DCP	55.1	90.2	29.9	151.2	40.9	11.8
0.4DCP	55.5	105.3	33.0	152.5	41.7	9.3
0.5DCP	54.7	88.5	32.2	151.6	41.5	10.0
0.1D1B	56.5	98.6	33.4	144.7; 153.1	41.6	8.8
0.1D3B	55.4	100.8	30.6	143.6; 152.8	41.7	11.9
0.1D5B	54.4	100.5	33.5	144.3; 153.2	43.4	10.6
0.1D7B	45.5	92.5	36.8	142.8; 152.6	46.3	10.2
0.3D1B	58.4	89.2	30.2	151.9	40.6	11.1
0.3D3B	58.1	93.7	37.3	152.1	42.8	5.9
0.3D5B	59.5	93.8	38.7	151.1	39.9	1.1
0.3D7B	59.3	93.0	38.8	151.7	41.3	2.6
0.5D1B	60.5	98.4	38.2	151.5	42.1	4.1
0.5D3B	59.2	100.9	38.5	150.8	43.3	5.1
0.5D5B	60.7	101.0	38.5	151.5	40.4	2.0
0.5D7B	58.4	97.0	35.7	150.1	41.9	6.6

9.4.5.2 Thermal Properties of 0.3D5B Sample from Compression

Molding

In the case of various time for compression molding, the results showed that the T_g of sample decreased with the increase compression time as seen in Figure 9.19. This suggested that PLA chain was degraded when increase in compression time. At the various temperature, it seen that the temperature at 200 °C showed the T_g higher than temperature at 190 °C. The highest T_g was at 200 °C for 5 min which means that this condition was minimize to reduce the thermal properties of the sample as seen in Figure 9.19. The T_{cc} was shifted to lower temperature with

the increase in compression time. Moreover, the T_m of sample exhibited two peaks (Figure 9.20). The increase both temperature and time did not affect on the T_m of the sample (Table 9.4). So, the temperature and time are important factors for the compression or processing condition because PLA chain was more sensitive to heat.

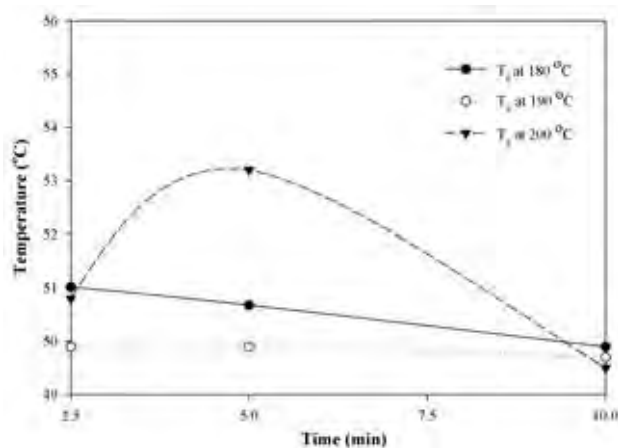


Figure 9.19 The plot of T_g of 0.3D5B sample from compression molding at various temperature and time.

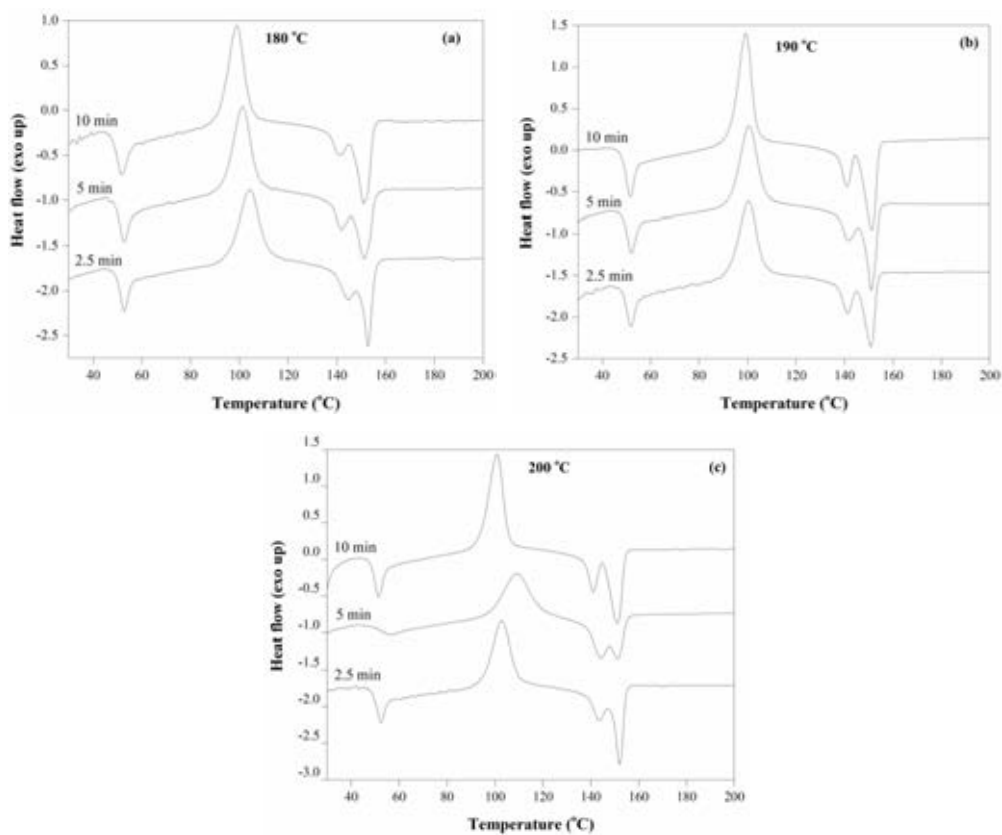


Figure 9.20 DSC thermograms of 0.3D5B sample of (a) 180 °C, (b) 190 °C, and (c) 200 °C.

Table 9.4 Thermal properties of 0.3D5B sample from compression molding at various condition

Condition of compression molding	T_g (°C)	T_{cc} (°C)	ΔH_{cc} (J/g)	T_{m1}; T_{m2} (°C)	ΔH_m (J/g)	χ_c (%)
180 °C for 2.5 min	51.0	104.3	45.3	144.5: 152.9	48.1	3.0
180 °C for 5 min	50.7	101.4	45.4	141.6: 151.1	47.4	2.2
180 °C for 10 min	49.5	98.7	48.4	141.0: 152.1	50.7	2.5
190 °C for 2.5 min	49.9	100.5	46.1	141.3: 151.2	47.8	1.8
190 °C for 5 min	49.9	100.6	51.6	141.4: 151.1	53.4	1.9
190 °C for 10 min	49.7	99.2	56.7	141.0: 151.5	57.9	1.3
200 °C for 2.5 min	50.8	103.0	46.0	143.5: 152.3	47.9	2.0
200 °C for 5 min	53.2	109.0	44.9	144.2: 151.2	46.3	1.5
200 °C for 10 min	49.5	100.9	57.2	141.0: 151.2	58.4	1.3

9.4.6 Thermo–Mechanical Properties

Figure 9.21a and Table 9.5 show the effect of temperature on storage modulus (E'), which relates directly to the stiffness of materials. At ambient temperature, E' of DCP/PLA is higher than that of PLA. It can be seen that E' of DCP/PLA also increased with the increasing DCP content because the crosslinking improved the modulus of the material. In the case of DCP/PLA/Bis–EMAs as seen in Figure 9.22a–9.24a, the E' increased with increasing Bis–EMAs up to 5 phr.

In the glass transition region, the E' of all samples is decreased. As the temperature is higher than T_g , the E' of all samples shows an abrupt increase which is attributed to cold crystallization. At temperature higher (>100 °C), DCP/PLA and DCP/PLA/Bis–EMAs are higher the E' than that of PLA. This means that DCP/PLA and DCP/PLA/Bis–EMAs can bear loads at higher temperatures better than that of PLA because the development of rigidity obtained from cold crystallization. At 120 °C, DCP/PLA and DCP/PLA/Bis–EMAs still show greater rigidity when compared to PLA. This can be noted that crosslinking structures showed bear load at temperature beyond the glass transition region.

Figure 9.21b and Table 9.5 show the loss modulus (E''), or ability of the material to dissipate energy, which is related to viscosity. DCP/PLA shows higher magnitude peak of the E'' when compared to PLA. The E'' of DCP/PLA slightly increased with increasing DCP content. This suggests that the addition of DCP improved the viscosity of PLA [19]. In Figure 9.22b–9.24b, the E'' peak of DCP/PLA/Bis-EMAs slightly increased with increasing Bis-EMAs content. This can be attributed to the crosslinking structure lead to promote high viscosity. The ratio of E' to E'' is measured as a loss factor, or $\tan \delta$, as observed in Figure 9.22a–9.24a and Table 9.5. Damping reveals that the molecular motion of PLA is greater when compared to DCP/PLA/Bis-EMAs. The limited molecular motion in DCP/PLA/Bis-EMAs agrees well to the stiffness due to crosslinking structure.

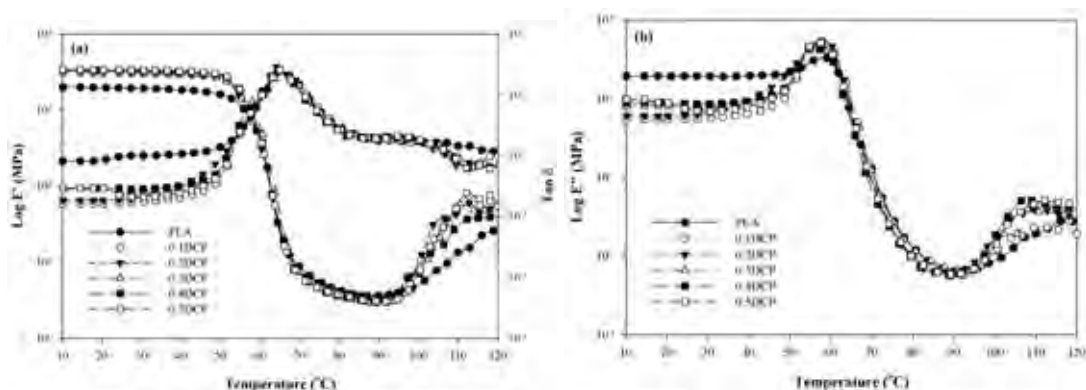


Figure 9.21 Temperature dependence of (a) E' and $\tan \delta$, and (b) E'' of PLA and DCP/PLA.

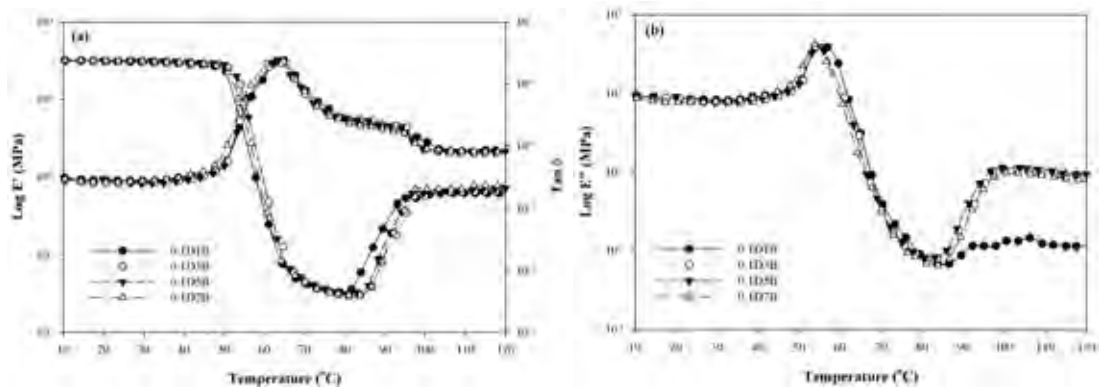


Figure 9.22 Temperature dependence of (a) E' and $\tan \delta$, and (b) E'' of 0.1DCP/PLA/Bis-EMAs content.

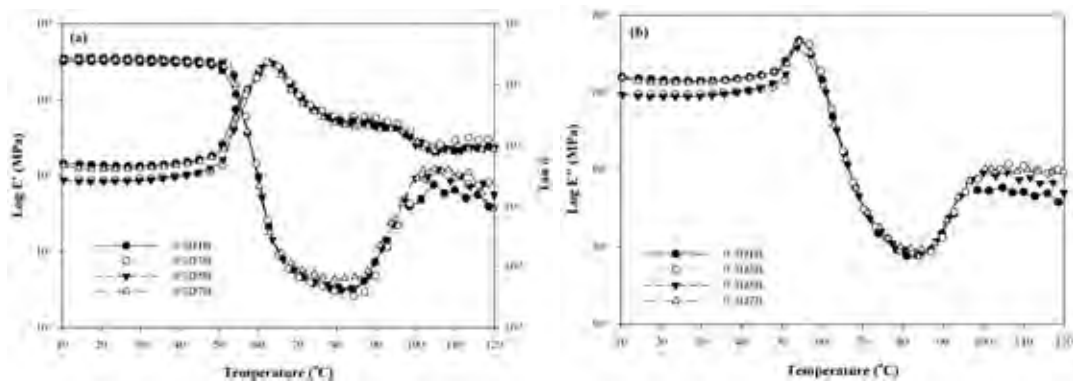


Figure 9.23 Temperature dependence of (a) E' and $\tan \delta$, and (b) E'' of 0.3DCP/PLA/Bis-EMAs.

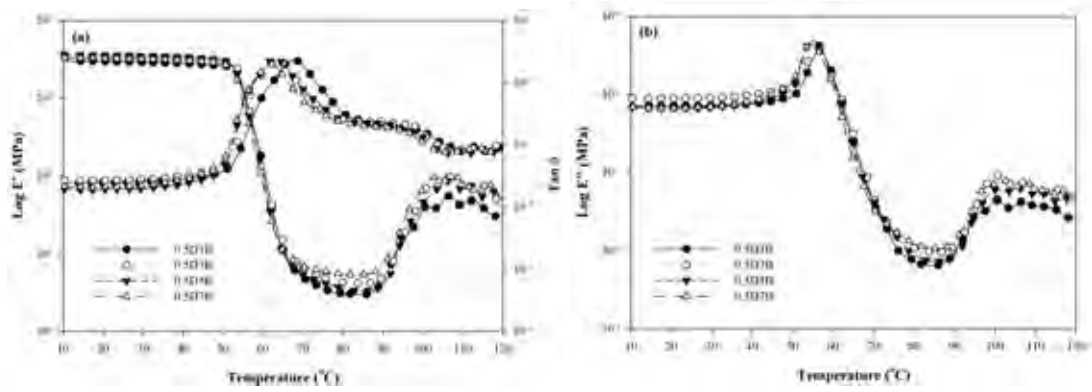


Figure 9.24 Temperature dependence of (a) E' and $\tan \delta$, and (b) E'' of 0.5DCP/PLA/Bis-EMAs content.

Table 9.5 Thermo–mechanical properties of PLA, DCP/PLA, and DCP/PLA/Bis–EMAs

Sample	T _g (°C)	30 °C		80 °C		100 °C		120 °C	
		E' (MPa)	E''(MPa)	E' (MPa)	E''(MPa)	E' (MPa)	E'' (MPa)	E' (MPa)	E''(MPa)
PLA	64.3	1925.04±40.32	193.00±12.95	4.21±0.84	1.19±0.01	5.74±1.02	0.96±0.21	31.72±6.03	3.27±1.06
0.1DCP	64.6	3021.09±56.29	57.14±10.06	2.70±0.03	0.63±0.01	10.77±2.11	1.21±0.43	54.16±5.11	1.90±0.59
0.2DCP	64.1	3199.53±38.01	66.85±8.43	2.41±0.11	1.22±0.04	12.56±1.04	1.76±0.69	43.95±5.86	2.40±0.67
0.3DCP	64.0	3219.72±49.75	77.48±9.12	2.69±0.04	1.02±0.05	10.04±1.90	1.13±0.08	52.11±6.03	3.86±0.41
0.4DCP	64.4	3257.51±62.05	85.69±7.05	2.56±0.14	0.68±0.04	7.07±0.98	1.84±0.14	40.00±2.49	3.38±0.48
0.5DCP	64.9	3322.11±50.30	69.49±8.21	2.41±0.16	0.72±0.01	7.92±2.32	1.44±0.60	54.36±5.92	3.61±0.52
0.1D1B	64.9	3084.15±48.56	81.56±10.23	3.56±0.02	0.91±0.03	52.81±6.09	2.53±0.45	60.79±9.39	2.53±0.68
0.1D3B	64.6	3105.07±83.48	86.05±9.40	2.93±0.03	0.78±0.06	55.55±9.42	9.42±2.59	64.37±11.94	9.23±0.21
0.1D5B	63.2	3185.93±29.54	81.32±8.52	3.11±0.03	0.81±0.02	60.71±11.56	9.05±1.38	70.00±9.02	8.84±1.11
0.1D7B	60.6	3160.29±31.93	76.49±6.59	3.00±0.05	0.68±0.08	68.69±6.52	8.30±2.09	76.85±9.35	8.24±0.85
0.3D1B	62.6	3100.15±40.54	141.22±9.63	3.07±0.05	0.76±0.09	48.53±3.21	5.32±1.02	42.95±5.39	3.89±0.72
0.3D3B	62.3	3461.30±47.58	94.79±7.76	2.96±0.09	0.90±0.02	43.33±2.09	8.99±1.53	77.91±10.38	8.73±0.68
0.3D5B	63.6	3475.32±53.40	87.98±5.69	3.44±0.17	0.93±0.01	91.66±5.28	9.06±1.20	55.89±7.93	5.01±0.42
0.3D7B	62.8	3283.17±50.28	135.54±11.60	4.26±0.03	1.00±0.02	90.99±3.95	10.22±3.29	36.94±3.50	9.29±1.08
0.5D1B	68.7	2889.69±39.59	71.23±9.54	3.09±0.05	0.77±0.02	40.24±2.11	4.45±0.43	34.05±4.02	3.17±0.92
0.5D3B	64.9	3321.82±47.80	89.43±8.59	4.26±0.08	1.08±0.01	67.40±8.42	9.06±1.30	61.04±7.49	5.39±0.47
0.5D5B	61.7	3503.96±41.05	67.41±8.90	3.71±0.03	0.99±0.01	45.42±4.65	5.86±1.04	40.31±5.03	3.49±0.21
0.5D7B	62.1	3175.07±39.46	69.01±5.62	5.37±0.04	1.32±0.04	62.57±5.04	6.88±1.22	46.89±4.60	4.42±0.19

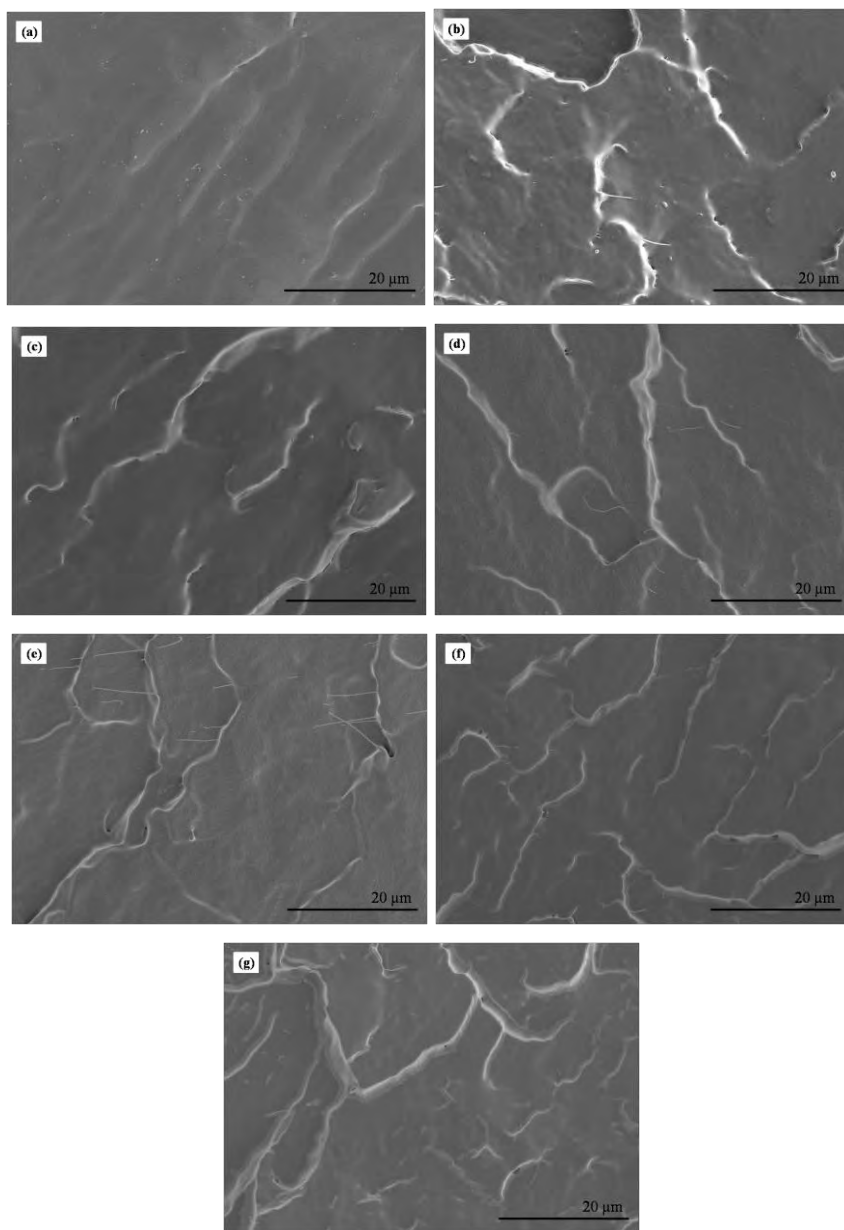
9.4.7 Morphological Properties

Figure 9.25 Morphological images of (a) PLA, (b) 0.1D1B, (c) 0.1D5B, (d) 0.3D1B, (e) 0.3D5B, (f) 0.5D1B, and (g) 0.5D5B.

The morphology of PLA reveals a smooth and uniform fractured surface as seen in Figure 9.25a. DCP/PLA/Bis-EMAs show rough surface which is observed in Figure 9.25b–9.25g. This can be suggested that the chains entanglement of crosslinking structure is strongly interaction between PLA chains lead to promote rough surface. Moreover, the fracture surface is rougher when increase in Bis-EMAs content.

In addition, the biodegradation of crosslinked PLA must be further studied. Mitomo et al. [2] studied the biodegradation rate of crosslinked PLA by irradiation. They found that the biodegradation was significantly delayed with the introduction of crosslink because of suppressing the penetrating of microorganisms into polymer gels and increased with increasing irradiation dose due to degradation of crosslinked molecules. This results also found in Quynh et al. [20]. In this work, it may be suggested that DCP/PLA samples have higher biodegradation rate than that of PLA because this system occur some chain scission. In the case of DCP/PLA/Bis-EMAs, the biodegradation of this system may decrease when compared to PLA. This suggests that crosslinked PLA was successfully produced in the presence of Bis-EMAs which retards the degradation.

9.4.8 Mechanical Properties

Mechanical properties of PLA and crosslinked PLA samples are shown in Figure 9.26 and Table 9.6. The introductions of DCP and Bis-EMAs into PLA show increase of Young's modulus and decrease of elongation at break. This suggests that PLA material was stiffened when crosslink structure was introduced to PLA. In the case of 0.3DCP/PLA/Bis-EMAs, the tensile strength firstly increases and then decreases with increasing Bis-EMAs content up to 7 phr. It can be seen that the highest tensile strength is obtained from 0.3D5B sample. Moreover, at the same introductions of Bis-EMAs contents, which are 0.3D7B and 0.5D7B samples, do not significantly changes of tensile strength and Young's modulus values. From this result, it can be noted that the optimums of tensile strength and Young's modulus were at a 5 phr Bis-EMAs.

Impact strength of PLA and crosslinked PLA is shown in Table 9.6. Impact strength of crosslinked PLA slightly decreased when compared to PLA. This suggests that crosslinked PLA has higher rigidity than PLA due to network structure. Moreover, it can be seen that impact strength of 0.3DCP/PLA/Bis-EMAs decreases with increasing Bis-EMAs content up to 5 phr. The lowest impact strength is obtained from 0.3D5B.

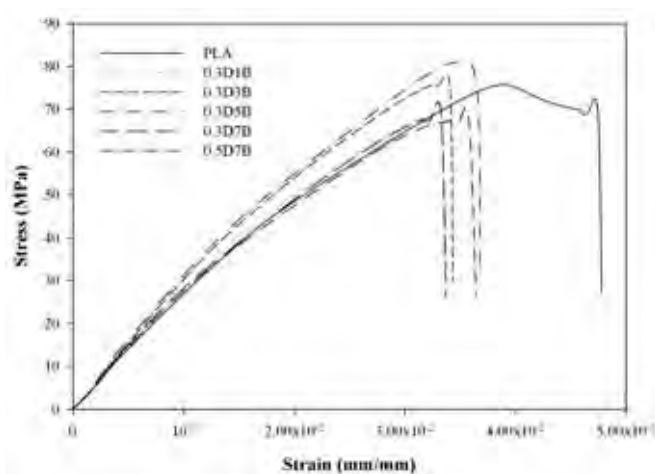


Figure 9.26 Stress–strain curves of PLA, 0.3D1B, 0.3D3B, 0.3D5B, 0.3D7B, and 0.5D7B samples.

Table 9.6 Mechanical properties of PLA, 0.3D1B, 0.3D3B, 0.3D5B, 0.3D7B, and 0.5D7B

Sample	Tensile strength (MPa)	Young's modulus (MPa)	Elongation at break (%)	Impact strength (J/m)
PLA	66.15±7.46	2681.98±156.61	5.00±0.30	55.10±1.20
0.3D1B	67.54±5.29	3155.40±179.15	3.00±0.40	55.10±1.00
0.3D3B	69.51±3.54	3343.79±147.81	3.00±0.20	51.30±2.50
0.3D5B	72.62±1.89	3453.64±75.30	4.00±0.20	47.50±1.20
0.3D7B	65.70±4.50	3196.24±144.56	3.00±0.30	51.30±1.50
0.5D7B	64.21±4.22	3084.17±114.96	4.00±0.30	52.50±1.40

9.5 Conclusion

This work reveals that crosslinking structures can be introduced into PLA by the initiation of DCP in the presence of Bis-EMAs. The rheological properties showed that DCP/PLA revealed the enhancement of G' and η^* when added DCP over 0.3 phr. In the case of DCP/PLA/Bis-EMAs, the G' and η^* of 0.1DCP/PLA/Bis-EMAs were decreased when compared to PLA because the introduction of 0.1 phr DCP did not enough to generate radicals of PLA chains and Bis-EMAs. This case was undesired crosslinking reaction of PLA in the presence of Bis-EMAs. In addition, 0.3DCP/PLA/Bis-EMAs and 0.5DCP/PLA/Bis-EMAs revealed improvement in G' and η^* due to effectively introduced crosslinking structure. The optimums of G' and η^* were at a 5 phr Bis-EMAs. TGA results revealed that DCP/PLA was better thermal stability when compared to PLA. The thermal stability of DCP/PLA/Bis-EMAs did not significantly change with increasing Bis-EMAs content. DSC results demonstrated that T_g , T_{cc} , and T_m of DCP/PLA slightly shifted to lower temperature when compared to PLA. The thermal properties of 0.1DCP/PLA/Bis-EMAs decreased with increasing Bis-EMAs content. In the case of 0.3DCP/PLA/Bis-EMAs and 05DCP/PLA/Bis-EMAs, T_g and T_{cc} were

increased when compared to PLA because the crosslinking structure inhibited chain motion. The tensile strength and Young's modulus of 0.3DCP/PLA/Bis-EMAs were increased while the impact strength of 0.3DCP/PLA/Bis-EMAs was decreased with increasing Bis-EMAs up to 5 phr. The thermo-mechanical properties showed that the E' and E'' of DCP/PLA were higher than that of PLA. In the case of DCP/PLA/Bis-EMAs, the E' and E'' increased with increasing Bis-EMAs up to 5 phr. The morphology properties of DCP/PLA/Bis-EMAs showed rough surface due to the chains entanglement of crosslinking structure. This work concluded that the chemical crosslinked PLA was successfully produced in the presence of Bis-EMAs was at 5 phr with the introduction of DCP over 0.3 phr.

9.6 Acknowledgement

Financial support has been granted by Rachadapisek Sompoch Endowment, Chulalongkorn University, Thailand.

9.7 References

- [1] Satyanarayana, K.G., Arizaga, G.G.C., Wypych, F. (2009) Biodegradable composites based on lignocellulosic fibers—An overview. Progress in Polymer Science, 34, 982–1021.
- [2] Mitomo, H., Ayako, K., Tran, M.Q., Naotsugu, N., Fumio, Y. (2005) Improvement of heat stability of poly(L-lactic acid) by radiation-induced crosslinking. Polymer, 46, 4695-4703.
- [3] Quynh, T.M., Mitomo, H., Nagasawa, N., Wada, Y., Yoshii, F., and Tamada, M. (2007) Properties of crosslinked polylactides (PLLA & PDLA) by radiation and its biodegradability. European Polymer Journal, 43, 1779–1785.

- [4] Yang, S.L., Wu, Z.-H., Meng, B., and Yang, W. (2009) The Effects of Dioctyl Phthalate Plasticization on the Morphology and Thermal, Mechanical, and Rheological Properties of Chemical Crosslinked Polylactide. Journal of Polymer Science: Part B: Polymer Physics, 47, 1136–1145.
- [5] Zenkiewicz, M., Rytlewski, P., and Malinowski, R. (2010) Compositional, physical and chemical modification of polylactide. Journal of Achievements in Materials and Manufacturing Engineering, 43, 192–199.
- [6] Changgang, X., Xuegang, L., Xiurong, Z., and Lili, L. (2009) Research on Crosslinking of Polylactide using Low Concentration of Dicumyl Peroxide. Materials Science Forum, 620, 189–192.
- [7] Huang, Y., Zhang, C., Pan, Y., Wang, W., Jiang, L. and Dan, Y. (2013) Study on the effect of Dicumyl Peroxide on Structure and Properties of Poly(Lactic Acid)/Natural Rubber Blend. Journal of Polymers and the Environment, 21, 375–387.
- [8] Yang, S.L., Wu, Z.-H., Yang, W., and Yang, M.-B. (2008) Thermal and mechanical properties of chemical crosslinked polylactide (PLA). Polymer Testing, 27, 957–963.
- [9] Lee, K.Y., Blaker, J.J., and Bismarch, A. (2009) Surface functionalisation of bacterial cellulose as the route to produce green polylactide nanocomposites with improved properties. Composites Science and Technology, 69, 2724–2733.
- [10] Wang, Y., Yang, L., Niu, Y., Wang, Z., Zhang, J., Yu, F., and Zhang, H. (2011) Rheological and Topological Characterization of Electron Beam Irradiation Prepared Long-Chain Branched Poly(lactic Acid). Journal of Applied Polymer Science, 122, 1857–1865.
- [11] Shin, B.Y., Han, D.H., and Narayan, R. (2010) Rheological and Thermal Properties of the PLA Modified by Electron Irradiation in the Presence of Functional Monomer. Journal of Polymers and the Environment, 18, 558–566.
- [12] Winter, H.H., and Chambon, F. (1986) Analysis of Linear Viscoelasticity of a Crosslinking Polymer at the Gel Point. Journal of Rheology, 30(2), 367–382.

- [13] Kaustabh, G., Xiao, Z.S., Robert, M., Jack, L., Glenn D.P., Miriam H.R., and Richard A.F.C. (2005) Rheological Characterization of in Situ Cross-Linkable Hyaluronan Hydrogels. Biomacromolecules, 6, 2857–2865.
- [14] Huang, Y., Zhang, C., Pan, Y., Wang, W., Jiang, L., and Dan, Y. (2013) Study on the Effect of Dicumyl Peroxide on Structure and Properties of Poly(Lactic Acid)/Natural Rubber Blend. Journal of Polymer Environment, 21, 375–387.
- [15] Bhardwaj, R., and Mohanty, A.K. (2007) Modification of Brittle Polylactide by Novel Hyperbranched Polymer-Based Nanostructures. Biomacromolecules, 8, 2476–2484.
- [16] Di, Y., Iannace, S., Maio, R.D., and Nicolais, L. (2005) Reactively Modified Poly(lactic acid): Properties and Foam Processing. Macromolecular Materials and Engineering, 290, 1083–1090.
- [17] Kim, E.S., Kim, B.C., and Kim, S.H. (2004) Structural Effect of Linear and Star-Shaped Poly(L-lactic acid) on Physical Properties. Journal of Polymer Science: Part B: Polymer physics, 42, 939-946.
- [18] Frone, A.N., Berlioz, S., Chailan, J.-F., and Panaitescu, D.M. (2013) Morphology and thermal properties of PLA-cellulose nanofibers composites. Carbohydrate Polymers, 91, 377–384.
- [19] Semba, T., Kitagawa, K., Ishiaku, U.S., and Hamada, H. (2006) The Effect of Crosslinking on the Mechanical Properties of Polylactic Acid/Polycaprolactone Blends. Journal of Applied Polymer Science, 101, 1816–1825.
- [20] Quynh, T.M., Mitomo, H., Nagasawa, N., Wada, Y., Yoshii, F., and Tamada, M. (2007) Properties of crosslinked polylactides (PLLA & PDLA) by radiation and its biodegradability. European Polymer Journal, 43, 1779–1785.

CHAPTER X

DISCUSSION OF WHOLE RESEARCH

10.1 Comparing between Peanut shell/PLA Composites with Polyethylene Glycol (form chapter V) and Peanut shell/PLA Composites with Triacetin (form chapter VI)

Plasticized PNS/PLA composites are prepared using two plasticizers, PEG and triacetin. The plasticized composites with triacetin show lower thermal properties than that of plasticized composites with PEG. The adding of triacetin show slightly decrease in decomposition temperature than that of adding PEG suggesting the higher volatility of triacetin when compared to PEG due to lower molecular weight.

The higher of tensile strength and modulus of plasticized composites are obtained using PEG instead of triacetin. This contributes to higher crystallinity of plasticized composites with PEG enhance the strength. However, the highest elongation at break and impact strength are obtained for the plasticized composites with triacetin with the best solubility parameter in relation to PLA.

The storage and loss modulus are reduced by the addition of PEG and even more decreased with triacetin. Thus the plasticized composites with triacetin are better processibility than the plasticized composites with PEG. If comparing between PEG and triacetin, the span of storage modulus is narrower in case of PEG than triacetin. Meaning that for high temperature usage, the triacetin plasticized composites are susceptible to deform easier than PEG plasticized ones. When increasing temperature beyond T_g , there was an event that the storage modulus abruptly increased suggesting cold crystallization to occur. So the properties of both plasticized composites are summarized in Table 10.1.

Table 10.1 Properties of the PNS/PLA composite with triacetin versus with PEG

Properties		PEG vs. Triacetin
Thermal properties	T_d, T_g, T_{cc}, T_m	>
% crystallinity		>
Mechanical properties	Tensile strength	>
	Young's modulus	>
	Elongation at break	<
	Impact strength	<
Thermo-mechanical properties	Storage modulus	>
	Loss modulus	<
Biodegradable properties		≈

10.2 Comparing between Bagasse/PLA Composite Films with Single and Double Plasticizers (form chapter VIII)

The bagasse/PLA composite with double plasticizers is better for processing into film than single plasticizer. The single-plasticized composite shows better mechanical properties than the double-plasticized composite. The optimum plasticizer (single and double plasticizers) is thus a compromise between the process requirements and the desired material stiffness. Table 10.2 summarizes the properties of both composite films.

Table 10.2 Properties of composite films with single plasticizer versus with double plasticizers

Properties		Single vs. Double
Thermal properties	T_d, T_g, T_{cc}, T_m	>
% crystallinity		<
Mechanical properties	Tensile strength	>
	Young's modulus	>
	Elongation at break	<
Thermo-mechanical properties	Storage modulus	>
	Loss modulus	>

10.3 Comparing between Peanut shell/PLA Composite Film (form chapter VII) and Bagasse/PLA Composite Film (form chapter VIII)

Table 10.3 shows the properties of peanut shell and bagasse fiber. It can be seen that bagasse is higher the density, decomposition temperature, and aspect ratio than that of peanut shell.

Table 10.3 The density, decomposition temperature, and aspect ratio of peanut shell and bagasse fiber

Properties	Peanut shell	Bagasse fiber
Density (g/cm^3)	1.63	1.74
$T_{d(\text{max})}$ ($^{\circ}\text{C}$)	339.5	340.2
Aspect ratio	2.52-5.16	6.67-10.29

At the same amount of fiber and plasticizer loading, the bagasse/PLA composite film is higher thermal properties than that of peanut shell/PLA composite film as seen in Table 10.4. The mechanical properties of bagasse/PLA composite film increased when compared to peanut shell/PLA composite film. This is due to the

bagasse fiber is higher aspect ratio than peanut shell that provides the better reinforcement properties.

Table 10.4 Properties of 10PNS10T film versus 10BAG10T film

Properties		10PNS10T vs. 10BAG10T
Thermal properties	T_d, T_g, T_{cc}, T_m	<
% crystallinity		<
Mechanical properties	Tensile strength	<
	Young's modulus	<
	Elongation at break	<
Thermo-mechanical properties	Storage modulus	<
	Loss modulus	<

10.4 Comparing between Polyethylene (PE), Black Biodegradable (PBAT), Polylactic Acid (PLA), and Peanut shell/PLA Composite Films with use as a Mulch Films

Table 10.5 shows properties of mulch films from benchmark (PE and PBAT films), PNS/PLA film, Bagasse/PLA film. It can be seen that PNS/PLA film shows the highest Young's modulus while the elongation at break is the lowest. The elongation at break of PNS/PLA and bagasse/PLA films must be improved for mulch film application for the future. The tensile strength of PNS/PLA film is higher than PBAT film but it is lower than PE film. Water vapor permeability of PNS/PLA film is higher than that of PBAT and PLA films but it is lower water vapor permeability than PE film. In addition, the advantage of PNS/PLA and bagasse/PLA films over the PE film is a biodegradable property. For PNS/PLA film, it provides the nitrogen < 2.60 % which is a good source of fertilizer for the crop production.

Table 10.5 Properties of mulch films which are PE, PBAT, PLA, PNS/PLA, and bagasse/PLA films

Properties	PE film	PBAT film	PLA film	PNS/PLA film	Bagasse/PLA film	Test method
Film thickness (μm)	25.0 \pm 1.0	218.0 \pm 22.0	100.0 \pm 14.0	135.4 \pm 29.0	136.47 \pm 6.32	-
Young's modulus (MPa)	10.9 \pm 0.4	40.1 \pm 5.8	2155.5 \pm 35.2	2203 \pm 42.2	721.06 \pm 68.0	ASTMD822
Tensile strength (MPa)	25.8 \pm 8.4	6.1 \pm 1.6	20.7 \pm 3.4	9.5 \pm 2.6	4.35 \pm 0.3	ASTMD822
Elongation at break (%)	336.0 \pm 159.0	530.0 \pm 102.0	4.2 \pm 1.0	2.9 \pm 0.8	5.78 \pm 1.6	ASTMD822
Water vapor permeability ($\times 10^{-6}$ g/m.Pa.day)	0.01049 \pm 0.0012	2.5 \pm 0.11	0.77 \pm 0.053	0.42 \pm 0.021	-	ASTM E96-01

Note: PNS/PLA composite film=10PNS5T, Bagasse/PLA composite film=10BAG10T10G

10.5 Comparing between Biocomposite, Plasticization, and Chemical Crosslinking Techniques

The composites are prepared using three techniques which are biocomposite, plasticization, and chemical crosslinking. Table 10.6 shows the properties of the samples from three techniques. For biocomposite technique, the composites from this technique show the improvement of tensile strength, biodegradability, Young's modulus as well as storage modulus. This is due to the addition of natural fiber as reinforcement in polymer matrix increases those properties of the composite. In the case of plasticization technique, the samples show decrease in thermal properties such as glass transition temperature because of the plasticizing effect. Moreover, this technique improves the elongation at break of the sample. For the chemical crosslinking, the crosslinking samples do not change in the decomposition

temperature, and are slightly decreased the glass transition temperature. In this work, the chemical crosslinking did not successful to improve the thermal properties.

Table 10.6 Properties of the sample from biocomposite, plasticization, and chemical crosslinking methods

Properties		Biocomposite	Plasticization	Chemical crosslinking
Thermal properties	T _d ,	-	--	Negligible change
	T _g , T _{cc} , T _m	-	--	-
% crystallinity		++	++	-
Mechanical properties	Tensile strength	+	--	N/A
	Young's modulus	+++	---	N/A
	Elongation at break	---	+++	N/A
Thermo-mechanical properties	Storage modulus	+++	---	++
	Loss modulus	++	--	++
Biodegradable properties		+++	+++	N/A

Note: The symbols, that increase from high to low, are +++, ++, and +, respectively.

The symbols, that decrease from high to low, are ---, --, and -, respectively.

10.6 Processing Techniques

Properties of natural fiber reinforced PLA composites depend on many factors, for instance fiber/matrix adhesion, volume fraction of fiber, fiber aspect ratio, fiber orientation, and stress/transfer efficiency through the interface, as well as processing techniques [1].

Processing techniques have a significant incidence on the final properties of the composites because they define the degree of dispersion or agglomeration of the fibers, and fiber orientation which have a stronger effect in the mechanical properties of the composites and can be reflected on other potential properties such as barrier properties.

Moreover, crystalline development in PLA has a dominant influence on the mechanical properties. Since the difference processing techniques have difference effect on the developed crystalline of PLA.

10.7.1 Injection molding

There are two major differences in the crystalline development in PLA molding conditions. The first one is that the polymer is crystallizing during or right after it has been sheared and oriented by the flow. The polymer flow is known to potentially increase the nucleation process since bundles of highly oriented polymer chains can act as nuclei unto which secondary crystals grow in the direction perpendicular to flow. The second major difference is the much higher cooling rate found in molding processes [2]. Since the enhanced nucleation rate and higher cooling time have opposite effect on developed crystalline of PLA lead to improve the mechanical properties.

For injected sample, the cycle time of 60 s with molding at 30–40 °C (as mentioned in Chapter IV–Chapter VI) is the time required to develop sufficient rigidity through crystallization in the molded parts prior to ejection. When compared to blown film extrusion, injection molding has more developed crystalline in PLA sample and obtained better mechanical properties.

10.7.2 Blown film extrusion

Properties of the film, such as tensile strength, flexural strength, toughness, and optical properties, drastically change depending on the orientation of the molecules. As the transverse direction properties decrease, the machine direction properties increase. For instance, if all the molecules were aligned in the machine direction, it would be easy to tear the film in that direction, and very difficult in the transverse direction (as mentioned in Chapter VII–Chapter VIII).

Blown film has a less effective cooling process than injection molding. Injected sample cooling is done by means of water, which has significantly higher specific heat capacities than the air that is used in the blown film cooling process. The higher specific heat capacity allows the substance to absorb more heat with less change in the substance temperature. Compared to injected sample, blown film has a more complicated and less accurate method to control thickness.

10.7.3 Compression Molding

Compression molding is the process of applying heat to materials, using hydraulic pressure to create a basic shape. The mold itself is typically heated to melt the materials. This allows materials to be shaped using molds. This process is conducted in a compression mold. Sample from this process is poorer mechanical properties than that of sample from injection and blown film extrusion because the orientation of the molecules in material does not occur in the compression molding.

10.7 References

- [1] Sanchez-Garcia, M.D., E. Gimenez, and J.M. Lagaron, Morphology and barrier properties of solvent cast composites of thermoplastic biopolymers and purified cellulose fibers. Carbohydrate Polymers, 2008. 71: p. 235–244.
- [2] Li, H. and M.A. Huneault, Effect of nucleation and plasticization on the crystallization of poly(lactic acid). Polymer, 2007. 48: p. 6855–6866.

CHAPTER XI

CONCLUSIONS AND RECOMMENDATIONS

11.1 Conclusions

This research focuses on three techniques, compounding (biocomposite), plasticization, and chemical crosslinking, as proposed solutions to overcome the aforementioned shortcomings associated with PLA. For compounding and plasticization techniques, the results revealed that natural fibers (peanut shell and bagasse) and plasticizers strongly alter crystallization behavior of PLA such that thermal stability and mechanical properties of plasticized composites differ from those of PLA. TGA results revealed that plasticized composites showed less heat stability; they start to decompose at temperatures greater than 100 °C due to the loss of moisture and plasticizers decomposition. The decrease in decomposition temperature of plasticized composites indicated a poor intermolecular interaction caused by plasticizing effect. In the case of adding natural fibers, the decomposition temperature of composites decreased with increasing natural fibers content due to low thermal stability of natural fibers.

DSC results showed that either natural fibers or plasticizers can act as nucleating agent for crystallization of PLA, and the combination of natural fibers and plasticizers caused melt crystallization of PLA. The crystallinity of plasticized composites increased largely and contributes to enhance the mechanical properties. Furthermore, plasticized composites showed two melting temperatures when compared to PLA. The addition of plasticizers decreased glass transition temperature of PLA.

Mechanical properties informed that an increase in plasticizers content decreased tensile strength due to the loosening of intermolecular interaction. However, elongation at break of plasticized PLAs was improved. In the case of adding natural fibers into PLA, tensile strength and Young's modulus increased with increasing natural fibers. Plasticized composites revealed that tensile strength decreased while Young's modulus increased with increasing both natural fibers and plasticizers.

The morphological study demonstrated that poor interfacial adhesion between natural fibers and PLA matrix, and natural fibers aggregated in PLA matrix. In addition, plasticized composites showed good distribution of natural fibers because the presence of plasticizers improved the distribution of natural fibers during extrusion.

For the thermo-mechanical properties, the storage and loss modulus of PLA increased with the addition of natural fibers. On the other hand, they are reduced by the addition of plasticizers. At room temperature, plasticized composites were higher storage modulus when compared to plasticized PLAs. When increasing temperature beyond glass transition temperature, the storage moduli of plasticized PLAs and plasticized composites abruptly increased suggesting cold crystallization to occur.

The biodegradation study revealed that the addition of natural fibers into PLA improved biodegradation of PLA. In case of adding plasticizers, plasticized composites showed slightly increase degradation rate with increasing plasticizers content. It can be explained that increase in plasticizers content resulted in a large amount of plastically deformed polymer on fracture surfaces. Thus the results concluded that the addition of natural fibers together plasticizer improved the biodegradation of PLA.

Water vapor permeability showed that plasticized PLAs were lower water vapor permeability than that of PLA. The adding natural fiber into plasticized PLAs improved the barrier properties to water because the presence of natural fiber is thought to increase the tortuosity. The water vapor permeability of plasticized composites decreased, which means that decreased moisture loss. One property of much film was reduced the water consumption. So, the plasticized composites showed a decrease in water vapor permeability which can use as a much film.

In the study of chemical crosslinked PLA, the results revealed that crosslinking structures can be introduced into PLA by an initiation of DCP in the presence of Bis-EMAs as a crosslinking agent. The rheological properties showed that storage modulus and complex viscosity of DCP/PLA improved when added DCP over 0.3 phr. In the case of DCP/PLA/Bis-EMAs, the optimums of storage modulus and complex viscosity were at a 5 phr Bis-EMAs. The thermo-mechanical properties showed that storage modulus and loss modulus of DCP/PLA showed

higher than that of PLA. In the case of DCP/PLA/Bis-EMAs, storage modulus and loss modulus increased with increasing Bis-EMAs up to 5 phr. The thermal stability of DCP/PLA/Bis-EMAs did not significant change when compared to PLA. Moreover, the thermal properties of 0.3DCP/PLA/Bis-EMAs and 0.5DCP/PLA/Bis-EMAs increased with increasing Bis-EMAs content. This work can be concluded that the optimum reaction for chemical crosslinking PLA in the presence of Bis-EMAs was at 5 phr Bis-EMAs. And the thermal properties of crosslinking PLA were improved when introduction of DCP above 0.3 phr in the presence of 5 phr Bis-EMAs.

11.2 Recommendations

The recommendation of the future work will be based:

- Study the fiber surface treatment to improve adhesion between fiber and matrix.
- Study the effect of aspect ratio of fibers on the mechanical properties and barrier properties.
- Study the composite film as a mulch film for the crop production in the real scale experiment.
- The composite film will be improving elongation at break for use as mulch film. For example, blending PLA with PBAT to increase elongation at break.
- Study the biodegradable properties of crosslinking PLA.
- Study the processing condition of crosslinking PLA, such as screw speed or reaction time, and temperature in order to find the optimum condition of crosslinking PLA for processing.

REFERENCES

- Averousa, L. and Boquillon, N. (2004) Biocomposites based on plasticized starch: thermal and mechanical behaviours. Carbohydrate Polymers, 56, 111–122.
- Anderson, K.S. and Hillmyer, M.A. (2006) Melt preparation and nucleation efficiency of polylactide stereocomplex crystallites. Polymer, 47, 2030–2035.
- Akgu, M. and Tozluoglu, A. (2008) Utilizing peanut husk (*Arachis hypogaea* L.) in the manufacture of medium-density fiberboards. Bioresource Technology, 99, 5590–5594.
- Bharadwaj, R.K. (2001) Modeling the Barrier Properties of Polymer-Layered Silicate Nanocomposites. Macromolecules, 34, 9189–9192.
- Bilba, K. and Arsene, M.A. (2008) Silane treatment of bagasse fiber for reinforcement of cementitious composites. Composites: Part A, 39, 1488–1495.
- Bilck, A.P., Grossmann, M.V.E., and Yamashita, F. (2010) Biodegradable mulch films for strawberry production, Polymer Testing, 29, 471–476.
- Bax, B. and Mussig, J. (2008) Impact and tensile properties of PLA/Cordenka and PLA/flax composites. Composites Science and Technology, 68, 1601–1607.
- Bledzki, A.K., Jaszkiwicz, A., and Scherzer, D. (2009) Mechanical properties of PLA composites with man-made cellulose and abaca fibres. Composites: Part A, 40, 404–412.
- Bhattacharya, A., Rawlins, J.W., Ray, P. (2009) Polymer Grafting and Crosslinking. Published by John Wiley & Sons, Inc., Hoboken, New Jersey.
- Cabot Corporation. "Masterbatch Selection Guide for Agricultural Film Applications". 2008. 15 November 2013. < www.cabot-corp.com/plastics >
- Chang, L. and Woo, E.M. (2011) Effects of molten poly(3-hydroxybutyrate) on crystalline morphology in stereocomplex of poly(L-lactic acid) with poly(D-lactic acid). Polymer, 52, 68–76.
- Cao, Y., Shibata, S., and Fukumoto, I. (2006) Mechanical properties of biodegradable composites reinforced with bagasse fibre before and after alkali treatments. Composites: Part A, 37, 423–429.

- Cerqueira, E.F., Baptista, C.A.R.P., and Mulinari, D.R. (2011) Mechanical behaviour of polypropylene reinforced sugarcane bagasse fibers composites. Procedia Engineering, 10, 2046–2051.
- Design, A. M. b. (2014) Chapter 3 polymer matrix composites.
<https://www.princeton.edu/~ota/disk2/1988/8801/880106.PDF>, 3 March.
- Finkenstadta, V.L., and Tisserat, B. (2010) Poly(lactic acid) and Osage Orange wood fiber composites for agricultural mulch films. Industrial Crops and Products, 31, 316–320.
- Faruk, O., Andrzej, K.B., Hans-Peter, F., and Mohini, S. (2012) Biocomposites reinforced with natural fibers. Progress in Polymer Science, 37, 1552–1596.
- Fasina, O.O. (2008) Physical properties of peanut hull pellets. Bioresource Technology, 99, 1259–1266.
- Fu, S.-Y. and Lauke B. (1996). Effects of fiber length and fiber orientation distributions on the tensile strength of short-fiber-reinforced polymers. Composites Science and Technology, 56, 1179–1190.
- Fu, S.-Y., Xu, G., and Mai, Y.-W. (2002). On the elastic modulus of hybrid particle/short-fiber/polymer composites. Composites: Part B, 33, 291–299.
- Garthe, J.W. and Kowal, P.D. (1993) Managing Used Plastic Mulch Film: Degradable Versus Non-Degradable. Agricultural and Biological Engineering.
- Graupner, N., Herrmann, A.S., and Müssig, J. (2009) Natural and man-made cellulose fibre-reinforced poly(lactic acid) (PLA) composites: An overview about mechanical characteristics and application areas. Composites: Part A, 40, 810–821.
- Gurit. “Reinforcement Properties for Composite Materials”. 11 Jun 2013. 4 Dec 2013 < <http://www.azom.com/article.aspx?ArticleID=978>>
- Galagan, Y., Hsu, S.-H., Su W.-F. (2010). Monitoring time and temperature by methylene blue containing polyacrylate film. Sensors and Actuators B: Chemical, 144, 49–55.
- Grillet, A.M., Wyatt, N.B., Gloe, L. M. (2012). Polymer gel rheology and adhesion. Rheology edited by Dr. Juan De Vicente, March 2012
<<http://www.intechopen.com>>.

- Hemvichian, K., Nagasawa, N., and Tamada M. (2009) Effects of Radiation-Induced Crosslinking on the Thermal Stability of Poly(Lactic Acid) and Cellulose Acetate Blends. Paper presented at The 11th Conference on Nuclear Science and Technology. Bangkok.
- Henton, D.E., Patrick, G., Jim, L., and Jed, R. Natural Fibers, Biopolymers, and Biocomposites. Poly(lactic Acid) Technology. 4 Nov 2013.
<[http://www.jimluntllc.com/pdfs/poly\(lactic_acid\)_technology.pdf](http://www.jimluntllc.com/pdfs/poly(lactic_acid)_technology.pdf)>
- Huda, M.S., Lawrence, T.D., Amar K.M., and Manjusri, M. (2006) Chopped glass and recycled newspaper as reinforcement fibers in injection molded poly(lactic acid) (PLA) composites: A comparative study. Composites Science and Technology, 66, 1813–1824.
- Harrell, Design for Sustainable Development Spring. 2010, 4 Nov 2013.
- HallStar, The function and selection of ester plasticizers. Thechnical Publication. 16 Nov 2013 <http://www.hallstar.com/techdocs/The_Function-Selection_Ester_Plasticizers.pdf>
- Kijchavengkul, T., Rafael, A., Maria, R., Mathieu, N., and Thomas F. (2008) Assessment of aliphatic–aromatic copolyester biodegradable mulch films. Part I: Field study. Chemosphere, 71, 942–953.
- Li, H. and Huneault, M.A. (2007) Effect of nucleation and plasticization on the crystallization of poly(lactic acid). Polymer, 48, 6855–6866.
- Lemmouchi, Y., Marius, M., Ana, M.D.S., Allan, J.A., Etienne, S., and Philippe D. (2009) Plasticization of poly(lactide) with blends of tributyl citrate and low molecular weight poly(D,L-lactide)-b-poly(ethylene glycol) copolymers. European Polymer Journal, 45, 2839–2848.
- Martin, O. and Averous, L. (2001) Poly(lactic acid): plasticization and properties of biodegradable multiphase systems. Polymer, 42, 6209–6219.
- Murariu, M., Amália, D.S.F., Mirosław, P., Leila, B., Michaël, A., and Philippe, D. (2008) Poly(lactide) (PLA)–CaSO₄ composites toughened with low molecular weight and polymeric ester-like plasticizers and related performances. European Polymer Journal, 44, 3842–3852.
- Ochi, S. (2008) Mechanical properties of kenaf fibers and kenaf/PLA composites. Mechanics of Materials, 40, 446–452.

- Oksman, K., Skrifvars, M., and Selin, J.-K. (2003) Natural fibres as reinforcement in polylactic acid (PLA) composites. Composites Science and Technology, 63, 1317–1324.
- Ogliari, F.A., Caroline, E., Cesar, H.Z., Carmen, B.B.F., Susana, M.W.S., Fla' vio, F.D., Cesar, L.P., Evandro, Piva. (2008) Influence of chain extender length of aromatic dimethacrylates on polymer network development. Dental Materials, 24, 165–171.
- Pradhan, R., Misra, M., Erickson, L., and Mohanty, A. (2010) Compostability and biodegradation study of PLA-wheat straw and PLA-soy straw based green composites in simulated composting bioreactor. Bioresource Technology, 101, 8489–8491.
- Pillin, I., Montrelay, N., and Grohens, Y. (2006) Thermo-mechanical characterization of plasticized PLA: Is the miscibility the only significant factor?. Polymer, 47, 4676–4682.
- Piorkowska, E., Kulinski, Z., Galeski, A., and Masirek, R. (2006) Plasticization of semicrystalline poly(L-lactide) with poly(propylene glycol). Polymer, 47, 7178–7188.
- Quynh, T.M., Hiroshi, M., Naogutsu, N., Yuki, W., Fumio, Y., Masao, T. (2007) Properties of crosslinked polylactides (PLLA & PDLA) by radiation and its biodegradability. European Polymer Journal, 43, 1779–1785.
- Ren, J., Hongye, F., Tianbin, R., and Weizhong, Y. (2009) Preparation, characterization and properties of binary and ternary blends with thermoplastic starch, poly(lactic acid) and poly(butylene adipate-co-terephthalate). Carbohydrate Polymers, 77, 576–582.
- Rahman, M. and Brazel, C.S. (2004) The plasticizer market: an assessment of traditional plasticizers and research trends to meet new challenges. Progress in Polymer Science, 29, 1223–1248.
- Ramis, X. and Salla, J. M. (1997). Time-Temperature Transformation (TTT) Cure Diagram of an Unsaturated Polyester Resin. Journal of Polymer Science: Part B: Polymer physics, 35, 371–388.

- Scarascia-Mugnozza, G., Evelia, S., Giuliano, V., Mario, M., Barbara, I., and Stefania, P. (2006) Mechanical properties decay and morphological behaviour of biodegradable films for agricultural mulching in real scale experiment. Polymer Degradation and Stability, 91, 2801–2808.
- Suryanegara, L., Nakagaito, A.N., and Yano, H. (2009) The effect of crystallization of PLA on the thermal and mechanical properties of microfibrillated cellulose-reinforced PLA composites. Composites Science and Technology, 69, 1187–1192.
- Sanchez-Garcia, M.D. and Lagaron, J.M. (2010) On the use of plant cellulose nanowhiskers to enhance the barrier properties of polylactic acid. Cellulose, 17, 987–1004.
- Shogrena, R.L., Doane, W.M., Garlotta, D., Lawton, J.W., and Willett, J.L. (2003) Biodegradation of starch/polylactic acid/poly(hydroxyester-ether) composite bars in soil. Polymer Degradation and Stability, 79, 405–411.
- Song, J., Weihua, Z., Yangyang, B., Fengyun, S., and Runping, H. (2011) Adsorption characteristics of methylene blue by peanut husk in batch and column modes. Desalination, 265, 119–125.
- Stael, G.C., Tavares, M.I.B., and Almeida, J.R.M. (2001) Impact behavior of sugarcane bagasse waste–EVA composites. Polymer Testing, 20, 869–872.
- Tao, Y., Yan, L., and Jie, R. (2009) Preparation and properties of short natural fiber reinforced poly(lactic acid) composites. Transactions of Nonferrous Metals Society of China, 19, 651–655.
- Tsuji, H. and Ikada, Y. (1999) Stereocomplex formation between enantiomeric poly(lactic acid)s. XI. Mechanical properties and morphology of solution-cast films. Polymer, 40, 6699–6708.
- Vieira, M.G.A., Mariana, A.S., Lucielen O.S., and Marisa M.B. (2011) Natural-based plasticizers and biopolymer films: A review. European Polymer Journal, 47, 254–263.
- Verasan, J., Sae-jiew, A., and Mutharat, P. (2014). Releasing of plant available fertilizer nutrient from plant media. http://www.rdi.ku.ac.th/kasetresearch52/04-plant/janjarus/plant_00.html.

- Wu, C.S. (2009) Renewable resource-based composites of recycled natural fibers and maleated polylactide bioplastic: Characterization and biodegradability. Polymer Degradation and Stability, 94, 1076–1084.
- Wilson, K., Hong, Y., Chung, W.S., and Wayne, E.M. (2006) Select metal adsorption by activated carbon made from peanut shells. Bioresource Technology, 97, 2266–2270.
- Winter, H.H., and Chambon, F. (1986). Analysis of linear viscoelasticity of a crosslinking polymer at the gel point. Journal of Rheology, 30(2), 367–382.
- Yokohara, T. and Yamaguchi, M. (2008) Structure and properties for biomass-based polyester blends of PLA and PBS. European Polymer Journal, 44, 677–685.
- Yu, T., Jie, R., Shumao, L., Hua, Y., and Yan, L. (2010) Effect of fiber surface-treatments on the properties of poly(lactic acid)/ramie composites. Composites: Part A, 41, 499–505.
- Yang, S.L., Wu, Z.H., Yang, W., and Yang, M.B. (2008) Thermal and mechanical properties of chemical crosslinked polylactide (PLA). Polymer Testing, 2008, 27,957–963.
- Yang, S.L., Wu, Z.H., Meng, B., and Yang, W. (2009) The Effects of Dioctyl Phthalate Plasticization on the Morphology and Thermal, Mechanical, and Rheological Properties of Chemical Crosslinked Polylactide. Journal of Polymer Science: Part B: Polymer Physics, 47, 1136–1145.
- Żenkiewicz, M., Rytlewski, P., and Malinowski, R. (2010) Compositional, physical and chemical modification of polylactide. Journal of Achievements in Materials and Manufacturing Engineering, 43(1).
- Zhang, X., Yi, X., and Xu, Y. (2008) Phase separation time/temperature dependence of thermoplastics-modified thermosetting systems. Chemical Engineering of China, 2(3), 276–285.

APPENDICES

Appendix A Stress–Strain Curves of Sample Films in Chapter VII

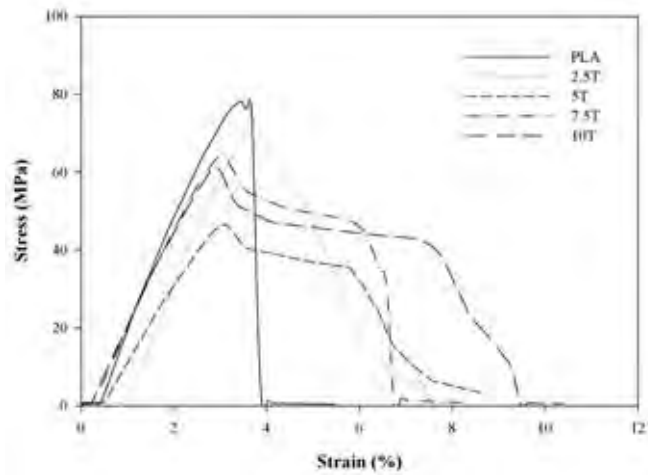


Figure A1 Stress–strain curves of plasticized PLA films.

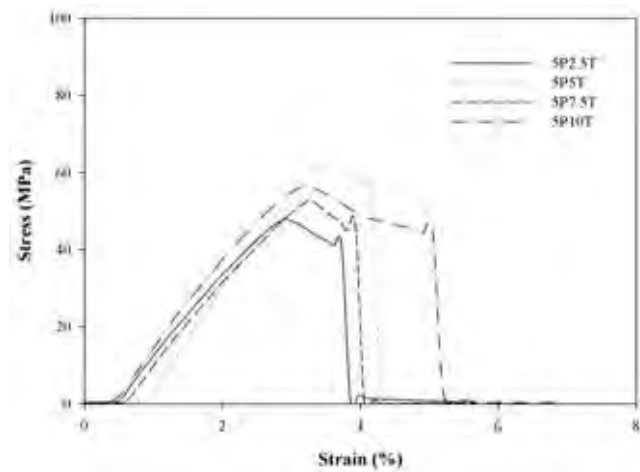


Figure A2 Stress–strain curves of plasticized 5PNS/PLA composite films.

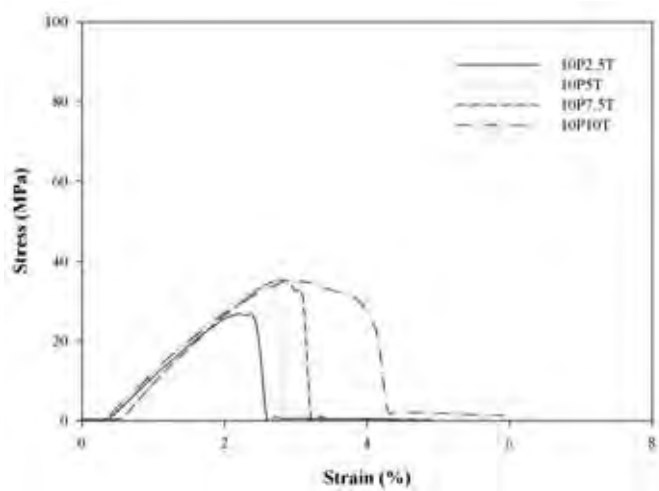


Figure A3 Stress–strain curves of plasticized 10PNS/PLA composite films.

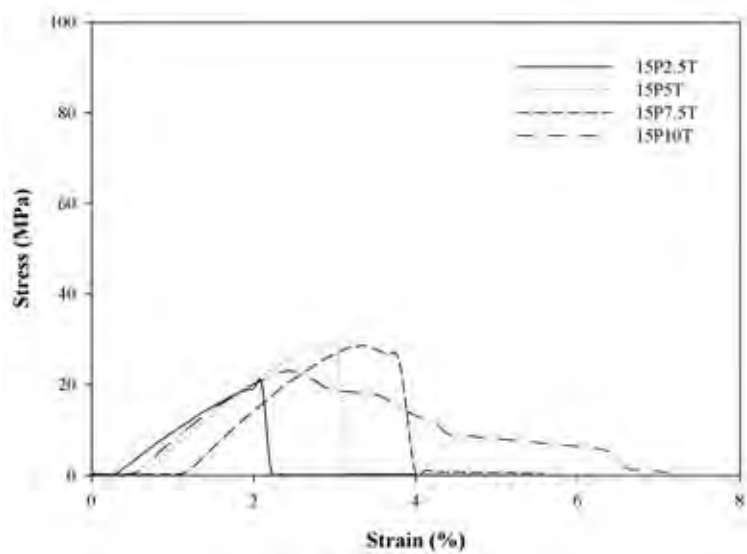


Figure A4 Stress–strain curves of plasticized 15PNS/PLA composite films.

Appendix B Calculation Cost of Samples in Each Chapter

Materials	Prices
1. Polylactic acid	100 baht/kg
2. Peanut shell powder	120 baht/kg
3. Bagasse powder	137 baht/kg
4. Polyethylene glycol	1,260 baht/L
5. Triacetin	4,000 baht/L
6. Glycerol	5,640 baht/L
7. Irganox 1010	110 baht/kg.
8. QUENT 68	150 baht/kg
9. Dicumyl peroxide	2,115 baht/100g
10. Bisphenol A ethoxylate dimethacrylate	7,830 baht/500mL

Table B1 Cost of samples in Chapter IV

Sample	Cost/kg	Cost/25kg
10PNS	103.30	2,582.50
20PNS	105.50	2,637.50
30PNS	107.30	2,687.50
40PNS	109.30	2,732.50

Table B2 Cost of samples in Chapter V

Sample	Cost/kg	Cost/25kg
30P2.5PEG	138.80	3,70.00
30P5PEG	170.30	4,257.50
30P7.5PEG	201.80	5,045.00
30P10PEG	233.30	5,832.50
30P12.5PEG	264.80	6,620.00

Table B3 Cost of samples in Chapter VI

Sample	Cost/kg	Cost/25kg
30P2.5TRI	207.30	5,182.50
30P5TRI	307.30	7,682.50
30P7.5TRI	407.30	10,182.50
30P10TRI	507.30	12,682.50
30P12.5TRI	607.30	15,182.50

Table B4 Cost of samples in Chapter VII

Sample	Cost/kg	Cost/25kg
2.5T	201.30	5,032.50
5T	301.30	7,532.50
7.5T	401.30	10,032.50
10T	501.30	12,532.50
5P2.5T	202.30	5,057.50
5P5T	302.30	7,557.50
5P7.5T	402.30	10,057.50
5P10T	502.30	12,557.50
10P2.5T	203.30	5,082.50
10P5T	303.30	7,582.50
10P7.5T	403.30	10,082.50
10P10T	503.30	12,582.50
15P2.5T	204.30	5,107.50
15P5T	304.30	7,607.50
15P7.5T	404.30	10,107.50
15P10T	504.30	12,607.50

Table B5 Cost of samples in Chapter VIII

Sample	Cost/kg	Cost/25kg
10BAG	105.00	2,625.00
10T	501.30	12,532.50
10T10G	1065.30	26,632.50
10BAG10T	505.00	12,625.00
10BAG10T10G	1069.00	26,725.00

Table B6 Cost of samples in Chapter IX

Sample	Cost/kg	Cost/25kg
0.1DCP	121.15	3,028.75
0.2DCP	142.30	3,557.50
0.3DCP	163.45	4,086.25
0.4DCP	184.60	4,615.00
0.5DCP	205.75	5,143.75
0.1D1B	277.75	6,943.75
0.1D3B	590.95	14,773.75
0.1D5B	904.15	22,603.75
0.1D7B	1217.35	30,433.75
0.3D1B	320.05	8,001.25
0.3D3B	633.25	15,831.25
0.3D5B	946.45	23,661.25
0.3D7B	1,259.65	31,491.25
0.5D1B	362.35	9,058.75
0.5D3B	675.55	16,888.75
0.5D5B	988.75	24,718.75
0.5D7B	1301.95	32,548.75

CURRICULUM VITAE



Name: Chamaiporn Yamoum

Date of Birth: September 1, 1985

Nationality: Thai

University Education:

2008 – Present Ph.D. student in major of Polymer Science, The Petroleum and Petrochemical College, Chulalongkorn University, Thailand

2004 – 2007 Bachelor Degree of Chemical Engineering, Faculty of Engineering and Industrial Technology, Silpakorn University, Thailand

Publications:

1. Yamoum, C.; Magaraphan R. (2011) Peroxide Cured Natural Rubber/Fluoroelastomer/High-Density Polyethylene via Dynamic Vulcanization. Journal of Polymer Engineering & Science, 51(8). 1484–1488.
2. Yamoum, C.; Magaraphan R. (2013) Thermal Behaviors and Mechanical Properties of PLA–Bagasse Composite Film. Journal of Biobased Materials and Bioenergy, 7. 639–647.
3. Yamoum, C; Magaraphan R. (2015) Effect of Peanut Shell Content on Mechanical, Thermal, and Biodegradable Properties of Peanut Shell/Polylactic Acid Biocomposites. Polymer Composites, DOI 10.1002/pc.23627.
4. Yamoum, C; Magaraphan R.; Joao Maia (2016) Rheological and Thermal Behavior of PLA Modified by Chemical Crosslinking in the Presence of Ethoxylated Bisphenol A Dimethacrylates. Polymers for Advanced Technologies, 28. 102–112.

Proceedings:

1. Yamoum, C.; Magaraphan R. (2009, Jan 14-16) Dynamic Vulcanization of Fluoroelastomer/ Natural Rubber and High-Density Polyethylene with peroxide Proceeding of Pure and Applied Chemistry International Conference (PACCON 2009).

2. Yamoum, C.; Magaraphan R. (2013, Jan 25) Effect of Carboxymethylcellulose on Plasticized Polylactide. Proceeding of Advanced Materials Research, 658. 19-24.

Presentations:

1. Yamoum, C.; Magaraphan R. (2009, Jan 14-16) Dynamic Vulcanization of Fluoroelastomer/ Natural Rubber and High-Density Polyethylene with peroxide. Poster presented at Pure and Applied Chemistry International Conference (PACCON 2009), Phitsanulok, Thailand.
2. Yamoum, C.; Magaraphan R. (2011, May 29-31) Reactive blends of Polylactic acid and modified cellulose from biomass. Poster presented at 2nd International Symposium - Frontiers in Polymer Science, Lyon, France.
3. Yamoum, C.; Magaraphan R. (2011, November 13-17) Reactive Blends of Polylactic acid and Modified Cellulose from Biomass for Biodegradable Film Application. Poster presented at The 12th Pacific Polymer Conference, Jeju island, Korea.
4. Yamoum, C.; Magaraphan R. (2011, November 13-17) Green Composites of Polylactic acid Filled with Carboxymethylcellulose for Biodegradable Film Application. Poster presented at The 12th Pacific Polymer Conference, Jeju island, Korea.
5. Yamoum, C.; Magaraphan R. (2011, December 20-21) Development and Thermal Behavior of Carboxymethylcellulose/Polylactic acid Composite Films. Poster presented at The third Thai-Japan, Bioplastics and Biobased Materials Symposium (AIST-NIA-TBIA Joint Syposium), Bangkok, Thailand.
6. Yamoum, C.; Magaraphan R. (2011) Biomass-Filled Bioplastic Compounds for Injection Molding. Oral presented at The 2nd Research Symposium on Petroleum, Petrochemicals, and Advanced Materials and the 17th PPC Symposium on Petroleum, Petrochemicals, and Polymers, Bangkok, Thailand.

7. Yamoum, C.; Magaraphan R. (2012, January 11-13) Thermal Behavior of PLA Composite Films with Bagasse Fibers. Poster presented at Polymer Chemistry in Pure and Applied Chemistry International Conference (PACCON 2012), Chiangmai, Thailand.
8. Yamoum, C.; Magaraphan R. (2012, June 2012) Green Composites of Polylactic Acid/Peanut Shell Fiber for Biodegradable Application. Oral presented at InterPlas Thailand 2012, Bangkok, Thailand.